

Linking cooling by nature and urban drought reduction to irrigation measures.

Tackling the urban heat island and droughts simultaneously.

A.M. Kool



Linking cooling by nature and urban drought reduction to irrigation measures.

Tackling the urban heat island and droughts
simultaneously.

by

A.M. Kool

to obtain the degree of Master of Science,
at the Delft University of Technology,
to be defended publicly on Thursday July 29, 2021 at 11:45 AM.

Abstract

To reduce the Urban Heat Island (UHI) effect Green Infrastructure (GI) is seen as a key measure. Though, often the need for water to evaporate is neglected. This study focuses on showing the effects of irrigation and increased soil moisture contents on GI within urban areas to reduce the UHI-effect. ENVI-met, a micro-climate model, is used to model various scenarios for a tropical day and a heatwave in the Netherlands. For two Dutch urban areas, with different building typology and subsoil, the current situation, a greener scenario and various soil moisture profiles have been modelled to show the effects of increased soil moisture content on thermal comfort and the UHI-effect.

Student number: 4248791
Project duration: September 2, 2019 – July 22, 2021
Thesis committee: Dr. ir. F.H.M. van de Ven, TU Delft Water Resources Management
Dr. F.L. Hooimeijer, TU Delft Urbanism
Dr. ir. G.H.W. Schoups, TU Delft Water Resources Management
L. Valkenburg, MSc., TAUW bv.

An electronic version of this thesis is available at <http://repository.tudelft.nl/>.



Preface

During secondary school I already got attracted to Civil Engineering, entering a paper bridge contest, building a small arched wooden bridge for one of my courses and I attended a floating homes curriculum at the same University I am graduating from. These interests, together with growing up in a very green-blue neighborhood in the Netherlands, inspired me to study Civil Engineering. During my bachelors at TU Delft I always wanted to build bridges and find the best structural solution. Soon I found out the human side behind the field, and our responsibility as engineers to tackle the larger problems in the world like the environmental challenges we face. This lead me to study water management at TU Delft, trying to find a balance between the technical and human world, while finding helpful solutions the environmental challenges.

This path has lead me to my thesis, to the begin of creating a better sustainable and durable world for man and nature.

First of all, I would like to thank my committee for guiding me trough my master's thesis. Special thanks to Frans van de Ven and Leon Valkenburg. Frans for always being understanding and picking my mind towards my next steps, guiding me to this end result. Leon thank you for giving me the opportunity to start the research within TAUW b.v. and showing me the work field. Most of all I would like to thank you for your patience and understanding during the laptop crash and initial software problems that occurred during my research. To both Gerrit and Fransje, thank you for you insights and keeping my mind open to new insights and a different approach to certain problems, this was very helpful.

At last, I would like to give a huge thank you to my friends and family. Thank you for keeping me motivated, thank you for pulling me through and thank you for the relaxing moments during these special times. Thank you to my baseball team and club members at HitManics, you gave me, when needed, the right kind of distraction to keep me motivated, in shape and going through my thesis.

When looking back at my student life, I am happy and pleased with all the new knowledge, experience and friends I have gained through the years! Now it is time to look forward and begin a new chapter in my life with the MSc. degree in Civil Engineering. I am ready to dive in the big ocean that is ahead of me.

If you lack the will to dive, you lack the will to win.

A.M. Kool
July 22, 2021

Summary

Climate change and the Urban Heat Island

Worldwide the climate is changing, temperatures are rising, while droughts and heavy precipitation occur more frequently. Furthermore, due to urbanisation, the implementation of impermeable surfaces has increased, lowering the vegetated fraction, which caused the urban temperatures to rise and streets to flood more often. The increase of temperature in urban areas with respect to rural areas is called the Urban Heat Island (UHI) effect. Previous research showed that the growing built environment strengthened this phenomenon. But the urban heat island can be reduced by implementing green infrastructure on various scales. At the neighborhood scale greening the gardens and public spaces showed previously promise by reducing the UHI-effect up to 30%. But droughts reduce the water availability for evaporation, possibly strengthening the UHI-effect, increasing urban temperatures, which already increase due to climate change. Although green infrastructure seems to have potential, it is often disregarded that green infrastructure needs soil moisture to enable cooling through evaporation. Potentially, increasing the water availability for vegetated surfaces could increase evaporation, thus lowering the UHI-effect. Increasing the water availability can be done by applying urban irrigation and water retention measures, like in sponge-city design. Another possible benefit from applying irrigation is to reduce droughts and limit the consequences from droughts, like increased soil settling.

Research goal and method

The goal of this study is to link cooling by nature and urban drought reduction to irrigation measures. To do this the research simulated two Dutch urban areas within ENVI-met, a microclimate model, to determine the effect of irrigation on green infrastructure and droughts with respect to thermal comfort within urban areas. The first case is the Bredalaan in Eindhoven with a sandy subsoil and consists of low rise street and block building typologies with a low vegetated fraction. The second case is the Oranjeboomstraat in Rotterdam with a clayey subsoil. The Oranjeboomstraat has also a low vegetated fraction, but instead of a low rise built environment a mid rise built environment is simulated. For each location their current scenario is simulated for a single extremely warm day with five different soil moisture profiles from dry till wet plus irrigation. Besides, for the current and greener scenario each, a heatwave of five days is simulated with meteorological parameters from the nearest weather station. For these scenarios each a dry and wet-irrigated soil profile is simulated.

The daily simulations enable research into the effects of the soil physical characteristics and increased soil moisture availability on the evaporation rates, temperature and thermal comfort of the cases. While the series simulation shows the relationship of green infrastructure and thermal comfort, being influenced by the soil moisture content.

Results and conclusion

These simulations showed a positive effect of irrigation on the evaporation rate and thermal comfort. The daily simulations showed that, with respect to a dry soil, irrigation results in an increased evaporation of 100% for a sandy soil and 170% for a clayey soil. The increase of evaporation caused a reduced air temperature of 0.5-1.5°C, but no significant median PET reduction was found.

The scenarios showed the influence of greening on the air temperature. Increasing green infrastructure could lead to higher temperatures, but reducing the PET by increasing shading. Furthermore, when the green fraction is increased and irrigation is also applied the air temperature is reduced by 1.5°C daily, while irrigating the current situation results in approximately a 1°C reduction.

An increased soil moisture content due to irrigation enables, for different soil types, an increase of evaporation and reduce the urban temperature. But a dry soil, even with increased green fraction, could increase the UHI-effect. So applying green infrastructure is beneficial to decrease ambient temperature as long as drought reduction measures, possibly irrigation of vegetation, are implemented simultaneously.

Contents

Abstract	i
Preface	iii
Summary	v
Table of contents	ix
List of Figures	xi
List of Tables	xv
Abbreviations	xvii
1 Introduction	1
1.1 Problem description	2
1.2 Problem statement	2
1.3 Research goal and questions	3
1.3.1 Research questions	3
1.4 Research method and boundaries	4
1.5 Further outline of the document	4
2 Context of the urban environment	5
2.1 The Urban Heat Island	6
2.1.1 The energy and water balance regarding the Urban Heat Island	6
2.1.2 The influencing factors of the Urban Heat Island	7
2.1.3 The meteorological influence: the occurrence of a warm day.	7
2.1.4 Urban characteristics influencing the Urban Heat Island	7
2.1.5 Surface water and the Urban Heat Island	10
2.1.6 Green area and the Urban Heat Island	11
2.1.7 Measuring and predicting the Urban Heat Island	12
2.1.8 Adaptations to reduce the Urban Heat Island	13
2.2 Drought in the Netherlands	15
2.2.1 The Dutch definition of drought.	15
2.2.2 The urban water balance in the Netherlands	16
2.2.3 Distribution, severity and occurrence of drought	17
2.2.4 The effect of drought on the urban environment	17
2.2.5 Water retention measures	18
2.3 The (un)saturated zone	21
3 Methodology	23
3.1 The system of interest: The urban environment	24
3.2 Modelling the atmosphere and urban environment.	24
3.2.1 ENVI-met	25
3.2.2 Limitations and assumptions	26
3.2.3 Interpretation of the output data of ENVI-met	26
3.3 Research method: application of the model	27
3.3.1 The different aspects of the approach.	27
3.3.2 Elaboration of the different scenarios with respect to the research questions	28

4	Case studies and data retrieval	29
4.1	General description of the case study.	30
4.2	Locations and the characteristics of the build environment	30
4.2.1	Geographical location of the cases	30
4.2.2	Building typology of the cases	32
4.2.3	Characteristics of the build environment.	34
4.3	Meteorological environment of the case studies.	38
4.4	Soil composition of the case studies	39
4.5	Overview of the cases and simulations	41
4.5.1	Scenarios of the series simulations	41
4.6	A short comparison of the two cases	42
5	Results of the models	45
5.1	Results of the single day simulations of both cases	46
5.1.1	Results of single day simulations regarding simulated air temperature and PET	46
5.1.2	The relationship of the soil moisture content and simulated air temperature of the single day simulation	52
5.1.3	The relationship of the air temperature and evaporation of the single day simulation	53
5.1.4	The relationship of the soil moisture content and evaporation	54
5.2	Results of the series simulations of both cases	57
5.2.1	Results of series simulations regarding simulated air temperature, PET and UHI-effect	57
5.2.2	Results of series simulations regarding soil moisture content.	65
5.2.3	Results of series simulations regarding hourly evaporation rates.	65
5.3	Comparison of the scenarios	68
5.3.1	Relative air temperature with respect to the current situation	68
5.3.2	Relative physiological equivalent temperature with respect to the current situation	71
6	General discussion	75
6.1	Case studies and data retrieval	76
6.1.1	Case study location and characteristics.	76
6.1.2	The influence of the Sky View Factor on the results	76
6.1.3	The effects of increased vegetation on the case studies	77
6.1.4	The influence of the subsoils composition on the results	77
6.2	Usage of ENVI-met.	78
6.2.1	Numerical stabilization of ENVI-met	79
6.3	Comparison of the results	80
6.3.1	Comparison of the results with RIVM's UHI-model	80
6.3.2	Comparison of the results with TNO's UHI-model.	80
6.3.3	Comparison of the PET.	80
7	Conclusion & recommendations	83
7.1	Conclusions.	84
7.2	Recommendations	85
7.2.1	Further research	86
7.2.2	Application of measures in urban areas.	86
	Bibliography	91
A	Appendix - Detailed ENVI-met description	93
A.1	Atmospheric model of ENVI-met	93
A.2	Built environment and building systems of ENVI-met	93
A.3	Vegetation model of ENVI-met	94
A.4	Soil model of ENVI-met	96
A.5	Input data of ENVI-met	97
A.5.1	ENVI-met's database system.	97

A.5.2	Parent–child relationships within the database	98
A.5.3	The adjustable parameters within each database.	99
B	Appendix - Multi criteria analysis of second location	101
B.1	The characteristics of the Oranjeboomstraat in Rotterdam	101
B.1.1	Physical properties of the Oranjeboomstraat, Rotterdam	101
B.2	Multi criteria analysis for Eindhoven	101
C	Appendix - Wind evaluation of the street profile.	103
D	Appendix - additional tables and graphs of the results	111
E	Appendix - Comparison of ENVI-met and KNMI data	113
E.1	Input Eindhoven	113
E.2	Input Rotterdam	122

List of Figures

2.1	General conceptualization of the Urban Heat Island.	6
2.2	Distribution of tropical days over the Netherlands.	7
2.3	Causes of the urban heat island.	8
2.4	The relationship between the population density and the UHI in Northern America and Europe.	9
2.5	The relationship between the height-width ratio (H/W) and the maximum UHI, based on data of European, Northern American and Australian data.	9
2.6	The relationship between the green area and surface temperature within 88 Dutch' neighborhoods.	11
2.7	Relationship between the fraction of incoming radiation used for evaporation and the vegetated fraction of a city.	12
2.8	The relation between the surface and air temperature within Rotterdam.	13
2.9	The average diurnal and nocturnal UHI effect measured in Utrecht by bike.	14
2.10	Processes influencing the groundwater level within a reservoir.	16
2.11	Yearly water balance of De Bilt, The Netherlands	17
2.12	Standardized Gumbel probability plot of the cumulative precipitation deficit in the Netherlands.	18
2.13	Spatial distribution of the evaporation and maximum precipitation deficit in the Netherlands.	18
2.14	Cross-section of the subsoil circumstances, explaining the unsaturated zone. And the characteristic water content curve for specific soils.	21
3.1	Schematic representation of the system of interest.	24
3.2	The architecture of the ENVI-met model.	25
3.3	Nesting grids with three and five cells.	27
4.1	Overview of the case locations and different dominant soil classes in the Netherlands.	29
4.2	Presentation of the two cases and their respective study area and locations of the cross-sections (left: Oranjeboomstraat(Google LLC., 2015, January 10/2015), right: Bredalaan(Google LLC., 2020, April 16/2020)).	30
4.3	The spacematrix of the eighth different building typologies for individual housing blocks.	31
4.4	The spacematrix of the six different building typologies for fabrics.	31
4.5	The three building sections of the Bredalaan. Block A, B and C are given together with the case study area.	33
4.6	The two building blocks of the Oranjeboomstraat.	33
4.7	Impression of both cases.	35
4.8	All cross-sections with height information of the Oranjeboomstraat.	36
4.9	All cross-sections with height information of the Bredalaan.	37
4.10	The sky view factor of each case. At the bottom of the maps the average value and the standard deviation are given, to indicate the range of values.	37
4.11	The average annual precipitation and reference evaporation over 1971-2010	38
4.12	Eindhoven's average precipitation, evaporation over 1986-2015 and daily values of 2018 between April and October.	39
4.13	Rotterdam's average precipitation, evaporation over 1988-2015 and daily values of 2018 between April and October.	39
4.14	caption	40
4.15	Lithoclass of the Bredalaan and the Oranjeboomstraat.	40
4.16	Overview of the case studies, the scenarios, type of simulations and the relative soil moisture content.	41

4.17	Three dimensional presentation of the increased green infrastructure scenarios for both the Bredalaan and Oranjeboomstraat.	42
5.1	Presentation of the air temperature development at the Bredalaan in Eindhoven and Oranjeboomstraat in Rotterdam.	47
5.2	Heatmap of the Bredalaan showing the warmest and coldest areas within the area for a 10% and 100% relative soil moisture content.	48
5.3	Heatmap of the Oranjeboomstraat showing the warmest and coldest areas within the area for a 10% and 100% relative soil moisture content.	48
5.4	Absolute temperature difference between a 10% and 100% relative soil moisture content for both the Bredalaan and Oranjeboomstraat.	48
5.5	UHI effect heat maps of the driest and wettest scenario of both cases.	49
5.6	Presentation of the PET development at the Bredalaan in Eindhoven and Oranjeboomstraat in Rotterdam.	50
5.7	Presentation of the extreme air temperature, 90 th and 100 th percentile, development of green infrastructure at the Bredalaan in Eindhoven and Oranjeboomstraat in Rotterdam.	51
5.8	Relationship between the relative soil moisture content and temperature around green infrastructure for both cases.	52
5.9	The air temperature and evapotranspiration of the green infrastructure at 9 a.m. and 3 p.m. of the Bredalaan and Oranjeboomstraat.	53
5.10	Relationship between the soil moisture content and the evaporation.	55
5.11	The hourly evapotranspiration rate of both cases for various soil moisture profiles.	56
5.12	The simulated air temperature at the Bredalaan for several scenarios.	58
5.13	The simulated air temperature at the Oranjeboomstraat for several scenarios.	59
5.14	The PET at the Bredalaan for several scenarios.	61
5.15	The PET at the Oranjeboomstraat for several scenarios.	62
5.16	The UHI-effect at the Bredalaan for several scenarios.	63
5.17	The UHI-effect at the Oranjeboomstraat for several scenarios.	64
5.18	The relative soil moisture content with respect to field capacity at the Bredalaan for several scenarios.	66
5.19	The relative soil moisture content with respect to field capacity at the Oranjeboomstraat for several scenarios.	66
5.20	The hourly evapotranspiration rate at the Bredalaan for several scenarios.	67
5.21	The hourly evapotranspiration rate at the Oranjeboomstraat for several scenarios.	67
5.22	The change in median air temperature at the Bredalaan for several scenarios with respect to the current scenario.	69
5.23	The change in median air temperature at the Oranjeboomstraat for several scenarios with respect to the current scenario.	70
5.24	The change in median PET at the Bredalaan for several scenarios with respect to the current scenario.	72
5.25	The change in median PET at the Oranjeboomstraat for several scenarios with respect to the current scenario.	73
6.1	Relative wind velocity change at 27-7-2018 3 p.m. between the dry current scenario and dry greener scenario.	78
6.2	The UHI-effect based on infrared imagery.	82
6.3	PET map of both the Bredalaan and Oranjeboomstaat.	82
A.1	An overview of the database manager of ENVI-Met.	97
A.2	The plants' database can be adjusted on eight parameters.	100
A.3	The adjustable parameters of the roof and wall greening.	100
C.1	A relative height map of the Oranjeboomstraat.	103
C.2	Comparison A regarding wind from 34° and 124°	105

C.3	Comparison B regarding wind from 34° and 214°	106
C.4	Comparison C regarding wind from 124° and 214°	106
C.5	Comparison D regarding wind from 34° and 304°	107
C.6	Comparison E regarding wind from 124° and 304°	108
C.7	Comparison F regarding wind from 214° and 304°	109

List of Tables

The list of tables is presented in order of occurrence.

2.1	The seven causes of the Urban Heat Island	8
2.2	Average yearly and seasonal water balances of De Bilt, the Netherlands, over 1981-2010 (KNMI, 2020a)	17
2.3	Types of green roofs and their characteristics.	19
4.1	Urban form and density factors of the Bredalaan.	32
4.2	Urban form and density factors of the Oranjeboomstraat	33
4.3	Short comparison of the cases with respect to their characteristics.	43
5.1	Air temperature of green infrastructure of both cases with respect to the relative soil moisture content.	52
5.2	The average air temperature and evaporation rate of green infrastructure at the Bredalaan.	54
5.3	The average air temperature and evaporation rate of green infrastructure at the Bredalaan and Oranjeboomstraat.	54
5.4	The green infrastructure's average of evapotranspiration rates of both cases with respect to the relative soil moisture content.	54
5.5	Total daily evapotranspiration at each case for different soil moisture contents.	55
A.1	The parent-child-relationships within the database of ENVI-met.	99
A.2	The adjustable parameters within the soil database.	99
B.1	Multi criteria analysis to determine the second profile	102
C.1	The evaluated wind directions of the model.	104
C.2	Overview of the wind sensitivity simulation's input.	104
C.3	The mean air temperature, standard deviation, and minimum and maximum values between a 34° and 124° wind with respect to each other.	105
C.4	The mean air temperature, standard deviation, and minimum and maximum values between a 34° and 214° wind with respect to each other.	105
C.5	The mean air temperature, standard deviation, and minimum and maximum values between a 124° and 214° wind with respect to each other.	106
C.6	The mean air temperature, standard deviation, and minimum and maximum values between a 34° and 304° wind with respect to each other.	107
C.7	The mean air temperature, standard deviation, and minimum and maximum values between a 124° and 304° wind with respect to each other.	107
C.8	The mean air temperature, standard deviation, and minimum and maximum values between a 214° and 304° wind with respect to each other.	108
D.1	Air temperature data of the simulation with the driest soil moisture profile.	111
D.2	Air temperature data of the simulation with the wettest soil moisture profile.	111
D.3	Green infrastructure's air temperature data of the simulation with the driest soil moisture profile.	112
D.4	Green infrastructure's air temperature data of the simulation with the wettest soil moisture profile.	112
D.5	Green infrastructure's air temperature data of the simulation with the wettest soil moisture profile.	112
D.6	Green infrastructure's air temperature data of the simulation with the wettest soil moisture profile.	112

Abbreviations

An alphabetically ordered list of all used abbreviations is given to ease reading of the document. The list gives the abbreviation itself and, the meaning and first occurrence of the abbreviation.

Abbreviation	Meaning	Chapter
CFD	Computational Fluid Dynamics	A.1
FSI	Floor Space Index	4.2.2
GI	Green Infrastructure	1.1
GSI	Ground Space Index	4.2.2
KNMI	The Royal Netherlands Meteorological Institute or Koninklijk Nederlands Meteorologisch Instituut	2.2.1
L	Layers	4.2.2
LAD	Leaf Area Density	A.3
LID	Low Impact Development	1.1
OSR	Open Space Ratio	4.2.2
RAD	Root Area Density	A.3
PET	Physiological Equivalent Temperature	2.1.5
RSMC	Relative Soil Moisture Content with respect to field capacity	5.1.2
SVF	Sky View Factor	2.1.4
UHI	Urban Heat Island	1.1

Chapter - 1

Introduction

1.1 Problem description

Worldwide climate is changing, population is increasing and cities are expanding, which requires humanity to adapt to these situations. When looking into global climate there is a clear increase in temperature of 0.85 °C during the period between 1880 and 2012 (Stocker et al., 2013). Locally, in The Netherlands, climate change is researched by KNMI. Based on KNMI's research it can be assumed that in 2050 the average temperature has increased by 1-2°C with respect to their reference period of 1981 till 2010. Furthermore, a combined projected increase, in rainfall, evaporation and precipitation deficit, could lead to an increase of extreme weather events (Attema et al., 2014). These meteorological events increase probability of the five environmental themes, which are:

1. Coastal flooding;
2. Pluvial flooding;
3. Fluvial flooding;
4. Heat stress, and
5. Droughts.

These effects could damage infrastructure and society. When no actions are taken, the accumulated damage till 2050 could rise to €70 billion (Deltacommissie, 2017).

Therefore, the Deltacommissie sees a need to adapt urban environments, preparing cities to withstand the environmental challenges. Since coastal and fluvial flooding are dealt with on a national and regional scale, the adaptation of urban environments is mainly aimed at three of the five themes. Firstly, reducing pluvial flooding caused by intense rain showers. Secondly, reducing the Urban Heat Island (UHI), caused by heat stress in urban areas. Thirdly, increasing water availability to reduce soil settling, damage to foundations, and water quality and quantity related problems (Deltacommissie, 2017; Schrijvers et al., 2014; Stichting CAS, 2016). Cities in the Netherlands generally become rainproof by capturing, storing and draining the water (Dai, Wörner, and van Rijswick, 2018; Dai, van Rijswick, Driessen, and Keessen, 2018). The sponge city approach is to focus on Low Impact Development (LID) and Green Infrastructure (GI) to reduce pluvial flooding. Though, the same techniques can be used to reduce the UHI (Schrijvers et al., 2014). This reduction is driven by evaporation, which is dependent on water. Though, the dependency of water is threatened by droughts (Attema et al., 2014; Stocker et al., 2013).

1.2 Problem statement

Urban areas deal with increasing temperatures due the Urban Heat Island effect, which is strengthened by climate change (T. R. Oke, 2002). The Urban Heat Island effect can be reduced by various means, though the usage of vegetation for cooling seems most effective (Gunawardena, Wells, and Kershaw, 2017; Grimmond, 1999; C. Jacobs et al., 2020; Kleerekoper, van Esch, and Salcedo, 2012; L. Klok, Zwart, Verhagen, and Mauri, 2012; Ng, Chen, Wang, and Yuan, 2012). The vegetation provides shading and uses incoming radiation to vaporize soil water after extraction by the roots. However, the extraction of water is only possible if sufficient water is available (E.S Van der Meulen, 2015). When the soil water content is insufficient, part of the incoming radiation is used for heating surfaces instead of evaporation, which causes the urban temperatures to increase.

Insufficient soil water content is considered a drought. The drought period in the Netherlands is observed between April and September, with the drought severity defined by the KNMI as the maximum potential precipitation deficit (Rob Sluijter, Plieger, van Oldenborgh, Beersma, and de Vries, 2018). The potential precipitation deficit is the difference between the actual precipitation and the potential reference crop evaporation. The potential reference crop evaporation is based on the quantity of evaporation from a well-watered, well-maintained and well-fed meadow. Though, the potential reference crop evaporation is not representative for the actual urban evaporation for the following reasons.

Firstly, the maximum evaporation potential only applies for meadows in rural areas and not for other types of vegetation or urban environments. Secondly, urban areas are impermeable and have limited infiltration areas, therefore soil water availability is most probably lower than in rural areas. Thirdly, rural and urban areas have different environments due to the influences of the built environment. The built environment causes some areas to show fluctuating temperatures, some areas are warmer and others are colder, due less incoming

radiation from shading, and wind-flow variation due turbulence, dispersion and convergence. All these factors combined result in a high uncertainty of the urban evaporation rate and soil water availability.

While several researches have shown the potential of green infrastructure for reducing the Urban Heat Island, these researches neglect the soil moisture content. Therefore the effect of droughts or recent precipitation is not considered in these researches. To ensure sufficient soil water availability a majority of the precipitation has to be collected and maintained within an urban environment. Collecting and maintaining precipitation within an urban environment is referred to as the sponge city design (Dai, van Rijswijk, et al., 2018). The sponge city design uses low impact developments and green infrastructure to reduce damage due excess precipitation, while increasing the additional storage of water. The quantity of additional water stored within a sponge city can be seen as the sponge-capacity of a city. The additional stored water then can be reused for urban cooling through evaporation.

To summarize, urban areas deal with droughts and urban heat islands due impermeable surfaces, which possibly can be solved by implementing the sponge city design. The sponge city can introduce additional water storage capacity and green infrastructure. The retained water can be used for infiltration, reducing droughts, or irrigation, possibly reducing the urban heat island through the green infrastructure. Though evaporation rates, which influences the urban heat island reduction, depend on the soil moisture content and various parameters of the vegetation. All these factors have to be considered within the goal of the research.

1.3 Research goal and questions

In the previous paragraph it is concluded that cities cope with droughts and the urban heat island effect. Besides, the sponge city design seems to be a hopeful design strategy for tackling urban drought and heat simultaneously. Since sponge cities make use of green infrastructure and increase the sponge capacity by using additional storage of water, enabling infiltration of precipitation and possibly reuse of precipitation for irrigation. This is helpful since the UHI-effect can be reduced with green infrastructure, when sufficient soil water is available for the various kinds of vegetation. Besides if sufficient water is retained in the urban environment, this could solve drought related problems.

Previous research showed promising results regarding urban heat island reduction with green infrastructure, but ignored the relationship with soil moisture content. Besides sponge cities design, while making use of precipitation retention measures, could reduce urban droughts. Coupling these two problems and linking them to precipitation retention measures can be translated into the following research goal:

"Linking cooling by nature and urban drought reduction to irrigation measures."

The research goal can be split into three parts, which together form a coherent research. The first part is researching the relationship between precipitation retention measures and droughts. Secondly, the relationship between precipitation retention measures and urban evaporation for cooling. And at last the part is the relationship between droughts and evaporation for cooling, which can be seen as the relationship between the soil moisture content in the rootzone, the evaporation rate and the cooling effect of the vegetation.

1.3.1 Research questions

The main research question, to reach the research goal, is specified as:

"How are irrigation measures linked to cooling by nature and drought reduction?"

To answer this question some relationships need to be understood. The relationship between irrigation measures and cooling by nature, and the relationship between irrigation measures and drought reduction. Furthermore, there is an interest in the effect of the soil moisture or absence of soil moisture on the evaporation rates and temperature in urban areas. To establish these relationships and effects on each other the following three questions need to be answered:

"Which spatial adaptations can influence both the temperature and drought positively?"

"What is the effect of the soil moisture content on the urban evaporation rate of vegetation?"

"What is the effect of the soil moisture content on the urban temperature?"

Answering these questions is only sensible when the urban characteristics are taken into account. Urban areas show various differences in the urban characteristics. The urban characteristics that are most interesting are:

- Soil physical characteristics defined by different soil types;
- Percentage of impervious surface; and
- Vegetation type.

The soil physical parameters are interesting, since the parameters have an influence on the behaviour of the soil water. Therefore, the different soil types might respond differently to implemented measures. Thus specific measures could be more or less effective in different urban environments. Another factor influencing the soil water is the amount of impervious surfaces. The amount of impervious surfaces controls the amount of water infiltrating, thus recharging the amount of soil water. So the amount of impervious surfaces possibly influences the amount of soil moisture available for evaporation and thus cooling. Since, the rate of cooling is correlated with the evaporation rate, which depends partly on the vegetation type, there is an interest to see which vegetation types have the most influence on droughts and the urban temperatures. This can be translated into the following research questions:

"What is the effect of the soil physical characteristics on the irrigation measures?"

"How affects the impervious surface the drought severity, temperature and evaporation rates in the urban environment?"

"What is the effect of the soil physical parameters on the urban evaporation rate?"

These questions will be answered after a profound research. The steps taken, to answer the various research questions, are given in the upcoming paragraph. In chapter 3 the methodology is discussed further in detail.

1.4 Research method and boundaries

The research goal is to link irrigation measures to urban drought reduction and urban evaporation for cooling (by nature). To reach the goal, the research is divided into three parts. The first part is a literature study on the background information. Enabling to narrow down the research and get insights in the current state of research. This is necessary to define the methodology that is used.

Secondly, a micro-climate model is used to gain insights in the urban micro-climate. This enables research into the UHI, drought reduction, and urban adaptation.

The model is used for two case studies, the third aspect of this study. These cases are chosen to define the effects of spatial variability, urban characteristics and governance. More information on the cases is discussed in chapter 4.

1.5 Further outline of the document

After this introduction, the findings of the literature research are presented in chapter 2, Context of the urban environment. In order to perform this study a research method is necessary, which is described in chapter 3. Chapter 4 describes the case studies and scenarios on which the model is applied. The results of the models are given in chapter 5, Results of the models. The interpretation of these results is discussed in chapter 6. This is followed by the conclusions in chapter 7, which also gives recommendations.

Chapter - 2

Context of the urban environment

The research started with a literature study on the urban environment, which enables setting boundaries, deciding on the right models and making the right assumptions, to answer the research questions. The relevant background information gives insights into the urban environment, which is a detailed complex system. The urban environment is influenced by multiple factors, such as sub-systems, influencing processes and governance. To get understanding of these factors, the background information is elaborated during this chapter. Firstly, the three focus areas are discussed, which are:

1. The urban environment.
2. Sub-surface of the urban environment.
3. Governance and Dutch climate policies.

The given information leads to a comprehensive context of the research, which help answering the research questions given in Chapter 1.

The urban environment

This analysis provides the necessary information of the effects in the urban environment. To model the urban environment, there is a necessity to understand what occurs in the urban environment. The urban environment is the area where humanity lives in cities, towns, villages etc. The urban environment is influenced by meteorological, anthropogenic and biological factors, which will be discussed in this chapter.

2.1 The Urban Heat Island

The Urban Heat Island, according to T. R. Oke (2002), is the presence of higher air temperatures in (sub)urban areas. A conceptualization of the UHI can be seen in figure 2.1. Within the conceptualization a clear increase in temperature with building density is visualized. To understand this temperature increase, the mass and energy balances are explained. After this the influencing parameters within the urban environment are given. At last, several research examples are given regarding the severity, occurrence and meteorological influences.

2.1.1 The energy and water balance regarding the Urban Heat Island

To understand what the Urban Heat Island really is and why it occurs, a basic understanding of the driving natural and anthropogenic processes is necessary. The natural processes are driven by the radiation of the sun, whereas the anthropogenic sources come from industries, transportation and daily activities. Besides the anthropogenic, represented by Q_F , and natural sources amplify each other (T. R. Oke, 2002). Based on the incoming (Q^*) and outgoing (Q_H , Q_E) radiation, horizontal sensible and latent heat flux (ΔQ_A), and heat storage (ΔQ_S) an energy balance can be made.

Within the water balance the incoming fluxes are precipitation (p), water vapour due combustion (F) and inflow (I). Whereas the outgoing fluxes are evaporation (E), sewer outflow (Δr), net moisture advection (ΔA), and the change in water storage is given by ΔS . The energy balance is influenced by the water balance through evaporation. The energy and water balance, given in equations 2.1 and 2.2 respectively, based on T. R. Oke (2002), show their relationship.

$$Q^* + Q_F = Q_E + Q_H + \Delta Q_A + \Delta Q_S \quad (2.1)$$

$$p + F + I = E + \Delta r + \Delta S + \Delta A \quad (2.2)$$

The relationship, between the two balances, is given by the latent heat flux (Q_E) and evaporation (E) which are both influenced by vegetation and surface water. Besides, the balances are interlinked through the three anthropogenic parameters, Q_F , F , I . How these factors influence the balances is discussed in the next section.

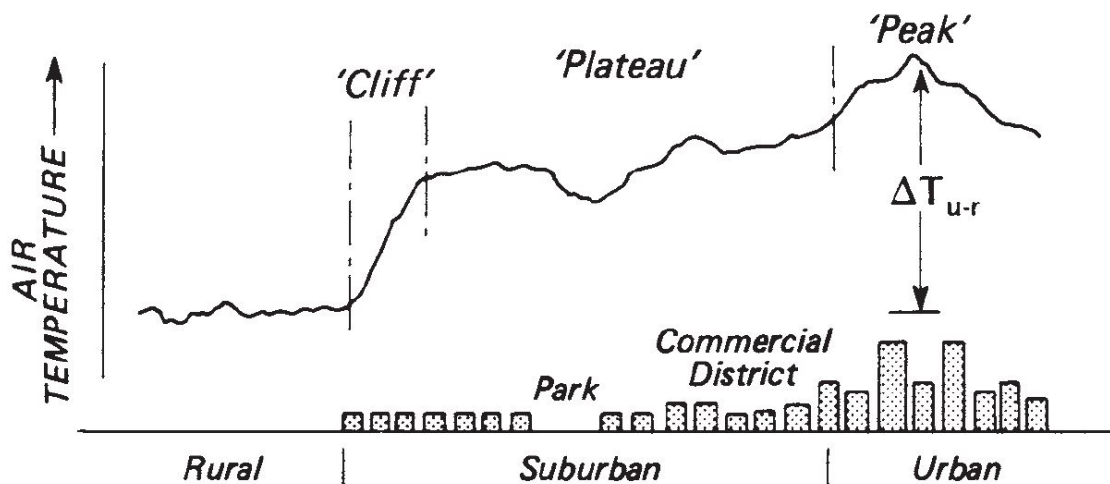


Figure 2.1: General conceptualization of the Urban Heat Island (T. R. Oke, 2002). A clear visual representation of the increasing air temperature over (sub)urban areas is given. This increase in air temperature is the higher within denser areas.

2.1.2 The influencing factors of the Urban Heat Island

The terms within the balances have their own specific influence on temperature change. The influence is connected to human activity directly and indirectly. These connections influence the temperature within the urban environment over time and space. This variation of temperature is influenced by three kind of factors:

1. Meteorological;
2. Location of the urban area and
3. Urban characteristics.

The meteorological factors, which will be discussed first, depend on weather events which occur and cannot directly be influenced. Secondly, the effects due to the specific global position of that location. The location determines the climate of that given area, which influences the meteorological factors. The third factor given are the urban characteristics with respect to rural areas. T. R. Oke (2002) gives seven hypothetical features of urbanization, which contribute to change in urban characteristics and how these influence the UHI. All three factors will be discussed separately in the upcoming sections.

2.1.3 The meteorological influence: the occurrence of a warm day

The Dutch definition of a warm day in the Netherlands is divided in two sets. The first set are the amount of summer days and the second set the amount of tropical days (KNMI, 2015).

A summer day is characterised by a maximum daily temperature of 25 °C or higher. Whereas a tropical day has a maximum daily temperature of 30 °C. From 1981-2010 on average 21 summer days occurred, with two to five of those days being tropical (KNMI, 2015). The amount of summer and tropical days is not equally distributed over the Netherlands. On average along the coast two days are characterised as summer days, while in the south-east six to eight summer days occur. Figure 2.2 shows the distribution of tropical days over the Netherlands.

Due climate change the amount amount of summer days will rise between 20-70% in 2050 (KNMI, 2015). In combination with the urbanisation of the Netherlands, the impact of the Urban Heat Island on urban areas will be larger (Deltacomissie, 2017).

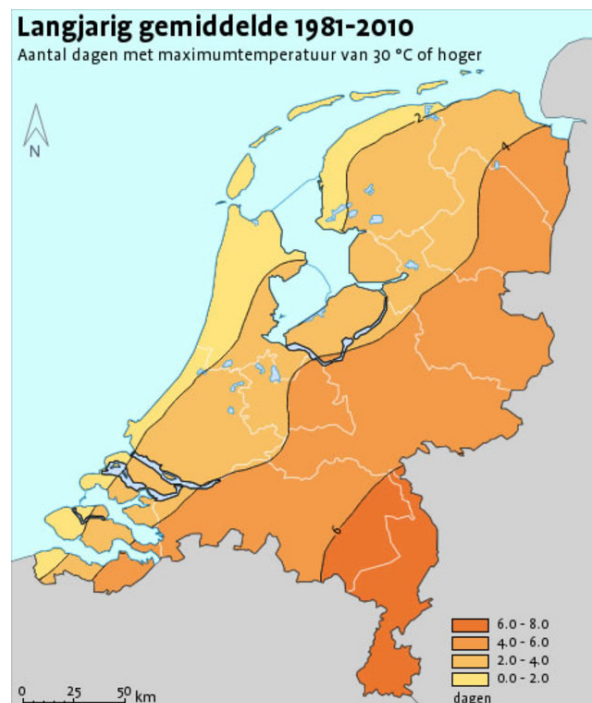


Figure 2.2: Distribution of tropical days over the Netherlands (KNMI, 2020b).

2.1.4 Urban characteristics influencing the Urban Heat Island

As described there are three main factors influencing the UHI. The first factor that is discussed are the urban characteristics. Based on T. R. Oke (2002) and Santamouris (2013), the seven causes are described and

visualized by Kleerekoper et al. (2012) in Figure 2.3:

1. Absorption of short-wave radiation from the sun in low albedo (reflection) materials and trapping by multiple reflections between buildings and street surface.
2. Air pollution in the urban atmosphere absorbs and re-emits longwave radiation to the urban environment.
3. Obstruction of the sky by buildings results in a decreased long-wave radiative heat loss from street canyons. The heat is intercepted by the obstructing surfaces, and absorbed or radiated back to the urban tissue.
4. Anthropogenic heat is released by combustion processes, such as traffic, space heating and industries.
5. Increased heat storage by building materials with large thermal admittance. Furthermore, cities have a larger surface area compared to rural areas and therefore more heat can be stored.
6. The evaporation from urban areas is decreased because of 'waterproofed surfaces' – less permeable materials, and less vegetation compared to rural areas. As a consequence, more energy is put into sensible heat and less into latent heat.
7. The turbulent heat transport from within streets is decreased by a reduction of wind speed.

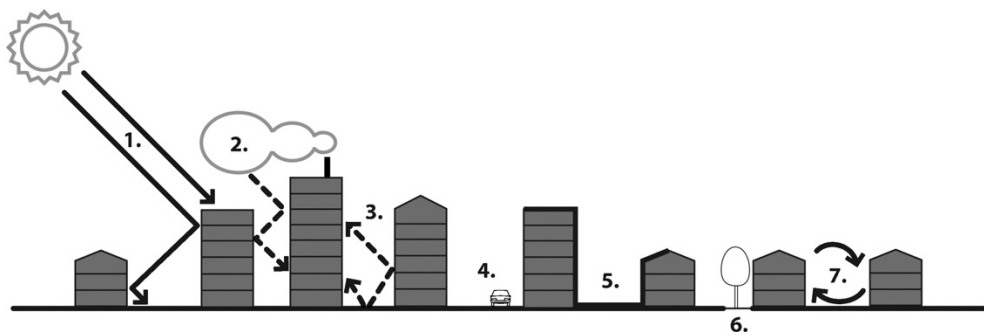


Figure 2.3: Causes of the urban heat island (Kleerekoper, van Esch, and Salcedo, 2012).

While figure 2.3 shows an example which causes contribute within the urban environment, Table 2.1 presents an overview of the seven causes and which term these possibly influence. All seven causes combined, possibly at the same location, cause higher temperatures.

Change of energy balance term	Urbanizing terms
<i>Influencing during day-time</i>	
Short-wave radiation increases	Increased paved and reflecting surfaces due changed canyon geometry.
Increase of sensible heat storage	Increased thermal admittance by usage of specific building materials.
Anthropogenic heat sources	Building and traffic heat losses.
Decreased evaporation	Increased impermeable surfaces.
Increased long-wave radiation from the sky	Air pollution causes greater absorption and reflection.
<i>Influencing during night time</i>	
Decreased long-wave radiation loss	Increased building height-street width ratio.
Decreased total turbulent heat transport	Reduction of wind speed due changed canyon geometry.

Table 2.1: The seven causes of the Urban Heat Island based on T. R. Oke (2002) divided in influencing period.

T. R. Oke (2002) tried to link these effects to the change of parameters of the previously stated energy and water balance, equations 2.1 and 2.2, respectively. Besides T. R. Oke (2002) makes the distinguish between affecting temperature during day and night, while during winter the anthropogenic heat source becomes dominant.

Building density, population and the Urban Heat Island

As described by T. R. Oke (2002) and presented in Figure 2.3, a major contribution to the UHI are the building's characteristics. Initially was perceived that this was due to the relationship with population density, since a higher population density in a city results in a larger anthropogenic heat source. But a higher population density results in a change of urban density. Population density is not a parameter of of a city, therefore describes T. R. Oke (1981) that the building height to street width ratio as a better representation of the maximum potential increase of the UHI or even more accurate the sky view factor.

Based on in-situ measurements in several towns and cities in Canada a relationship was found between the population density and the UHI-severity (T.R. Oke (1973)). After these measurements T.R. Oke (1973) compared North American and European cities. From this comparison T.R. Oke (1973) found two different relationships. Though, there was a stronger relationship with more confidence in Northern America versus European cities, see Figure 2.4 for the results. T. R. Oke (2002) describes that this relationship, in combination with the rural wind velocity, can be a method to determine the UHI-severity.

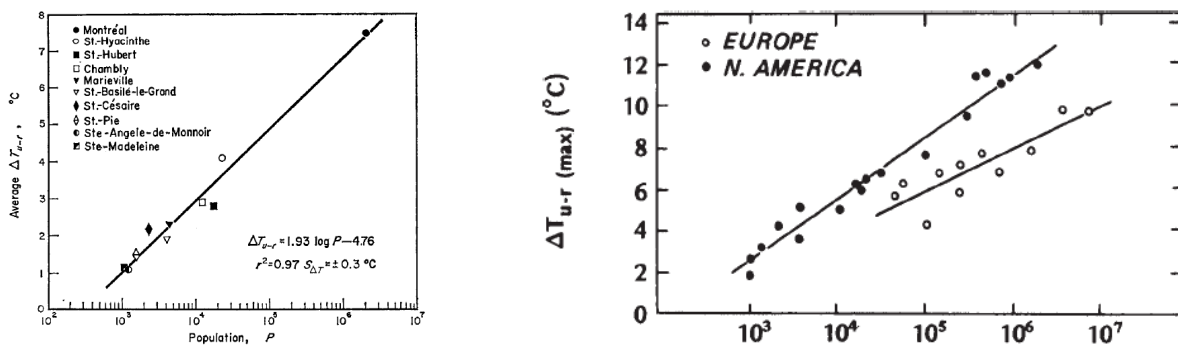


Figure 2.4: The relationship between the population density and the UHI in Northern America and Europe (T. R. Oke, 2002; T.R. Oke, 1973).

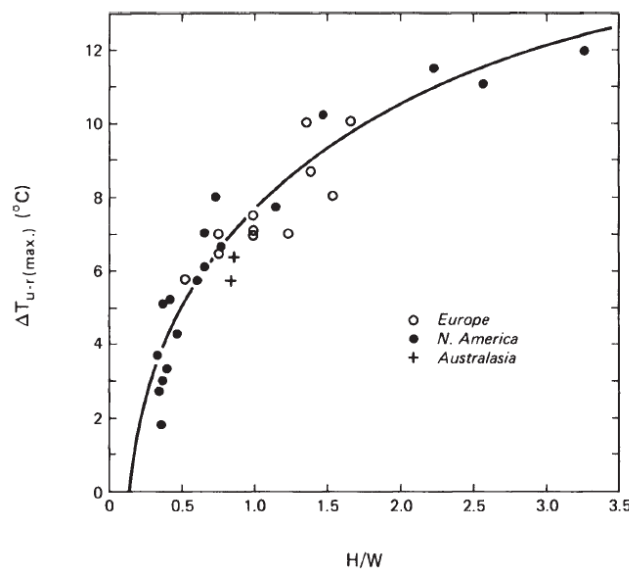


Figure 2.5: The relationship between the height-width ratio (H/W) and the maximum UHI, based on data of European, Northern American and Australian data T. R. Oke, 2002.

As can be shown in figure 2.5 the relationship between the height-width ratio (H/W) and the maximum UHI-effect. The maximum UHI-effect for a height-width ratio of 1, so as high buildings as wide streets, a maximum UHI-effect of 7°C is observed. Combining the maximum increase in temperature, due to the UHI-effect, and building height-street width ratio of each city gives a different relationship. Due to the dependency of specific characteristics of each city, the ratio is believed to predict the maximum UHI-effect rather than predicting local effects (T. R. Oke, 2002).

Figure 2.5 shows the correlation between the height-width-relationship and the maximum UHI-effect. Later T. R. Oke (1981) combined this data to find the same correlation for the nocturnal effects of the UHI. The model by T. R. Oke (1981) showed that the canyon geometry is one of the dominant factors within the thermal balance.

The height-width ratio is later redefined as the Sky View Factor (SVF), indicating the amount of clear sky that is visible from the calculated point or area, with 1 being in the open sky and 0 being in an enclosed environment. The SVF is therefore an indication on the total solar radiation which radiates on this point or area. The SVF is, according to T. R. Oke (2002), a better indicator to predict the UHI-effect in a city. The relationship is defined in equation 2.3, with the minimum UHI-effect at 1.39°C and the maximum at 15.27°C.

$$\Delta T_{UHI} = 15.27 - 13.88 * \psi_{sky} \quad (2.3)$$

Therefore can be concluded that the H/W-ratio or even more precise the SVF are two of the determining factors regarding the severity of the UHI. But several other parameters have an influence on the temperature in the urban environment. First the effect of surface water on the daily and nocturnal UHI-effect is discussed, after which the effects of green area is discussed.

2.1.5 Surface water and the Urban Heat Island

In the previous section it is concluded that higher buildings with respect to street width causes an increase in the UHI-effect. Besides as can be seen in Table 2.1 reduction of evaporation is a possible cause of the UHI. Urban evaporation originates from various sources. The main sources are plant and surface water evaporation. In the current section the influence of water bodies on the UHI is discussed after which the effects of vegetation is discussed.

Often it is assumed that water bodies, such as canals, ponds and fountains, have a cooling effect on the micro-climate. This effect is assumed to be most common during the warmest hours of a day (Broadbent, Coutts, Tapper, Demuzere, and Beringer, 2018; Gross, 2017). Though, due to the high specific heat capacity of water, heat convection within the water will store the warmth within the water body (T. R. Oke, 2002; Solcerova, van de Ven, and van de Giesen, 2019). At night time this results in warmer water temperatures. Therefore water bodies potentially increase night air temperatures and enhance the night-UHI (Hathway and Sharples, 2012; Solcerova et al., 2019; Steeneveld, Koopmans, Heusinkveld, and Theeuwes, 2014; Hove] et al., 2015). Which has led to the question if urban water bodies were really cooling the urban environment by C. Jacobs et al. (2020).

C. Jacobs et al. (2020) evaluated sixteen reference water bodies with different characteristics, such as orientation and tree-type. The reference water bodies were compared to the equal lay-out without water and specified design interventions. All these situations are modelled within ENVI-met for a 24-hour period under equal circumstances and then compared. From the analysis it could be concluded that surface water reduces the air temperature above the water at most with 0.8°C and on street-level with 0.6°C. While the perception of temperature, expressed in the Physiological Equivalent Temperature (PET) (Höppe, 1999; Walther and Goestchel, 2018), is above water 2°C and on street-level 1.9°C. Though, air temperatures were slightly increased by 0.3°C during night time. This effect is linked to the thermal inertia of water; it remains cooler than air during warming, while water stays warmer when air temperatures drop (Gunawardena et al., 2017). Furthermore, Solcerova et al. (2019) found that the sensible heat flux, which affects the air temperature, was about one tenth of all energy released by the surface water at night. The other energy fluxes, the latent heat flux and radiative cooling, had both a contribution of 40%. These two fluxes increase the PET slightly.

Therefore can be concluded that surface water has a small effect on the air temperatures during the day and night. Besides, previous research in Amsterdam showed the same small daytime cooling effect of small

urban water bodies (L. Klok, Rood, Kluck, and Kleerekoper, 2019, which is strengthened by this current research. Since it only influences the air temperature and PET in small fractions, the addition of surface water to reduce the UHI can be neglected. Gunawardena et al. (2017) strengthen this concept, even though water bodies possibly have a temperature reducing effect on a larger scale, like a city or neighbourhood scale. The design interventions showed more effective manners to cool down an area. The interventions are vaporization, shading and natural ventilation (C. Jacobs et al., 2020). In the upcoming section the effect of green area, which enables vaporization, is discussed.

2.1.6 Green area and the Urban Heat Island

While water bodies do not result in the satisfied temperature reduction, vaporization through green infrastructure is promising (Gunawardena et al., 2017; C. Jacobs et al., 2020; Kleerekoper et al., 2012). The decrease of green surfaces can be linked to increase of short-wave radiation and decreased evaporation within urban areas. Therefore, one of the hypotheses previously researched is: 'higher percentages of green area result in lower air temperatures'.

Based on remote sensing data and in-situ measurements of respectively surface and air temperatures a negative correlation is found between green areas and surface temperatures. Though, the stronger correlations occurred between green areas and surface temperatures (L. Klok et al., 2012). Within Rotterdam, the Netherlands, L. Klok et al. (2012) analyzed 88 neighborhoods with respect to their surface temperature and percentage of green. From this analysis is concluded that an increase of the surface temperature of 1.3 °C corresponds with an decrease of 10 % green area. The results of this analysis are represented in Figure 2.6.

This can be summarized as follows: to reduce the UHI on a larger scale green infrastructure is a valuable resource to increase vaporization. Though as C. Jacobs et al. (2020) describes the local shading effects of trees may not be neglected.

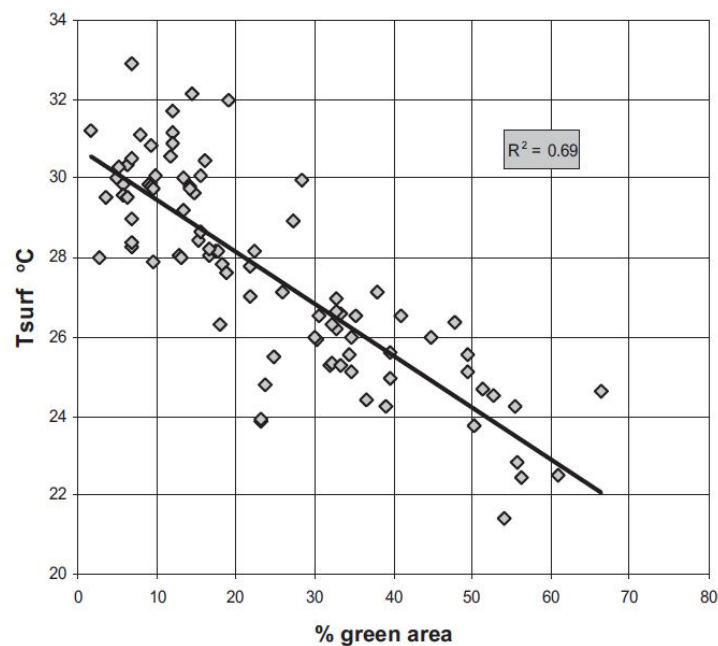


Figure 2.6: The relationship between green area and surface temperature within 88 Dutch' neighborhoods. (L. Klok, Zwart, Verhagen, and Mauri, 2012).

While L. Klok et al. (2012) did not relate the urban hydrological state in the research, earlier research showed a significant impact due water availability in urban areas (Grimmond, 1999).

Grimmond (1999) evaluated the water and energy balance of ten Northern-American cities, with respect to green areas. Taking into account their individual micro-climates, radiation and evaporation flux measurements were performed. Though, the most noticeable was the irrigation rate of the green areas. Some of the cities irrigated their green spaces, which resulted in a higher evaporation fraction with respect to the incoming radiation.

Grimmond (1999) clearly showed that evapotranspiration is an important flux within the urban energy and

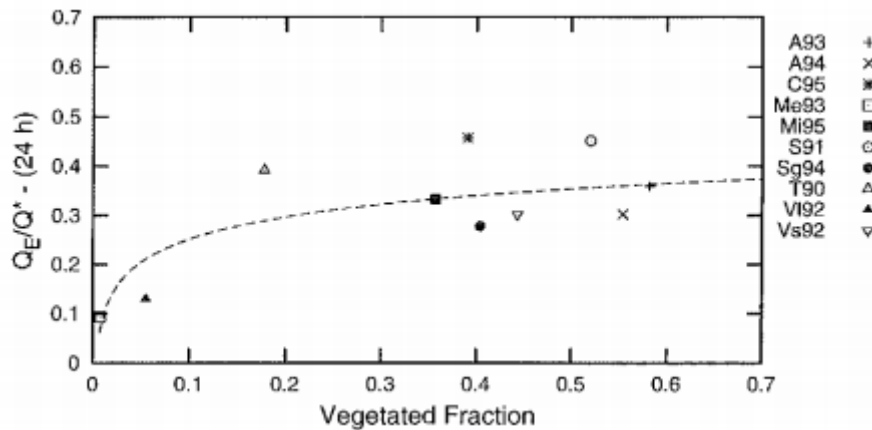


Figure 2.7: Relationship between the fraction of incoming radiation (Q_E/Q^*) used for evaporation and the vegetated fraction of a city. Where several cities as T90 and C95 were irrigated (Grimmond, 1999).

water balance, influencing one another. Urban areas which have more frequent precipitation or are irrigated, use higher fractions of incoming solar energy for evaporation, which result in lower temperatures. This concludes the different factors influencing the UHI-effect and their influences. Though how the UHI-effect can be measured has yet to be discussed. Therefore the upcoming section will further analyse the possibilities of measuring and predicting the UHI.

2.1.7 Measuring and predicting the Urban Heat Island

The previous sections showed that researchers use various ways of measuring the severity of the urban heat island. The approaches of the various ways will be discussed to determine which process can be regarded as most applicable for what situation. The different methods elaborated are:

1. Thermal infrared imaging;
2. In-situ temperature measurements and
3. Usage of a micro-climate model.

The first method regarded is the thermal infrared imaging. L. Klok et al. (2012) used thermal infrared imaging to find a correlation between green area and lower surface temperatures. Even though, L. Klok et al. (2012) also found a positive correlation between the surface and air temperature, see Figure 2.8. The land and air temperatures cannot simply be based on a correlation, since this requires knowledge of the surface characteristics. Because the dominating factors within the energy balance are surface area parameters, converting surface to air temperatures cannot simply be done (Voogt and Oke, 2003).

Another disadvantage is satellite data, which has a rather large resolution and is discontinuous. The resolution of the thermal infrared data is varying between 60x60 and 120x120 metres resolution, which is good for estimating the severity of the UHI (L. Klok et al., 2012). Besides, to ensure the air-surface temperature relationship can be established, a when adaptations with a smaller resolution want to be evaluated, this method is not suitable.

Though surface temperatures give a good estimate of the severity of an heat island, it is not a good estimate for the actual air temperatures in a specific area. Besides the resolution of the thermal variation varies between 60x60m, for Landsat satellites, and 1.1km to 4km for AVHRR satellites, which are both rather low resolutions for spatial transformations within Urban Areas. Since satellites move over a location, there is no continuous data available. Therefore the severity can be measured, but hourly variations are neglected. With in-situ meteorological measurements, hourly data can be retrieved.

The in-situ measurements were primarily used to either verify (L. Klok et al., 2012) other data, or to measure the severity of the UHI (Brandsma and Wolters, 2012; T. R. Oke, 2002; T.R. Oke, 1973). The benefits of in-situ measurements is the preciseness of the measurements. Though this is also the disadvantage. Since air temperatures in a city are highly fluctuating and influenced by local characteristics, possibly a distorted outcome is created. Nonetheless, it can give implications of the severity of the UHI.

As seen previously T.R. Oke (1973) uses in-situ measurements to show the relationship between population

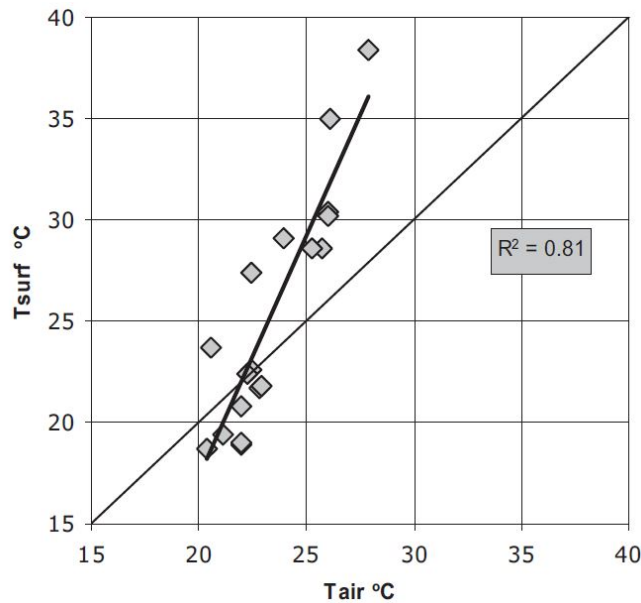


Figure 2.8: The relation between the surface and air temperature within Rotterdam, the Netherlands (L. Klok, Zwart, Verhagen, and Mauri, 2012).

and the UHI within a city. The same has been done within the Netherlands for the Utrecht region. A GPS and thermometer were mounted on a bike and daily data over three years was collected. Based on this data the average nocturnal and diurnal UHI-effect was calculated. This resulted an increase in temperature with an increase towards the city center with respect to the rural areas (Brandsma and Wolters, 2012).

The last common research method is the usage of a micro-climate model. Simple micro-climate models (T. R. Oke, 1981) were the step to more sophisticated models such as ENVI-met (Lenzholzer, Klemm, and Vasilikou, 2018). The simple models were based on air temperature and humidity (Lenzholzer et al., 2018). Later these were expanded with radiation balances (T. R. Oke, 1981), which was the step to holistic micro-climate models. One of the most-used software is ENVI-met, a numerical modeling method for the urban climate (ENVI-Met GmbH, 2019b; Huttner and Bruse, 2009). The several manners to use ENVI-met will be discussed now.

ENVI-met is used by various researchers within various climates and validated often. The validation of data was performed though either satellite (Toparlar et al., 2015) or in-situ measurements (Ayyad and Sharples, 2019; Bande et al., 2019; Forouzandeh, 2018; Kleerekoper, 2016; Ng et al., 2012; Wu, Dou, and Chen, 2019). While the various climates researched are:

1. Arid climate (Ali-Toudert and Mayer, 2007; Ayyad and Sharples, 2019; Bande et al., 2019)
2. Continental climate (Wu et al., 2019)
3. Oceanic climate (Forouzandeh, 2018; C. Jacobs et al., 2020; Kleerekoper, 2016; Toparlar et al., 2015)
4. Subtropical (Ng et al., 2012)

So ENVI-met is a promising software and therefore used often to research the urban environment on a local to neighborhood scale, though larger areas can be researched. Multiple researcher focused on various aspects of the urban environment, like the effect of urban greening (Ng et al., 2012; Kleerekoper, 2016), water bodies (C. Jacobs et al., 2020), building morphology (Ali-Toudert and Mayer, 2007), and urban planning (Wu et al., 2019; Ng et al., 2012). The results of these adaptations have resulted in effective measures which can be taken to reduce the UHI-severity. In the upcoming section these examples are discussed regarding their capabilities of reducing the UHI-effect.

2.1.8 Adaptations to reduce the Urban Heat Island

Within the Netherlands several measures have been recognized to reduce heat stress within an urban area. Researchers collected measures on different scales and aspects of the built environment to reduce the UHI-effect (Schrijvers et al., 2014, the scales were:

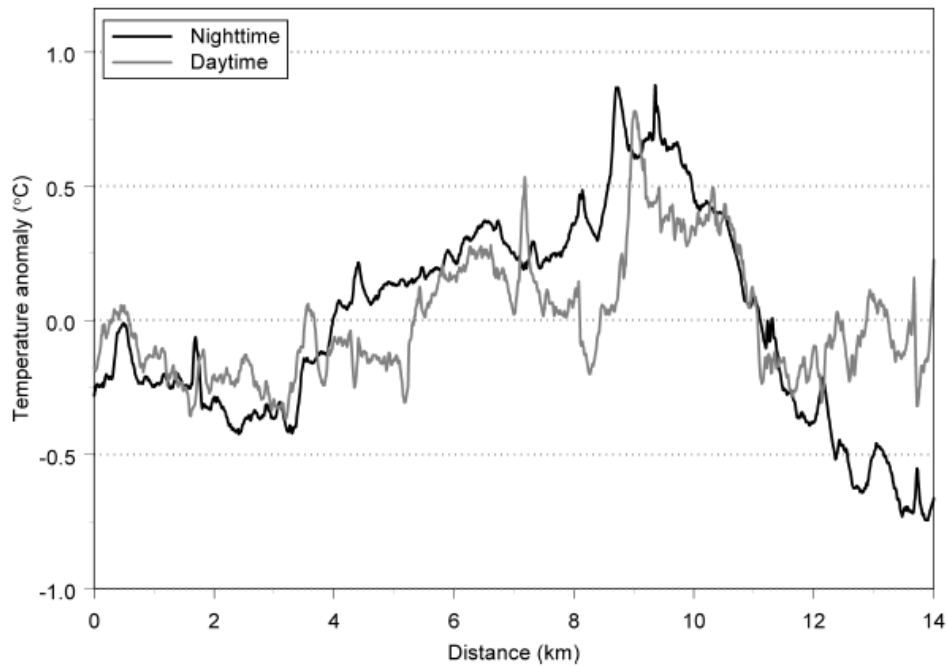


Figure 2.9: The average diurnal and nocturnal UHI effect measured in Utrecht by bike Brandsma and Wolters, 2012.

1. Building scale;
2. Street to neighborhood scale;
3. City and region scale.

First the heat stress reducing measures will be discussed for the building scale, after which the larger scales are briefly discussed. The building measures focus on three aspects. The first aspect is the application of green infrastructure, such as green roofs and façades, secondly the building characteristics and at last indoor climate measures.

The indoor climate measures are effective to reduce heat stress on a local scale, which do not contribute to reducing the UHI-effect. Though the usage of different building materials could have an effect on both indoor and outdoor climate. Alike green roofs, both intensive and extensive, and green façades could increase indoor and outdoor thermal comfort (Schrijvers et al., 2014).

According to Schrijvers et al. (2014) green façades and green roofs are promising implementations on street to neighborhood scale. Furthermore increased amount of vegetation, especially trees are effective to cool down on the street level. On the street till building scale the researchers focused on the public spaces as well as the building itself. Though later research showed that private gardens need to be taken into account (Williams, 2019). This is strengthened by research with GIS and Tyrgon, where 70% of gardens are grass will reduce the UHI-effect by about 30% (Witteveen, 2014). Furthermore was showed that green roofs show similar results on this scale.

At last on a city scale Schrijvers et al. (2014) only found the implementation of parks effective to reduce the Urban Heat Island. Which is strengthened by the earlier findings that a higher ratio of green area reduces the UHI-effect. Besides Schrijvers et al. (2014) focused on drought and pluvial flood reducing measures. To understand these measures, first the effects of droughts on the urban area will be discussed in the upcoming section.

2.2 Drought in the Netherlands

As showed in the previous sections can the urban heat island be tackled with green infrastructure. The reduction of the UHI-effect is dependent on the availability of water in urban areas as shown by Grimmond (1999). This is related to the evaporation rates of the green infrastructure depending on the available water. Droughts reduce the available water for transpiration, resulting in lower transpiration rates. Due the lower transpiration rates higher temperatures occur in the urban environment. The available water can be expressed in the soil moisture content in the soils. The soil moisture content is depending on the water table, precipitation and evaporation. In urban areas on average 9% of precipitation is available transpiration, in combination with drought stress about half of the potential evaporation rates are reached (E.S Van der Meulen, 2015). To further understand the effects of droughts in the Netherlands, firstly the definition of a drought has to be explained. After the definition of a drought the yearly water balance gives insight in what period within a year is interesting to contemplate on further. This enables to research the drought distribution, severity and occurrence of droughts in the Netherlands. These factors together enable research into the effect of droughts on the urban environment The theme of drought and its aspects is subsequently discussed in the following order:

- The definition of drought in the Netherlands, based on the potential precipitation deficit;
- The urban water balance in the Netherlands;
- Distribution, severity and occurrence of droughts; and
- The effects of drought on the urban environment.

2.2.1 The Dutch definition of drought

Droughts are globally researched and monitored which causes many perspectives and interpretations. To simplify the situation the Dutch definition of a drought will be considered. Drought in the Netherlands is measured the the Royal Netherlands Meteorological Institute (KNMI). The KNMI observes a yearly drought period between April and September and is based on the potential precipitation deficit. The potential precipitation deficit is the accumulated difference between the amount of precipitation and potential reference crop evaporation (Rob Sluijter et al., 2018).

Potential reference crop evaporation

The potential reference crop evaporation is the evaporation measured for a well-watered, well-maintained and well-fed meadow on a rural site (Rob Sluijter et al., 2018). The KNMI does not measure evaporation spatially since, according to the KNMI, the evaporation depends on too many factors. The actual grass evaporation will differentiate substantially from the reference crop evaporation due the following factors:

- Soil type;
- Groundwater level;
- Groundwater supply and/or discharge; and
- Surface characteristics.

The actual evaporation, also in urban areas, will therefore be influenced by these factors. Besides different kinds of vegetation are present in urban areas, which also have their own variable evaporation. A short explanation on how these factors will influence the evaporation rate is given in the upcoming section.

Factors influencing the reference crop evaporation

The influencing factors can be explained as followed. The soil type influences the infiltration and extraction capacity through the soil physical characteristics, for example the hydraulic conductivity and porosity. Vegetation depends on the soil moisture content within the rootzone. If the soil moisture content is at its maximum the soil is saturated. While if the soil moisture content is too low for vegetation to extract water is called the wilting point. The phase in between when there is a mixture of air and water, ideal for each type of vegetation, is called the field capacity (Brouwer, Goffeau, and Heibloem, 1985). The groundwater level has a large contribution. The higher the groundwater lever the more evaporation may occur, too low and no or little evaporation will occur.

The groundwater level is dependent on the surface characteristics and both groundwater supply and discharge. The more impermeable surfaces the less infiltration can occur on that specific site, which declines

the soil moisture availability. Furthermore, the groundwater level fluctuation is influenced by the groundwater supply and discharge (Fitts, 2013). Other factors influencing the groundwater level are pumping and river discharge, an overview of all processes are visible in Figure 2.10.

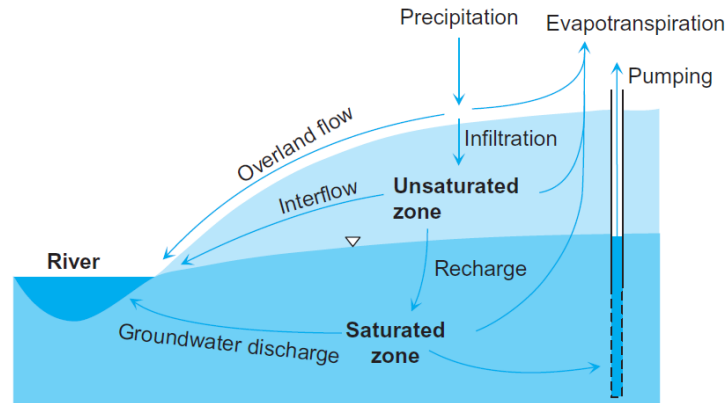


Figure 2.10: Processes influencing the groundwater level within a reservoir (Fitts, 2013).

Several of the processes are influenced by the surface characteristics. To begin with the rate of evaporation. Even though multiple factors contribute to the rate of evaporation, the amount of green area per square metre has a major influence. Respectively the second and third processes influenced are the amount of overland flow to water-bodies or sewerage system and infiltration to the subsurface. Both of these processes depend on the amount of impermeable surface and capacity of the sewerage.

Before the influences can be quantified a deeper understanding of the fluxes is necessary. To establish this understanding two aspects will be explained. The yearly water balance within the Netherlands, based on precipitation and evaporation, is discussed. This is complemented with the processes involved with urban water management and their ratios. These two components enable to quantify the fluxes roughly.

2.2.2 The urban water balance in the Netherlands

When looked at urban environments it substantially differs from rural areas, which also is expressed within the urban water balance. Based on urban water balance studies in the Netherlands conclusions can be drawn regarding the urban fluxes. Based on an extensive research in Lelystad, the Netherlands, an urban balance was found between precipitation, evaporation, infiltration and sewerage discharge (Van de Ven, 1990).

Based on the research by Van de Ven (1990) the incoming precipitation about 40% infiltrates to deep groundwater, 37% evaporates and about 23% is discharged through the sewerage. Though the yearly average precipitation is 827mm while the potential evaporation is 559mm over 1980–2010. Therefore, potentially 67.5% of the precipitation can be used for evaporation (KNMI, 2020a). Though, monthly variable precipitation and evaporation cause an imbalance, which is enhanced by urban drainage.

KNMI has extensive records of meteorological data, which are used for statistical analysis and weather forecasting. For statistical drought evaluations the KNMI distinguishes two main yearly periods, the autumn/winter period from October until March, and the spring/summer period from April until September. The distinction is made since on average in April the reference crop evaporation is higher than the precipitation. In September the reference evaporation starts to decline again, while the precipitation increases again, which is also visible in Figure 2.11.

The period of higher potential evaporation can also be regarded as the crop growing season. The crop growth rate is influenced by several factors for example precipitation and total of sun hours, which can be linked to potential evaporation. Based on precipitation and potential evaporation data, from 1981 to 2010, yearly and seasonal water balances can be made.

Table 2.2 presents the differences in water balance over these two periods and the yearly data. From the data can be derived that on average 80% of the potential evaporation occurs during the growing season, while 50% of precipitation occurs outside this season. This causes an imbalance in supply and demand, which leads to an average deficiency of 59 millimetre of water at the end of the growing season.

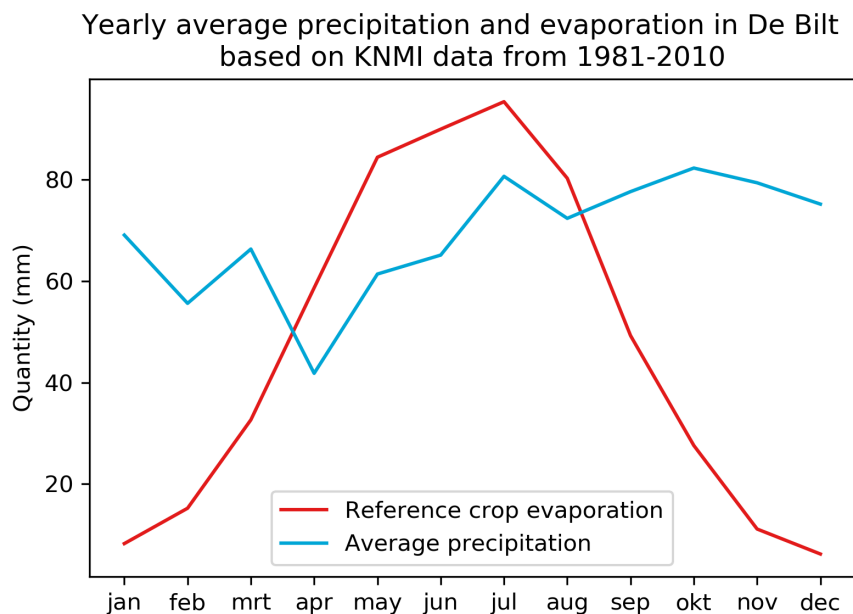


Figure 2.11: Yearly water balance of De Bilt, The Netherlands. Based on data from KNMI

	Precipitation	Potential evaporation	Water balance
Yearly	827	559	292
April–September	399	458	–59
October–March	428	101	327

Table 2.2: Average yearly and seasonal water balances of De Bilt, the Netherlands, over 1981-2010 (KNMI, 2020a)

Though, the deficiency does not give an implication in the real severity and duration of droughts. Besides, precipitation is spatially distributed, local variance in precipitation deficit will occur. Besides thermal and wind conditions cause variation in the potential evaporation. To give a better overview of the drought severity, the distribution, severity and occurrence of droughts in the Netherlands is discussed in the next section.

2.2.3 Distribution, severity and occurrence of drought

Dutch national weather data is collected by the Royal Dutch Meteorological Institute (KNMI) at 34 locations. Data from 18 stations was used for statistical analysis regarding the distribution and occurrence of a drought with a specific severity. A standardized Gumbel plot was made based on nation wide average precipitation and evaporation data from 1906–2000. Based on that period the drought of 1976 had the highest cumulative precipitation deficit with an occurrence of about once every 150 years (Beersma, 2007). In Figure 2.12 the results of this study is shown.

As stated earlier, there is a distribution of evaporation within the Netherlands. This distribution causes the maximum precipitation deficit to vary spatially. It can be seen, in Figure 2.13, that coastal regions have a higher yearly amount of evaporation with respect to the inland eastern part of the country. Besides, this results in a slightly higher probability at a more severe drought during the growth season.

A more severe drought will have a larger impact on the local environments. Besides 2018 was the fifth driest year ever, even though it has a projected return period of 30 years (R. Sluijter, Plieger, van Oldenborgh, Beersma, and de Vries, 2018). Though what is the effect of such a drought on the urban environment, the upcoming section shortly addresses these effects.

2.2.4 The effect of drought on the urban environment

On a global scale half of the earth is sensitive to droughts, possibly leading to long-term social, economic and environmental effects. Estimated is that the last century 11 million people have died due droughts, while 2 billion have been affected. Estimated is that the upcoming century these numbers only will grow due higher temperatures, dryer conditions and population growth (Spinoni, Naumann, Carrao, Barbosa, and Vogt, 2014).

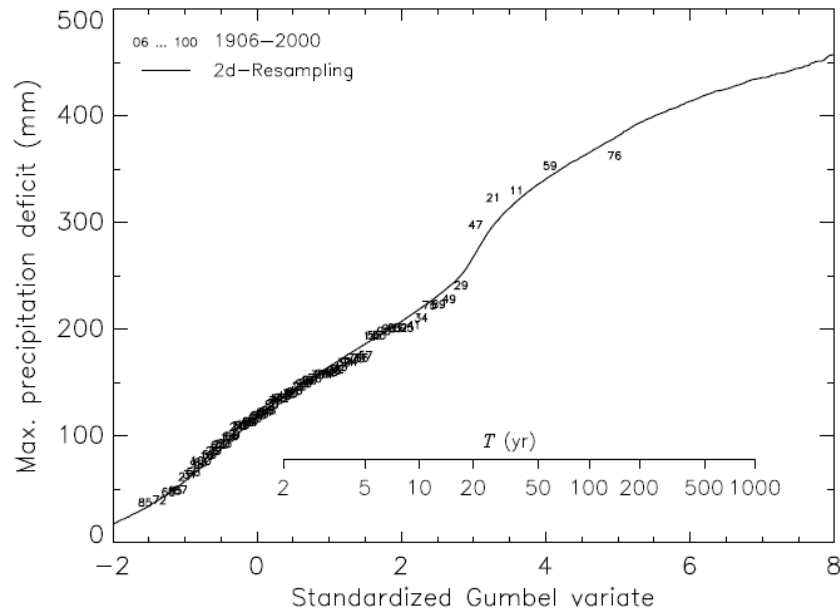


Figure 2.12: Standardized Gumbel probability plot of the cumulative precipitation deficit in the Netherlands (Beersma, 2007).

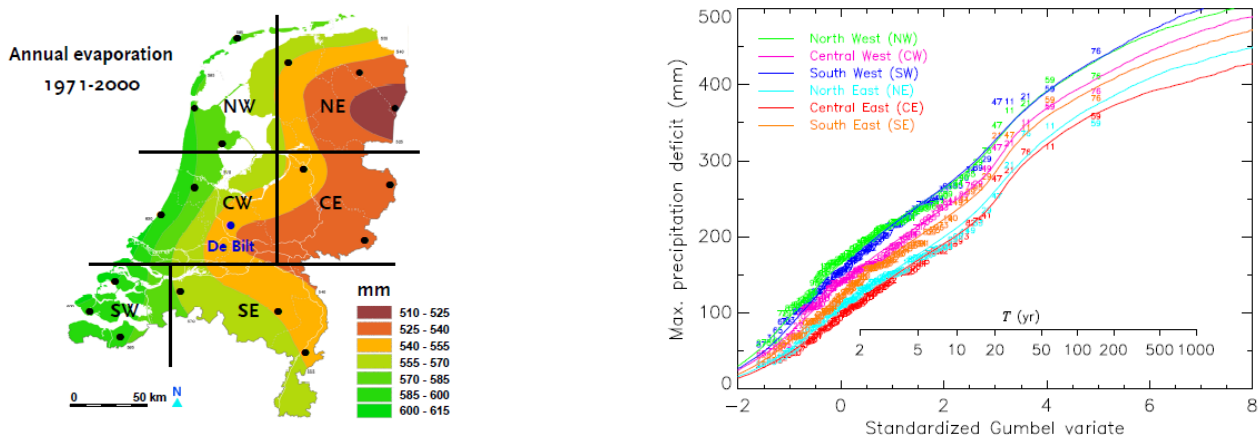


Figure 2.13: Spatial distribution of the evaporation (left) and maximum precipitation deficit (right) in the Netherlands (Beersma, 2007).

With respect to Dutch urban areas, it is expected that mainly urban areas in peat and clay regions will be affected. Land subsidence and oxidation of foundations and poles both could lead to damage to infrastructure. While green areas are dependent on the water availability (de Ven et al., 2011).

Furthermore, de Ven et al. (2011) acknowledges that the soil moisture content potentially will reach extreme low values due droughts. The droughts increase the chance of salinization of the subsoil, which could lower evaporation rates too. Though not enough information is known on this specific topic.

As a solution is given to reduce the quantity impermeable pavement, in combination with collecting all precipitation, store and reuse the precipitation and only discharge the excess water (Witteveen, 2014). This process is called the sponge city design. In the upcoming section the several implementations, which could lead to drought and flood reductions, are discussed.

2.2.5 Water retention measures

Previously is described that sponge cities could reduce pluvial floods and droughts. To understand why sponge cities reduce pluvial floods and droughts, a short description of the sponge city definition and its water retention measures is given.

As described by Dai, van Rijswijk, et al. (2018) a sponge city is: "A city built around the concept of managing water in an ecologically sustainable way." A sponge city aims to capture, store and re-use rainwater. Within

sponge city design there are measures focused on water infiltration, retention, storage, purification, drainage and reuse. While these implementations increase resilience and benefit multiple aspects, for example environmental, economic and social benefits (Li et al., 2019). These measures have been adapted for Dutch cities by Schrijvers et al. (2014) and divided into three scales and levels:

- | | |
|----------------------------------|---------------------------|
| 1. Building scale; | 1. Roof level; |
| 2. Street to neighborhood scale; | 2. Street level; |
| 3. City and region scale. | 3. And sub-surface level. |

Firstly on the building scale there are some measures which also benefit for reducing the UHI-effect, these are the green roofs and to a lesser extend green façades. More promising on the building scale are a blue roof, or water storage on the roof, rain barrels or underground storage tanks. Though, Schrijvers et al. (2014) also recognized the that private gardens need to be permeable. Increasing the permeability or infiltration capacity, is also the aim on street level. Depaving, in combination with infiltration units or ditches, will reduce droughts and pluvial flooding simultaneously. Furthermore implementations of wadis and disconnecting rainfall sewers result in beneficial situations. Though it is important that both public and private spaces are adapted to reach maximum potential (Witteveen, 2014; Williams, 2019). To distinguish the several measures their characteristics are described below ordered on the level.

Roof level water retention measures

At roof level various types of green roofs can be applied, an overview is presented in table 2.3. In principle are green roofs constructed with a layer of substrate and moss with possibly the addition of herbs and grasses. These basic type of green roofs are extensive green roofs. When is chosen for a thicker layer of substrate, even larger types of vegetation can be planted, like trees and bushes. A green roof with additional substrate and larger vegetation need more maintenance and are therefore called intensive green roofs.

Both types of green roofs reduce the UHI-effect due their increased albedo. Besides green roofs retain between 50–60% and 60–90% of precipitation, respectively extensive and intensive green roofs. When an extensive green roof is accessible and used for leisure this can be regarded as a roof garden. Furthermore green roofs can be applied at sloping roofs of 0-7°, for ideal water retention purposes, though till 35° is possible without extreme additional measures. If the ideal slopes are applied extensive roofs store up to 25 l/m², while intensive green roofs can store up to 160 l/m².

	Weight [kg/m ²]	Depth [cm]	Slope [°]	Vegetation	Water retention [%]	Discharge coefficient [-]	Water storage [l/m ²]
Intensive	320–570	45–126	0–5	Bushes, trees, grasses, and herbs	70–95	0.3–0.05	110–160
Extensive	80–130	7	0–5	Moss, herbs and grasses	50–60	0.5–0.4	25
Sloped	160–190	13	5–35	Moss, herbs and grasses	-	-	-
Roof garden	100–300	10–25	0–5	Moss, herbs, grasses and bushes	60–90	0.4–0.1	30–80

Table 2.3: Types of green roofs and their characteristics (Schrijvers et al., 2014).

Street level water retention measures

All measures at street level are the most visible with the urban landscape, since these physically change an urban area. These measures have the goal to store, retain and/or reduce runoff from the urban area, which is done by catching rain, diverting flow routes and create (sub-)street level storage.

Flow route diversion, to reduce the peak flow of the sewer, is achieved by (above) ground drainage and uncoupling of rainwater drainage. Uncoupling of rainwater drainage can be implemented at a local/household level. The uncoupled drainage pipes could discharge their water either directly or via drainage into a storage unit. Above ground storage can be implemented through storage tanks such as rain barrels, though subsurface

storage or storage within crawlspaces or cellars of houses could also be implemented. The stored water can later be reused for gardening or flushing toilets. Above ground drainage diverts flow towards a nearby water body or infiltration area, any excess water can be discharged out of the area.

Draining precipitation can be done by either natural or artificial gullies and ditches, or drainage pipes in the soil. All types of drainage have equal purpose; transport water to the perceived location. The location can be either surface water, storage location or infiltration area.

Types of infiltration areas

There are several possibilities to create a larger infiltration flux. Increasing the infiltration flux can be done by increasing the amount of permeable surfaces, improving soil quality or changing surface levels.

Firstly permeable surfaces are addressed, followed by changing the surface levels, while improving soil quality will be addressed in a later section. Within existing urban areas the current impermeable surfaces can be replaced by permeable surfaces. Permeable surfaces allow water to infiltrate into the subsoil enabling water to be retained within the area. For each specific type of surface there is a type of permeable surface available such that the surface area's function is not changed when the surface layer is adapted. For example asphalt of frequent used parking spaces can be replaced with porous or open-joint clinkers, while barely used parking areas can be designed with gravel or another loose material, or grass concrete pavement.

Another solution is to drain the water towards an infiltration field, which is designed to enable infiltration from surrounding buildings and/or roads. An infiltration field could be designed with (partial) lower street level to enable temporary water storage. An infiltration field could be designed to have multiple functions within an urban area, such as a play ground or it is part of the green infrastructure within the urban area.

A wadi is a ditch designed with additional infiltration and drainage capacity, which enables it to cope with excess precipitation situations. Wadis will infiltrate all precipitation within a day, which is exceeded once every 25 years. Ditches and gullies transport the water to an infiltration area or wadi to recharge groundwater and increase the soil moisture content.

Sub-surface water retention measures

The third level of measures addressed are the sub-surface water retention measures. Which can be split in two groups; storing water and increasing infiltration rates. Storing water can be achieved by installing tanks or crates under the surface level or pump water in an aquifer. Whereas increasing infiltration rates is achieved by improving the soil structure of permeable areas.

Water tanks are mostly used to store water from roofs or cleaner surfaces, which enables potential reuse within households or gardens. Crates can be used under impermeable surfaces such as asphalt or artificial sport fields. The water from either the storage tanks or crates can later be used for infiltration in the soils. By creating storage tanks or crates, water which would otherwise have been discharged from the area, is retained within the area.

Improving the soil structure is beneficial on three aspects. The first aspect is the infiltration capacity of the soil is increased, which reduces overland flow into surface water or sewerage. The second aspect is the increased storage within the pores of the soil, which enhances evaporation. The third aspect is from an ecological standpoint, adding organic material improves soil life.

The sub-surface water retention measures are enhanced by the surface and roof level water retention measures, since these increase the available water. A coherent system of drainage infiltration and storage measures should therefore be most beneficial to reduce droughts.

2.3 The (un)saturated zone

The previous sections stressed the need for availability of water regarding evaporation to reduce the Urban Heat Island and droughts. Though to reach higher infiltration and evaporation rates, while retaining water over longer periods to reduce droughts, the water related processes in the subsoil need to be understood. This section will therefore introduce the various terms and processes.

Within groundwater sciences there is a distinction made between two zones, the vadose or unsaturated zone and the saturated or phreatic zone (Fitts, 2013). Fitts (2013) defines the unsaturated zone as: 'The zone above the water table where the pore water pressure is less than atmospheric.' This can be explained as the area where the pores within the soil contain both air and water. The region where the pores only contain water is the saturated zone. When looked at the relationship between the water pressure in the soils and atmospheric pressure, it is regarded that the unsaturated zone is the region where the pressure is lower than atmospheric pressure. A vertical cross-section of these details is given in Figure 2.14

Water fluxes cause variation of water content within the unsaturated zone, both spatially as with depth. The amount of water within the unsaturated zone is also called the soil moisture, which refers to water which is available for root extraction. Fluctuations of water content has lead to a distinguish into three states within the soil. The first state is the saturation water content (θ_s), where the pores are completely filled with water. This occurs then at the top of this zone is the water table. The complete opposite is when there is so little water available that roots cannot extract the water from the soil. The moment this occurs, the soil is at wilting point. A specific value of water content between these values is the field capacity, at which vegetation can evaporate optimal (Brouwer et al., 1985).

Figure 2.14 shows how the water content with respect to the pressure head propagates within a soil. It can be seen that each soil has a specific curve for the water content (Fitts, 2013).

The amount of soil water is influenced by several factors and fluxes, earlier presented in Figure 2.10, such as infiltration, recharge of the saturated zone, interflow and evaporation. Infiltration is depending on the conditions of the surface, the more impermeable surfaces there are the lower the infiltration rates will be. Furthermore the evaporation rates depend on the available water in the root zone, which is the area beneath a plant where the roots are situated (Brouwer et al., 1985). When there is no water available within this zone vegetation cannot evaporate. Besides when the groundwater table is too low plants can almost not evaporate, while most of the water will recharge the saturated zone.

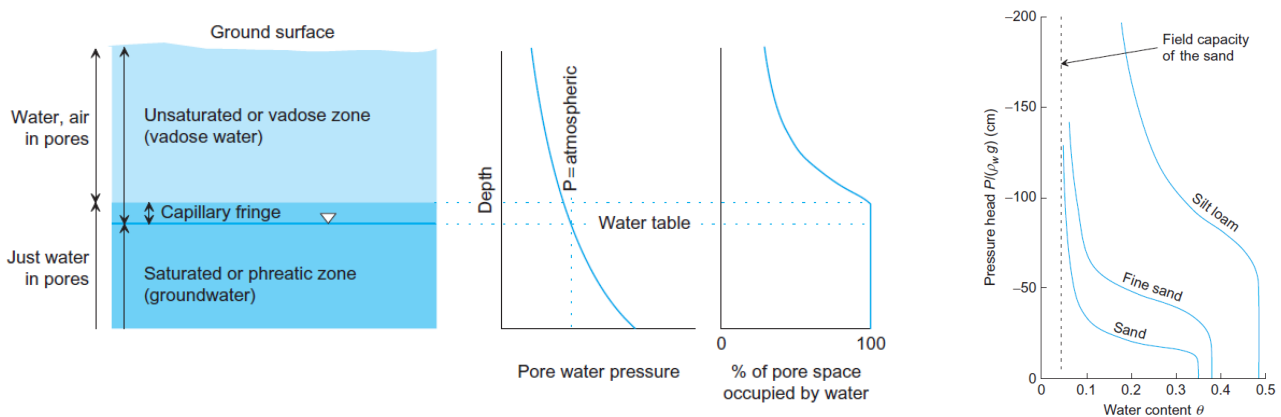


Figure 2.14: Cross-section of the subsoil circumstances, explaining the unsaturated zone. And the characteristic water content curve for specific soils. Given are the water content and the pressure head within the unsaturated zone (Fitts, 2013).

Chapter - 3

Methodology

After setting stating the research problem into more detail, the methodology now will be discussed to reach the research goal. The research goal, which is linking excess precipitation measures to drought reduction and urban evaporation for cooling (by nature), can be reached with a solid approach. The approach can be translated into the methodology. The methodology consists of two interlinked parts:

1. Case study;
2. Micro-climate model.

Firstly, the systems interacting with each other will be introduced. The introduction is followed with an explanation of the micro-climate model used. The micro-climate model used is ENVI-met, which purpose is discussed in detail. From there on the case study is described, focused on the location, assumptions and application of the models.

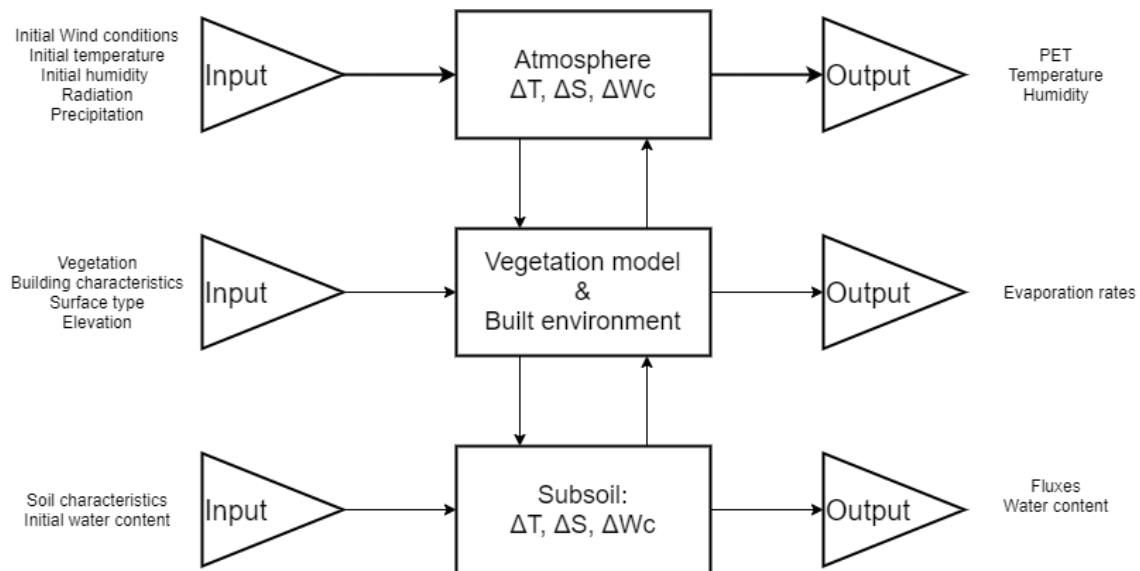


Figure 3.1: Schematic representation of the system of interest.

3.1 The system of interest: The urban environment

The scope of this research can be translated to a system of interest. The system of interest consists of all sub-systems and assets interacting together within that specific environment. The system of interest gives insight in the necessary capabilities of the used models, which can be linked to the sub-systems and assets of the system of interest.

Therefore, the system of interest of this research consists of the urban environment including the (sub-) soil and atmosphere. The urban environment acts as the boundary layer between the atmosphere and soil system.

The interest in temperature, soil moisture content and processes between, which occur mostly in the urban environment, all three aspects are necessary. These processes are for example evaporation and infiltration. A representation of the system of interest is given in Figure 3.1, each area has their own specific input and output.

Therefore, to accurately model the system of interest, all three areas should be covered in the models. Furthermore, the necessary output of the models should include the meteorological and soil-water parameters to contribute to answering the research questions. Which models will be used, why and what these will contribute to the research is discussed in the upcoming sections.

3.2 Modelling the atmosphere and urban environment

There is an interest into modelling the atmosphere, urban environment while taking the subsoil into account. Therefore a model of the urban environment should be capable of simulating three aspects. The first aspect is simulating the atmosphere and the urban environment, since this is the space where humanity interacts with. Secondly, the model should be able to model the natural processes which interact with the urban environment, such as solar radiation and precipitation. At last, it should be able of implementation of excess precipitation measures to link these to drought reduction and/or cooling.

The software ENVI-met, as seen in Chapter 2, is capable of doing so. ENVI-met is previously used by multiple researchers to evaluate green structures (Fahmy, Sharples, and Yahiya, 2010), for assessment of outdoor thermal comfort (Boukhabl and Alkam, 2012; Berkovic, Yezioro, and Bitan, 2012) and urban planning (Emmanuel, Rosenlund, and Johansson, 2007; Taleb and Abu-Hijleh, 2013). Furthermore, studies have validated that ENVI-met accurately models the outdoor thermal conditions (Toparlak et al., 2015; Ayyad and Sharples, 2019; Bande et al., 2019; Forouzandeh, 2018; Kleerekoper, 2016; Ng et al., 2012; Wu et al., 2019).

Firstly, the several components of ENVI-met are discussed. Secondly, the input and output of ENVI-met, together with the limitations and assumptions of the software. After which the relationships between model and the research questions are discussed.

3.2.1 ENVI-met

An holistic micro-climate modelling system available is ENVI-met. ENVI met enables modelling the interactions between the surface, plants and air in three dimensions, with a resolution down to 0.5m in space and between 1 – 5 seconds in time (ENVI-Met GmbH, 2019b). These interactions are driven by the main atmosphere model, which takes environmental and geographical parameters into account. An overview of the ENVI-met model architecture can be seen in figure 3.2, which shows the relevant components of the model. The relevant components are:

1. Atmospheric model;
2. Built environment & Building system;
3. Vegetation model; and
4. Soil model.

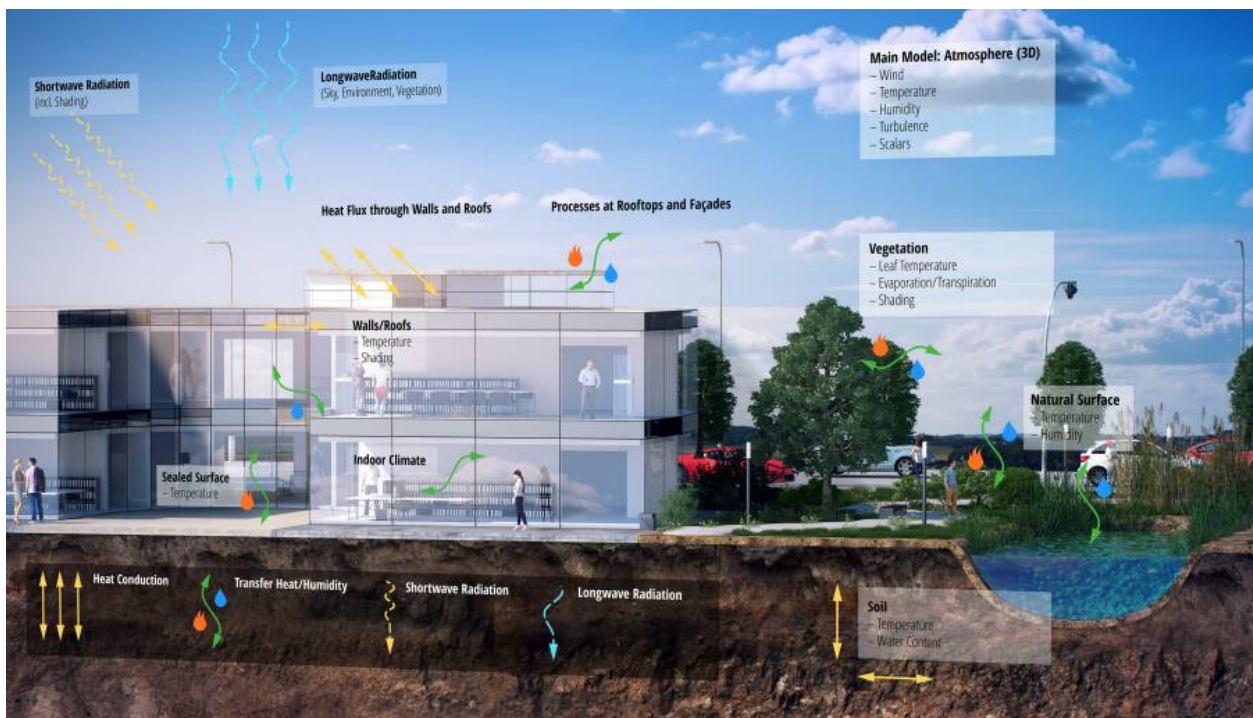


Figure 3.2: The architecture of the ENVI-met model. *Based on the main atmosphere model, the interactions between air, plants and infrastructure can be modelled (ENVI-Met GmbH, 2019b).*

All four components are shortly discussed, stating their basic principle, on which this is based and their relationship with the other components. Addressing these factors will create an understanding of the necessity for the research. A detailed overview of the formulas and processes within ENVI-met is available in appendix A.

The atmospheric model is used to model meteorological processes within the urban environment. This is done by maintaining a stable air flow within the model, while taking the energy and water balance into account. The two balances are based upon the incoming and outgoing fluxes of each system. As can be seen in figure 3.2, the atmosphere model, due its complexity, is influenced by the other three models.

The built environment is modelled to simulate the interaction with meteorological processes and create the context of the urban environment. The built environment in ENVI-met is given as input with the Spaces application. Within Spaces the built environment is given as parameters of the surface type and level, building height, materials and shape, but also vegetation and soil type are given as input to complete the entire local environment. The built environment is therefore setting the boundary conditions and context of the other three components of the model.

The vegetation model is used to simulate evaporation based on plant type and size, soil moisture content in the rootzone and meteorological circumstances. Taking into account these parameters during an iterative process the, evaporation rate of vegetation is determined. This evaporation rate then influences the atmospheric model increasing the humidity and lowering the temperature by using solar radiation.

The last component is the soil model which is used to model the soil water processes such as infiltration, transfer of water, and extraction by the roots (combined with the vegetation model). Besides water related processes, the soil model incorporates the adsorption, radiation and transmission of energy in the subsoil. The soil model interacts not only with the vegetation model directly, but also with the atmospheric model.

Spaces, ENVI-met database and ENVI-guide

The input for the is mostly done through the Spaces application, but the characteristics of the components in the spaces application is stored in a separate database. The database holds all variables of materials, soil profiles and vegetation. The standard values can be adapted or new components can be added to the database itself. A overview of the database and its parent-child relationships is given in A The database and spaces file together are used to initiate a simulation with the ENVI guide. The ENVI guide sets the boundaries for time, meteorology and the initial soil moisture content with respect to field capacity.

3.2.2 Limitations and assumptions

All software comes with several implications and limitations. This section will describe these and their influence on the research. To start with ENVI-met's spatial resolution, which is, as stated before, down to 0.5 and up to 10 metre. The model's height should be at least 30m and twice the height of the tallest structure. The height restriction is essential to minimize unwanted artificial effects such as jet stream effects near the top border (ENVI-Met GmbH, 2019b).

Furthermore, to create an stable area of interest, nesting grids can be applied. Nesting grids are additional boundary cells which help creating more stability at model borders and edges. The usage of nesting grids is optional. Though, as can be seen in figure 3.3, the flow nearby the border will stabilize when using five nesting grids.

Therefore, to create a stable model, the conditions regarding height and border stability should be met. Stability can be reached by having a grid three times higher as the highest building, with a minimum total height of 30m, and adding 5 nesting grids, such that there is as much distance available as the nearest structure is tall (ENVI-Met GmbH, 2019a).

The last limitation of ENVI-met is probably the most important limitation with respect to this research. The soil model, even if initially a lower value is given, sets the minimum soil moisture content with respect to field capacity at 10%. ENVI-met increases the soil moisture content to increase stability and assure that the simulation will start in a stable state and numerical problems do not occur during the simulation. So when a 0% relative soil moisture content is prompted, actually a 10% relative soil moisture content is simulated. This limits this study to not be able to study a drought without evaporation, but this comes as close as possible with this software.

3.2.3 Interpretation of the output data of ENVI-met

The output data of ENVI-met can be evaluated through multiple approaches. The first two approaches are interpretation through ENVI-met's data interpreter Biomet and Leonardo. The third approach is to extract and read files through a python package.

Data within ENVI-met can visually be displayed by ENVI-met's Leonardo application. The Leonardo application can create two and three dimensional maps of the modelled urban environment. The data within these maps can also be extracted from Leonardo to csv files, which can be used for statistical analysis. Biomet is capable of translating the atmospheric parameters into values representing the thermal comfort of the local climate, such as the Physiological Equivalent Temperature (PET), Standard Effective Temperature (SET) and Universal Thermal Climate Index (UTCI).

Since ENVI-met produces EDT/EDX files, which not easily can be processed, a python package is used. The package used is the xml.etree.ElementTree-package (Lundh, 1999–2008). This package decodes and converts the EDX/EDT files into easily processable data.

3.3 Research method: application of the model

Now that ENVI-met has been explained, the research method can be explained. The research method is split in several aspects, which are discussed in this section.

3.3.1 The different aspects of the approach

The approach is split in three different aspects, which are:

1. two base cases, with different characteristics and locations;
2. different soil physical parameters and soil moisture contents; and
3. different meteorological periods, single day with versus five day period.

The first aspect of the approach, the usage of two case studies, are discussed in detail the upcoming chapter. This enables giving a detailed description of the cases altogether.

The second aspect, the different characteristics for both cases, enable research into the effect of soil moisture content, influence of the soil characteristics, and evaporation rates on the urban thermal conditions. Furthermore, the amount of green surfaces within the urban environment is increased to create another scenario. These scenarios will give insight into the effects of impervious surfaces and the evaporation rates with respect to the thermal conditions.

The third aspect, varying the meteorological periods, allows to see daily trends and variations due local influences. The meteorological periods chosen are a tropical day on June 21, with dry and wet soil moisture contents, and meteorological period from July 27 till July 31 of 2018. The latter period traditionally has high temperatures and the peak of the drought-severity occurs at the end of this period, as seen in Chapter 1. During discussion of the cases, in the upcoming chapter, the meteorological period is elaborated in more detail.

The approach is chosen due the interest in the relationship between the soil moisture content, evaporation rate and temperature. This is enabled by a micro-climate model with different scenarios focused on green infrastructure and soil moisture content. ENVI-met generates data regarding the thermal conditions, while precisely modelling evaporation rates and soil moisture contents within the urban environment. Furthermore, applying these models to two case studies, allows research of different scenarios or circumstances. All simulations have a spatial resolution of 2x2m and a time-step of 2 seconds, while producing hourly output, enabling in depth analysis of the results.

Now that the different aspects of the research are clear, the relationship with the research goal questions can be made. This relationship is discussed in the next section.

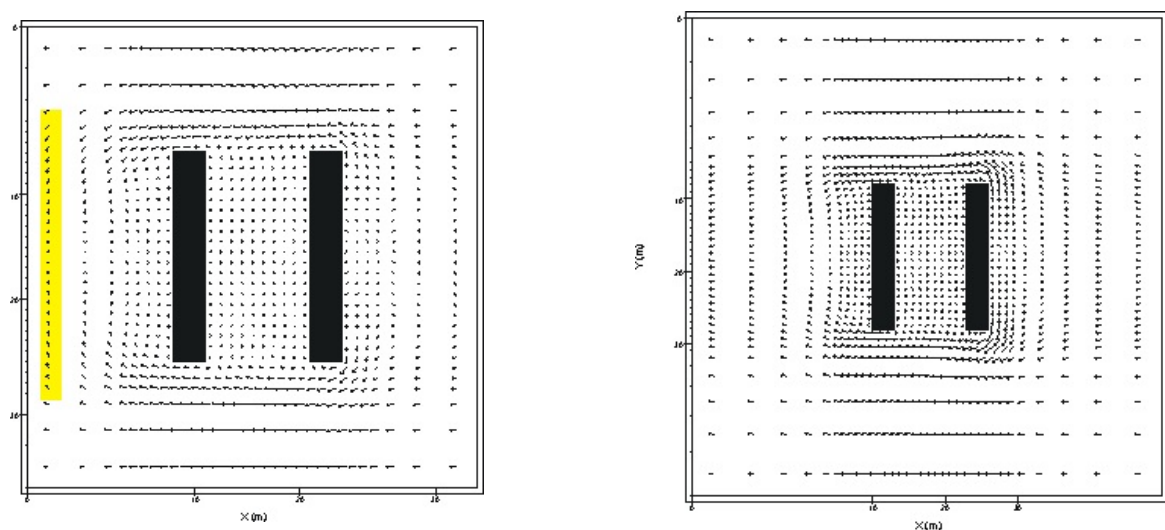


Figure 3.3: Nesting grids with three and five cells. *At the edge of the simulation with three nesting grids the flow did not stabilize, whereas the flow with five nesting grids did stabilize.*

3.3.2 Elaboration of the different scenarios with respect to the research questions

The case studies and their scenarios enable answering specific research questions. This is done by varying soil physical characteristics and urban characteristics, like amount of impermeable surfaces and green infrastructure. Varying these parameters gives insight into the second set of research questions. The changes in the model focus on both private and public space.

The soil physical characteristics, meteorological input and urban characteristics depend on the case studies and are therefore discussed in the next Chapter 4. The cases will focus on three aspects:

1. green area, including variation of vegetation type;
2. irrigation rate; and
3. soil moisture content with respect to field capacity.

The total increase of green area depends on the current situation, though it focuses on both the public and private spaces, since previous research showed that these both have a substantial impact on urban climate adaptation (Witteveen, 2014; Williams, 2019). The current percentage of green area is increased till 70%, since previous research has shown that this quantity of green reduces the UHI locally by 30% (Williams, 2019).

Irrigation and soil moisture variation are a comprehensive set. Together these allow to analyse the effect of precipitation retention measures on the UHI and evaporation rates in the urban environment. For the daily simulations the soil moisture content with respect to field capacity varies from 0-100% in increments of 25% with at 100% the addition of irrigation, such that the soil moisture content is constantly at field capacity. For the longer meteorological period the soil moisture content is either 0% or 100% combined with irrigation.

More information on the cases is given in the next chapter, discussing the specific location, size and characteristic of each case study.

Chapter - 4

Case studies and data retrieval

The methodology enables research into the urban environment. To research the urban environment and its systems, a case study will be given. The case study consists of two neighborhoods which are alike in building typology, though with different subsoil. The first case study is the Bredalaan in Eindhoven, with a sandy subsoil. The second case study is the Oranjeboomstraat in Rotterdam, with a clayey subsoil. The Oranjeboomstraat was chosen initially, since this was part of a research project by BNA to design the house and urban environment as the water cooling machine of the city (Architecten", 2019). Based on the Oranjeboomstraat a Multi-Criteria-Analysis was performed to determine the second case location, these results are presented in appendix B.

This chapter discusses the locations, characteristics and meteorological and soil data of the cases. Besides, some additional information is given on the possible adaptations suggested by local governance. These aspects result in the scenarios for both cases. The results of the scenarios are presented in Chapter 5.

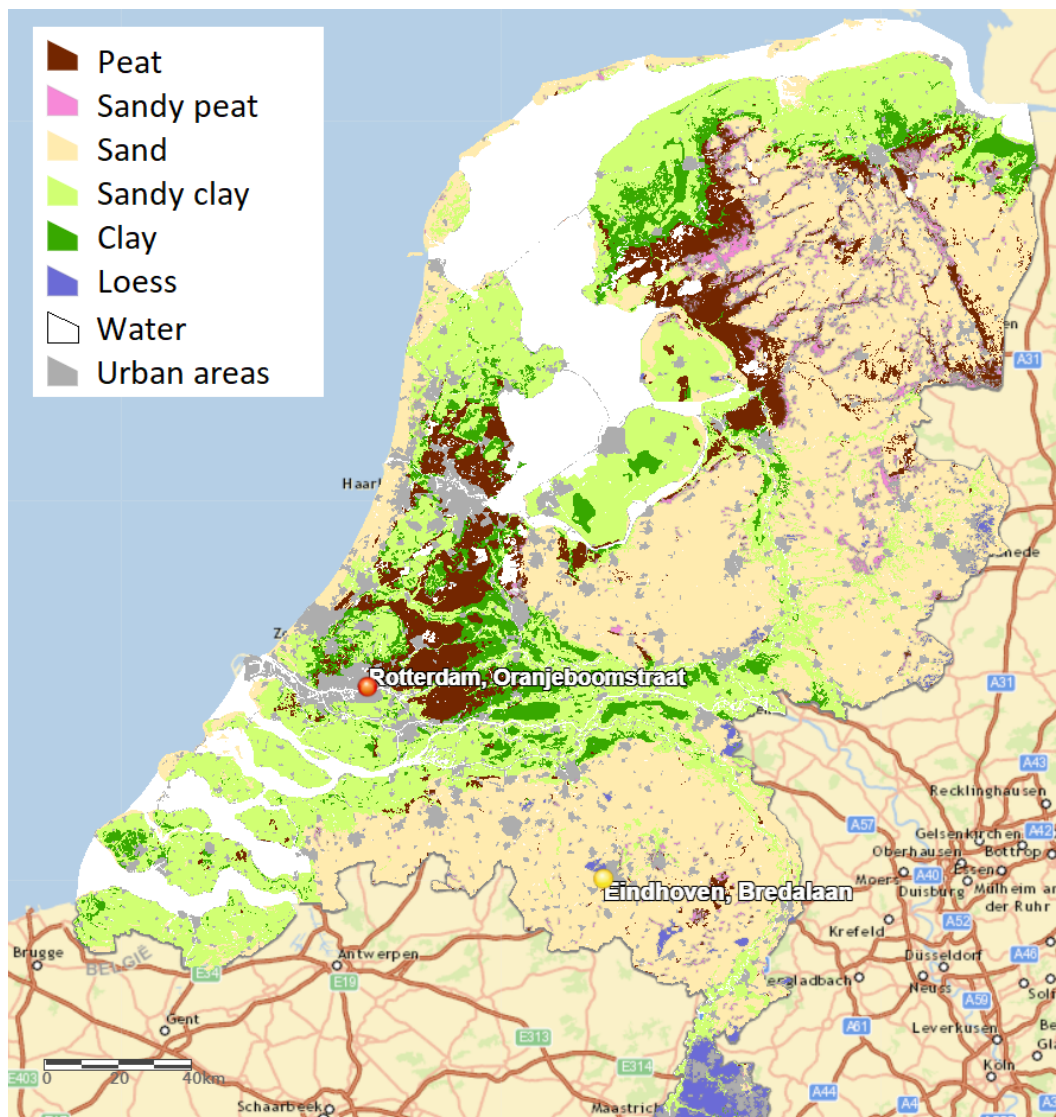


Figure 4.1: Overview of the case locations and different dominant soil classes in the Netherlands (Alterra, 2006).

4.1 General description of the case study

The case study enables answering the research questions by three means. Firstly, the case studies create context of the urban environment in which the research is done. Secondly, the case studies create the boundary conditions for the research by their respective urban environments. And thirdly the cases allow to alter the urban environments, changing the boundary conditions, and simulate possible scenarios, while enabling comparisons of different scenarios and circumstances.

To create a clear picture of both environments the locations are discussed alongside each other regarding five aspects, which set the local boundary conditions, These are:

- Location;
- Building typology;
- Meteorological data;
- Soil composition;
- And local governance.

The aspects are discussed in the upcoming section, after which the simulated scenarios are explained.

4.2 Locations and the characteristics of the build environment

The location of the case studies determines factors such as environment and soil structure of the location. Besides each location comes with challenges and opportunities due the influence of local governance and climate. Within this section their respective locations and characteristics are discussed alongside each other.

4.2.1 Geographical location of the cases

Within Eindhoven the Bredalaan is used as a case study and in Rotterdam the Oranjeboomstraat is studied. Figure 4.1 shows both locations of the case studies with respect to each other and the most common soil classes. As it can be seen is Eindhoven situated in southeastern Netherlands, in the province of Noord-Brabant. The geographical coordinates are $51^{\circ}26'22.8''N$ $5^{\circ}26'16.4''E$. Figure 4.1 also shows that in the region around Eindhoven a sandy subsoil is most common. Furthermore, figure 4.2 shows the study area of the Bredalaan with an area of 108x136m, which also consists part of the Wielantstraat.

The Oranjeboomstraat in Rotterdam is located at west coast of the Netherlands. The geographical coordinates are $51^{\circ}54'25.9''N$ $4^{\circ}30'31.4''E$ and the case study is 120x120m, including part of the Persoonshaven at the northeastern border of the case area. Rotterdam is in the province of Zuid-Holland, surrounded by more clayey-peaty subsoil. Section 4.4 gives a more detailed subsoil composition of both cases.

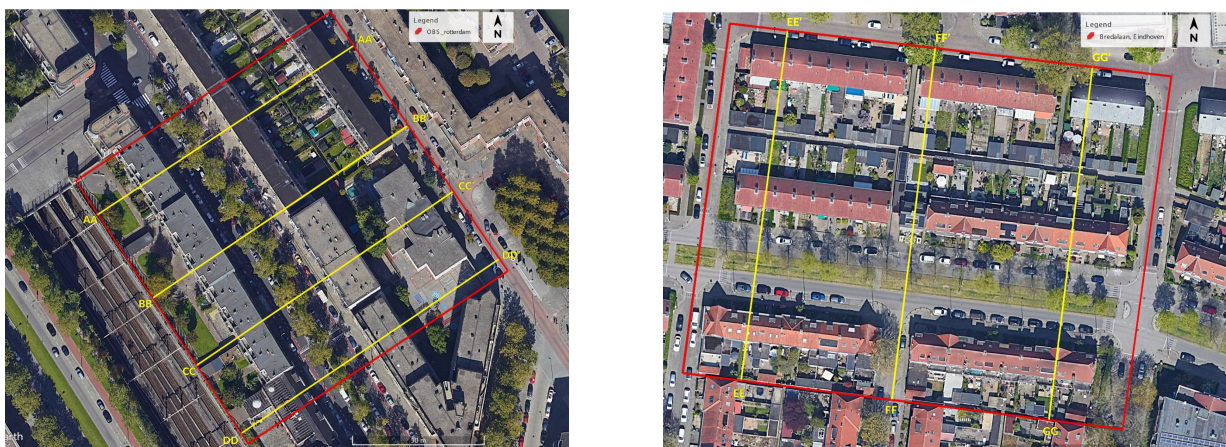


Figure 4.2: Presentation of the two cases and their respective study area and locations of the cross-sections (left: Oranjeboomstraat(Google LLC., 2015, January 10/2015), right: Bredalaan(Google LLC., 2020, April 16/2020)).

Spacematrix for individual housing blocks

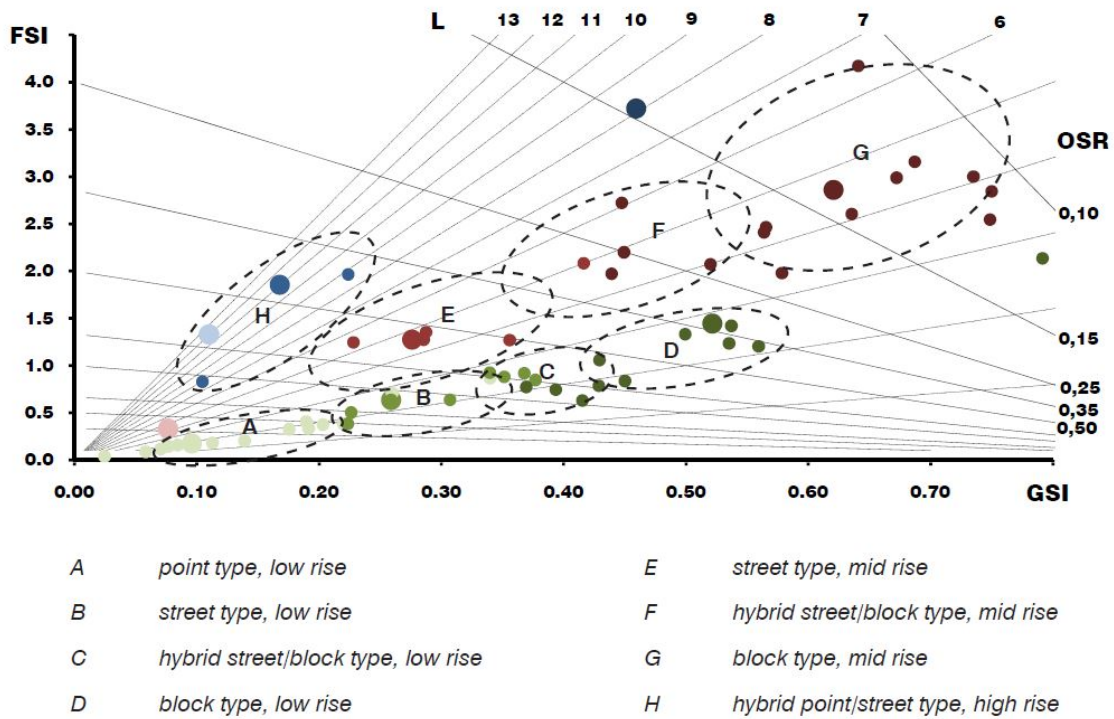


Figure 4.3: The spacematrix of the eighth different building typologies for individual housing blocks found by Berghauser Pont and Haupt (2009).

Spacematrix for the fabric scale

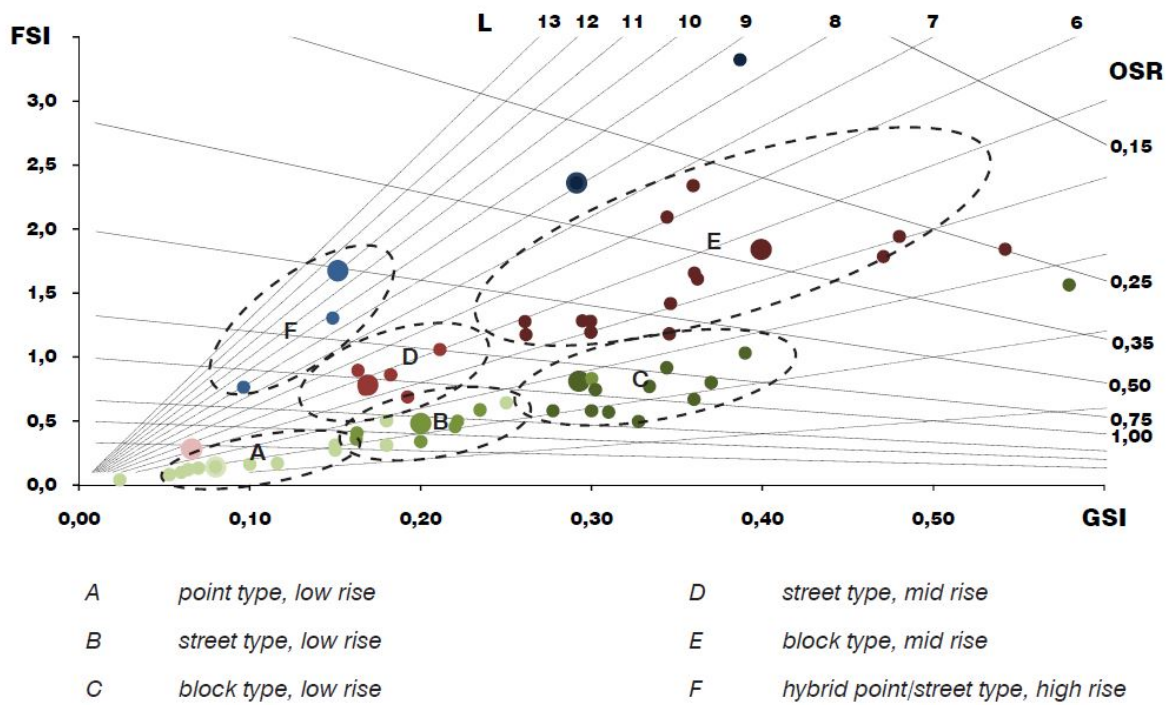


Figure 4.4: The spacematrix of the six different building typologies for fabrics found by Berghauser Pont and Haupt (2009).

4.2.2 Building typology of the cases

Each built environment has their own characteristics and therefore their own building typology. To determine the building typology of the cases, the Urban Density and Urban form are determined for housing blocks individually and combined. Determination of the building typology is done using the Spacematrix of Berghauser Pont and Haupt (2009). The Spacematrix uses urban dimensions to determine several factors, which determine the build typology of each building block individually and the fabric combined. The spacematrix parameters or urban density and form factors are (Berghauser Pont and Haupt, 2009):

- Floor Space Index (FSI);
- Ground Space Index (GSI);
- Open Space Ratio (OSR); and
- Layers (L).

The FSI is calculated by dividing the total living area by the total area of the housing block. The indicates the amount of living space per square metre of ground area. The GSI is calculated by dividing the sum of the "footprint" of all buildings by the total area. The OSR is determined as 1-GSI divided by the FSI, giving the ratio of spaciousness of an area. The amount of layers is determined by dividing the FSI by the GSI.

Subsequently these four values indicate the building typology of the individual or combined housing blocks of the case areas. Which is done by finding the corresponding cluster for these parameters in the spacematrixes of Berghauser Pont and Haupt (2009), visible in figures 4.3 & 4.4. These matrices and the relationships were found not only for Dutch build areas, but also within other European cities. The other European cities show similar relationships with for these factors as Dutch urban areas. Therefore, the FSI, GSI, OSR and L are calculated for each case for the individual building blocks and combined. All surface areas and dimensions are based upon the Kadaster (n.d.), which measure and register data of real estate in the Netherlands.

The spacematrix of the Bredalaan

The spacematrix of the Bredalaan are determined for the three individual building blocks of the case and the combination of these three. An overview of the three sections and their building blocks with respect to the case area are visible in figure 4.5, showing the three blocks A, B and C.

Based on the kadaster data of the housing blocks in region A of figure 4.5, the total plot area of all the houses combined is 6882 m², while the total living area is 4851 m² and the foundation sizes are 2175 m². This results in a FSI, GSI and OSR of 0.70, 0.32 and 0.97 m²/m² respectively. For building block B surface values of 6360 m², 5873 m² and 2526 m² were found for the total plot area, living space and foundation area. This resulted in a FSI, GSI and OSR of 0.92, 0.40 and 0.65 m²/m² respectively. For the third block areas of 6591 m², 5317 m² and 2380 m² where found resulting in a FSI, GSI and OSR of 0.81, 0.36 and 0.79 m²/m². When taking the streets and alleys into account the parameters give a FSI, GSI and OSR of 0.58, 0.26 and 1.28 for the fabric of the Bredalaan.

Table 4.1 shows the overview, amount of building layers and building typology of the Bredalaan. The Bredalaan has for the fabric a build typology of a low rise street type with respect to the factors, which corresponds with the spacematrix of the individual building blocks. The individual building blocks have a low rise hybrid or street type building typologies. Besides can be observed that the amount of layers is relatively constant over the case area with about 2.2-2.3 layers.

	Bredalaan A	Bredalaan B	Bredalaan C	Bredalaan fabric
FSI [m ² /m ²]	0.70	0.92	0.81	0.58
GSI [m ² /m ²]	0.32	0.40	0.36	0.26
OSR [m ² /m ²]	0.97	0.65	0.79	1.28
L [-]	2.23	2.33	2.23	2.27
Building typology	Low rise street type	Low rise block type	Low rise block type	Low rise street type

Table 4.1: Urban form and density factors of the Bredalaan.

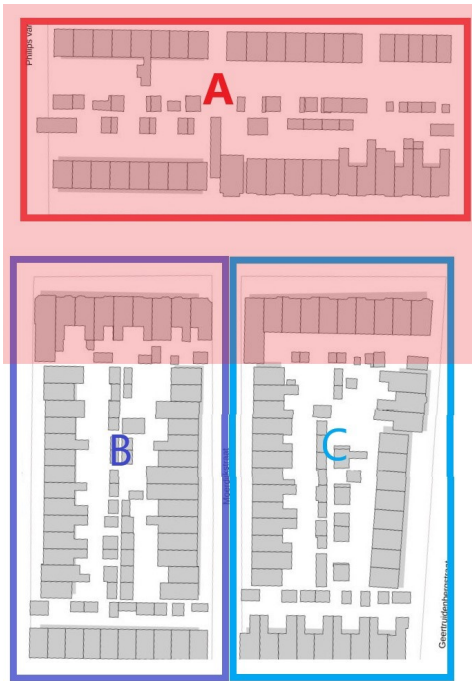


Figure 4.5: The three building sections of the Bredalaan. Block A, B and C are given together with the case study area.

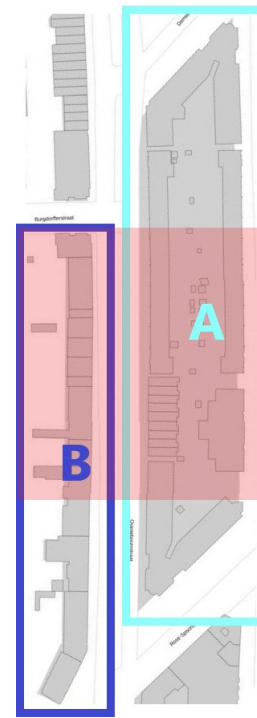


Figure 4.6: The two building blocks of the Oranjeboomstraat. Block A and Block B are given together with the case study area.

The spacematrix of the Oranjeboomstraat

For the Oranjeboomstraat the same approach is used to determine the FSI, GSI, OSR and layers of the building blocks. Figure 4.6 shows the case study of the Oranjeboomstraat and the two building blocks of the Oranjeboomstraat.

To determine the building typology of building block A the total area, living space and built area are defined from kadaster data. Based upon this data the total area is 13170 m², the total living space is 14176 m², while the built area is 7320 m². This results in a FSI of 1.05, GSI of 0.54 and OSR of 0.43, which results in a block type low rise building typology. Building block B shows a lower values with a total area of 7335 m², living space of 9297 m² and built area of 3375 m². This results in a FSI, GSI and OSR of 1.27, 0.46 and 0.43 m²/m² respectively, which is also related to a low rise block type building typology.

When combining the data and taking the streets into account the factors for the fabric can be determined. This resulted in a total area of 33500 m², giving a 0.70, 0.32 and 0.97 FSI, GSI and OSR respectively for the fabric. In figure 4.4 this results in a low rise block type build typology for the Oranjeboomstraat. Taking the amount of layers in consideration a large difference is observed between both building blocks, which results in an average of 2.2 layers in the case area.

At the end of this chapter a short overview of all the considered information is given and a comparison is made.

	Oranjeboomstraat A	Oranjeboomstraat B	Oranjeboomstraat fabric
FSI [m ² /m ²]	1.08	1.27	0.70
GSI [m ² /m ²]	0.56	0.46	0.32
OSR [m ² /m ²]	0.41	0.43	0.97
L [-]	1.94	2.75	2.19
Building typology	Low rise block type	Low rise block type	Low rise block type

Table 4.2: Urban form and density factors of the Oranjeboomstraat

4.2.3 Characteristics of the build environment

For both locations a short description is given of the local build environment. Firstly, the building and roofing materials are addressed, according to Google street-view imagery. Secondly, the street profile is discussed according to the green area, type of vegetation and type of surfaces. Thirdly, the building-height of the individual buildings is discussed, which completes the context of the cases.

Building materials of the cases

This sections begins with addressing the roofing style and material. After which the paving materials and building height and ages are discussed, based upon figure 4.7, showing impressions of both locations.

Figure 4.2 shows clearly the roofing materials used throughout both cases. The roofing material of the Oranjeboomstraat is mostly grey shingles or possibly stones. With respect to the Bredalaan shows the figure red roof tiles, with exception of the most north-eastern building which has light grey tiles. Furthermore, in both cases most of the garden sheds seem to have shingles and at the Bredalaan red tiles are used for some sheds. All buildings at the Oranjeboomstraat have flat roofs, while the Bredalaan's main buildings have sloped roofs, in the next part this is discussed in detail.

To get an understanding of the building materials Google Earth's street view imagery is used. Four figures of each location are used to show the building materials and street profile, which are discussed in the next section, the impression is presented in figure 4.7. The houses at the Bredalaan consist of mostly red brick buildings with gabled roofs, while the Oranjeboomstraat has a mixture of red and yellow bricks. Furthermore, most buildings at the Oranjeboomstraat are four stories high, while the Bredalaan mostly is build up to three stories. The Bredalaan is characterized by front gardens and gardens at the back of the buildings, while front gardens are not present at the Oranjeboomstraat.

Building ages of the cases

The building ages are estimated through the Dutch cadastre (Kadaster, n.d.). Two eras can be distinguished at the Oranjeboomstraat. The red brick buildings of the Oranjeboomstraat are from around 1900, while the more yellow buildings are from the late 1900's. The Bredalaan's buildings are built in the period between 1930–1950, with exception of the buildings with the grey roofs. The building in the middle of the case area is build in 1960, while in 2018 the others were built.

Street profile and pavement materials of the cases

Based on figures 4.2 and 4.7 the street profile, street material and width can be determined. Furthermore, the types of green, like grasses or trees, along the streets are addressed.

To start with the Oranjeboomstraat's case dimensions. As stated before the entire cross-sectional area is considered, has a width of 120 metres. The back gardens on the most western building block are 16–18m deep, while the gardens in between the other two blocks span a width of 28m. The exception is the area between the highest building of the middle row, the garden of this building is only 10m wide. The street is characterized by wide concrete brick pavements (+/-2m) on both sides of the street, with adjacent grey basalt bricks for parking (+/-2m) followed by red (+/-2m) and then black(+/-4m) asphalt. The center of the street is characterized by a green grass area of about 4 metres, with adjacent basalt brick pavement, destined as parking locations. In between every two to three parking spots there is a tree planted. The total width of the street becomes 28 metres from facade to facade.

The Persoonshaven, which is the northeastern border of the case area, is characterized by concrete pavement, followed by a basalt brick parking area and road, which figure 4.7 image A.3 shows this clearly.

Secondly, the profile materials and case dimensions of the Bredalaan. As seen in figure 4.7, an equal division of the main street profile is visible, with exception of an additional bike lane and parking and an addition of small gardens on the front of each building. Due to these changes the total width from facade to facade is 30 metres, which is 2m wider with respect to the Oranjeboomstraat. The southern gardens are 12m and northern gardens together with the path in between 30 metres. The Wielantstraat, visible in figure 4.7 B.3 and B.4, shows a similar division of the surface as the Persoonshaven in Rotterdam. The sole exception is the amount of trees, while Rotterdam has every 6-8m a tree, the Wielantstraat shows only a couple of larger trees.

The street surface of the streets that connect the Bredalaan and Wielantstraat, is the last aspect addressed. The material used is red bricks from crossing to crossing, while the crossings show grey basalt bricks.

Height of the buildings in the case areas

The building heights are based upon a National Height Database (AHN) which uses calibrated laser altimetry data measured with planes (Actueel Hoogtebestand Nederland, 2020). This technique results in an accuracy of 5cm per square metre. AHN3's data is used for several sections to create an understanding of the building height within the cases.

The Oranjeboomstraat is characterised by three building blocks in North-West/South-Eastern trajectory. Perpendicular to this direction four cross-sections, visible in figure 4.2, are chosen to establish a detailed height



A.1



B.1



A.2



B.2



A.3



B.3



A.4

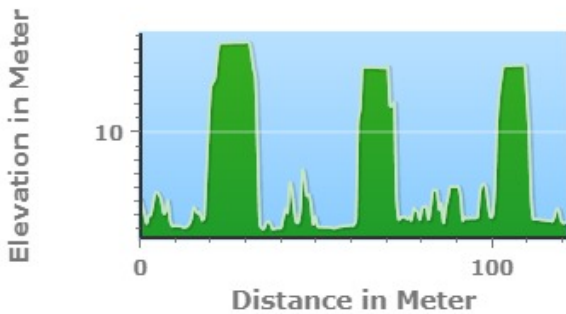


B.4

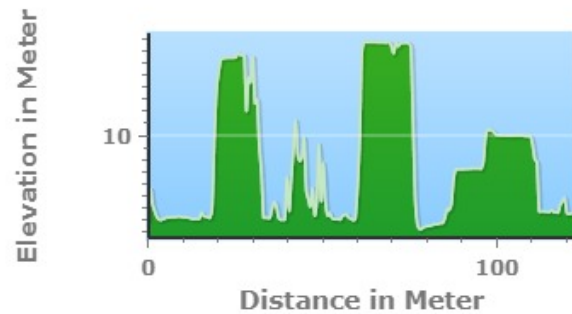
Figure 4.7: Impression of both cases. On the left and right hand side four pictures of each case are visible, the Oranjeboomstraat and respectively Bredalaan (Google LLC., 2015, January 10/2015; Google LLC., 2020, April 16/2020).

profile of these buildings. AHN's data concludes that the most western building blocks have flat roofs with an elevation of 13-15m with respect to ground level. But at the southern border there is a building with an height of 8m with respect to ground level. The building blocks in the middle of the three rows vary from 11-14m, The most southern block of the Oranjeboomstraat is 12m and the building adjacent to this one has a height of 14m. Furthermore, the garden of this building lies 1m lower than the surrounding areas.

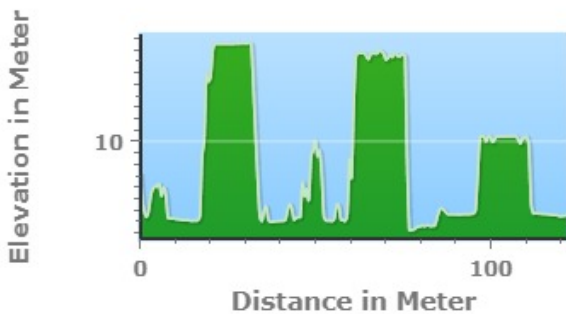
The third row of buildings consists of two different buildings. The most northern building has an height of 11m, while the southern building is 7m with a lower section of 4m. A detailed overview of the cross-sections is visible in figure 4.8,



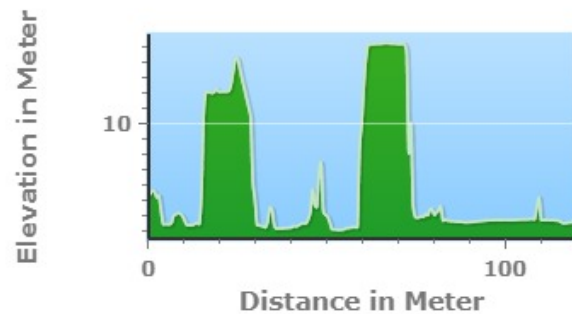
Cross-section AA-AA' of the Oranjeboomstraat.



Cross-section CC-CC' of the Oranjeboomstraat.



Cross-section BB-BB' of the Oranjeboomstraat.



Cross-section DD-DD' of the Oranjeboomstraat.

Figure 4.8: All cross-sections with height information of the Oranjeboomstraat (Actueel Hoogtebestand Nederland, 2019).

The identical approach is used to determine the height of the building's at the Bredalaan. For this location three cross-sections are chosen to determine the building height. From the cross-sections can be concluded that all main buildings have gable-roofs, while on some corners the roofs are constructed as cross-gables.

The buildings are east-west oriented and built into three rows. The most northern buildings have sloped roofs from 5-7m, likewise the building height of the most eastern row of buildings of the middle row is 5-7m high too. The house in the middle of this row, as can be seen in cross-section FF-FF' in figure 4.9, is slightly higher and is sloped from 5-9m, with a small 3m high extension. The other three buildings have sloped roofs from 6-10m.

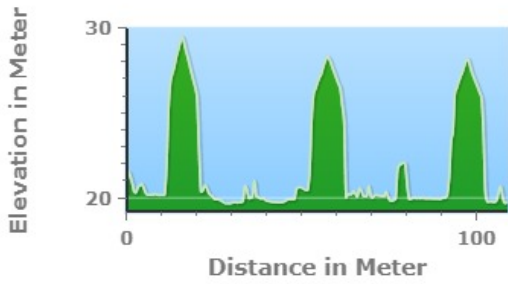
The average building height of the Oranjeboomstraat is slightly higher with respect to the Bredalaan. Furthermore, the Bredalaan has sloped roofs, while the Oranjeboomstraat has flat roofs. At last, there are garden sheds spread through-out both locations, these have heights varying from 3-4 metre.

The sky view factor of the cases

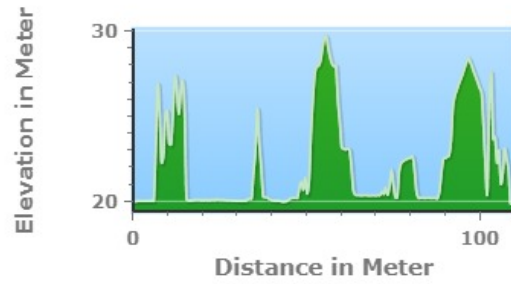
Based on the buildings height and vegetation within the cases, the SVF can be determined for the case area. Figure 4.10 shows the distribution of the SVF for both cases together with the average value and standard deviation.

The SVF of the Oranjeboomstraat of 0.470 is slightly lower than the SVF of the Bredalaan with 0.475. This means that at the Oranjeboomstraat less direct sunlight shines on the ground surfaces, possibly causing a

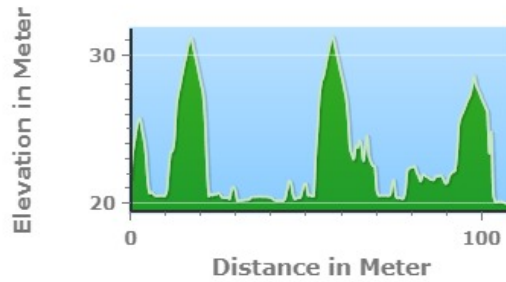
lower increase of the UHI-effect.



Cross-section EE-EE' of the Bredalaan.



Cross-section FF-FF' of the Bredalaan.



Cross-section GG-GG' of the Bredalaan.

Figure 4.9: All cross-sections with height information of the Bredalaan (Actueel Hoogtebestand Nederland, 2019).

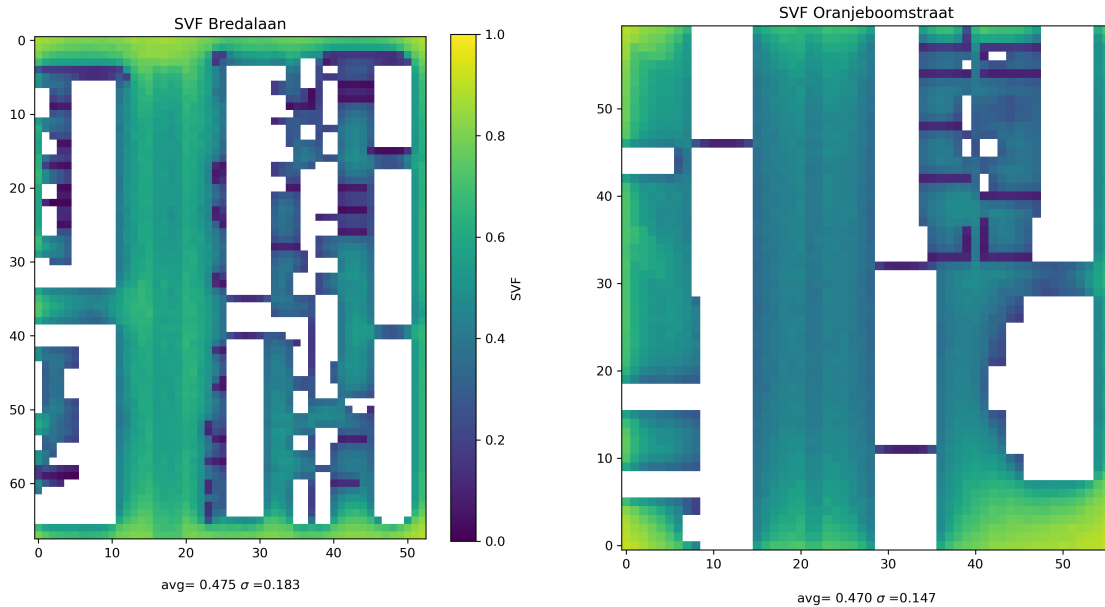


Figure 4.10: The sky view factor of each case. At the bottom of the maps the average value and the standard deviation are given, to indicate the range of values.

4.3 Meteorological environment of the case studies

The Bredalaan and Oranjeboomstraat are discussed according to their meteorological measurements at Eindhoven's weather station near Eindhoven Airport, and respectively Rotterdam's weather station near Rotterdam-The Hague Airport. Eindhoven's weather station is situated 4.4 km from the Bredalaan, while the distance between Rotterdam's weather station and the Oranjeboomstraat is 7.8 km. Besides meteorological circumstances, the potential severity of the urban heat island is discussed.

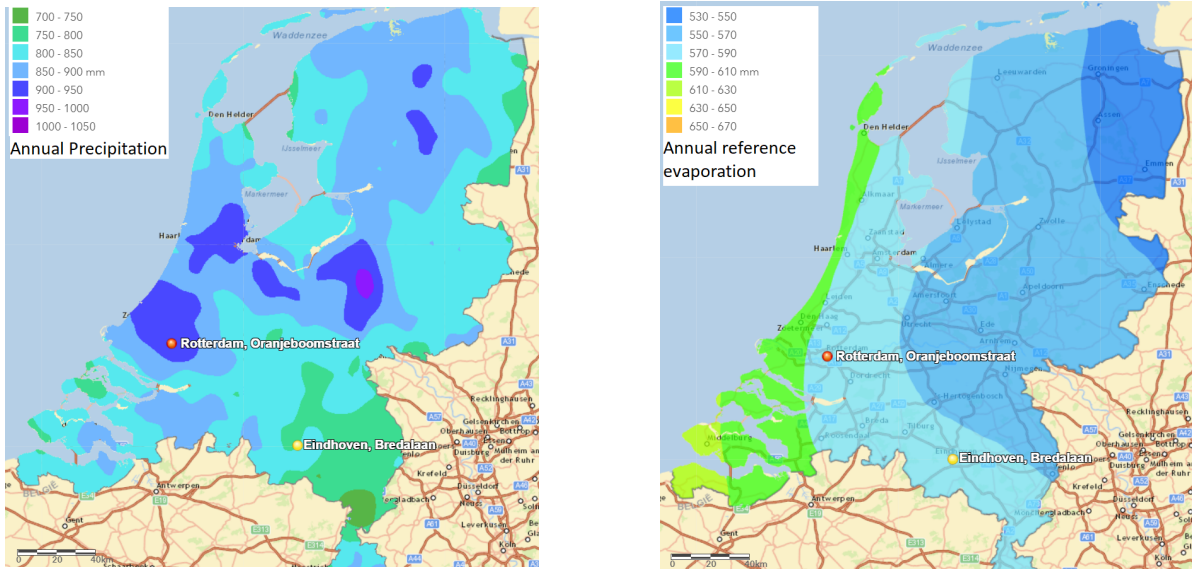


Figure 4.11: The average annual precipitation and reference evaporation over 1971-2010 (KNMI; ESRI, 2020a; KNMI; ESRI, 2020b)

Within meteorology it is interesting to look at yearly average trends and extremes. These give an impression of the climate of the cases. Therefore the trends between 1986 and 2015 are given, while 2018, the year of interest, is shortly discussed. Trends indicate the general state of a system, while the extremes show the potential threats and opportunities to the system. The trends and extremes are discussed regarding three meteorological events:

- Temperature;
- Precipitation;
- And drought.

An overview of both locations with respect to their average precipitation and evaporation is given in figure 4.11. As can be seen, the yearly evaporation rates are in the same range, while there is a substantial difference in precipitation. Eindhoven's Bredalaan copes with 700-750mm of precipitation, while Rotterdam's Oranjeboomstraat copes with 900-950mm. Figures 4.12 & 4.13 look into the detailed values of the monthly average precipitation and potential evaporation. These clearly show, that over a 30-year time-span from 1986-2015, a trend of a dry April and wet July occurs, while the potential evaporation reaches an average peak of about 95–100mm in July. Given the standard deviations of the reference crop evaporation, it can be observed that the evaporation is rather stable over the years, while the precipitation fluctuates heavily. The standard deviation for the potential evaporation lies between 1.2 and 15 mm per month, while the standard deviation for precipitation ranges from about 20–40mm per month.

Observing solely 2018, a severe drought occurred with a maximum precipitation deficit of respectively 322mm in Eindhoven and 263mm in Rotterdam. As earlier shown in Chapter 2, based on standardized Gumbel variate, a return period can be determined for this specific drought. For the southeastern region of the Netherlands figure 2.13 shows a return period of about 35 years for the precipitation deficit of 322mm, while for a drought of 263mm a return period of about 15 years. Figure 4.12 shows the development of these specific droughts over 2018 for Eindhoven.

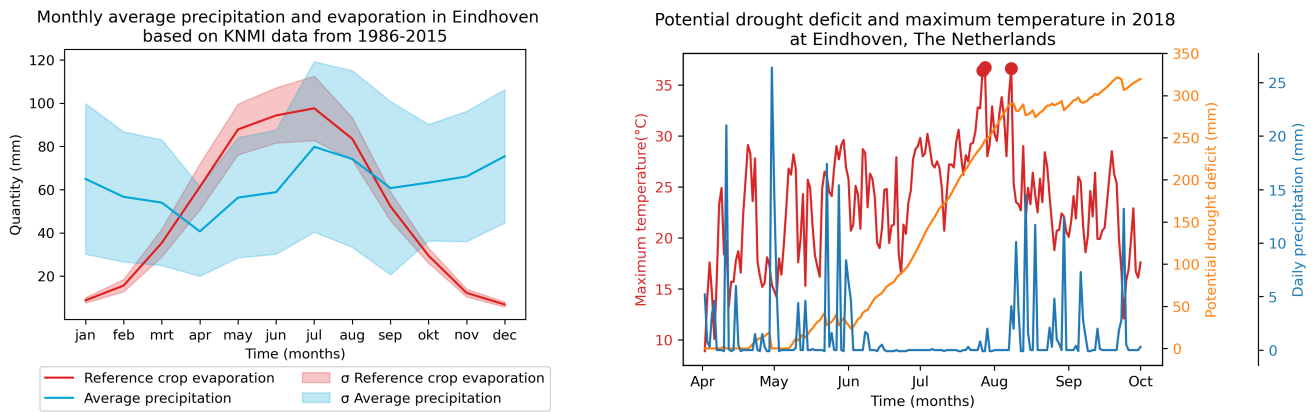


Figure 4.12: On the left an overview of Eindhoven's average precipitation and evaporation over 1986-2015 with monthly standard deviations given. On the right the daily temperature and precipitation with the development of the potential precipitation deficit of 2018 between April and October. The red dots show temperature peaks of 36.4°C , 36.7°C and 36.6°C (Data used from KNMI, 2020a).

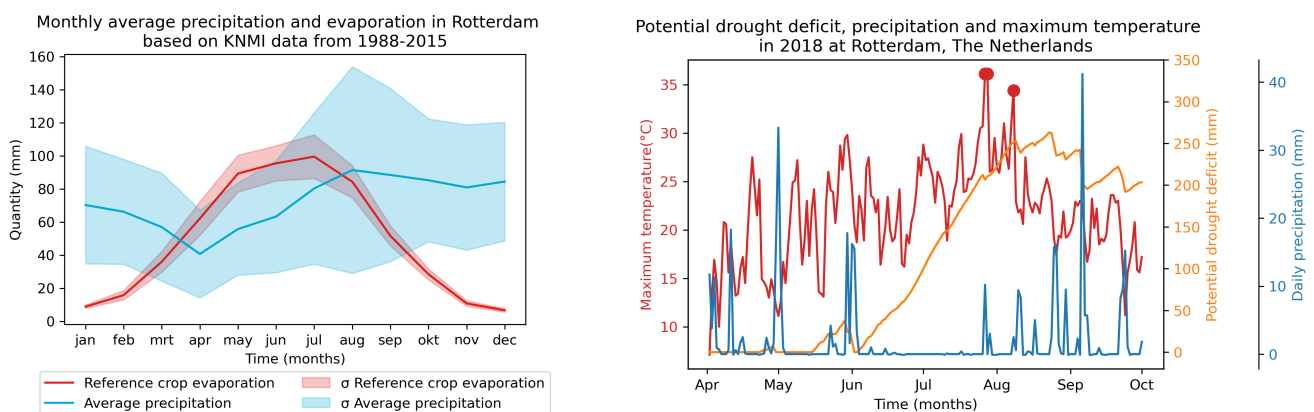


Figure 4.13: On the left an overview of Rotterdam's average precipitation and evaporation over 1988-2015 with monthly standard deviations given. On the right the daily temperature and precipitation with the development of the potential precipitation deficit of 2018 between April and October. The red dots show temperature peaks of 36.1°C , 36.1°C and 34.4°C (Data used from KNMI, 2020a).

Figure 4.12 shows 2018's crop growth season, from April till September, with the drought severity peak occurs at the end of August, simultaneously with an heat wave with the three warmest days of 2018. These peaks occurred on 26 and 27 July, and 7 August with temperatures of 36.4°C , 36.7°C and 36.6°C respectively.

For Rotterdam, a comparable pattern as in Eindhoven can be seen in the monthly average evaporation rate. These have standard deviations between 0.95 and 13mm. Looking at 2018, an identical curve till September is seen with respect to the potential drought deficit, peaking around this time. The temperature trend is also comparable with a heatwave in the same period with temperature peaks of 36.1°C , 36.1°C and 34.4°C .

To conclude, the yearly evaporation rates do not fluctuate severely between years, while precipitation quantity varies greatly. Specifically, Eindhoven's 2018 drought trend's maximum occurs nearly simultaneously with extreme temperatures. The period from July 24 till August 8 is interesting to research and to see the effects of these simultaneous peaks.

Severity of the Urban Heat Island

A prediction of the local severity of the UHI is shown in figure 4.14. This effect is predicted based upon population density, wind velocity on a representative day, percentage of green area, amount of surface water and impermeable surfaces. This results at the Bredalaan in an estimated UHI-effect from 1.4°C till more than 2°C , while in Rotterdam the effect shown is between 1.2°C and 1.6°C . The lower increase at Rotterdam can be a result from the cooling effect from the river nearby.

4.4 Soil composition of the case studies

The soil structure of both locations is important for modelling purposes and possible implementation of water retention measures and the possible effect on evaporation. The soil profile and compositions are based on

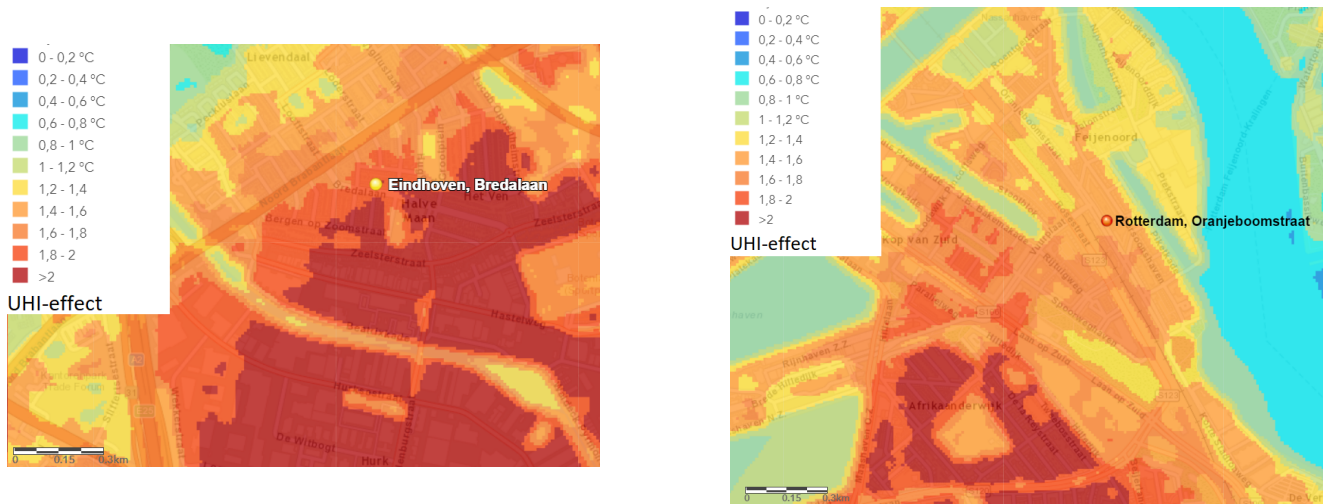


Figure 4.14: The predicted UHI-effect in both Rotterdam and Eindhoven. This model is based on several anthropological, spatial and meteorological parameters.(KNMI; ESRI, 2020c).

GeoTOP v1.4 (Basisregistratie Ondergrond, 2020). GeoTOP is a detailed model of the top layers of the Dutch subsoil based on 430.000 boreholes over the Netherlands. Therefore, small deviations of the actual soil composition could occur. Since every soil type has a specific range of parameters, which determine its characteristics, the composition should be approximated as closely as possible. The model has a resolution of 100x100m and 50cm vertically and therefore usable for this study. Furthermore, GeoTOP’s database also consists of profiles of nearby drill samples, which could be used for further reference.

Based on GeoTOP’s model it can be concluded that the top layer in the Bredalaan is of anthropogenic matter (TNO, 2020a), followed by layers of loamy or clayey sand and fine sand. The deeper layers consist of again loamy or clayey sand and fine sand.

The most probable lithoclass in the Oranjeboomstraat based on GeoTOP consists solely of anthropogenic matter until a depth of 3.5m (TNO, 2020b), since this is not detailed enough the lithoclass of a nearby borehole is chosen. The borehole chosen is at the nearby Jalonstraat with serial number: B37H0129. This borehole shows a sandy layer followed by a clay and sandy clay layer(TNO, 2020c). Figure 4.15 shows the soil profiles of both locations.

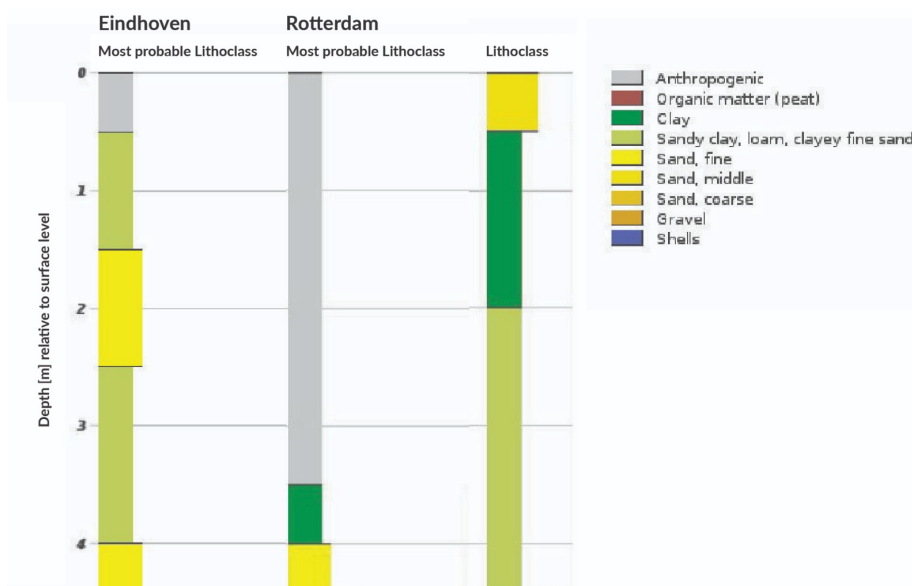


Figure 4.15: Lithoclass of the Bredalaan and the Oranjeboomstraat based on GeoTOP, with an additional Lithoclass from a borehole at the Jalonstraat in Rotterdam (TNO, 2020a; TNO, 2020b; TNO, 2020c).

4.5 Overview of the cases and simulations

The upcoming paragraphs give a complete overview of the different scenarios and type of simulations of the cases. After this overview, the most noteworthy input parameters are given. Discussing the input parameters gives a tangible idea of the cases, different scenarios and type of simulations.

Case studies	Type of simulation	Scenario of simulation	Relative soil moisture content
Bredalaan and Oranjeboomstraat	Day	Current	0%
			25%
	Series	Current	50%
			75%
Series	Greener	100%	
			Dry (0%) Irrigated (100%)

Figure 4.16: Overview of the case studies, the scenarios, type of simulations and the relative soil moisture content.

To strengthen the understanding of the case's approach, figure 4.16 shows an overview of the approach. Within the figure the two cases are displayed, which type of simulations are performed, the scenarios applied and the initial soil moisture content. To elaborate on figure 4.16, there are two case studies and for both case studies a simulation with the duration of day and a series of five days is applied.

The single day simulation is only performed on the current scenario with five relative soil moisture contents with respect to field capacity in the subsoil. On the other hand, for the series, besides the current scenario, a greener scenario is simulated. For the series only two soil moisture contents are calculated.

So there are five single day and four series simulation per case bringing the total number of simulations at eighteen. In the upcoming paragraph the current and greener scenario of both cases is discussed. After which, the meteorological parameters of the single day and series simulation are shortly discussed.

4.5.1 Scenarios of the series simulations

For each case four scenarios are simulated. First of all the current situation is addressed without irrigation. The second scenario applied is the usage of irrigation on the current situation, i.e. the simulation is started at 100% relative soil moisture content and ENVI-met simulates irrigation to keep this value stable. The third scenario increases the amount of green infrastructure within each case area. The fourth scenario simulated both irrigation and an increased green infrastructure. Figure 4.17 shows both cases' increased green infrastructure. The largest changes in green infrastructure are the increased amount of green infrastructure from façade to façade, the Bredalaan in the front gardens of the houses and the Oranjeboomstraat's public green has increased. Besides, the back gardens of each case have increased amount of green infrastructure too.

For both the front and back gardens has been chosen to increase the amount of grass and the amount of hedges in between two plots. Furthermore, where possible in the back gardens small trees up to 5 metre are added to create shade and increase evapotranspiration.

Meteorological input parameters of the cases

First the meteorological parameters of the single day simulation are given, after which the input of the series simulation is discussed.

For each case a single day, June 21 from 4 a.m. till June 22 4 a.m., is simulated with, by KNMI's definition, tropical temperatures and humidity. The temperatures and humidity vary between 18°C to 35°C, and 60 to 70% respectively during these runs. Furthermore, the simulations are performed with a wind velocity at 10m of 1 m/s with a direction perpendicular on the general orientation of the cases, 7° and 123° for Eindhoven and Rotterdam respectively. Appendix C shows the sensitivity of the Oranjeboomstraat to wind changes on the

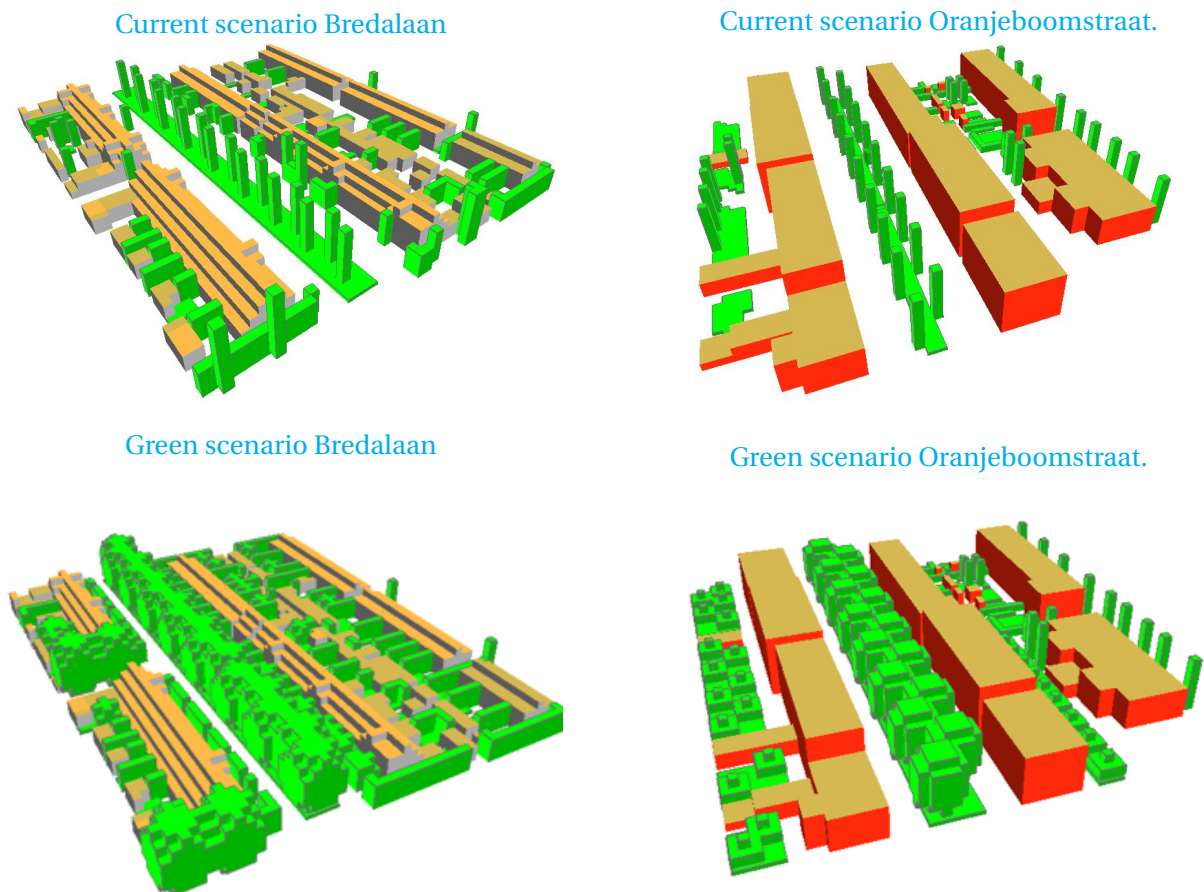


Figure 4.17: Three dimensional presentation of the increased green infrastructure scenarios for both the Bredalaan and Oranjeboomstraat. Both locations have an increased amount of green infrastructure from façade to façade, the Bredalaan in the front gardens of the houses and the Oranjeboomstraat's public green has increased. Besides, the back gardens of each case have increased green infrastructure too.

average temperature within the case area.

For the five sequential days, 4 a.m. July 27 till 4 a.m. August 1st, are simulated with meteorological data from the Royal Dutch Meteorological Institute (KNMI). For each case meteorological data from the closest weather station, Eindhoven and Rotterdam respectively, is used. The input data retrieved from KNMI that is used is:

- Temperature;
- Wind direction;
- Wind velocity;
- Precipitation; and
- Humidity.

Furthermore, due stability issues within ENVI-met several wind parameters have been adjusted to create a stable simulation. For an overview of the input data and the manipulated values, see Appendix E

4.6 A short comparison of the two cases

The two cases are briefly discussed, to show their similarities and distinctions for each other. Their overall dimensions, material usage and green fractions are given.

The dimension and characteristics of the cases are shortly compared in table 4.3, showing both the Oranjeboomstraat and Bredalaan. As can be seen there is a 40° difference in orientation. When comparing the building heights, there is a difference of one till two stories or on average 5 metre, but when observing tables

4.1 & 4.1 the amount of building layers are relatively similar. The building ages have a wide range throughout both cases, with both cases buildings of the early, mid and late twentieth century.

Comparing the case size, vegetation ratio and street profile dimensions, shows comparable garden depths, street profile width and total size of the cases. When comparing the surface usage of both locations it can be seen that the locations have a comparable vegetated fraction and a difference in built area. This means, while having comparable case sizes, that the public space differs slightly between both cases. When comparing the total amount of living space it can be seen that there is a difference of about $5500m^2$. Due the lower amount of living space the the spaciousness or OSR of the Bredalaan is higher than of the Oranjeboomstaat, which means that at the Bredalaan there is more area available for implementations in (public) space.

Due these differences have these locations a different building typology. The Bredalaan consists of a low rise street building typology. At the Oranjeboomstraat the ratio of urban area and built area are slightly higher, while the total living area is different, resulting in a building typology of a low rise rise block type building block.

At last the differences in soil composition are discussed. Both cases have a antropogenic soil layer, which is simulated as a sandy layer within ENVI-met. Below the top 0.5m the difference in main soil layer starts to become clearer. Where in Rotterdam a clay layer is followed by a sandy clay layer, the Bredalaan in Eindhoven has a clayey sand layer, below which a sand layer, a sandy clay and another sand layer is present. Therefore the shallow roots will extract water from similar layers, while at average root depth vegetation has to extract water form a different type of layer. Deeper roots at both cases will again extract water from similar layers.

	Oranjeboomstraat	Bredalaan
Orientation	145-325 ^o	105-285 ^o
Building height (Low, average, high [m])	8, 14, 16	7, 9, 10
Youngest building	1995	1960*
Oldest building	1898	1920
Garden depth [m]	13	14
Street Profile dimensions (Façade-façade [m])	29	30
Total size case [m ²]	14400	14416
Total built area [m ²]	4925	3500
Total living area [m ²]	13200	7765
Green surface ratio initial situation [-]	0.17	0.21
Green surface ratio greener scenario [-]	0.40	0.36

Table 4.3: Short comparison of the cases with respect to their characteristics. *A group of buildings is renovated around 2018.

Chapter - 5

Results of the models

This chapter presents the results of the simulated urban environment. Firstly, the results of the daily simulations with variable soil moisture profiles are presented. Secondly, an elaboration of the influence of the soil composition on the results of the daily simulations is given. These two elaborations are followed by the discussion of the two cases regarding the heatwave of 2018 in The Netherlands. For this period several urban scenarios are simulated.

Multiple parameters are presented for each simulation type. Firstly, the simulated air temperature and PET are discussed and compared. Secondly, the extremes within each case are observed regarding thermal extremes, occurrence and location. Thirdly, the resulting urban heat island effect with respect to the inflow, or local urban heat island effect, is presented. Lastly, the relationships between the soil moisture content, simulated air temperature and evaporation are presented. The next chapter discusses this study and its results in detail, see chapter 6

5.1 Results of the single day simulations of both cases

The single day simulations create a controlled meteorological and urban environment, which can be used as reference output for the heat wave's time series. Besides, the single day simulations enables to identify which output parameters are relevant to this research. Furthermore, these simulations give insight in the range of their values.

For both cases several meteorological and ground water parameters are chosen as input for these simulations. Chosen is to simulate a dry, warm to hot June 21st from 4 a.m. to 4 a.m. the following day with temperatures and humidity varying between 18°C to 35°C, and 60 to 70% respectively. June 21st is chosen as the reference date, because it is the day with the most daylight. The simulations are performed with varying soil moisture contents with respect to field capacity, with 0% meaning the roots can not extract water and 100% being at field capacity. Furthermore is chosen for a constant low wind speed of 1 m/s with a direction perpendicular on the general orientation of the cases, 7° and 123° for Eindhoven and Rotterdam respectively.

5.1.1 Results of single day simulations regarding simulated air temperature and PET

The simulations results are discussed regarding simulated air temperature and PET. Starting with the air temperature in Eindhoven and Rotterdam during the entire series. After discussion of the air temperature and PET, the extreme air temperatures and PET of green infrastructure for both cases are shown.

The first section shows the temperature development for various soil humidities for both cases, supported with tables of the driest and wettest soil humidities of one of the cases. This data is shown to understand the effect of the average soil moisture content with respect to air temperature. Besides, analyzing the spatial distribution in heat maps gives insights in the warmer areas within each case, which potentially benefit from irrigation.

The second section presents the PET development between 8 a.m. and 7 p.m. for the driest and wettest soil. This gives an indication in the ranges of the PET and effect of irrigation on the PET, which shows the effect of irrigation on the PET.

The third section show the temperatures of green infrastructure to show the effect of irrigation on the air temperature. Since the previous paragraphs showed a relationship between the temperature of green area and the soil moisture content, this relationship is explored further

Simulated air temperature of the cases

To begin with figure 5.1, these graphs shows the temperature development for all five relative soil moisture contents for the simulated period. It can be seen that both cases follow an almost identical temperature profile with a maximum median just below 32.5°C, but both reaching temperatures around 35°C.

When zooming into the data points and their respective locations in figures 5.2 and 5.3, it can be seen that the warmest locations are at the edges of the areas for both a dry and wet soil. What is more noticeable is that the average and maximum air temperature are lower for both areas.

When looking at the temperature difference [ΔT] in figure 5.4, it can be seen that almost all data points within both areas become cooler from irrigating and maintaining the soil of the green areas saturated. Tables D.1 and D.2 in Appendix D show the hourly temperature data for a dry and irrigated Oranjeboomstraat. Furthermore, the larger temperature reduction seems to be around green infrastructure, section 5.1.1 analyzes this relationship further.

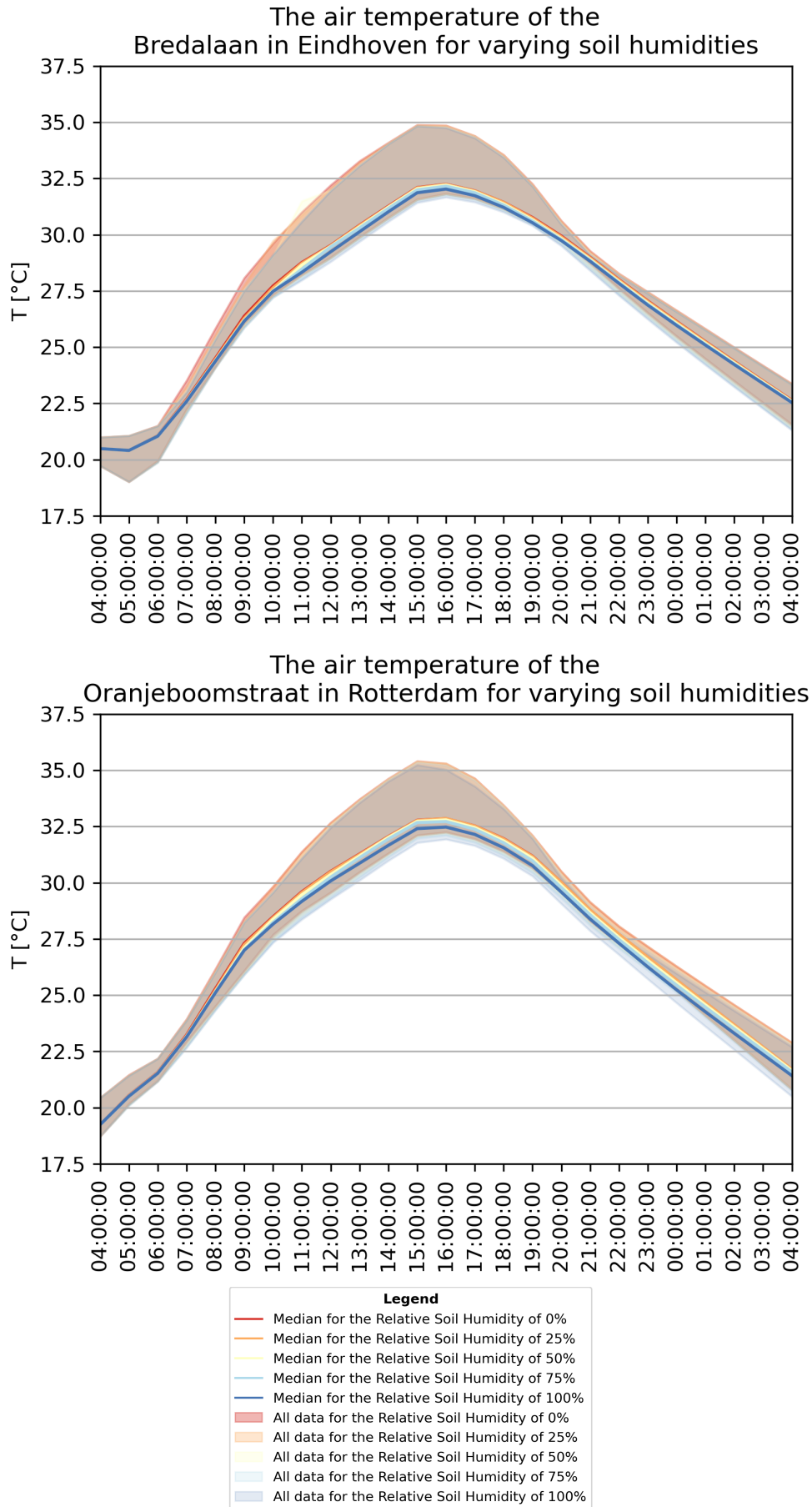


Figure 5.1: Presentation of the air temperature development at the Bredalaan in Eindhoven and Oranjeboomstraat in Rotterdam.

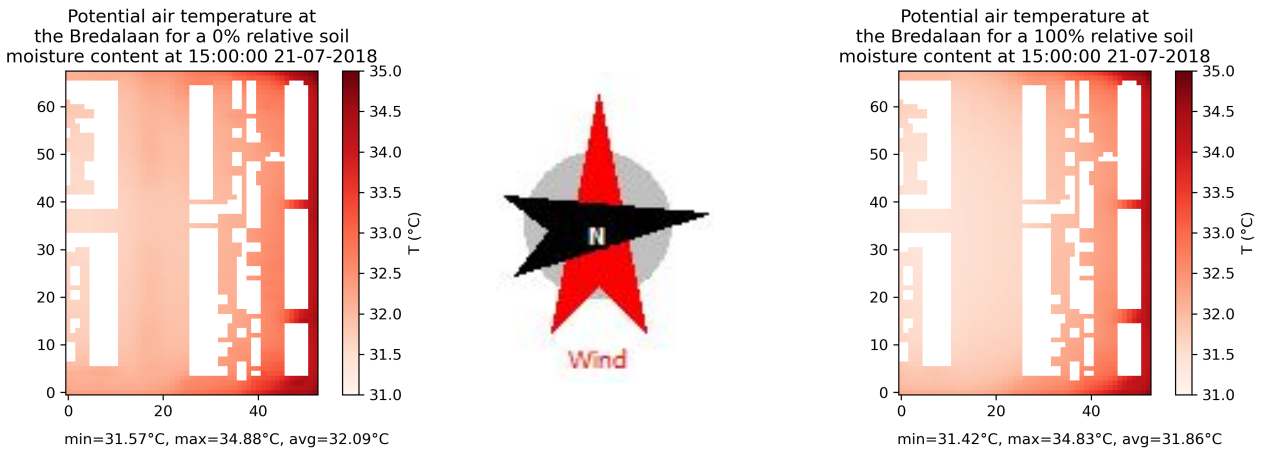


Figure 5.2: Heatmap of the Bredalaan showing the warmest and coldest areas within the area for a 10% and 100% relative soil moisture content.

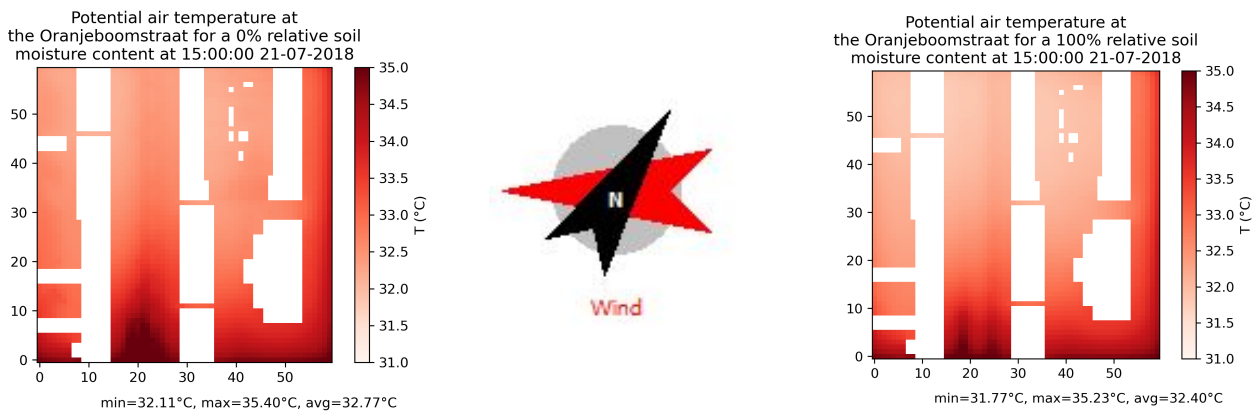


Figure 5.3: Heatmap of the Oranjeboomstraat showing the warmest and coldest areas within the area for a 10% and 100% relative soil moisture content.

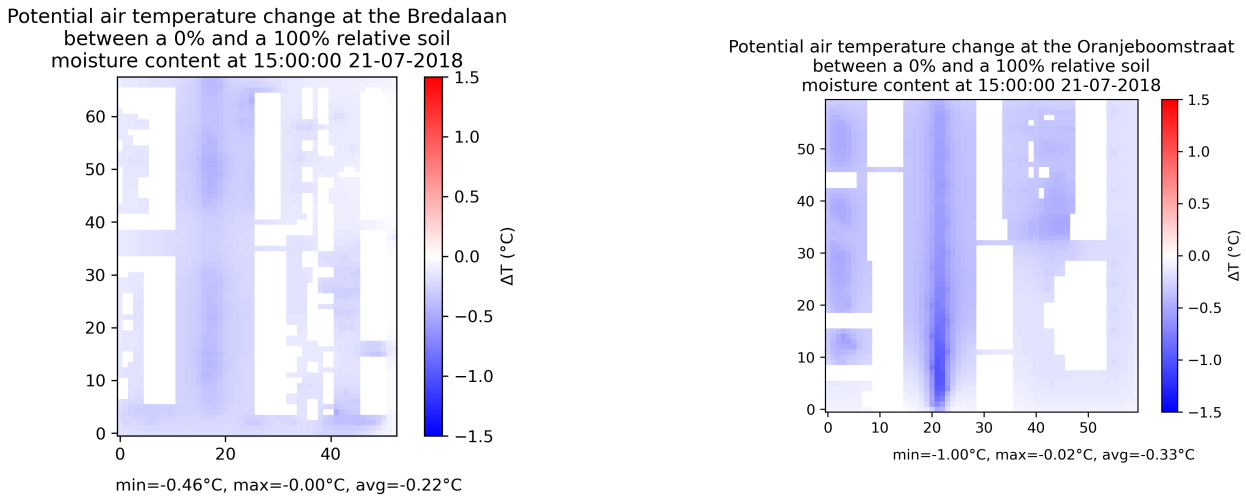


Figure 5.4: Absolute temperature difference between a 10% and 100% relative soil moisture content for both the Bredalaan and Oranjeboomstraat.

Results of the single day simulations regarding the Urban Heat Island effect of the cases

The Urban Heat Island effect is described as the difference in temperature between rural and urban atmospheres. In this instance the simulated urban heat island effect is the temperature difference between the inflow at the start of each simulated hour and the temperature at the end of the hour. This paragraph shows the UHI-effect at both cases at several moments of the day and for several soil moisture contents.

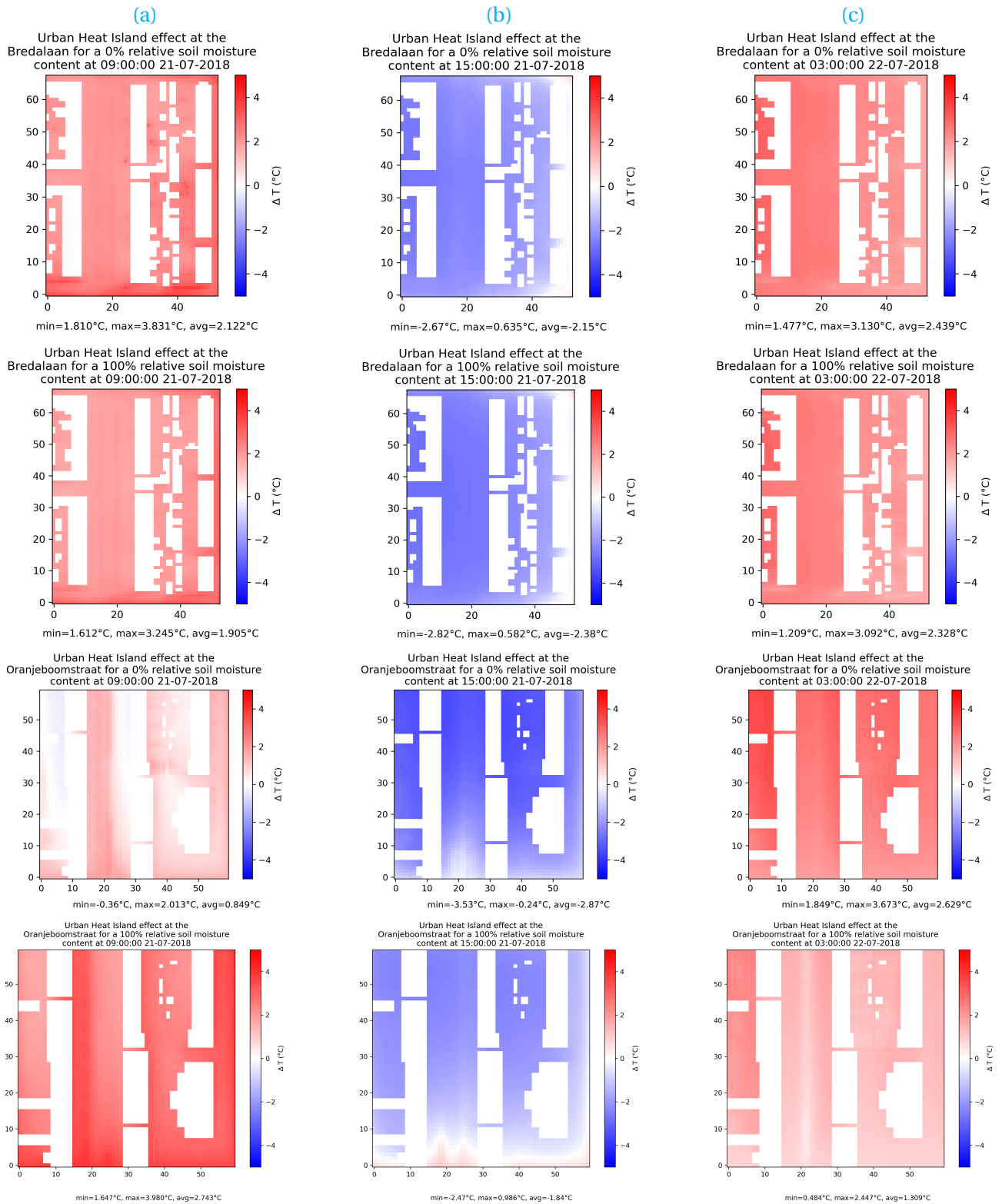


Figure 5.5: UHI effect heat maps of the driest and wettest scenario of both cases. Column a shows the UHI-effect at 9 a.m., b at 3 p.m. and c at 3 a.m.

The heat maps in figure 5.5 show the effect of the urban environment on the air temperature at both cases at 9 a.m., 3 p.m. and 3 a.m. for the driest and wettest scenario calculated. These graphs show that the urban environment increases the average air temperature by 2.12 to 1.90°C in Eindhoven at 9 a.m., while the Oranjeboomstraat in Rotterdam shows an increased temperature of 0.54 to 0.85°C. At 3 p.m. both cases show a lower temperature up to -2.87°C on average at an irrigated Oranjeboomstraat. During the night the nocturnal UHI-effect rises till 2.44-2.33°C and 2.44-1.31°C.

Results of the single day simulations regarding PET of the cases

The Physiological Equivalent Temperature or PET is calculated for a standardized human (according to ISO 7730), to understand how the average human would experience the simulated environment. Since the PET is influenced heavily by solar radiation, only the results between 8 a.m. and 7 p.m. are observed.

Figure 5.6 shows the perceived temperature of both cases rise up to 65°C with a minimum of about 25°C. Irrigating green infrastructure results in a reduction of the minimum PET values, though it does not show a significant reduction of the median PET value, i.e. locations that are already perceived as colder than the median become even colder from irrigation. This suggests that, like the simulated air temperature reduction, irrigation has a positive effect on the PET around green infrastructure.

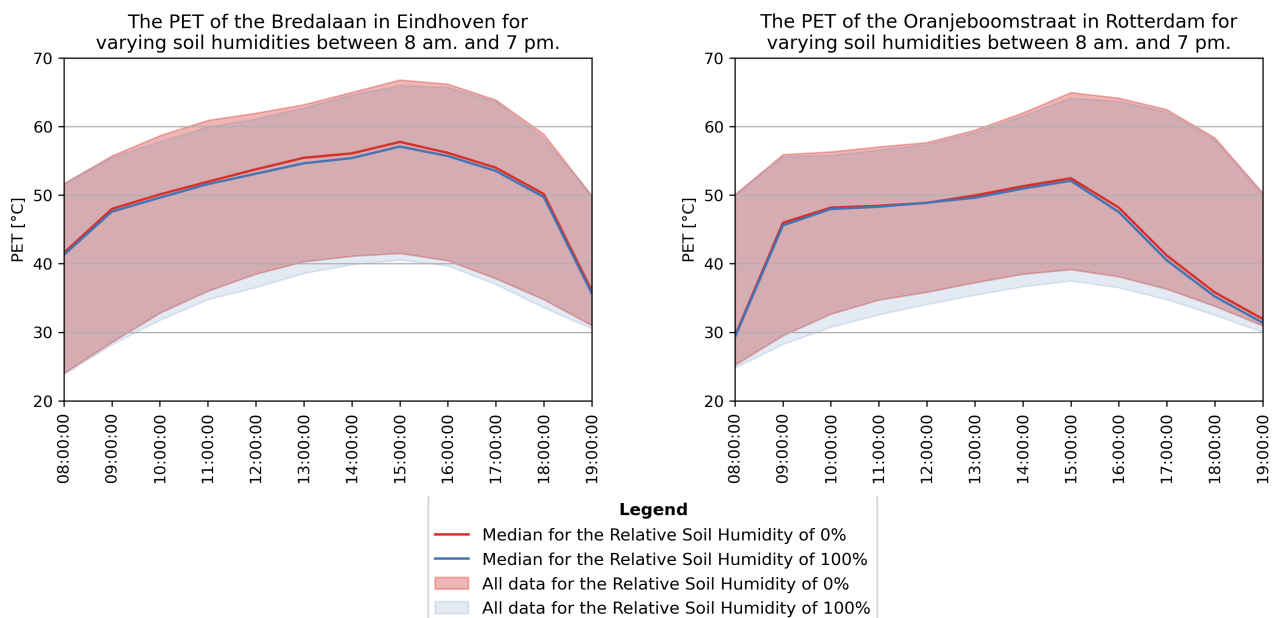


Figure 5.6: Presentation of the PET development at the Bredalaan in Eindhoven and Oranjeboomstraat in Rotterdam. *Both locations show a peak in PET around 3 p.m. maxing out around 65°C for both the 100% and 10% relative soil humidity.*

Results of the single day simulations regarding extreme temperatures around green infrastructure

To show the effect on the green infrastructure by the increased soil moisture content due irrigation, this section presents the hourly extreme air temperature values between the 90th and 100th percentile accompanied by the median value. Doing so gives an insight in the effect of irrigation on just the green infrastructure. This is important to understand the effects of irrigation on local green infrastructure.

Figure 5.1 shows an envelope of the data falling between two sets of data: a relative soil moisture humidity of 10% and 100%. Furthermore, figure 5.4 shows the largest temperature change around green infrastructure. Therefore is chosen to plot the 10% and 100% relative soil moisture humidities in 5.7, showing the extreme air temperatures and median of green infrastructure.

As can be observed in figure 5.7, both graphs show a temperature reduction in both median and extreme temperatures. The reduction of the median value is about 0.5°C during the peak of the day, while the absolute minimum and maximum also decrease by 0.5°C for each case. Tables D.3, D.4, D.5 & D.6 in Appendix D give hourly median, maximum and minimum values for each case and scenario.

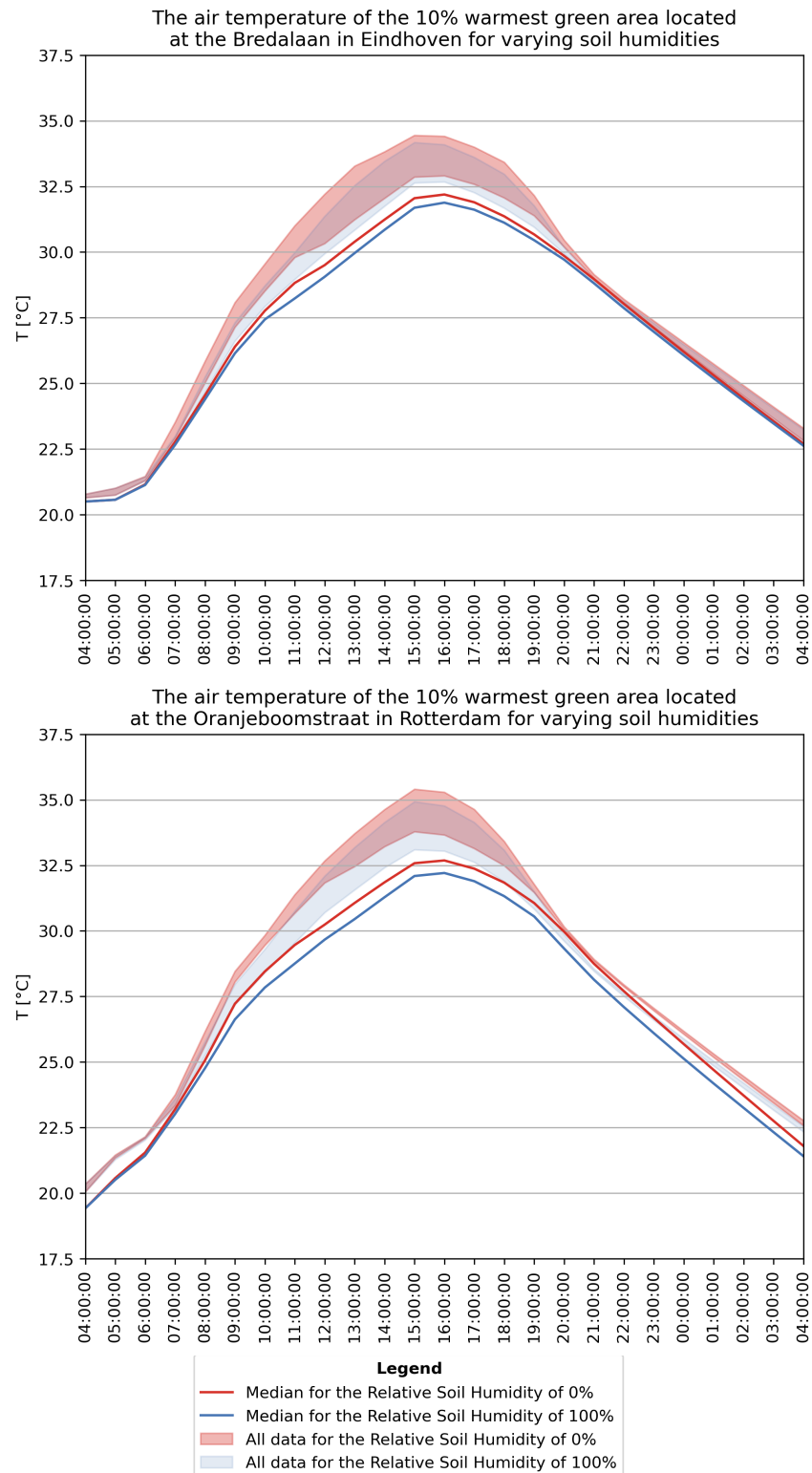


Figure 5.7: Presentation of the extreme air temperature, 90th and 100th percentile, development of green infrastructure at the Bredalaan in Eindhoven and Oranjeboomstraat in Rotterdam.

5.1.2 The relationship of the soil moisture content and simulated air temperature of the single day simulation

Based on the previous sections, a relationship between an increase of soil moisture content and a decrease in temperature is established. To strengthen this relationship, this section presents temperature data with respect to the relative soil moisture content. The data is presented with four graphs and a table of the average values.

Figure 5.8 presents the air temperature values at both 9 a.m. and 3 p.m. for green area with respect to their relative soil wetness to field capacity (RSMC).

All four graphs show at both 9 a.m. and 3 p.m. a reduction of the average temperature while the soil moisture increases. Furthermore, the minimum and maximum air temperature at 9 a.m. are lower for a wetter soil, with small differences between the 75 and 100% relative soil moisture content. At 3 p.m. a similar pattern is seen, though the temperature differences between the three drier soils has become smaller. Table 5.1 presents the average temperature data with respect to the soil moisture profile at 9 a.m. and 3 p.m. for both cases. The Bredalaan has a temperature reduction of 0.3 at both 9 a.m. and 3 p.m., while the Oranjeboomstraat shows at, respectively 9 a.m. and 3 p.m, a temperature reduction of 0.6 and 0.5 °C.

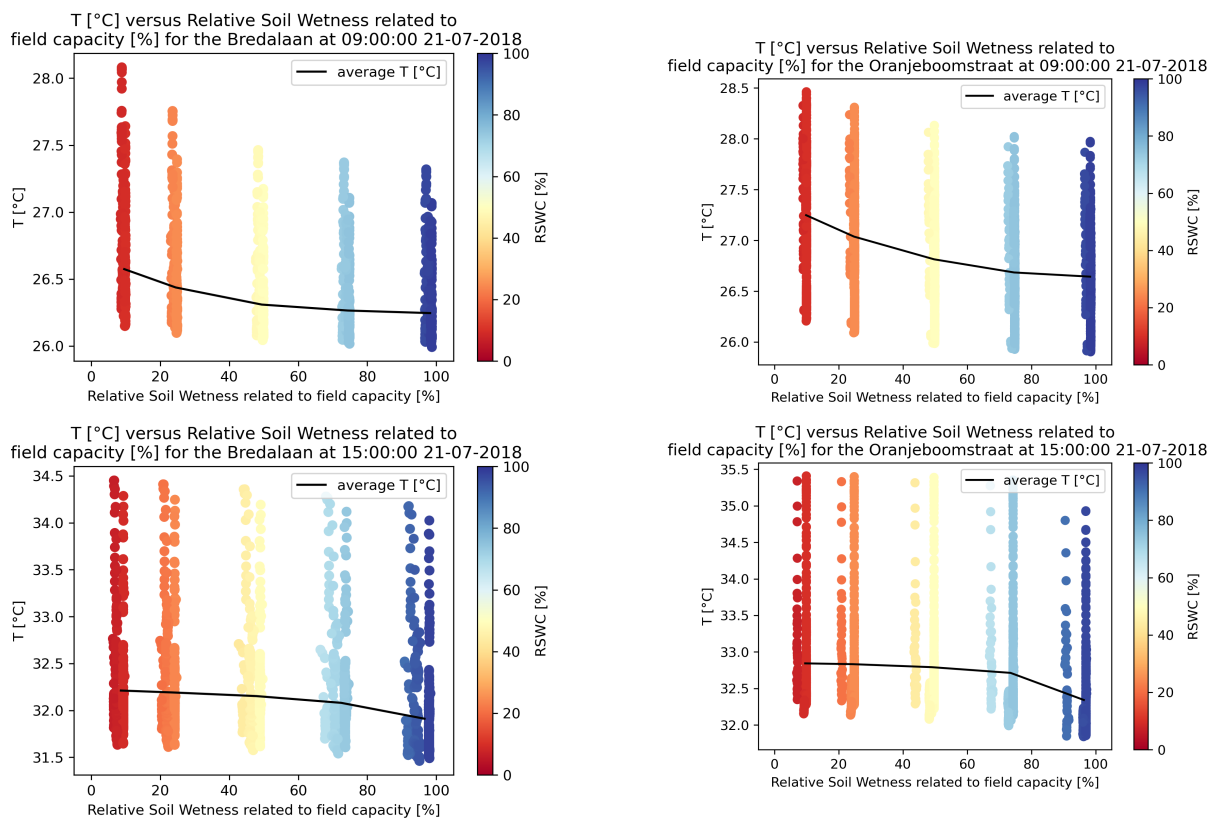


Figure 5.8: Relationship between the relative soil moisture content and temperature around green infrastructure for both cases. *Both cases show a downward trend of the average temperature value for an increase in relative soil moisture content.*

Location(↓)	RSMC (→)	10%	25%	50%	75%	100%
Bredalaan	T [°C] at 9 a.m.	26.57	26.44	26.31	26.27	26.25
	T [°C] at 3 p.m.	32.21	32.19	32.15	32.08	31.91
Oranjeboomstraat	T [°C] at 9 a.m.	27.25	27.04	26.81	26.68	26.64
	T [°C] at 3p.m.	32.84	32.83	32.79	32.71	32.34

Table 5.1: Air temperature of green infrastructure of both cases with respect to the relative soil moisture content.

5.1.3 The relationship of the air temperature and evaporation of the single day simulation

A higher soil moisture content resulted in lower average temperatures. Whether this is caused by higher soil moisture contents or some other effect is now the question. To answer this, the results of both cases at 9 a.m. and 3 p.m. with respect to air temperature and hourly evapotranspiration rate of green infrastructure are presented. With four graphs, showing the interpolated average temperature and hourly evaporation rate for soil moisture profile, presenting the relationship of the air temperature and evaporation. Tables 5.2 & 5.3 show the average temperature and evapotranspiration data.

Figure 5.9 shows a temperature reduction with increasing evaporation rates for all five soil moisture profiles. The Oranjeboomstraat shows at both times strong clusters of evaporation rates, probably linked to vegetation type or location, while the evaporation at the Bredalaan has a larger spread. The average trend of evaporation and air temperature at stays stable over time. For the Oranjeboomstraat, at 9 a.m. the average evaporation increases from 0.26 to 0.52 mm evaporation per hour, with an increased relative soil moisture content from 10 to 100%, results in a temperature reduction of 0.5 °C. At 3 p.m. the evaporation increases from 0.14 to 0.55 mm/h with an average air temperature decrease from 32.6 to 32.2 °C.

At 9 a.m. the average evaporation of the Bredalaan's vegetation increases from 0.44 to 0.74 mm/h with a temperature reduction from 26.6 to 26.2 °C. While at 3 p.m. the evapotranspiration increases from 0.25 to 0.40 mm/h, while the average temperature decreases by 0.4 °C till 31.9°C.

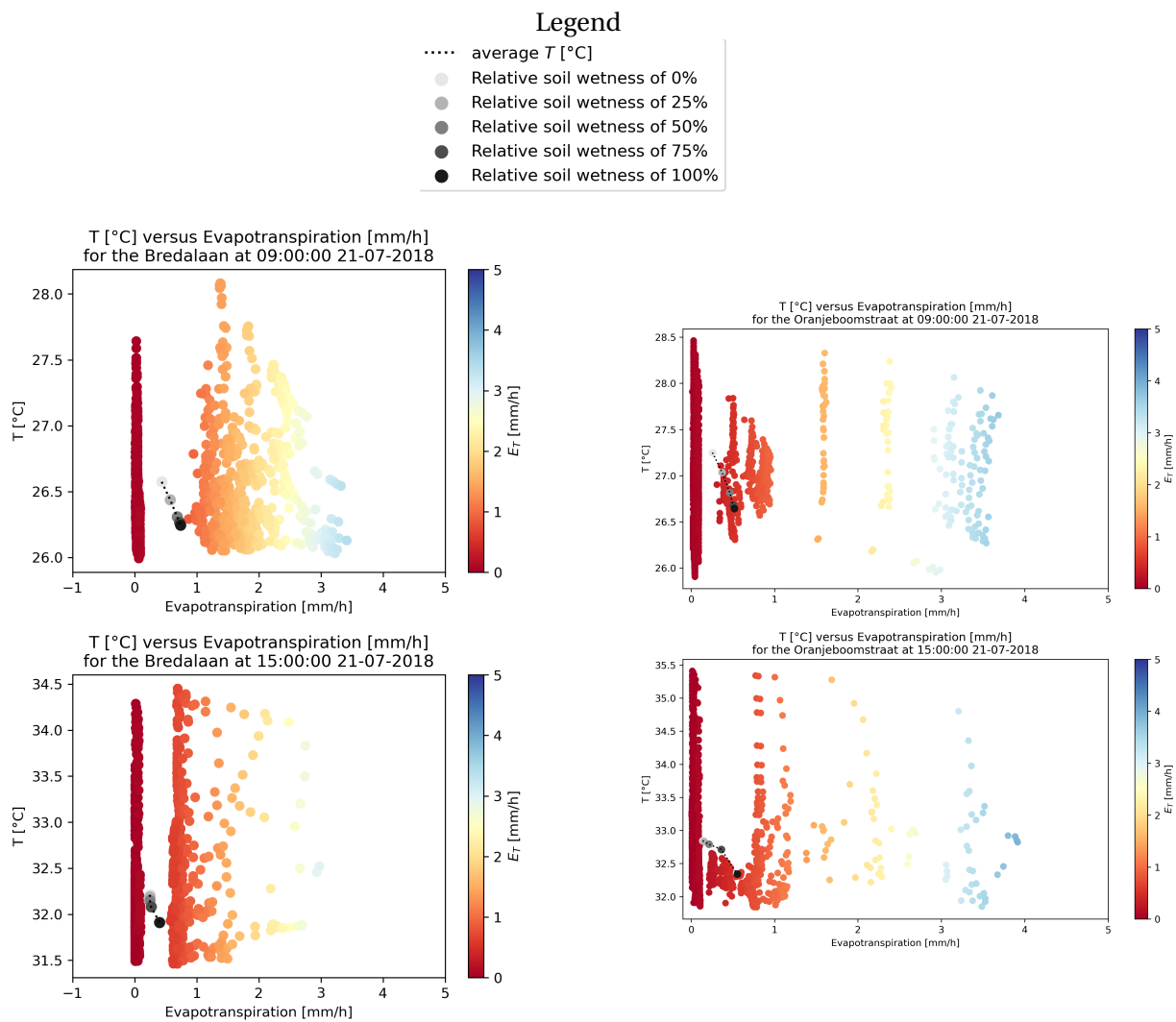


Figure 5.9: The air temperature and evapotranspiration of the green infrastructure at 9 a.m. and 3 p.m. of the Bredalaan and Oranjeboomstraat. *The Bredalaan shows at both times a large spread of evapotranspiration values with respect to temperature values. The Oranjeboomstraat shows clusters of evapotranspiration with a distribution of air temperature.*

Values of the average evaporation and temperature at the Bredalaan

Time(↓)	RSMC (→)	10%	25%	50%	75%	100%
9 a.m.	E_T [mm/h] at 9 a.m.	0.44	0.57	0.68	0.72	0.74
	T [°C]	26.6	26.4	26.3	26.3	26.2
3 p.m.	E_T [mm/h] at 3 p.m.	0.25	0.24	0.24	0.27	0.40
	T [°C]	32.2	32.2	32.2	32.1	31.9

Table 5.2: The average air temperature and evaporation rate of green infrastructure at the Bredalaan. *With increasing RSMC the average evaporation rates increase while the average temperature decreases.*

Values of the average evaporation and temperature at the Oranjeboomstraat

Time(↓)	RSMC (→)	10%	25%	50%	75%	100%
9 a.m.	E_T [mm/h]	0.26	0.37	0.46	0.5	0.52
	T [°C]	26.6	26.4	26.3	26.3	26.2
3 p.m.	E_T [mm/h]	0.14	0.15	0.21	0.36	0.55
	T [°C]	32.9	32.8	32.8	32.7	32.3

Table 5.3: The average air temperature and evaporation rate of green infrastructure at the Oranjeboomstraat. *With increasing RSMC the average evaporation rates increase while the average temperature decreases.*

5.1.4 The relationship of the soil moisture content and evaporation

After presenting the relationships between evaporation and temperature and, soil moisture content and temperature are established it is now time too see if there is an relationship between the soil moisture content and the evaporation. To illustrate this the evaporation rates larger than 0.15 mm per hour are shown with respect to the relative soil moisture content. These graphs show, together with the average data in table 5.4, the relationship between the soil moisture content and evapotranspiration rates. At last the sum of hourly evapotranspiration rates is presented with respect to the soil moisture content.

Figure 5.10 presents the evaporation larger than 0.15 mm per hour with respect to the corresponding relative soil moisture content at 9 a.m. and 3 p.m. for both cases. These that soil containing more moisture increase the average evaporation rate early in the morning with 1.7 to 2 mm/h maximally. During the afternoon the evaporation at the Oranjeboomstraat reaches a maximum increase of 3 mm/h, while the Bredalaan increases maximally 2 mm/h. Furthermore, the Oranjeboomstraat shows two distinct clusters, one with higher and one with lower evapotranspiration rates. At the Bredalaan the evaporation rates' distribution increases with increasing wetness, while in the afternoon only the wettest profile shows a large range of evapotranspiration rates. Table 5.4, showing the average evapotranspiration values, presents declining average evapotranspiration rates in the afternoon for both cases.

Location(↓)	RSMC (→)	10%	25%	50%	75%	100%
Bredalaan	E_T [mm/h] at 9a.m.	0.44	0.57	0.68	0.72	0.74
	E_T [mm/h] at 3 p.m.	0.25	0.24	0.24	0.27	0.40
Oranjeboomstraat	E_T [mm/h] at 9 a.m.	0.06	0.09	0.12	0.13	0.13
	E_T [mm/h] at 3 p.m.	0.03	0.04	0.05	0.09	0.14

Table 5.4: The green infrastructure's average of evapotranspiration rates of both cases with respect to the relative soil moisture content.

The hourly evaporation rate of both cases is presented in figure 5.11, showing the total hourly evaporation rates for all five soil moisture profiles over time. The Bredalaan's wettest soil profile shows a maximum evaporation at 11 a.m. of 4.8 mm/h, after which the evapotranspiration decreases till 3 p.m. before it reaches another peak at 6 p.m. For the drier profiles the evapotranspiration fulfills its maximum potential at 8 to 10 a.m. before it decreases till 2 to 3 p.m. before it reaches another peak right before sundown.

The Oranjeboomstraat, on the other hand, shows a more gradual gradient over the day, with a peak at noon of about 2.27 mm/h for the wettest soil profile. The drier profiles follow the same pattern as the Bredalaan,

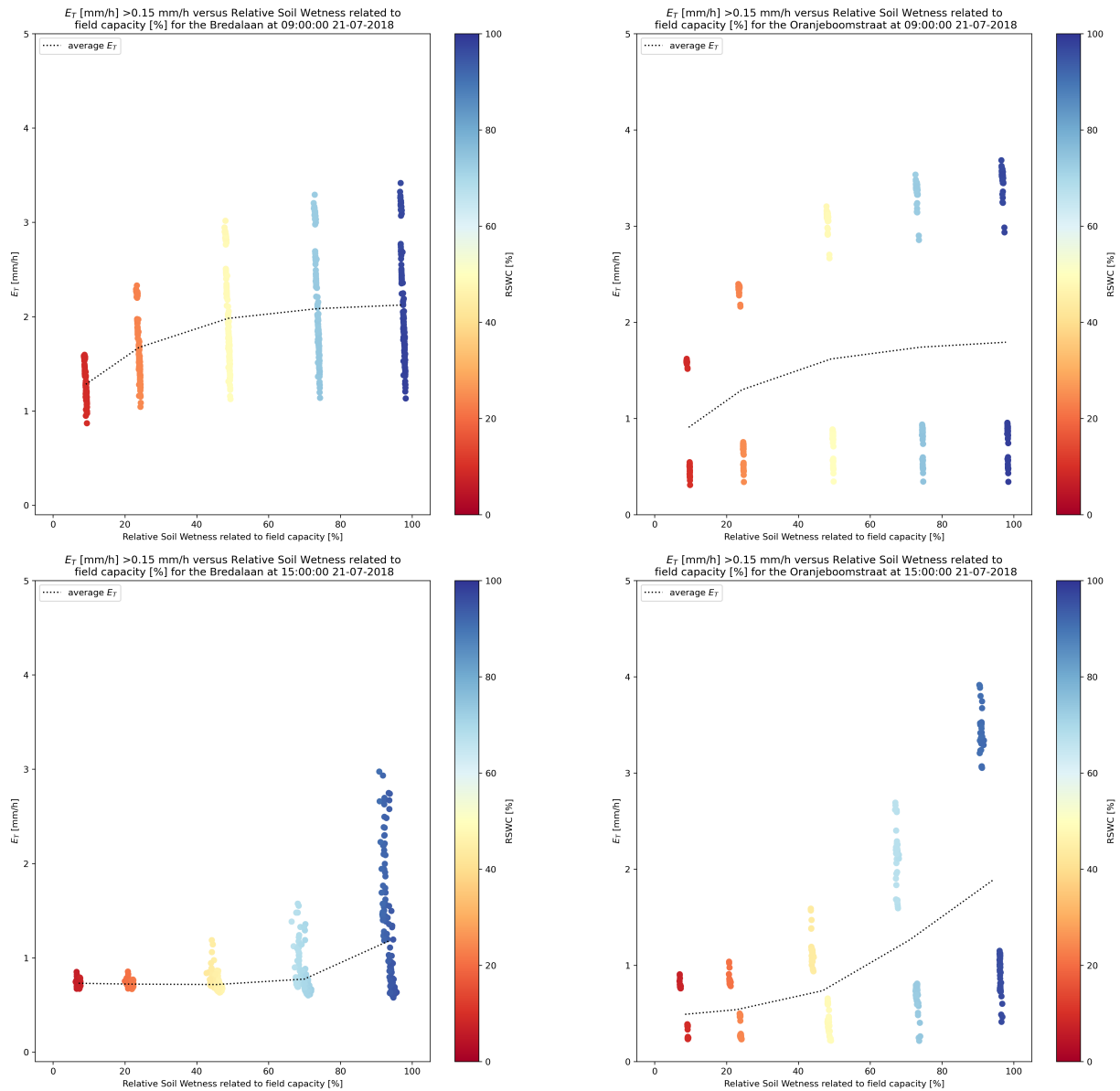


Figure 5.10: Relationship between the soil moisture content and the evaporation at 9 a.m. and 3 p.m. for both cases. *Both cases show an increased evaporation with increased soil wetness. The Bredalaan shows a large distribution of evapotranspiration, while the Oranjeboomstraat develops clusters of evapotranspiration.*

suggesting that this is caused by a shortage of water. In addition to figure 5.11, table 5.5 shows the total daily evapotranspiration values of both cases for each relative soil moisture profile. Showing that the Bredalaan evaporates for the dryer soil moisture profiles about 50% more water, while for the wettest moisture profiles it drops from 35 till 25%.

Location(↓)	RSMC (→)	10%	25%	50%	75%	100%
Bredalaan	[mm/d]	4.5	5.2	6.8	7.9	9.1
Oranjeboomstraat	[mm/d]	2.7	3.5	5.1	6.4	7.2

Table 5.5: Total daily evapotranspiration at each case for different soil moisture contents.

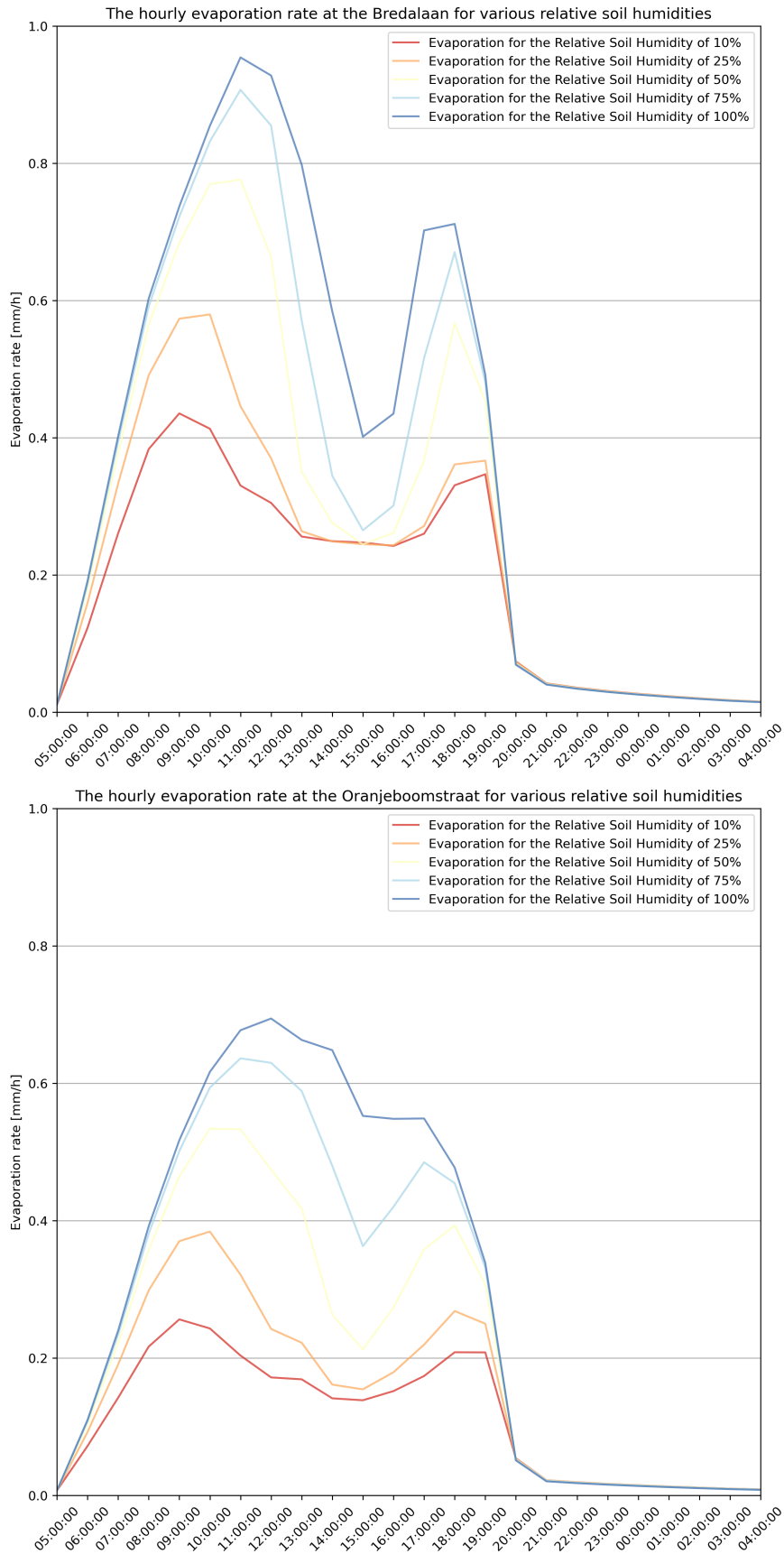


Figure 5.11: The hourly evapotranspiration rate of both cases for various soil moisture profiles. *The Bredalaan's maximum evapotranspiration rate reaches a maximum of about 0.95 mm/h, while the Oranjeboom's maximum evapotranspiration is only 0.7 mm/h. Though, both cases show similar trends of evapotranspiration rates.*

5.2 Results of the series simulations of both cases

After discussing the effects of soil wetness and evapotranspiration on the current situation of both cases, it is now time to discuss the effect of increasing green infrastructure and/or irrigation on the current situation. This is done by stating the meteorological input parameters and the increased green infrastructure of both cases. After which the results of the time series is presented, the following aspects are presented:

- Air temperature development, including UHI-effect;
- Physiological Equivalent Temperature, or PET, development; and
- Total evapotranspiration values.

5.2.1 Results of series simulations regarding simulated air temperature, PET and UHI-effect

The simulated air temperature, PET and UHI-effect are all discussed regarding the four scenarios for each case. Firstly, all four scenarios' air temperature for both cases is shown. These graphs show the median air temperature and the spread of the data, This enables comparing hourly median, minimum and maximum temperatures with respect to each other. Secondly, the same graphs are presented for the PET, enabling comparison of the scenarios with respect to the PET. Thirdly, the UHI-effect of all three cases is observed for all four scenarios.

Simulated air temperatures of the four scenarios

Figures 5.12 & 5.13 show the simulated air temperature for all four scenarios at respectively the Bredalaan and Oranjeboomstraat. To start with the Bredalaan of figure 5.12. The graph shows a data gap for all four scenarios between 8 p.m. 27-7 and 4 a.m. 28-7 due instability within the model. Besides, there are two smaller data graphs for the greener, and greener irrigated scenario at 11 p.m. 29-7 till 4 a.m. 30-7 and 10 p.m. 31-8 till 4 a.m. 1-8 due instability.

Focusing on each daily median peak temperature, the greener irrigated scenario is relatively coolest and the greener scenario is warmest. As can be observed, the temperature of the just irrigated scenario is also cooler than the current scenario. When looking at the maximum temperatures overall a maximum temperature of 45°C is reached for the greener scenario with a dry soil, while at the same time the irrigated scenario shows at that time a maximum temperature below 40°C.

As second the Oranjeboomstraat's results are discussed based on figure 5.13, showing the air temperatures from 4 a.m. 27/7/2018 till 4 a.m. 1/8/2018. The Oranjeboomstraat has a data gap for all scenarios between 11 p.m. 31-8 till 4 a.m. 1-8 due instability. With respect to the maximum daily median air temperature the trend is similar to the Bredalaan, with the greenest scenario relatively warmest and greener irrigated scenario coolest. Though in these results there is only a small difference between maximum air temperature of the scenarios is visible.

Physiological equivalent temperature of the four scenarios

Figures 5.14 & 5.15 show the PET of the four scenarios. Figure 5.14 shows the development of the PET from 4 a.m. 27/7/2018 till 4 a.m. 1/8/2018. To begin with the current situation. As can be seen is the maximum perceived temperature about 50% higher than the air temperature in figure 5.12 presents. This can be explained by the high influence of radiation on the calculated PET. This also explains the low PET during the night. Furthermore, there can be observed that the range of data of the PET fluctuates with solar radiation too. When the current situation is shortly compared with the irrigated scenario it can be seen that the median values follow approximately the same trend, albeit it with slightly lower values. This does not only account for the median values, also the minimum and maximum values follow similar trends.

The greener scenario shows reduced median temperatures over the entire course of the day, but slightly higher nocturnal PET values are observed. Maximum values show a minimal reduction, while the minimum values show a slightly larger reduction. Comparing the irrigated greener scenario to the current scenario, an even better performance is achieved regarding PET reduction. Alike the irrigated scenario compared to the current situation, follows the irrigated greener scenario a similar median trend with respect to the greener scenario with a dry soil.

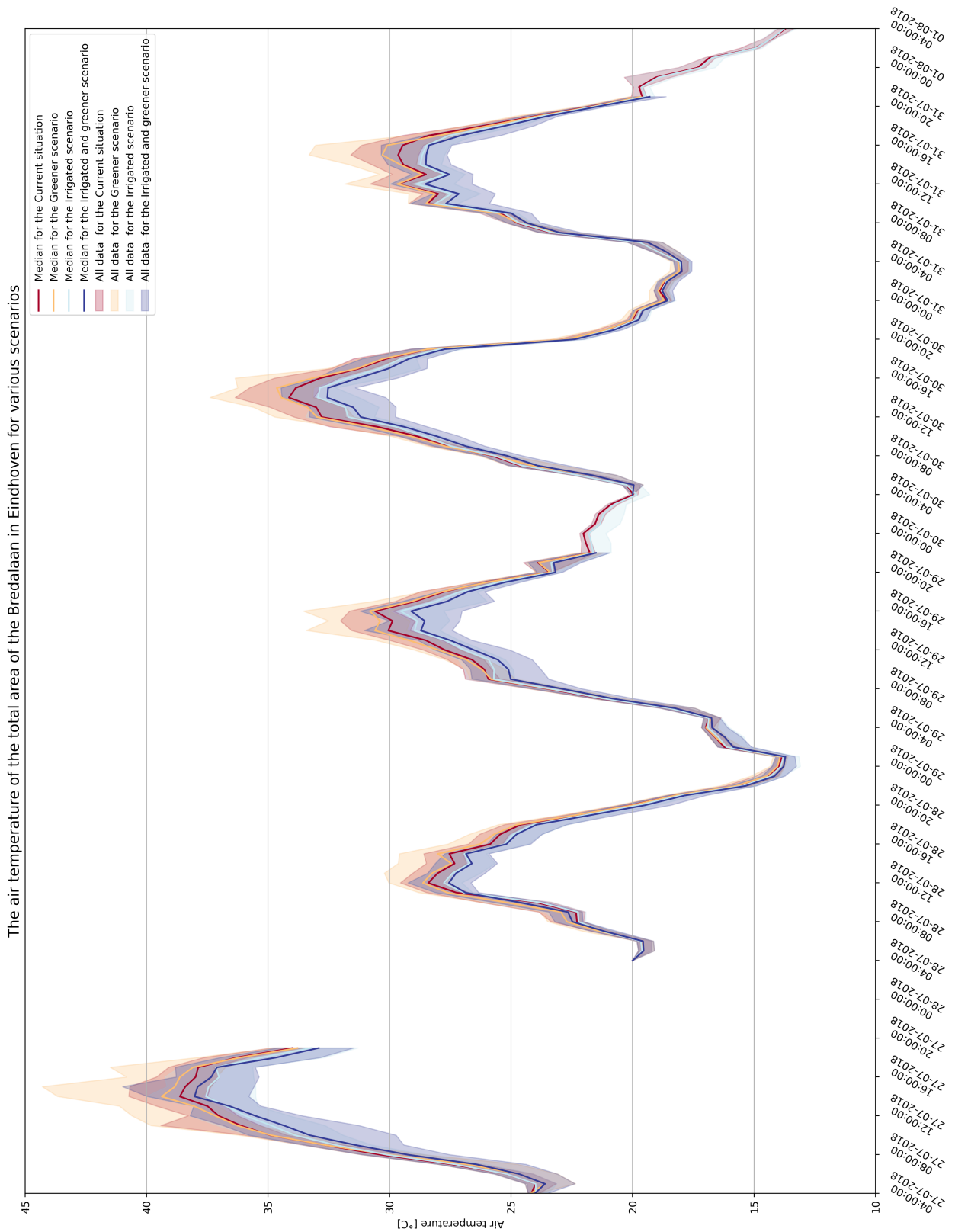


Figure 5.12: The simulated air temperature at the Bredalaan for several scenarios. *The air temperatures from 4 a.m. 27/7/2018 till 4 a.m. 1/8/2018 for four scenarios is presented.*

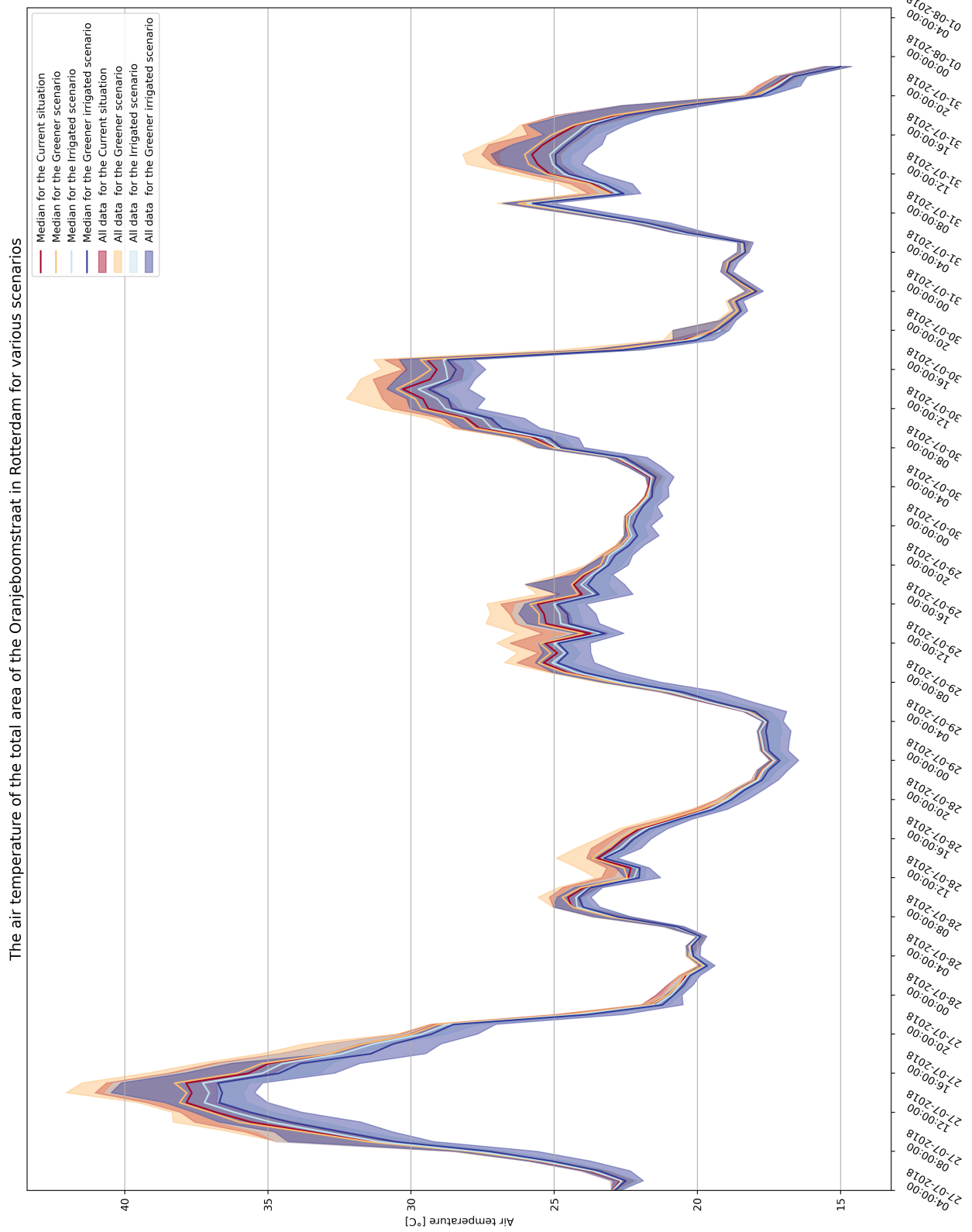


Figure 5.13: The simulated air temperature at the Oranjeboomstraat for several scenarios. *The air temperatures from 4 a.m. 27/7/2018 till 4 a.m. 1/8/2018 for four scenarios is presented.*

When analyzing the results of figure 5.15 for the Oranjeboomstraat its PET values, it can be seen that similar trends are visible between the scenarios as at the Bredalaan. But, what is remarkable is that the differences between the four scenarios are smaller.

As an example, on July 30 the median temperatures of the Oranjeboomstraat are at the peak within 5°C of each other while at the Bredalaan the difference is in the range of 10°C .

The urban heat island effect of the four scenarios

The UHI-effect of the scenarios is presented to show the hourly influence of the urban environment on the meteorological state of the cases with respect to the air temperature. The UHI-effect indicates whether a cooling effect is caused by the urban environment or rather a warming effect. Figures 5.16 & 5.17 show the development of the UHI-effect of the four scenarios for each case.

To begin with figure 5.16 showing the UHI-effect of the Bredalaan. As can be seen shows the greener scenario the largest warming effect with respect to the other cases. The greenest scenario reaches the largest daily warming effect between $4\text{--}9^{\circ}\text{C}$. The largest cooling effect is observed for the two irrigated scenarios showing a minimum cooling effect between $1\text{--}4^{\circ}\text{C}$, while the median for both scenarios reaches a $1\text{--}2^{\circ}\text{C}$ warming effect. But in the current scenario the urban area seems to be warming-up the urban environment from sunrise till sunset with daily median values between $1\text{--}3^{\circ}\text{C}$. The greener scenario shows often a similar trend as the current scenario, but with slightly higher maximum values and lower minimum values. Besides can be observed that the UHI-effect declines faster after the daily peak for the greener scenario than the current scenario.

Figure 5.17 shows the UHI-effect development at the Oranjeboomstraat for all four scenarios. The current scenario shows the second largest UHI-effect with a daily median warming effect of about 2°C . The current scenario shows a slight cooling effect during the night, while the other three scenarios show an even larger cooling effect with respect to the rural temperatures.

Furthermore, the irrigated and irrigated greener scenarios also show a lower UHI-effect from sunrise till sunset with the median warming effect around 1°C , while the daily maximum effect is between $3\text{--}5^{\circ}\text{C}$, with small differences between these two cases.

The greener scenario for the Oranjeboomstraat gave a similar result as at the Bredalaan, resulting in the highest daily maximum of $3\text{--}6.5^{\circ}\text{C}$, but lower median nocturnal UHI-effect as the current scenario resulted in.

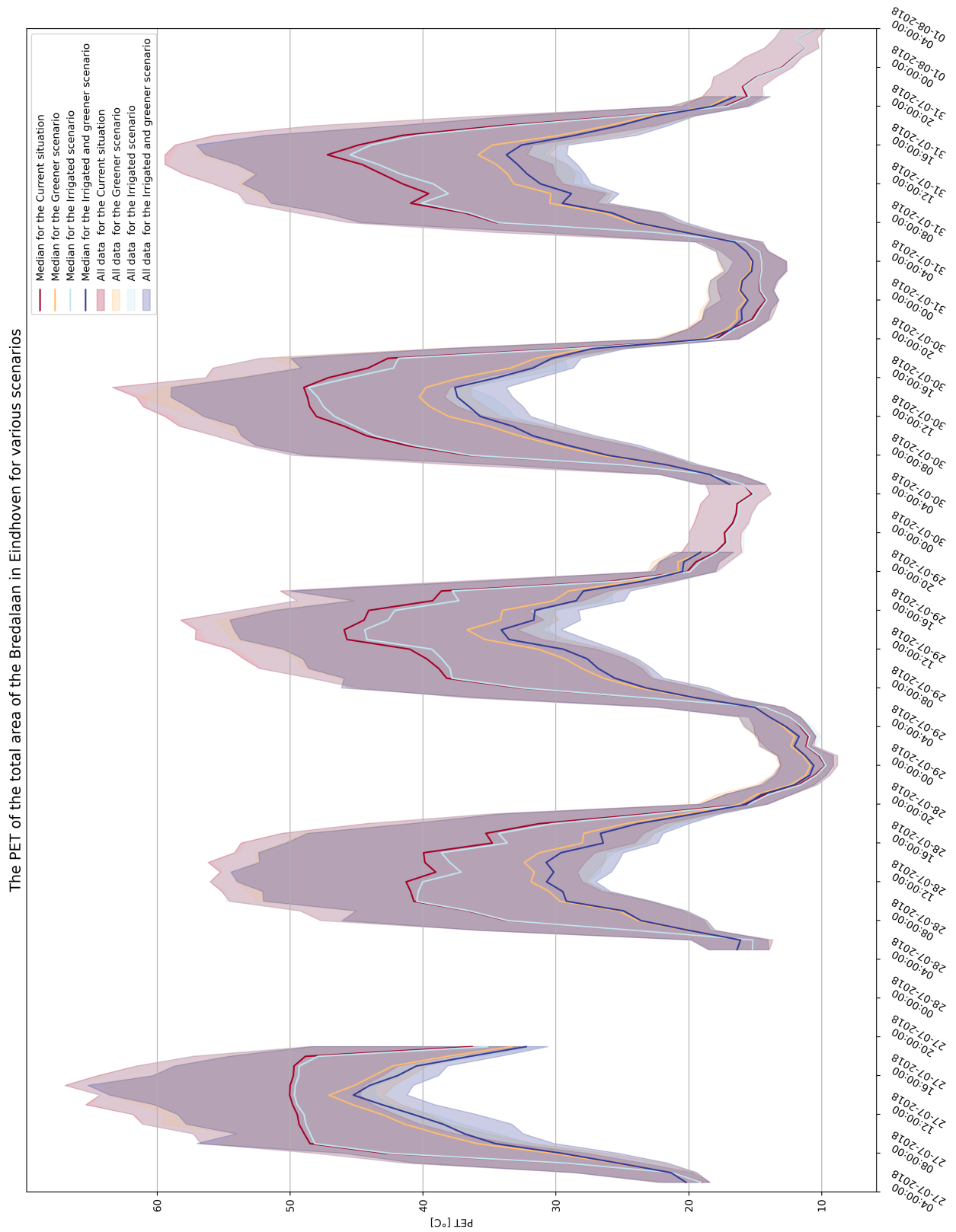


Figure 5.14: The PET at the Bredalaan for several scenarios. *The PET from 4 a.m. 27/7/2018 till 4 a.m. 1/8/2018 for four scenarios is presented.*

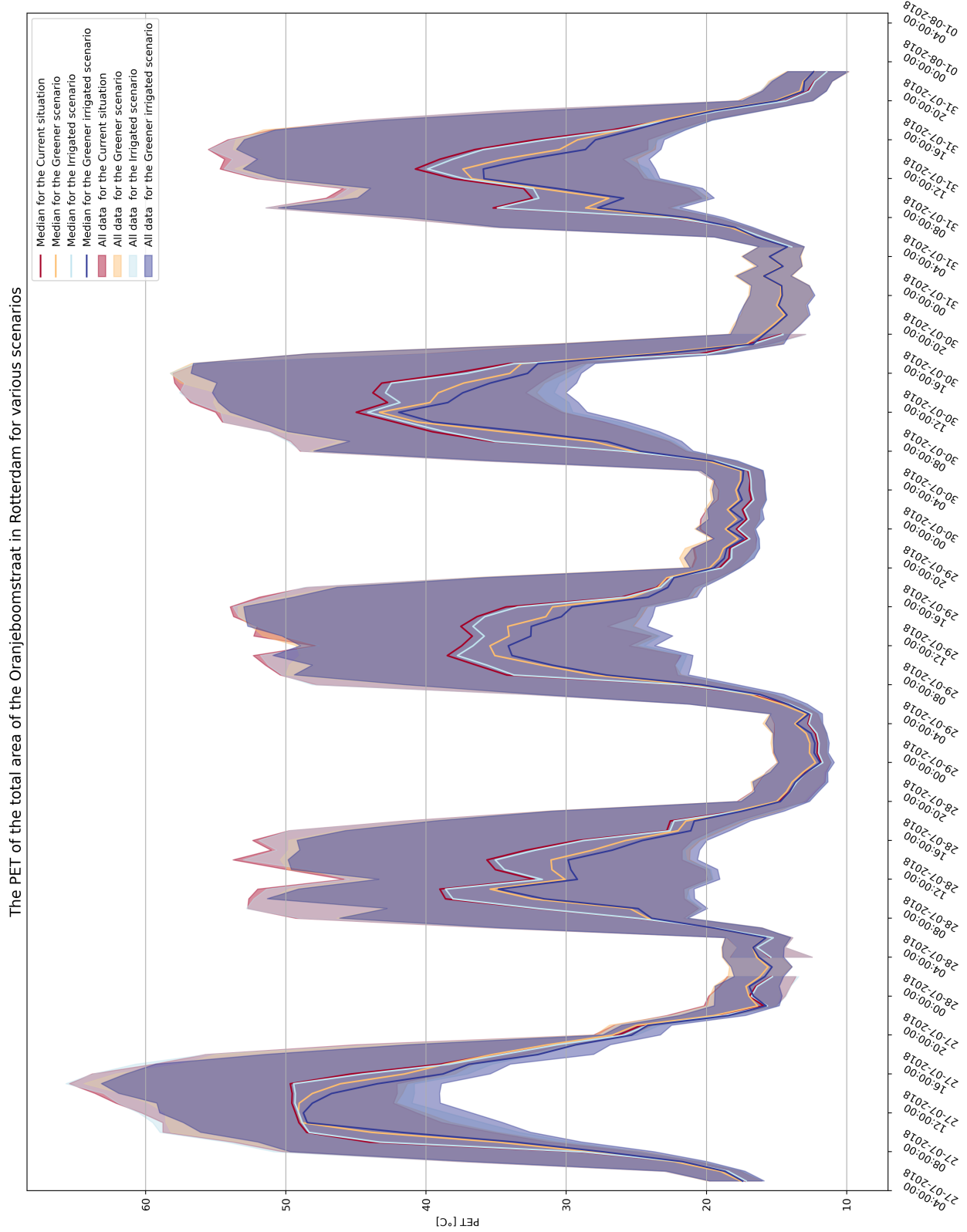


Figure 5.15: The PET at the Oranjeboomstraat for several scenarios. *The PET from 4 a.m. 27/7/2018 till 4 a.m. 1/8/2018 for four scenarios is presented.*

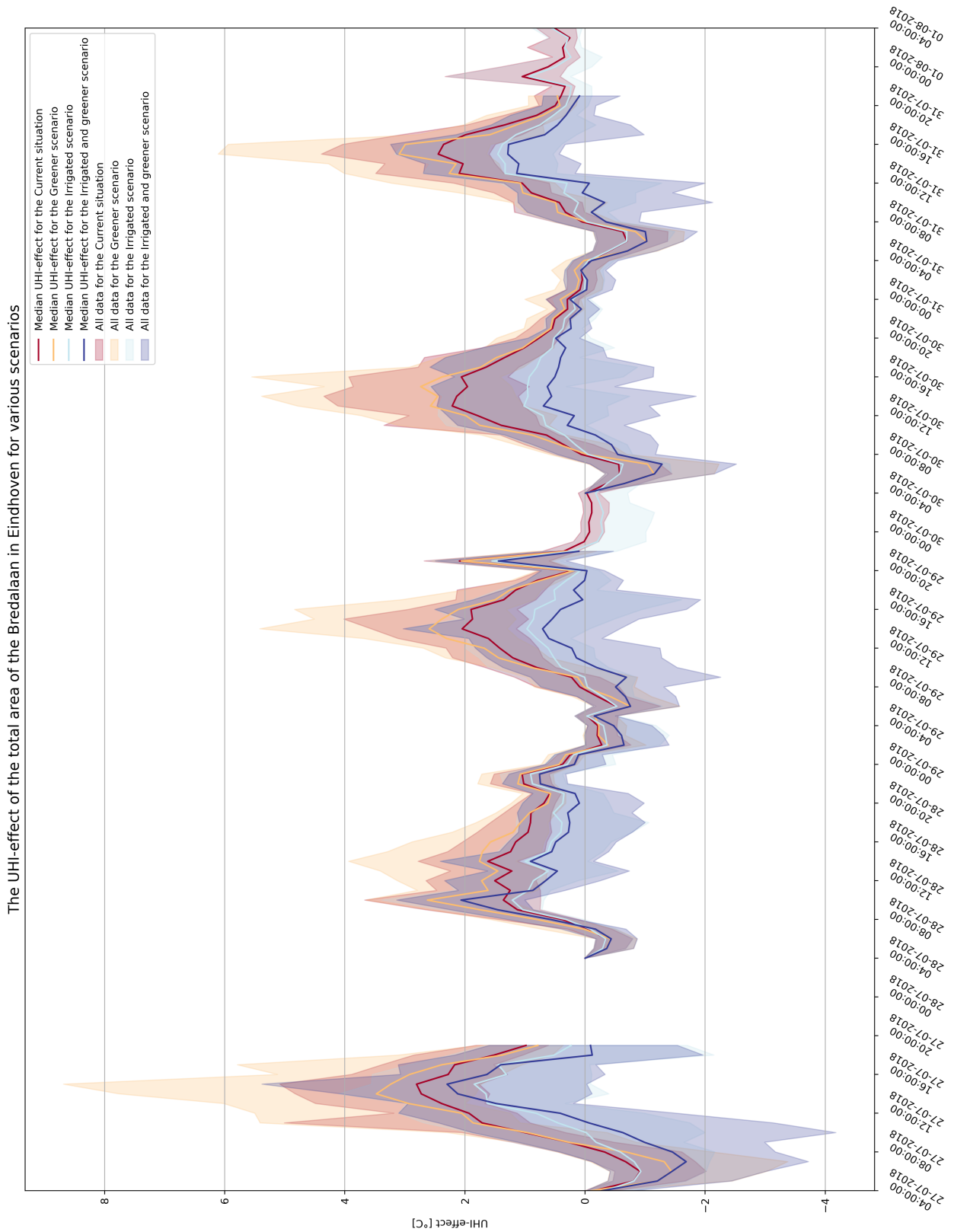


Figure 5.16: The UHI-effect at the Bredalaan for several scenarios. *The UHI-effect from 4 a.m. 27/7/2018 till 4 a.m. 1/8/2018 for four scenarios is presented.*

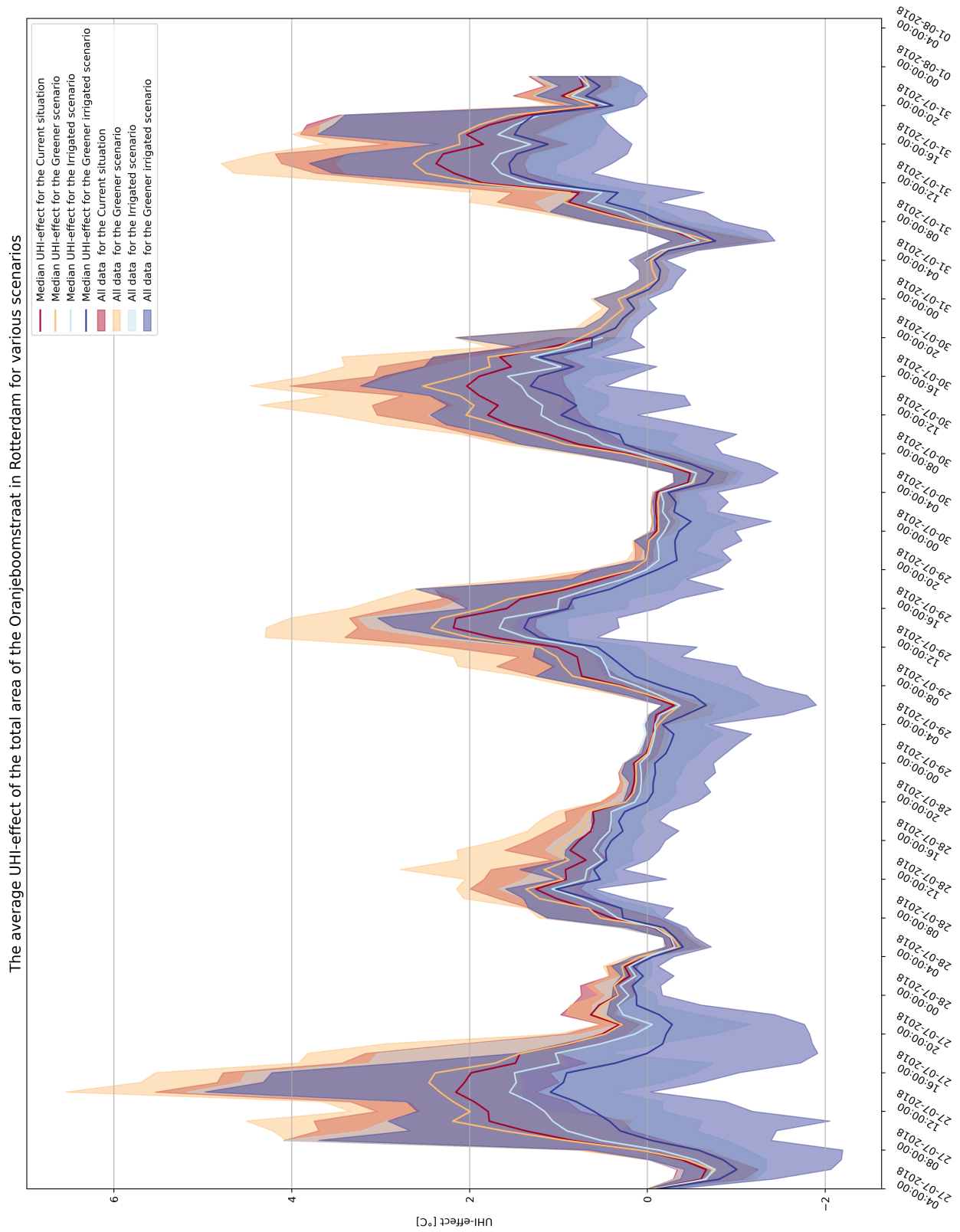


Figure 5.17: The UHI-effect at the Oranjeboomstraat for several scenarios. *The UHI-effect from 4 a.m. 27/7/2018 till 4 a.m. 1/8/2018 for four scenarios is presented.*

5.2.2 Results of series simulations regarding soil moisture content

For both cases two dry and two irrigated simulations were performed. To show the development of the relative soil moisture content (RSMC) with respect to field capacity the results are presented in this section. The RSMC is important since this indicates the water availability for root extraction. Figures 5.18 & 5.19 show the development of the RSMC with respect to field capacity over the simulated period.

When observing the relative soil moisture content of the Bredalaan in figure 5.18, the two type of simulations are clearly visible. The irrigated and dry profiles show two clear clusters, the irrigated scenarios floating between 90-100%, while the dry profiles fluctuate between 0-10% RSMC. The current and irrigated scenario show smaller RSMC reductions during the day, while the greener and greener irrigated scenarios show a large reduction of RSMC.

In contradiction with the Bredalaan, the Oranjeboomstraat in figure 5.19 shows smaller soil moisture reductions. Though at the Oranjeboomstraat the same two groups of dry and irrigated can be distinguished from one and another. These scenarios fluctuate between about 7-10% and 94-100% respectively.

To establish why the Oranjeboomstraat shows a smaller reduction of RSMC, the evaporation rates of both cases should be observed. The next section therefore presents the hourly evapotranspiration rates.

5.2.3 Results of series simulations regarding hourly evaporation rates.

To understand the differences in RSMC change at both cases, the evapotranspiration rates are presented in this section. Furthermore, the evapotranspiration rates, when compared to the relative temperature change, can give more insights in their relationship. Figures 5.20 & 5.21 show the hourly evapotranspiration rates at both cases for the four scenarios.

When observing figure 5.20, it can be seen that all five days show similar patterns over the several days and the same pattern between the different scenarios. Furthermore, each scenario individually reaches a constant maximum over the period. The current situation shows a daily maximum rate of about 0.5 mm/h, whereas the irrigated scenario reaches 1.5 mm/h, the greener scenario 2.25 mm/h and the irrigated greener scenario 4-4.5 mm/h.

The Oranjeboomstraat in figure 5.21 shows lower evapotranspiration rates, though with similar trends. Again there are repetitive patterns with each scenario reaching a daily maximum rate. The current situation shows a daily maximum rate of about 0.25 mm, whereas the irrigated scenario reaches 0.75 mm/h, the greener scenario 0.8 mm/h and the irrigated greener scenario 1.5-2 mm/h.

Both cases show consistent evapotranspiration rates over the simulation periods for each scenario. Though, both locations show large differences in maximum evapotranspiration rates between each other and between the different scenarios.

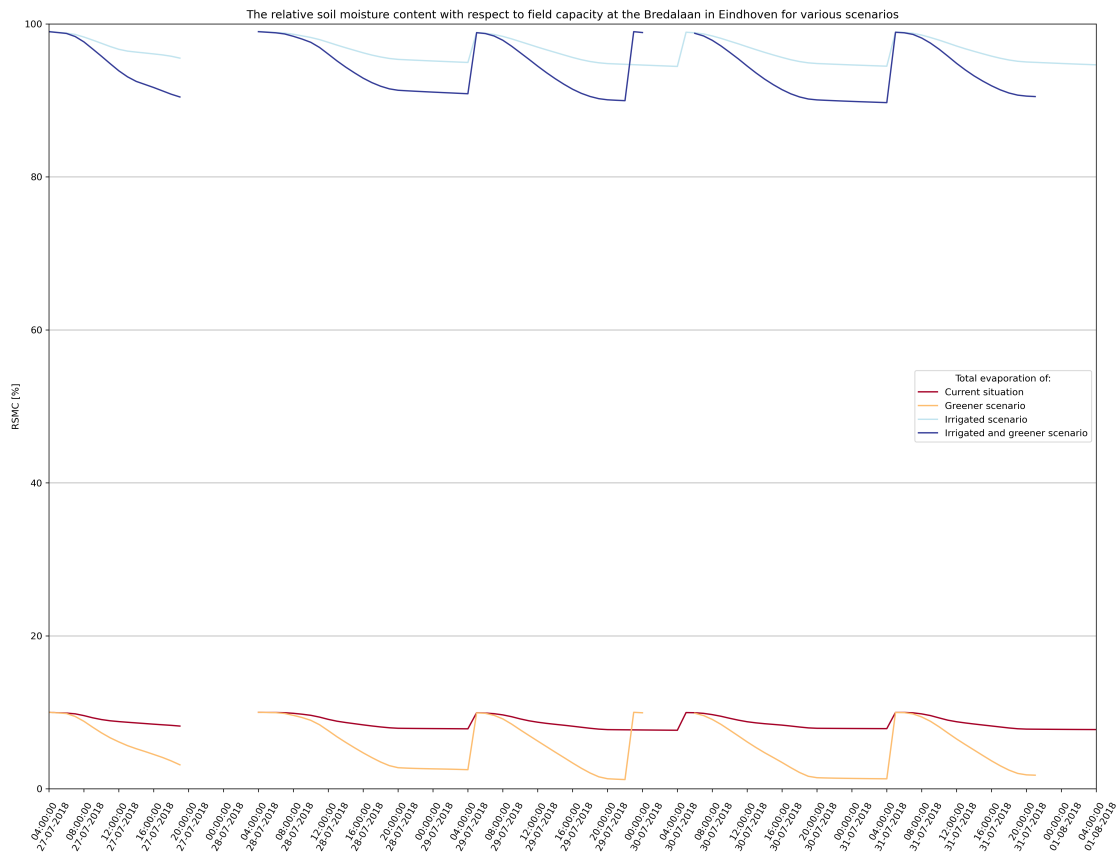


Figure 5.18: The relative soil moisture content with respect to field capacity at the Bredalaan for several scenarios. *The relative soil moisture content with respect to field capacity change from 4 a.m. 27/7/2018 till 4 a.m. 1/8/2018 for three scenarios is presented.*

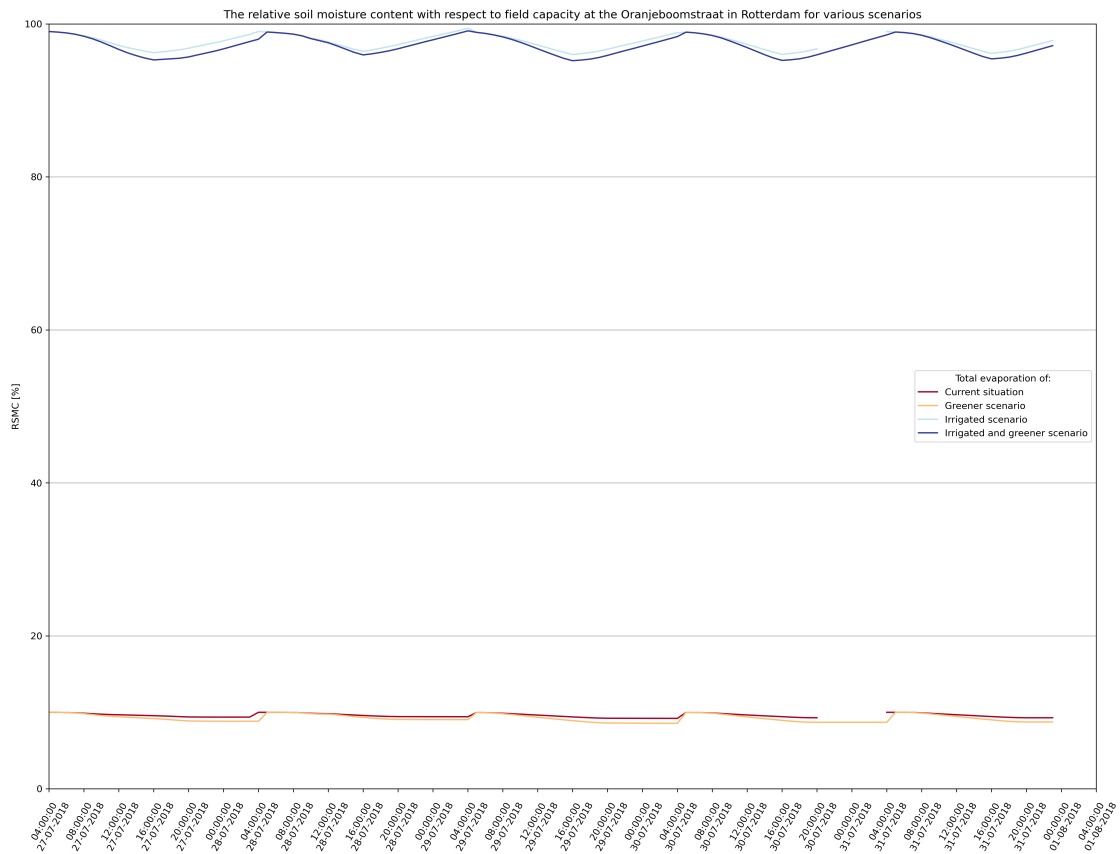


Figure 5.19: The relative soil moisture content with respect to field capacity at the Oranjeboomstraat for several scenarios. *The soil moisture content with respect to field capacity change from 4 a.m. 27/7/2018 till 4 a.m. 1/8/2018 for three scenarios is presented.*

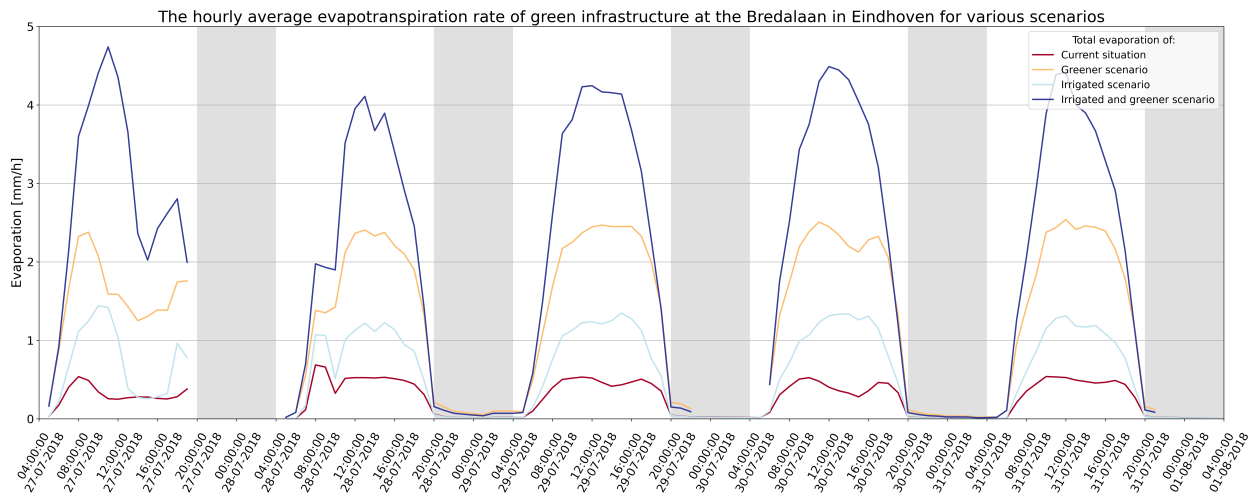


Figure 5.20: The hourly evapotranspiration rate at the Bredalaan for several scenarios. *The relative soil moisture content with respect to field capacity change from 4 a.m. 27/7/2018 till 4 a.m. 1/8/2018 for three scenarios is presented.*

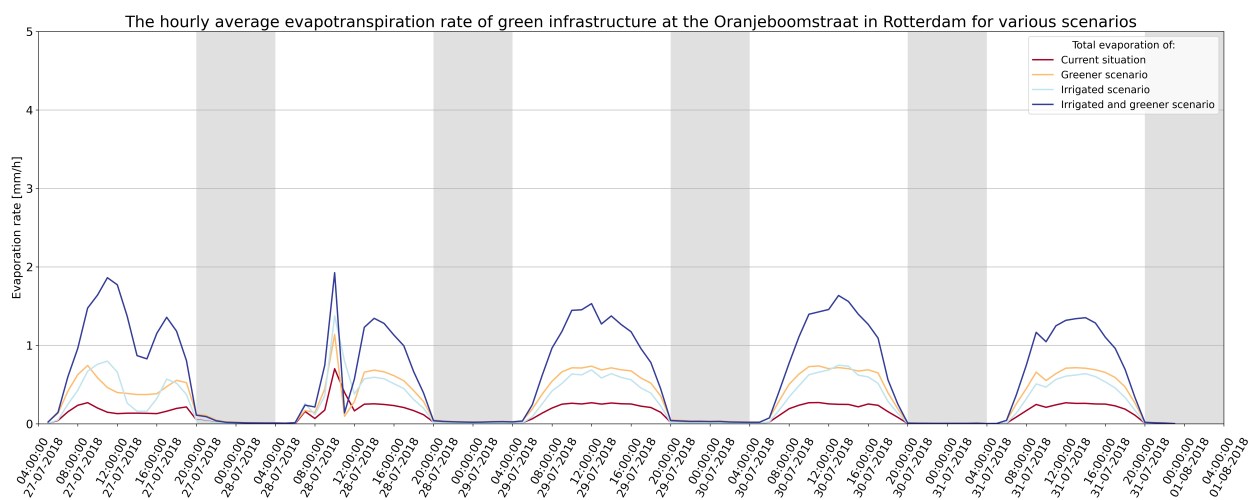


Figure 5.21: he hourly evapotranspiration rate at the Oranjeboomstraat for several scenarios. *The soil moisture content with respect to field capacity change from 4 a.m. 27/7/2018 till 4 a.m. 1/8/2018 for three scenarios is presented.*

5.3 Comparison of the scenarios

Within the upcoming paragraphs the scenarios are compared with each other for simulated air temperature and the PET. First, the relative temperature change is discussed. Secondly, the relative PET change is discussed. Showing these results will give an understanding in the effect of the measures on the urban climate with respect to air and perceived temperature.

5.3.1 Relative air temperature with respect to the current situation

To further analyze the data the relative air temperatures with respect to the current situation are presented in this paragraph, which is presented as the difference in median temperature change. Presenting the median relative temperature change enables in depth analysis of the effect of each measure simulated. Figures 5.22 & 5.23 show the relative temperature change with respect to the current situation.

To start with the Bredalaan. The greener scenario shows during early mornings the median temperature is cooler than the current situation, though this changes during the day to an increased temperature. During the day it shows a temperature increase over most of the simulated period. This scenario shows a maximum increase of 1.25°C , but at the warmest moment of the day there is an average temperature increase of about 0.65°C .

The irrigated scenario resulted in reduced median air temperature over almost the entire series. A maximum temperature reduction of 1.25°C is reached on the early morning of July 27, while the other days show a maximum reduction in the afternoon. The maximum reduction in the afternoon is about 1.0°C .

The greener irrigated scenario is relatively the coldest scenario on average. Though at 8 a.m. of July 28 a maximum temperature increase of 0.6°C is calculated. A maximum decrease of 2°C is reached at midnight of July 30. The scenario reduces the temperature most effectively between 8 a.m. and noon, and in most cases between noon and 4 p.m. with almost always reaching 1.5°C reduction.

Secondly, the Oranjeboomstraat in figure 5.23, presents the relative temperature change with respect to the current situation. The greener scenario shows warmer air temperatures during most of the series, with a maximum of 0.5°C . The irrigated scenario shows colder temperatures over the entire series down to 0.75°C . Furthermore, the irrigated scenario has the largest effect between 9 a.m. and noon, with an exception on the July 30 and 31. On these two days the maximum effect is reached between noon and 4 p.m.

The greener irrigated scenario resulted in lower median temperatures for all simulated days. The effect is slightly better than the irrigated scenario, since the greener irrigated scenario shows temperature reductions of larger than 1.25°C , but on most days at least 0.75°C .

Shortly comparing both cases, can be observed that similar patterns were found with reduced temperatures for the irrigated and greener irrigated scenarios. Both cases show reduced nocturnal and daily peak temperatures.

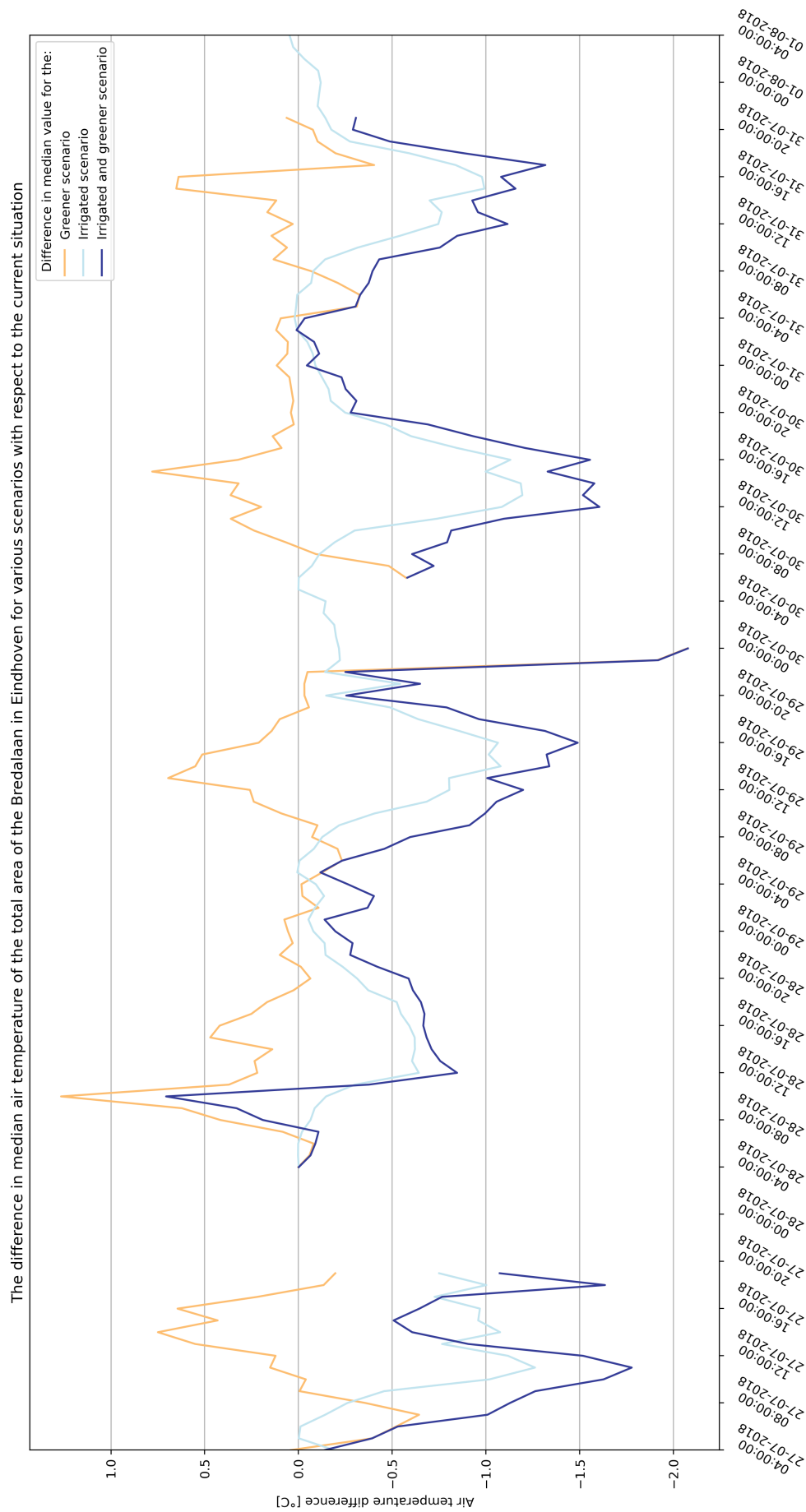


Figure 5.22: The change in median air temperature at the Bredalaan for several scenarios with respect to the current scenario. *The change in median air temperature from 4 a.m. 27/7/2018 till 4 a.m. 1/8/2018 for three scenarios is presented.*

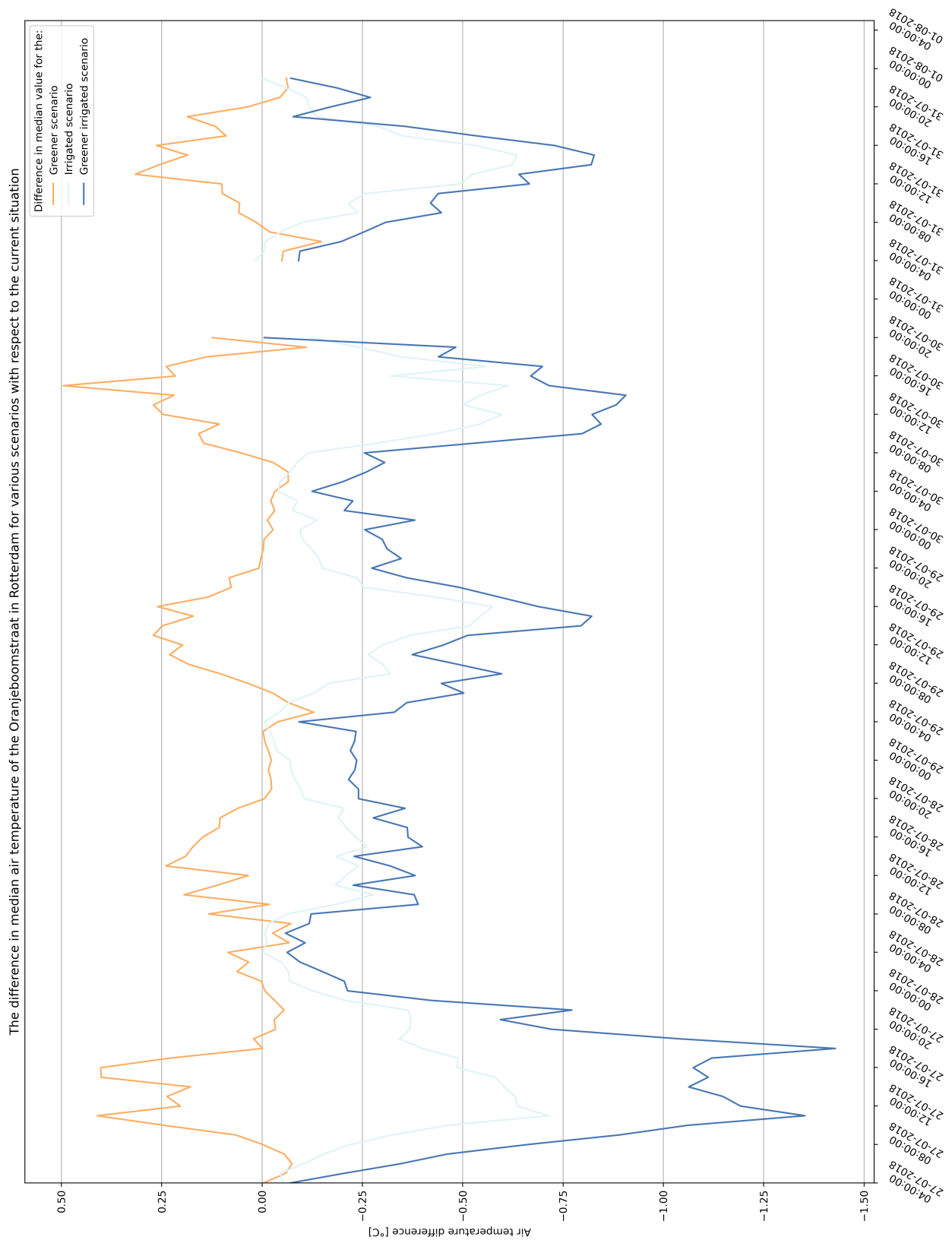


Figure 5.23: The change in median air temperature at the Oranjeboomstraat for several scenarios with respect to the current scenario. The change in median air temperature from 4 a.m. 27/7/2018 till 4 a.m. 1/8/2018 for three scenarios is presented.

5.3.2 Relative physiological equivalent temperature with respect to the current situation

Just as observed that for each case both the irrigated and irrigated greener scenarios are cooler than the current scenario, while the greener scenario results in higher air temperatures. To understand the effects of the scenarios on the perception of a human on this temperature the relative change in PET is observed with respect to the current scenario. Figures 5.24 & 5.25 show the relative PET for the Bredalaan and Oranjeboomstraat respectively.

The relative PET of the Bredalaan shows for all three scenarios a decrease in PET from sunrise till sunset, while the just irrigated scenario also shows a nocturnal reduction. The irrigated scenario, furthermore, shows a median PET reducing effect of 0–2°C. The greener and irrigated greener scenario both result in a larger daily median reduction of 11–14°C.

The large reduction in PET of the last two scenarios comes from the increased amount of green providing shade. When comparing these scenarios with each other, it can be seen that the irrigated greener scenario shows a larger reduction of PET, presumably due to the larger amount of evaporation. The difference between these two scenarios is up to two degrees Celsius.

Figure 5.25 shows the relative PET change of the Oranjeboomstraat's scenarios with respect to the current scenario. A similar trend is visible with the irrigated scenario cooler during the entire simulated period and the other two scenarios having higher PET during the night but lower during the day. The greener scenario shows a reduction in PET of 6–9°C, while the irrigated greener scenario shows a reduction of 7–10°C. This additional degree of reduction corresponds with the difference between the current situation and irrigated scenario which shows a reduction of 1°C.

What is remarkable is that there is one large difference with respect to the Bredalaan. The Oranjeboomstraat shows for two of the three scenarios two diurnal peaks, this is most certainly caused by the orientation of the cases and the direction from which the solar radiation reaches the cases. The angle of the solar radiation with respect to the orientation determines the area of shade in the cases.

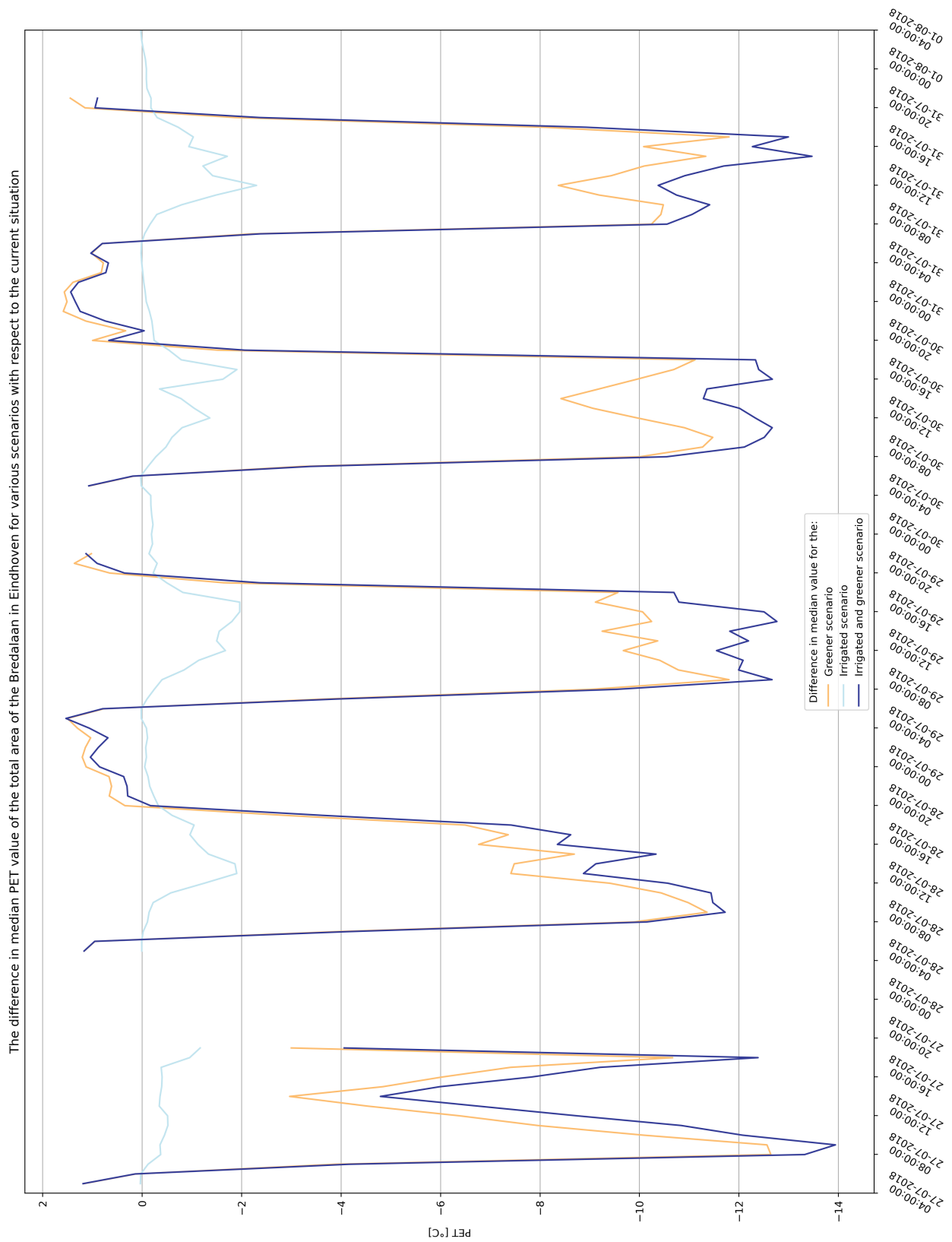


Figure 5.24: The change in median PET at the Bredalaan for several scenarios with respect to the current scenario. *The change in median PET from 4 a.m. 27/7/2018 till 4 a.m. 1/8/2018 for three scenarios is presented.*

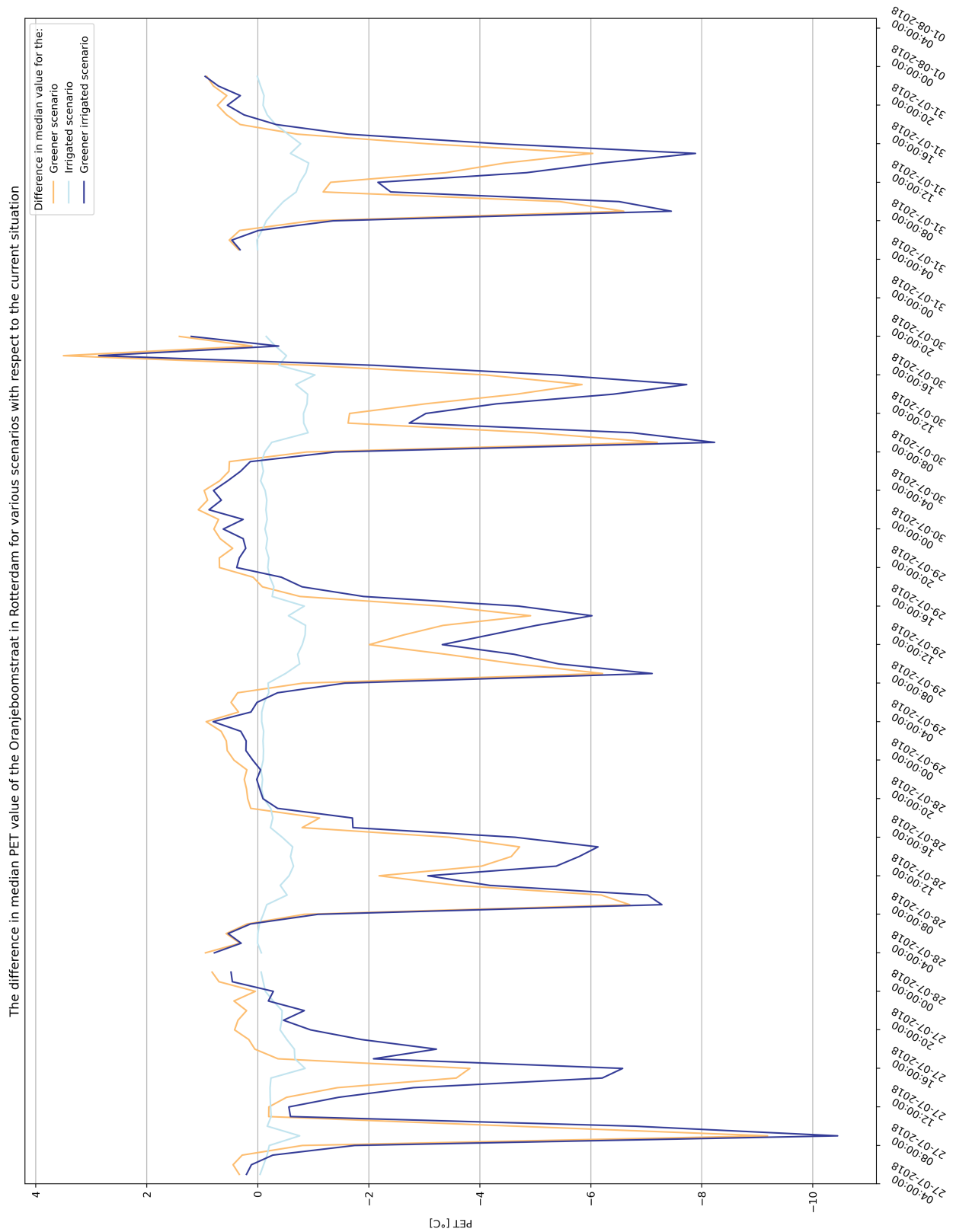


Figure 5.25: The change in median PET at the Oranjeboomstraat for several scenarios with respect to the current scenario. *The change in median PET from 4 a.m. 27/7/2018 till 4 a.m. 1/8/2018 for three scenarios is presented.*

Chapter - 6

General discussion

Before conclusions are drawn the robustness of the study and its results are discussed. The used approach and methodology are addressed, while also the validation and accuracy of the results are discussed. Firstly, the approach is evaluated through evaluation of the chosen case areas, data retrieval and model decision. The model decision focuses on the reevaluation of the usage of ENVI-met as software, also addressing the ability to reproduce the chosen process for possible future studies. Furthermore, the validity and transferability of the results are discussed and the data is further interpreted.

6.1 Case studies and data retrieval

This study focuses on two cases within the Netherlands, the Bredalaan in Eindhoven and the Oranjeboomstraat in Rotterdam. Within this section the decision for these locations is reevaluated and analyzed.

Both locations have similar typologies, but with a height difference, (see chapter 4), environment and size, therefore these locations are good for comparison. Though some key differences might have influenced the outcome of the study. These differences are shortly addressed to understand their influence. Besides, the applicability and transferability of these results with respect to other locations is addressed.

6.1.1 Case study location and characteristics

Within this study is chosen to simulate Eindhoven and Rotterdam for its different soil composition addressing a sandy and clayey subsoil. Based on their grain size and saturated hydraulic conductivity these two are their opposites. Clay particles are smaller than 0.002 mm with a hydraulic conductivity of $10^{-10} - 10^{-6}$ cm/s and sand is between 0.05–2.0 mm with a hydraulic conductivity of $10^{-4} - 1$ cm/s.

This leaves a large range in between these two soils, to understand the range of effects it is actually necessary to start with the extremes. Both soil classes widely present within the Netherlands, therefore choosing these two locations is representative for the Netherlands.

Besides soil composition, the building typology and urban design of both cases is representative for urban areas in the Netherlands. In suburban areas three storeys is the average, like at the Bredalaan, while four till five storeys is average in slightly denser populated areas, like at the Oranjeboomstraat. Furthermore, the design of both street profiles with parking, space for pedestrians and bikes, and a large lane of grass and trees is common, as well as the (front) gardens of the cases.

Besides, the meteorological circumstances of both cases is also representative for the Netherlands due the small differences in these parameters. Even though Rotterdam has a slightly higher average annual precipitation than Eindhoven, the potential drought deficit and maximum temperatures during the simulated period of 2018 were in the same range.

To summarize, the modelled cases are representative cities for the Netherlands regarding building typology and urban planning, soil composition and meteorological environment. Therefore, these cases were highly usable for research. Although, there is still a need to understand how urban vegetation and irrigation perform in other soil classes and what their influence is on the UHI-effect.

6.1.2 The influence of the Sky View Factor on the results

The sky view factor (SVF) indicates the amount of clear sky is visible from the calculated point or area. The SVF is a good indicator to predict the UHI-effect in an urban area. To determine the sensitivity of the SVF on this study is the average SVF of each case calculated and used in equation 2.3 to determine the predicted UHI-effect. Figure 4.10 shows the SVF within each case. The images clearly show, points closer to buildings and vegetation result in a lower SVF. Due the higher buildings and/or vegetation, the Oranjeboomstraat has a slightly lower average SVF of 0.470, while the Bredalaan has a higher standard deviation. A lower SVF implicates more radiation is converted into warmth by the surrounding urban objects. Based on the UHI-effect formula from T. R. Oke (2002) in equation 2.3, an average UHI-effect of 8.75 and 8.68°C is expected at respectively the Oranjeboomstraat and Bredalaan.

Recent study in Utrecht, the Netherlands, compared local measurements and calculations of the SVF based on remote sensing data. Besides, this study also included a reduced UHI-effect due the vegetation fraction (Dirksen, Ronda, Theeuwes, and Pagani, 2019). They found in their study that the UHI-effect was more sensitive to the SVF than the vegetation fraction. According to this study, the sensitivity to the SVF is linked to the resolution of the study. In calculating the SVF and vegetation fraction the recommendation is to have a resolution of 1m, while the SVF of figure 4.10 are based on a resolution of 2 metres.

Even-though the resolution of the SVF's calculation is lower than recommended, the difference in sky view factor translates into the difference in temperature between both cases. Figure 5.7, where a slightly lower

median and maximum temperature is visible for the Bredalaan, is in correspondence with the expected UHI-effect based on solely the SVF. Therefore, a slight difference in building height and vegetation fraction cause the difference in SVF and therefore a possible difference in maximum UHI-effect, with the Oranjeboomstraat being warmer than the Bredalaan.

6.1.3 The effects of increased vegetation on the case studies

The results in chapter 5 showed that the increased amount of vegetation without irrigation led to an increase of temperature, while the amount of evaporation in the case areas increased. The placement of green infrastructure is a main approach to reduce heat stress (Berardi, Jandaghian, and Graham, 2020; Kleerekoper et al., 2012; Zhao, Sailor, and Wentz, 2018). While Kleerekoper et al. (2012) focused a study on the larger scale effects of trees, Berardi et al. (2020) and Zhao et al. (2018) researched the local effects of tree placements.

Kleerekoper et al. (2012) addressed that trees show a reduced local effect, while on the large scale trees do have a temperature reducing effect. This can be in the form of parks or wide spread trees throughout the city. Kleerekoper et al. (2012) addresses green roofs and façades as an other viable implementation of green infrastructure. But Kleerekoper et al. (2012) also addresses the need for water based on a study by Schmidt (2006), focusing on rain water harvesting for irrigation. A vegetation placement research by Zhao et al. (2018) in Arizona, the United States, showed with ENVI-met the effects of different tree placements in front gardens. Zhao et al. (2018) found a reduced temperature for placement of single and double trees in the front garden. Even-though Zhao et al. (2018) found a reduced temperature, of 0.11 °C when placing trees in between two houses, the study did not include irrigation or soil moisture requirements, therefore is assumed that the default soil moisture content of ENVI-met is used. The default settings set a initial soil moisture content of 50% for the top 20cm and 60% for the deeper layers. Therefore the trees could still evaporate, while during the greener scenario the water availability is reduced.

Another study focused on the general fraction of green area in two Canadian neighborhoods in the Toronto area. Here too a temperature reduction of as high as 1.5 and 2 °C. Unfortunately also this study only researched with the standard soil moisture content of ENVI-met of 50-60%.

The reason of the increased temperature for the dry green scenario therefore has to found in another field of work. T. R. Oke (2002) described the Urban Canopy as an influence on the wind and therefore the temperature in the urban canyon between two façades. Therefore, shows figure 6.1 the relative wind velocity change between the dry current and dry greener scenario for 3 p.m. of July 27 in the middle of both cases.

As can be seen increases the wind velocity above both canyons slightly, while in between the façades and the back gardens a wind reduction evolves.

In the greener scenario the specific placement of green therefore reduces the air exchange between the between the canopy layer in the canyon and the higher air layer of the urban boundary layer, resulting in an increased canyon temperature.

6.1.4 The influence of the subsoils composition on the results

To understand how changes in soil composition affect the results some parameters are shortly discussed. Within this study the following soil parameters were included:

- Water content at saturation;
- Water content at field capacity;
- Water content at wilting point;
- Matrix potential;
- Hydraulic conductivity;
- Volumetric heat capacity; and
- Clapp & Hornberger constant

The water content at different water fractions, matrix potential in ENVI-met are based upon 1446 of 1800 soil samples from the United States (Roger B. Clapp and Hornberger, 1978). These samples have been tested to obtain several parameters and were classified into eleven groups based on mean clay fraction. All these parameters are determined with centimetre accuracy. Due the rather large sample size and process of the study these parameters have been taken over within this study.

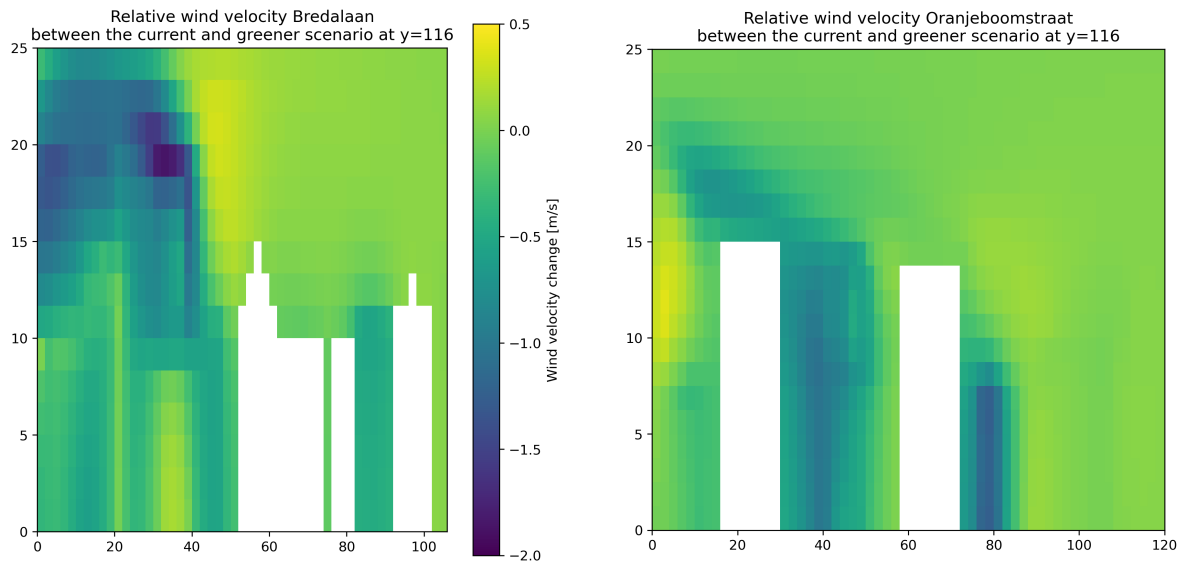


Figure 6.1: Relative wind velocity change at 27-7-2018 3 p.m. between the dry current scenario and dry greener scenario.

Within chapter 5 figures ??, 5.10, 5.18 & 5.19 show the effect of these parameters on the water availability, temperature and evaporation. As an example the relative soil moisture content with respect to field capacity for a sandy-soil hovers between $0.0068\text{--}0.135 \text{ m}^3 \text{ H}_2\text{O}/\text{m}^3 \text{ soil}$, while clayey soils hover between $0.286\text{--}0.367 \text{ m}^3 \text{ H}_2\text{O}/\text{m}^3 \text{ soil}$. So per cubic metre sandy-soil 0.1282 m^3 water can be extracted, while from the clay-soils only 0.081 m^3 water can be extracted. Besides, due the large difference in hydraulic conductivity $176 * 10^{-6}$ and $1.3 * 10^{-6} \text{ m/s}$ for respectively sand and clay, the groundwater flow is higher in the sandy soil. This higher flow velocity allows for recharge of water, enabling the higher evapotranspiration rates.

Based on these parameters, Roger B. Clapp and Hornberger (1978) found a relationship and came up with the Clapp & Hornberger constant this determines the relationship of the unsaturated hydraulic conductivity to determine the wetting front suction. A higher Clapp & Hornberger parameter results in a higher wetting front suction (Roger B. Clapp and Hornberger, 1978).

Due the Clapp & Hornberger constant' effect on the wetting front suction within unsaturated soil it influences the saturation rate and therefore the soil moisture content in the soil (R. B. Clapp, Hornberger, and Cosby, 1983). A change in the Clapp & Hornberger constant therefore influences indirectly the evaporation rate, heat and water transfer within the soil. Besides a difference in matrix potential at saturation, of -0.121 m for sandy soils and -0.405 m for clayey soils within ENVI-met, causes the differences in evaporation pattern for irrigated soils of figure 5.11. Due the higher matrix potential the soils recharge by irrigation is higher, enabling a more constant evaporation rate in the afternoon. Assuming the GeoTop soil composition are within margin of error, the accuracy of the Clapp & Hornberger constant is important to the soil system of ENVI-met.

No studies validating this approach to ENVI-met its soil and groundwater model were found. Therefore, more research should be done to confirm the approach by ENVI-met, possibly comparing it to (unsaturated) groundwater models.

6.2 Usage of ENVI-met

In the previous paragraph the relationship between this study and ENVI-met is already shortly addressed. Multiple aspects of the software potentially have an influence on the preciseness and accuracy of the results. Due its nature of a CFD model a critical aspect is stability of numerical values for wind, energy or temperature, and water and moisture content. Within this section the validation and verification of the results is discussed by addressing the internal models of ENVI-met. This is done by evaluating literature addressing the validation and verification results of ENVI-met as the microclimate model.

6.2.1 Numerical stabilization of ENVI-met

During this study the simulations failed numerous times due floating point errors or panic dumps. To reduce these kind of errors and shorten simulation time, three measures have been taken. The first measure taken is an increased horizontal and vertical resolution from 1 to 2 metre, to shorten simulation time. Secondly, nesting grids were applied to increase stability of the inflow. Thirdly, the wind direction change and/or wind velocity have been adapted to reduce instability.

Effect of a larger resolution

Within CFD software it is often ordinary that the grid or cell size should be independent from the results for a sufficiently fine raster, and the simulation should stay stable for any finer resolutions. However not many studies have analyzed the grid/cell-size with respect to cell independency for ENVI-met (Crank, Sailor, Ban-Weiss, and Taleghani, 2018). Since within this study the gridsize has been increased, the effects from increasing the grid have to be addressed.

Two studies are discussed to show the influence. Crank et al. (2018) used six vertical resolutions, from 0.75 to 2m, on a imaginary case study and compared the air temperature at 2m with respect to each other. While Maggiotto, Buccolieri, Santo, Leo, and Sabatino (2014) used three horizontal and three vertical resolutions.

Maggiotto et al. (2014) performed a convergence study for both horizontal and vertical resolution of 4, 2 and 1 metre. This convergence study showed a maximum air temperature difference of 2% at 2m height for a horizontal and vertical resolution of 2m with respect to measured data. For the vertical resolutions Crank et al. (2018) showed small fluctuation of the results of ENVI-met. The temperature increased slightly while decreasing the vertical grid resolution. The temperature change in ENVI-met is therefore less sensitive for resolution changes than spatial adaptations resulting in temperature changes.

At last, ENVI-met allows for vertical mesh refinement, splitting the lowest cell into five equal cells, but a refined mesh adjacent to all horizontal and vertical boundaries is not implementable. This could increase the accuracy of heat transfer at walls and at the rooftop boundaries.

Increasing the spatial resolution from 1m to 2m had a positive effect on stability of the model, while according to Maggiotto et al. (2014) 2 metre resolution is the ideal resolution for ENVI-met. Besides usage of the vertical mesh refinement increased accuracy of the model.

Effect of nesting grids

To increase stability the model was expanded with nesting grids which are extra empty grid cells at the border of the model. The nesting grids improve numerical stability, reduce numerical errors and the chance of floating point errors. Usage of the nesting grid has a therefore a useful addition to the model, although these cells have an effect on the air flow approaching the study area. The surface of these cells represents the urban environment around the case areas. Therefore, while increasing stability, it increases the temperature of the inflow slightly, but does not affect the outcome of the results, since the nesting grids are applied for all simulations. It could be said that the nesting grids increase the approximation of the characteristics of the urban area.

Effect of data manipulation

Within this study hourly weather station data of KNMI is used to determine the inflow within ENVI-met. The rural temperatures of the weather stations is changed to the local temperatures due the UHI-effect of the simulated urban environment within ENVI-met. ENVI-met updates the inflow characteristics every thirty minute interval. Therefore the data from KNMI has been interpolated from 60 to 30 minute intervals. The data is interpolated by averaging the hourly data to 30 minute intervals, with exception of precipitation, which is divided over both intervals. This data is used for the initial series simulations, unfortunately this often resulted in floating point errors or instabilities in the flow field.

These instabilities are caused by sudden changes between wind velocity and/or wind directional changes of the KNMI data. To reduce instability the meteorological data is adapted in several instances. The changes are presented in Appendix C To research out the influence of changing the wind directions a short study regarding wind directional change and the effects on air temperature is performed on the case of the Oranjeboomstraat.

This short study is performed on the base case of June 21 with temperature fluctuating between 18 and 28 °C. This study compared four wind directions with each other and showed that the relative mean and standard deviations in all comparisons hovered around 0°C. So therefore this did not result in significant changes.

6.3 Comparison of the results

Since the results are not validated with local measurements, the outcomes of this study are compared to other models. At first the results of this study are compared to the UHI-effect model of the National Institute for Public Health and the Environment (RIVM) (RIVM, 2018a) and a UHI-model from TNO based on satellite data (E. Klok, Schaminée, Duyzer, and Steeneveld, 2012). Secondly, the PET, or perceived temperature, results are compared to the National Heatmap of the PET (Goede, Timmermans, Moth, and de Niet, 2021), which is based on rural meteorological data and open source data to determine the local characteristics.

6.3.1 Comparison of the results with RIVM's UHI-model

Figure 4.14 shows the expected UHI-effect based on the model of the RIVM (2018a). This model is based on yearly average temperature differences between rural and urban areas, taking into account wind speed, vegetation, impermeable surfaces, population density and land use.

The initial maximum UHI-effect is adjusted on the average wind velocity and population density. Based on the amount of surface water, green and impermeable surfaces within 1km of an area the maximum UHI-effect is locally adjusted. Based on locally available green within 30m the UHI-effect is adjusted even further (RIVM, 2018b).

Figure 4.14, based on this study, shows a maximum UHI-effect of larger than 2°C at the Bredalaan, Eindhoven, and 1.6-1.8°C at the Oranjeboomstraat Rotterdam. This can be compared to the results presented in figures 5.5, 5.16 and 5.17. To first compare the results to figure 5.5, it can be seen that in the Oranjeboomstraat shows a maximum UHI-effect of 3.2 and 3.8°C for a wet and dry soil respectively, while the Oranjeboomstraat showed a maximum of 2.0-4.0°C for a dry and wet soil respectively. When comparing the current and irrigated current situation of figures 5.16 and 5.17 with respect to the RIVM model. The Bredalaan has a maximum UHI-effect of 4-5°C for the current situation, while the irrigated scenario fluctuates daily between 3 and 5°C.

The difference between RIVM's model and this study is caused by RIVM's usage of the average UHI-effect observation, while this study observed the peak UHI-effect over a heatwave and a day with extreme temperatures. Furthermore, this study focuses on a 2 by 2 metre resolution, while RIVM's study resolution is initially 250m, which is adjusted at the 10m resolution for the various factors.

When spatially comparing the warmer areas between the models it can be observed within this study ENVI-met neglects the effect of nearby surface water, since this was outside the research area. Due the larger range of RIVM's model the Persoonshaven, located on the North-East of the Oranjeboomstraat, is cooler than the Oranjeboomstraat, which is not shown in the results of this study.

6.3.2 Comparison of the results with TNO's UHI-model

Before anything can be said of ENVI-met its estimation of the UHI-effect, are the results compared to TNO's model. TNO's model estimated the maximum peak UHI-effect based on infrared imagery on a 1 by 1km scale for June 16 2006 at daytime and July 17 2006 nighttime. This measured data for rural areas is then interpolated for the urban areas and then compared to the original data to determine the UHI-effect, which resulted in figure 6.2 by E. Klok et al. (2012).

Figure 6.2 shows a maximum UHI-effect for both Eindhoven and Rotterdam of 8°C. Due the low resolution of 1x1km local influences are not accounted for within this model and is it hard to make an exact comparison with both the cases, but the range of the extremes at both cases for the current scenario of 5°C, shows a similar range of UHI-effect.

6.3.3 Comparison of the PET

The National heatmap PET is made with meteorological data of July 1 2015, which has the occurrence in the Netherlands of every once in a thousand summer days (Goede et al., 2021). For this day the average PET between noon and 6 p.m. is determined by using the following data:

Meteorological data used:

- Temperature;
- Radiation;
- Wind velocity;
- Humidity; and
- Solar angle.

Spatial data used:

- Land use;
- SVF;
- Object height;
- Vegetation ratio; and
- Trees.

These parameters are used to calculate the PET for a 2 by 2m resolution with the following formula from de Nijs et al. (2019):

$$PET_{sun} = -13.26 + 1.25T_a + 0.011Q_{gl} - 3.37\ln(u) + 0.078T_w + 0.0055Q_{gl}\ln(u) + 5.56\sin(\phi) - 0.0103Q_{gl}\ln(u)\sin(\phi) + 0.546B_b + 1.94SVF \quad (6.1)$$

$$PET_{shade,night} = -12.14 + 1.25T_a - 1.47\ln(u) + 0.060T_w + 0.015SVFQ_d + 0.0060(1 - SVF)\sigma(T_a + 273.15)^4 \quad (6.2)$$

Where:

- T_a is the air temperature at 2m[°C];
- T_w is the wet bulb temperature at 2m[°C];
- u is the wind velocity at 1.2m[m/s];
- σ is the Stefan Boltzmann constant;
- Q_d is the diffusive radiation[W/m²];
- Q_{gl} is the global radiation[W/m²];
- ϕ is the solar angle; and
- B_b is the Bowen ratio.

Within this calculation the meteorological factors are all comparable with respect to ENVI-met its calculation. The calculation of ENVI-met is based upon Gagge, Stolwijk, and Nishi (1972) and adapted by Höppe (1999) for usability. ENVI-met's calculation takes objects, air temperature, meant radiant temperature, horizontal wind velocity, the specific humidity and anthropological factors into account. RIVM's PET map is an approach of the Höppe model and adjusted for a specific range.

Now comparing the results of RIVM's model with the ENVI-met calculation. Figure 6.3 shows the PET map of both cases of Goede et al. (2021). It can be seen that the values show substantially lower extreme values than this study showed in figures 5.14 & 5.15, due averaging the outcomes of Goede et al. (2021) study. ENVI-met seems to show higher values than figure 6.3, but for July 28 2018 the values seem to be in the same range for both cases their current scenario. Furthermore, the minimum PET temperature at both cases in the interval the last four days in figures 5.14 & 5.15 seems to be lower in ENVI-met. The results of ENVI-met show a larger range due which comfortable and warmer locations can be distinguished more easily. Both models give a good estimation of the PET on a warm summer day, enabling localization of hotspots which have a need to be adapted to cope with heat stress.

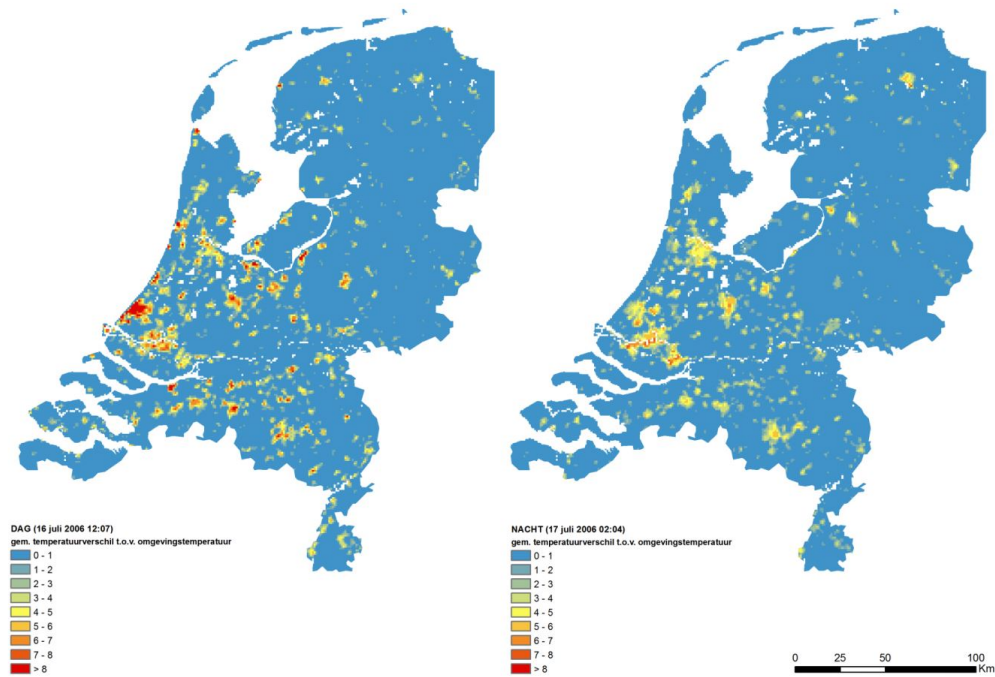
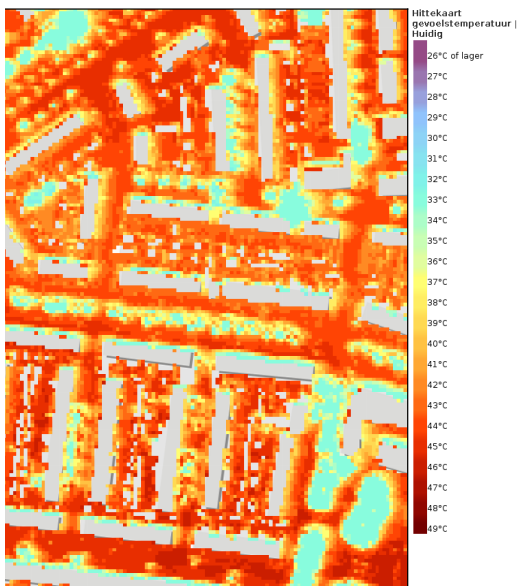


Figure 6.2: The UHI-effect based on infrared imagery for daytime (left) and nighttime (right) (E. Klok, Schaminée, Duyzer, and Steenveld, 2012)

Bredalaan



Oranjeboomstraat

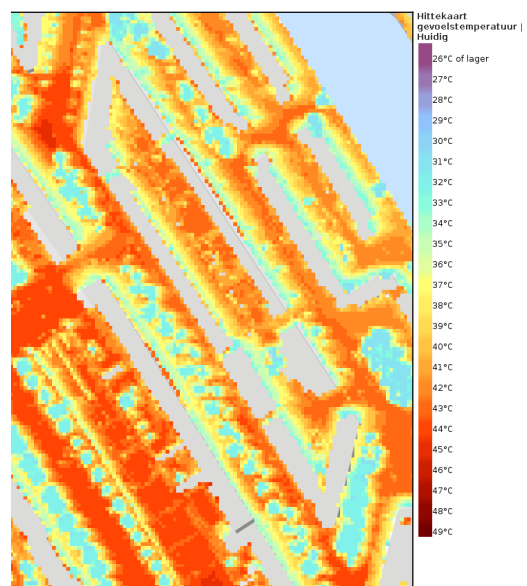


Figure 6.3: PET map of both the Bredalaan and Oranjeboomstaat by Goede, Timmermans, Moth, and de Niet (2021).

Chapter - 7

Conclusion & recommendations

This chapter concludes the research by answering the main research questions. Subsequently, Section 7.2 explains the recommendations for changes in the urban environment and further research.

7.1 Conclusions

This study aimed to show the effects of irrigation on urban drought, temperatures and thermal comfort, with the intend to reduce the UHI-effect in urban areas. This lead to the main question of how irrigation measures are linked to cooling by nature and drought reduction. This is accompanied with three questions regarding the soil moisture content and the relationship with respect to the urban temperature and evaporation rate of vegetation, but also which spatial adaptations influence temperature and drought positively. These questions are defined as 1) What is the effect of the soil moisture content on the urban evaporation rate of vegetation? 2) What is the effect of the soil moisture content on the urban temperature? And 3) Which spatial adaptations can influence both the temperature and drought positively? This question focuses on which measures could be taken to increase permeability or storage of water, while also increasing thermal comfort.

At last the effects of impervious surfaces and different soil physical characteristics on the performance of the irrigation measures and the urban evaporation rate is given based on this study.

The link between irrigation measures cooling by nature and drought reduction

Irrigation and drought reduction both increase water availability, the water availability enables higher evaporation rates which reduce ambient temperatures. Often is perceived that making a urban area greener will reduce urban temperatures, which is true when enough soil water for evaporation is available. Though, when droughts occur within urban areas insufficient water is available for evaporation, this could lead to increased temperature with respect to urban areas with lower ratios of green vegetation. But when sufficient water is available the UHI-effect and PET can both be reduced substantially during both day and nighttime.

The effect of soil moisture content on the evaporation rate

With respect to the tropical day simulation for the current situation, a clear increase of evaporation rates was visible at both locations. The Bredalaan showed a slightly lower ratio of increase of evaporation at 10% to 100% field capacity with respect to the Oranjeboomstraat, but a higher daily average evaporation was achieved at the Bredalaan. Remarkably, the Oranjeboomstraat showed an evaporation increase with almost 100% by increasing the field capacity from 10% to 50%, while the Bredalaan only showed an increase of 50%. Furthermore could be seen that higher evaporation rates, when irrigation is applied, maintain a natural pattern with respect to expected daily patterns of reference crop evaporation, while the dryer scenarios show a reduced evaporation rate between approximately 10 a.m. and 4 p.m.

When comparing the trend of the daily simulation with the series simulation for the current scenario shows a daily increase of 200% when irrigation is applied at both the Bredalaan and Oranjeboomstraat. But when comparing the dry greener scenario with respect to the irrigated greener scenario of both cases, the same increase in average evapotranspiration rate was observed. Therefore can be concluded that irrigation increases the evaporation with respect to dry soil up to 200% on average.

The effect of the soil moisture content on the urban temperature

Increase of the soil moisture content not only increases the evaporation rate but it also reduces urban temperatures. Increasing the soil moisture content reduces not only the average temperature but also reduces extreme temperatures within both case studies. The maximum daily simulated median temperature reduction due irrigation was between 0.5°C and 1.25°C . Furthermore, irrigation is effective in cooling urban areas faster after sundown, thus not only reducing the daily UHI-effect but also lowering the nocturnal UHI-effect.

Spatial adaptations that influence both the temperature and drought positively

Within this research is focused on two kinds of spatial adaptations, irrigation enabling transformations and green infrastructure implementations. With regards to irrigation enabling transformations only the effects of irrigation itself is modelled, while for green infrastructure two different scenarios could be compared.

For both cases an increase of vegetated fraction in gardens and public spaces is modelled. In gardens is focused on grasses, low vegetation and hedges, while for public spaces is focused on trees and grasses. Adding vegetation without adding water resulted in an increase of air temperature, while reducing the PET. When the soil of the vegetation was kept moist and irrigated the temperatures were reduced in each case. Furthermore, applying irrigation in the current situation already proves promising reducing temperatures.

The effects of the soil physical characteristics

Using two case studies with different subsoils allows comparison of the two soil types with each other. The two primary soil types within the subsoils in Eindhoven and Rotterdam are sand and clay respectively. While the irrigation measures increased evaporation this also decreased air temperature. For both cases a different trend could be observed for both the dry and irrigated scenarios.

To focus on the irrigated scenarios and the effect of the subsoil on the performance of the irrigation. It could be seen in figure 5.11 that at the Oranjeboomstraat a natural trend can be seen with respect to the evaporation, a single peak with a sinusoidal trend. For the same case, but with drier soil moisture profiles, a reduced evaporation can be observed between noon and 4 p.m. The irrigation in the wettest scenario not only increased the evaporation, but due having a clayey soil it showed resilience and the soil performed as a sponge, keeping the soil moist.

When looking at the Bredalaan for all scenarios a reduced evapotranspiration can be observed between 1 p.m. and 4 p.m. The sandy subsoil allows the vegetation to use all available water as soon as possible. The high hydraulic conductivity allows for a higher discharge capacity of water, but due this high hydraulic conductivity the soil dries out too quickly and the irrigated water cannot reach the roots as fast as necessary. A drier soil reduces the hydraulic conductivity and adhesive forces of water particles are reduced, resulting in a less resilient trend.

This difference in soils is caused by difference in the water content at wilting point, which is higher for a clayey soil than a sandy soil.

This can be seen in the evaporation rates of with respect to the two soils. While the sandy soil in the current situation reached a maximum evaporation rate of 0.9 mm/h for a soil at field capacity, the clayey soil performed about 20% worse with an evaporation rate of 0.70 m³/h. Even starting at lower relative soil wetness resulted in higher evaporation rates for a sandy soil over the clayey soil.

But when comparing the results for a relative soil wetness of 75 and 100% something remarkable is visible. Due the high evapotranspiration rates in sandy soils the hourly rate starts to decline rapidly after a peak at 11 a.m. The sandy soil can not satisfy the demand for water by the vegetation, while the clayey subsoil does not show this event. For the sandy subsoil this event not only occurred in a daily simulation, but also during the time series.

On the warmest day of the series simulation on July 27, the exact same event actually also takes place for the clayey subsoil. Therefore, this type of event is not only linked to just the soil physical parameters, but also to the evaporation demand. Since the evaporation demand of the vegetation in ENVI-met is reduced when water stress occurs.

The effects of impervious surfaces on drought severity, temperature and evaporation rates

From the literature study in chapter 2, it was already clear that there is a link between the UHI-effect and impervious surfaces, higher rates of imperviousness resulted in a stronger UHI-effect. Furthermore, the presence of impervious surfaces means that vegetation is not present, thus evaporation does not occur either. Therefore impervious surfaces increase drought, reduce evaporation rates and increase the ambient temperature.

This can be solved by changing impervious surfaces to porous paving materials, or reduce the amount of impervious surfaces. Furthermore can be thought of redirecting precipitation to an area destined for infiltration. These measures would allow higher soil moisture contents and thus increase evaporation, reducing the UHI-effect.

7.2 Recommendations

The recommendations are divided into recommendations regarding the urban transformation and further research. This is done to distinguish the applicability of this research in practice and the need for further research.

7.2.1 Further research

This study focused on two specific cases which were representative for respectively low rise street/block building typology with sandy soils and low rise block building typology with clayey subsoils. Within the Netherlands more than just these combinations occur, so research into the other combinations could be useful, alike comparison of this study to another clayey or sandy urban case area.

Regarding the other soil classes a peaty or loamy soil or combination of soils could give more insights in the behaviour of irrigation measures and the potential of coping with the urban heat island.

Another study which could be helpful is validating the soil model of ENVI-met and comparing it with (unsaturated) ground water models, such as MODflow, to compare the performance of ENVI-met top other models. This could need some adaptations within ENVI-met since within the software it is unable to specify individual soil moisture levels for each cell. Furthermore, ENVI-met can not handle soil moisture contents higher than field capacity or lower than 10% of field capacity as initial values.

Furthermore could be thought of calibrating an validating ENVI-met models after intensive temperature, soil moisture and sap flow monitoring. For example during a period of extreme heat in both areas, which could be modelled within ENVI-met. This could be done at either another location or at these cases.

This research is focused on a housing block till street level scale. On this scale the implementation of irrigation and increased vegetation seems promising to reduce the UHI, but a city is larger than a single housing block. Therefore, research into the effects on a larger scale could be interesting. Currently a temperature reduction of 0.75-1.25°C by irrigating was found, but on a larger scale this possibly could be higher, especially in denser urban areas. A larger reduction could be expected since the peak UHI-effect is often in the center of a city. Cooling not only this area, but also the area around, possibly would strengthen each other decreasing the UHI-effect further.

7.2.2 Application of measures in urban areas

Applying green infrastructure without a plan could result in an increase of air temperature. Therefore the following aspects should be taken into account when trying to reducing the urban heat island with green infrastructure:

- The amount, type and location of vegetation;
- the amount of impermeable surface;
- the building typology;
- the subsoil classification;
- local climate; and
- infiltration and irrigation capacity of the area.

The amount type and location of vegetation determine the evapotranspiration demand of a urban area, which is influenced by the local build environment, local climate and subsoil classification, as could be seen in this study. The amount of impermeable surfaces, and infiltration capacity, combined with the evaporation demand a water balance of the area can be made and estimated what amount of water is available for evaporation. From here can be determined if an additional amount of water should be supplied for irrigation to increase the evaporation rate, additional vegetation can be implemented, impermeable surfaces replaces by porous paving or a combination of these measures.

Besides local storage of excess water could be taken into account, this excess water could later be used for irrigation. To determine the amount of excess water storage the local climate should be taken into account, this determines the average monthly precipitation and gives an indication of the expected evaporation for the reference crop evaporation.

Taking this approach would give an insight in how to maximize space for vegetation, to reduce the UHI-effect, while taking the water demand of the vegetation into account.

Bibliography

- Actueel Hoogtebestand Nederland. (2019). Ahn viewer.
- Actueel Hoogtebestand Nederland. (2020). Ahn proces. Retrieved from <https://www.ahn.nl/proces>
- Ali-Toudert, F., & Mayer, H. (2007). Effects of asymmetry, galleries, overhanging façades and vegetation on thermal comfort in urban street canyons. *Solar Energy*, 81(6), 742–754. doi:<https://doi.org/10.1016/j.solener.2006.10.007>
- Alterra. (2006). Grondsoortenkaart. Retrieved from <https://ahn.maps.arcgis.com/home/webmap/viewer.html?useExisting=1&layers=af7a17abd0d24ef989e8b0e476107d9f>
- An interactive vegetation svat model tested against data from six contrasting sites. (1998). *Agricultural and Forest Meteorology*, 92(2), 73–95. doi:[https://doi.org/10.1016/S0168-1923\(98\)00091-4](https://doi.org/10.1016/S0168-1923(98)00091-4)
- Architecten", " (2019). Stad-x-klimaat. Retrieved from <https://www.bna.nl/kennis/bna-onderzoek/stad-x-klimaat>
- Attema, J., Bakker, A., Beersma, J., Bessembinder, J., Boers, R., Brandsma, T., ... Haarsma, R., et al. (2014). Knmi'14: Climate change scenarios for the 21st century—a netherlands perspective. *KNMI: De Bilt, The Netherlands*.
- Ayyad, Y. N., & Sharples, S. (2019). Envi-MET validation and sensitivity analysis using field measurements in a hot arid climate. *IOP Conference Series: Earth and Environmental Science*, 329, 012040. doi:10.1088/1755-1315/329/1/012040
- Bande, L., Afshari, A., Al Masri, D., Jha, M., Norford, L., Tsoupos, A., ... Armstrong, P. (2019). Validation of uwg and envi-met models in an abu dhabi district, based on site measurements. *Sustainability*, 11(16), 4378. doi:<https://doi.org/10.3390/su11164378>
- Basisregistratie Ondergrond. (2020). Retrieved March 10, 2020, from <https://basisregistratieondergrond.nl/inhoud-bro/registratieobjecten/modellen/geotop-gtm/>
- Beersma, J. (2007). *Extreme hydro-meteorological events and their probabilities*. Retrieved from http://projects.knmi.nl/publications/fulltexts/thesis_beersma_21823.pdf
- Berardi, U., Jandaghian, Z., & Graham, J. (2020). Effects of greenery enhancements for the resilience to heat waves: A comparison of analysis performed through mesoscale (wrf) and microscale (envi-met) modeling. *Science of The Total Environment*, 747, 141300. doi:<https://doi.org/10.1016/j.scitotenv.2020.141300>
- Berghauser Pont, M., & Haupt, P. (2009). Space, density and urban form. Retrieved from <http://resolver.tudelft.nl/uuid:0e8cdd4d-80d0-4c4c-97dc-dbb9e5eee7c2>
- Berkovic, S., Yezioro, A., & Bitan, A. (2012). Study of thermal comfort in courtyards in a hot arid climate. *Solar Energy*, 86(5), 1173–1186. doi:<https://doi.org/10.1016/j.solener.2012.01.010>
- Boukhabl, M., & Alkam, D. (2012). Impact of vegetation on thermal conditions outside, thermal modeling of urban microclimate, case study: The street of the republic, biskra. *Energy Procedia*, 18, 73–84. doi:<https://doi.org/10.1016/j.egypro.2012.05.019>
- Brandsma, T., & Wolters, D. (2012). Measurement and statistical modeling of the urban heat island of the city of utrecht (the netherlands). *Journal of Applied Meteorology and Climatology*, 51(6), 1046–1060. doi:<https://doi.org/10.1175/JAMC-D-11-0206.1>
- Broadbent, A. M., Coutts, A. M., Tapper, N. J., Demuzere, M., & Beringer, J. (2018). The microscale cooling effects of water sensitive urban design and irrigation in a suburban environment. *Theoretical and Applied Climatology*, 134(1-2), 1–23. doi:<https://doi.org/10.1007/s00704-017-2241-3>
- Brouwer, C., Goffeau, A., & Heibloem, M. (1985). Irrigation water management: Training manual no. 1 - introduction to irrigation.
- Bruse, M. (2004). Envi-met implementation of the jacobs a- gs model to calculate the stomata conductance.
- Clapp, R. B. [R. B.], Hornberger, G. M., & Cosby, B. J. (1983). Estimating spatial variability in soil moisture with a simplified dynamic model. *Water Resources Research*, 19(3), 739–745. doi:<https://doi.org/10.1029/WR019i003p00739>. eprint: <https://agupubs.onlinelibrary.wiley.com/doi/pdf/10.1029/WR019i003p00739>

- Clapp, R. B. [Roger B.], & Hornberger, G. M. (1978). Empirical equations for some soil hydraulic properties. *Water Resources Research*, 14(4), 601–604. doi:10.1029/WR014i004p00601
- Crank, P. J., Sailor, D. J., Ban-Weiss, G., & Taleghani, M. (2018). Evaluating the envi-met microscale model for suitability in analysis of targeted urban heat mitigation strategies. *Urban Climate*, 26, 188–197. doi:https://doi.org/10.1016/j.uclim.2018.09.002
- Dai, L., van Rijswick, H. F. M. W., Driessen, P. P. J., & Keessen, A. M. (2018). Governance of the sponge city programme in china with wuhan as a case study. *International Journal of Water Resources Development*, 34(4), 578–596. doi:10.1080/07900627.2017.1373637
- Dai, L., Wörner, R., & van Rijswick, H. F. M. W. (2018). Rainproof cities in the netherlands: Approaches in dutch water governance to climate-adaptive urban planning. *International Journal of Water Resources Development*, 34(4), 652–674. doi:10.1080/07900627.2017.1372273
- de Nijs, T., Bosch, P., Brand, E., Heusinkveld, B., van der Hoeven, F., Jacobs, C., ... Steeneveld, G. (2019). Ontwikkeling standaard stresstest hitte. doi:10.21945/RIVM-2019-0008
- de Ven, F., Nieuwkerk, E. v., Stone, K., Veerbeek, W., Rijke, J., Herk, S. v., & Zevenbergen, C. (2011). *Building the netherlands climate proof: Urban areas*. Deltares and Utrecht: Programme office Knowledge for Climate.
- Deltacomissie. (2017). *Deltaprogramma 2018*. Den Haag: Ministerie van Infrastructuur en Milieu and Ministerie van Economische Zaken.
- Dirksen, M., Ronda, R., Theeuwes, N., & Pagani, G. (2019). Sky view factor calculations and its application in urban heat island studies. *Urban Climate*, 30, 100498. doi:https://doi.org/10.1016/j.uclim.2019.100498
- E.S Van der Meulen, S., R.J. Broslma. (2015). *Ecosystem services provision: Dependence of water quality and quantity* (No. 1220357-000-BGS-0003). Deltares.
- Emmanuel, R., Rosenlund, H., & Johansson, E. (2007). Urban shading—a design option for the tropics? a study in colombo, sri lanka. *International Journal of Climatology: A Journal of the Royal Meteorological Society*, 27(14), 1995–2004. doi:https://doi.org/10.1002/joc.1609
- ENVI-Met GmbH. (2019a). ENVI MET: Getting started, Part 5 of 7: Design Spaces. Retrieved from https://www.envi-met.com/learning-support/getting-started/
- ENVI-Met GmbH. (2019b). Technical model webpage. Retrieved from http://www.envi-met.info/doku.php?id=start
- Fahmy, M., Sharples, S., & Yahiya, M. (2010). Lai based trees selection for mid latitude urban developments: A microclimatic study in cairo, egypt. *Building and Environment*, 45(2), 345–357. doi:https://doi.org/10.1016/j.buildenv.2009.06.014
- Fitts, C. R. (2013). *Groundwater science* (Second Edition). doi:https://doi.org/10.1016/C2009-0-62950-0
- Forouzandeh, A. (2018). Numerical modeling validation for the microclimate thermal condition of semi-closed courtyard spaces between buildings. *Sustainable Cities and Society*, 36, 327–345. doi:https://doi.org/10.1016/j.scs.2017.07.025
- Gagge, A., Stolwijk, J. A., & Nishi, Y. (1972). An effective temperature scale based on a simple model of human physiological regulatory response. *Memoirs of the Faculty of Engineering, Hokkaido University*, 13(Suppl), 21–36.
- Goede, A., Timmermans, J., Moth, L., & de Niet, A. (2021). *Landelijke hittekaart gevoelstemperatuur*. Stichting Climate Adaptation Services, Witteveen+Bos Raadgevende ingenieurs B.V.
- Google LLC. (2015). Google earth pro. Retrieved from https://earth.google.com/web/@51.90718899,4.50871261,4.90668022a,265.10477886d,35y,359.9996h,0t,0r?utm_source=earth7&utm_campaign=vine&hl=en
- Google LLC. (2020). Google earth pro. Retrieved from https://earth.google.com/web/@51.43965910,5.43788497,222.15305156a,0d,35y,0.3146h,0.0000t,0.0000r?utm_source=earth7&utm_campaign=vine&hl=en
- Grimmond, T., C.S.B.; Oke. (1999). Evapotranspiration rates in urban areas. (259). Retrieved from https://iahs.info/uploads/dms/11465.235-243-259-Grimmond.pdf
- Gross, G. (2017). Some effects of water bodies on the environment—numerical experiments. *Journal of Heat Island Institute International Vol*, 12, 2.
- Gunawardena, K., Wells, M., & Kershaw, T. (2017). Utilising green and bluespace to mitigate urban heat island intensity. *Science of The Total Environment*, 584-585, 1040–1055. doi:https://doi.org/10.1016/j.scitotenv.2017.01.158

- Hathway, E., & Sharples, S. [S.]. (2012). The interaction of rivers and urban form in mitigating the urban heat island effect: A uk case study. *Building and Environment*, 58, 14–22. doi:<https://doi.org/10.1016/j.buildenv.2012.06.013>
- Heber Green, W., & Ampt, G. A. (1911). Studies on soil physics. *The Journal of Agricultural Science*, 4(1), 1–24. doi:[10.1017/S0021859600001441](https://doi.org/10.1017/S0021859600001441)
- Höppe, P. (1999). The physiological equivalent temperature – a universal index for the biometeorological assessment of the thermal environment. *International Journal of Biometeorology*, 43, 71–75. doi:<https://doi.org/10.1007/s004840050118>
- Hove], L. [, Jacobs, C., Heusinkveld, B., Elbers, J., Driell], B. [, & Holtslag, A. (2015). Temporal and spatial variability of urban heat island and thermal comfort within the rotterdam agglomeration. *Building and Environment*, 83, 91–103. Special Issue: Climate adaptation in cities. doi:<https://doi.org/10.1016/j.buildenv.2014.08.029>
- Huttner, S., & Bruse, M. (2009). Numerical modeling of the urban climate—a preview on envi-met 4.0.
- Jacobs, C., Klok, L., Bruse, M., Cortesão, J., Lenzholzer, S., & Kluck, J. (2020). Are urban water bodies really cooling? *Urban Climate*, 32, 100607. doi:<https://doi.org/10.1016/j.uclim.2020.100607>
- Jacobs, C. M. J. (1994). *Direct impact of atmospheric co2 enrichment on regional transpiration*. Wageningen Universiteit. Retrieved from <https://edepot.wur.nl/206972>
- Kadaster. (n.d.). Retrieved 2020, from <https://bagviewer.kadaster.nl/lvbag/bag-viewer/index.html>
- Kleerekoper, L. (2016). Urban climate design. A+ BE| *Architecture and the Built Environment*, (11), 1–424. doi:<https://doi.org/10.7480/abe.2016.11>
- Kleerekoper, L., van Esch, M., & Salcedo, T. B. (2012). How to make a city climate-proof, addressing the urban heat island effect. *Resources, Conservation and Recycling*, 64, 30–38. Climate Proofing Cities. doi:<https://doi.org/10.1016/j.resconrec.2011.06.004>
- Klok, E., Schaminée, S., Duyzer, J., & Steeneveld, G. (2012). *De stedelijke hitte-eilanden van nederland in kaart gebracht met satellietbeelden*. TNO Earth, Environmental and Life Sciences.
- Klok, L., Rood, N., Kluck, J., & Kleerekoper, L. (2019). Assessment of thermally comfortable urban spaces in amsterdam during hot summer days. *International journal of biometeorology*, 63(2), 129–141.
- Klok, L., Zwart, S., Verhagen, H., & Mauri, E. (2012). The surface heat island of rotterdam and its relationship with urban surface characteristics. *Resources, Conservation and Recycling*, 64, 23–29. Climate Proofing Cities. doi:<https://doi.org/10.1016/j.resconrec.2012.01.009>
- KNMI. (2015). *Knmi'14 climate scenarios for the netherlands: A guide for professionals in climate adaptation*. KNMI: De Bilt, The Netherlands.
- KNMI. (2020a). Daggegevens van het weer in nederland, de bilt. Retrieved from 'https://cdn.knmi.nl/knmi/map/page/klimatologie/gegevens/daggegevens/etmgeg_260.zip'
- KNMI. (2020b). Uitleg over tropische dagen. Retrieved from <https://www.knmi.nl/kennis-en-datacentrum/uitleg/tropische-dagen>
- KNMI; ESRI. (2020a). Annual average precipitation from 1971-2010. Retrieved from <https://ahn.maps.arcgis.com/home/item.html?id=36869216a0aa425aa03cb0edc158db53>
- KNMI; ESRI. (2020b). Annual average reference evaporation from 1971-2010. Retrieved from <https://esrinl-content.maps.arcgis.com/home/item.html?id=d2e4399aa3c9447f94d63acbddd8b75c4>
- KNMI; ESRI. (2020c). Expected urban heat island effect. Retrieved from <https://ahn.maps.arcgis.com/home/item.html?id=a16b8b0d540c4e598d416aaf7ee6bd28>
- Lenzholzer, S., Klemm, W., & Vasilikou, C. (2018). Qualitative methods to explore thermo-spatial perception in outdoor urban spaces. *Urban Climate*, 23, 231–249. ICUC9: The 9th International Conference on Urban Climate. doi:<https://doi.org/10.1016/j.uclim.2016.10.003>
- Li, Q., Wang, F., Yu, Y., Huang, Z., Li, M., & Guan, Y. (2019). Comprehensive performance evaluation of lid practices for the sponge city construction: A case study in guangxi, china. *Journal of Environmental Management*, 231, 10–20. doi:<https://doi.org/10.1016/j.jenvman.2018.10.024>
- Lundh, F. (1999–2008). ElementTree.py. Retrieved from <https://github.com/python/cpython/blob/3.6/Lib/xml/etree/ElementTree.py>
- Maggiotto, G., Buccolieri, R., Santo, M. A., Leo, L. S., & Sabatino, S. D. (2014). Validation of temperature-perturbation and cfd-based modelling for the prediction of the thermal urban environment: The lecce

- (it) case study. *Environmental Modelling & Software*, 60, 69–83. doi:<https://doi.org/10.1016/j.envsoft.2014.06.001>
- Ng, E., Chen, L., Wang, Y., & Yuan, C. (2012). A study on the cooling effects of greening in a high-density city: An experience from hong kong. *Building and Environment*, 47, 256–271. International Workshop on Ventilation, Comfort, and Health in Transport Vehicles. doi:<https://doi.org/10.1016/j.buildenv.2011.07.014>
- Oke, T. R. (1981). Canyon geometry and the nocturnal urban heat island: Comparison of scale model and field observations. *Journal of climatology*, 1(3), 237–254. doi:<https://doi.org/10.1002/joc.3370010304>
- Oke, T. R. (2002). *Boundary layer climates*. doi:<https://doi.org/10.4324/9780203407219>
- Oke, T. [T.R.]. (1973). City size and the urban heat island. *Atmospheric Environment (1967)*, 7(8), 769–779. doi:[https://doi.org/10.1016/0004-6981\(73\)90140-6](https://doi.org/10.1016/0004-6981(73)90140-6)
- Rijkswaterstaat. (2020). Actueel hoogtebestand nederland. Retrieved from <https://www.rijkswaterstaat.nl/zakelijk/open-data/actueel-hoogtebestand-nederland/index.aspx>
- RIVM. (2018a). Stedelijk hitte-eiland effect (uhi) in nederland. Retrieved from <https://nationaalgeoregister.nl/geonetwork/srv/dut/catalog.search#/metadata/a87f5ca8-f354-4ff6-adc3-70f1bf6b78e3?tab=general>
- RIVM. (2018b). Stedelijk hitte-eiland effect (uhi) in nederland. Retrieved from <https://www.atlasnatuurlijkkapitaal.nl/kaarten?config=58bf95bc-67bf-402d-a355-af211ad33949&gm-x=121187.11870218973&gm-y=467370.5793842884&gm-z=3.1666666666666665&gm-b=1544180834512,true,1;1554714019959,true,0.8;&activeTools=layercollection,search,info,bookmark,measure,draw&activateOnStart=layermanager>
- Santamouris, M. (2013). *Energy and climate in the urban built environment*. doi:<https://doi.org/10.4324/9781315073774>
- Schmidt, M. (2006). The contribution of rainwater harvesting against global warming. *Technische Universität Berlin, IWA Publishing, London, UK*, 9.
- Schrijvers, P., van der Hoeven, F., Wandl, A., Hensen, J., van den Dobbelsteen, A., Kleerekoper, L., ... Blocken, B. (2014). *Climate proof cities final report*. Climate Proof Cities consortium, Delft. Retrieved from <http://resolver.tudelft.nl/uuid:11ed06c0-d377-439e-8e3b-d7db3b5bd8d6>
- Schulze, E.-D., Turner, N., Gollan, T., & Shackel, K. (1987). Stomatal responses to air humidity and soil drought. In *'Stomatal Function'*. (Eds E. Zeiger, G. D. Farquhar and IR Cowan.) 311–321.
- Schurr, U., Gollan, T., & Schulze, E.-D. (1992). Stomatal response to drying soil in relation to changes in the xylem sap composition of helianthus annuus. ii. stomatal sensitivity to abscisic acid imported from the xylem sap. *Plant, Cell & Environment*, 15(5), 561–567.
- Sluijter, R. [R.], Plieger, M., van Oldenborgh, G., Beersma, J., & de Vries, H. (2018). *De droogte van 2018: Een analyse op basis van het potentiële neerslagtekort* (No. 117162). KNMI.
- Sluijter, R. [Rob], Plieger, M., van Oldenborgh, G. J., Beersma, J., & de Vries, H. (2018). *De droogte van 2018: Een analyse op basis van het potentiële neerslagtekort*. KNMI.
- Solcerova, A., van de Ven, F., & van de Giesen, N. (2019). Nighttime cooling of an urban pond. *Frontiers in Earth Science*, 7, 156. doi:10.3389/feart.2019.00156
- Spaan, B. " S. (2015). All buildings in the netherlands shaded by year of construction. Retrieved from <http://code.waag.org/buildings/>
- Spinoni, J., Naumann, G., Carrao, H., Barbosa, P., & Vogt, J. (2014). World drought frequency, duration, and severity for 1951–2010. *International Journal of Climatology*, 34(8), 2792–2804.
- Steenefeld, G., Koopmans, S., Heusinkveld, B., & Theeuwes, N. (2014). Refreshing the role of open water surfaces on mitigating the maximum urban heat island effect. *Landscape and Urban Planning*, 121, 92–96. doi:<https://doi.org/10.1016/j.landurbplan.2013.09.001>
- Stichting CAS. (2016). *Nationale klimaatadaptatiestrategie 2016*. Den Haag: ministerie van Infrastructuur en Milieu. Retrieved from <https://ruimtelijkeadaptatie.nl/overheden/nas/>
- Stocker, T. F., Qin, D., Plattner, G.-K., Tignor, M., Allen, S. K., Boschung, J., ... Midgley, P. M., et al. (2013). Climate change 2013: The physical science basis. *Contribution of working group I to the fifth assessment report of the intergovernmental panel on climate change*, 1535. Retrieved from https://www.ipcc.ch/site/assets/uploads/2018/02/WG1AR5_all_final.pdf
- Taleb, D., & Abu-Hijleh, B. (2013). Urban heat islands: Potential effect of organic and structured urban configurations on temperature variations in dubai, uae. *Renewable energy*, 50, 747–762. doi:<https://doi.org/10.1016/j.renene.2012.07.030>

- TNO. (2020a). Dino Locket Ondergrondmodellen. Retrieved December 2, 2020, from <https://www.dinolocket.nl/ondergrondmodellen>. (Coordinates:158515, 383385 (RD); Depth: 0-4.5m with respect to surface level)
- TNO. (2020b). Dino Locket Ondergrondmodellen. Retrieved March 10, 2020, from <https://www.dinolocket.nl/ondergrondmodellen>. (Coordinates:94563, 435730 (RD); Depth: 0-4.5m with respect to surface level)
- TNO. (2020c). Dino Locket Ondergrondmodellen. Retrieved March 10, 2020, from <https://www.dinolocket.nl/ondergrondmodellen>. (Coordinates:94468, 436094 (RD); Depth: 0-4.5m with respect to surface level)
- Toparlar, Y., Blocken, B., Vos, P., Heijst], G. [, Janssen, W., Hooff], T. [, ... Timmermans, H. (2015). Cfd simulation and validation of urban microclimate: A case study for bergpolder zuid, rotterdam. *Building and Environment*, 83, 79–90. Special Issue: Climate adaptation in cities. doi:<https://doi.org/10.1016/j.buildenv.2014.08.004>
- Turner, N. C. (1991). Measurement and influence of environmental and plant factors on stomatal conductance in the field. *Agricultural and Forest Meteorology*, 54(2), 137–154. doi:[https://doi.org/10.1016/0168-1923\(91\)90003-9](https://doi.org/10.1016/0168-1923(91)90003-9)
- Van de Ven, F. (1990). Water balances of urban areas. *INT ASSOC OF HYDROLOGICAL SCIENCES, WALLINGFORD,(ENGL)*. 1990. 198(3), 21–32. Retrieved from <https://iahs.info/uploads/dms/8508.21-32-198-van-de-Ven.pdf>
- Voogt, J., & Oke, T. [T.R]. (2003). Thermal remote sensing of urban climates. *Remote Sensing of Environment*, 86(3), 370–384. Urban Remote Sensing. doi:[https://doi.org/10.1016/S0034-4257\(03\)00079-8](https://doi.org/10.1016/S0034-4257(03)00079-8)
- Walther, E., & Goestchel, Q. (2018). The p.e.t. comfort index: Questioning the model. *Building and Environment*, 137, 1–10. doi:<https://doi.org/10.1016/j.buildenv.2018.03.054>
- Williams, E. (2019). *Integrating the household scale into climate adaptation planning*.
- Witteveen, A. (2014). *Rain, catch it if you can*. Retrieved from <https://repository.tudelft.nl/islandora/object/uuid%5C%3Aabbf06c9f-17c0-41a8-924e-141e9a331b44>
- Wu, Z., Dou, P., & Chen, L. (2019). Comparative and combinative cooling effects of different spatial arrangements of buildings and trees on microclimate. *Sustainable Cities and Society*, 51, 101711. doi:<https://doi.org/10.1016/j.scs.2019.101711>
- Zhao, Q., Sailor, D. J., & Wentz, E. A. (2018). Impact of tree locations and arrangements on outdoor microclimates and human thermal comfort in an urban residential environment. *Urban Forestry & Urban Greening*, 32, 81–91. doi:<https://doi.org/10.1016/j.ufug.2018.03.022>

Chapter - A

Appendix - Detailed ENVI-met description

Chapter 3, the methodology, is discussed stating the different aspects and processes of the ENVI-met model. To give more detail of these the individual applications within the model are discussed in detail. Furthermore the input system of ENVI-met is given.

A.1 Atmospheric model of ENVI-met

The basis of ENVI-met, as could be seen in figure 3.2, is the atmospheric model. The atmospheric model takes the natural processes and characteristics into account. These processes and characteristics, which are the forcing factors behind the model, are:

- short and long-wave radiation including shading and reflection;
- wind and turbulence and
- temperature and humidity.

Based on the data input of the simulation, an atmospheric model is created. The atmospheric model takes five calculation aspects into account. The first aspect is the wind flow field of the urban environment. A full three dimensional Computational Fluid Dynamics (CFD) model of the wind field is made. The CFD-model takes the buildings, vegetation and elevation into account, while solving the model for space and time. The second aspect the model takes into account is turbulence. The third aspect is pollutant dispersion, though since this is not relevant for this research, this will not be elaborated on further.

The fourth aspect are the radiative incoming and outgoing fluxes. The incoming and outgoing fluxes give a understanding of the energy balance within the urban environment. To make an good estimate of this energy balance, ENVI-met takes shading, reflection and vegetation all into account when making these calculations. The last aspect are the air temperature and humidity, which represent the outdoor thermal quality. The factors are calculated by the interactive processes between air, soil and structures.

Being the forcing factor between the simulation, it is important that these aspects are given correctly. Though, the output from the atmospheric model is essential to make a distinctive decision on impact. The output from ENVI-met is focused on meteorological parameters. These parameters, such as temperature, wind and humidity, are the meteorological parameters influencing the Physiological Equivalent Temperature (PET) (Höppe, 1999; Walther and Goestchel, 2018).

Since these parameters are influenced by the processes and infrastructure in the urban environment, a good simulation is essential.

A.2 Built environment and building systems of ENVI-met

An urban environment is defined by the lay-out of the infrastructure. The infrastructure consists of roads, drainage, buildings and supporting structures. In other words it is the built environment. The built environment can be defined in ENVI-met by the spaces application to a model of the urban environment. The model interact with the modelled environmental processes in the urban environment. These processes come down to airflow around and between buildings and, exchange of water and energy in the form of heat and radiation. To simulate these processes precisely, the built environment should be modelled as precisely as possible.

To create a precise model, ENVI-met uses the built-in Spaces application. The spaces application is a concept design application, which allows the user to set-up the model area. Within the model area six aspects are defined:

1. The model's geographical information, including elevation data;
2. The model's resolution;
3. The soil profile;
4. The surface layer;
5. The built environment; and
6. The vegetation.

The geographical information and model's resolution are both defined for the entire model, whereas the other parameters can be defined for each cell individually as building blocks. The model is constructed with these building blocks to approach the desired urban environment. These building blocks can later be adapted to further define building materials, glass location, and green roofs and facades. All the materials and their characteristics can be adapted through their parameters in the database system.

The built environment creates the context of the urban environment, which enables research within the urban environment. The buildings and vegetation interact with the atmosphere, while the vegetation also interacts with the soil model. Therefore to understand these interactions the vegetation model is discussed in the next section.

A.3 Vegetation model of ENVI-met

The vegetation model of ENVI-met is interacting with the atmosphere and soil model within ENVI-met. Within ENVI-met two types of vegetation are represented. The first type is 3D-generated plants and secondly simple vertical plants, such as grass and simple trees. These two types of vegetation result into the same processes; water extraction from the soil and providing shading and cooling by evaporation.

To understand the evapotranspiration rate of the vegetation and the water extraction by the roots, their relationship and processes are given in the upcoming paragraphs. Water extraction from the soil is dependent on the available soil moisture in the root profile, influencing the evaporation rate of the vegetation. The initial rate of evaporation depends on the temperature of the leaves, or foliage temperature. The foliage temperature is calculated through the energy balance on the leaf structure, which directly influences the transpiration rate. The transpiration rate, on the other hand, reduces the leaf temperature. Therefore this in an iterative process, together with the CO_2 availability and water stress level in the soil (Bruse, 2004).

The stomata model is based on the correlation between the photosynthetic rate and stomatal resistance, or $A-g_s$ correlation, and the relationship with the relative soil moisture content of equation A.3 is based upon Calvet's adaption to water stress for the Jacob's model ("An interactive vegetation SVAT model tested against data from six contrasting sites", 1998; C. M. J. Jacobs, 1994). Equation A.1 shows the relationship and equation A.2 shows the net photosynthetic rate of a leaf. The photosynthetic rate is dependent on the CO_2 fixation of the plant. The CO_2 -fixation is either C_3 or C_4 , while the vast majority being C_3 plants (C. M. J. Jacobs, 1994).

$$g_s = 1.6 * \frac{A_n}{(C_s - C_i)} \quad (A.1)$$

Where

g_s is the stomatal resistance [mm/s];
 A_n ; is the photosynthetic rate [$mg\ CO_2/m^2\ s$];
 C_s ; is the CO_2 concentration at the surface of the leaf [$mg\ CO_2/m^3$]; and
 C_i ; is the intercellular CO_2 concentration [$mg\ CO_2/m^3$].

$$A_n = A_g - R_l - R_d \quad (A.2)$$

Where

A_g ; is the gross photosynthetic rate [$mg\ CO_2/m^2\ s$];
 R_l ; is the light respiration rate [$mg\ CO_2/m^2\ s$]; and
 R_d ; is the dark respiration rate [$mg\ CO_2/m^2\ s$].

To include the soil water stress within the model the relationship between the volumetric soil moisture content with respect to the wilting and field capacity of the soils is included in the model. This relationship is described as following by Bruse (2004) and C. M. J. Jacobs (1994) as:

$$\xi = \frac{\theta - \theta_w}{\theta_{fc} - \theta_w} \quad (\text{A.3})$$

where

- ξ ; is the relative available soil moisture content;
- θ ; is the soil moisture content in the soil at that time [$m^3 \text{H}_2\text{O}/m^3 \text{soil}$];
- θ_w ; is the soil moisture content at wilting point [$m^3 \text{H}_2\text{O}/m^3 \text{soil}$]; and
- θ_{fc} ; is the soil moisture content at field capacity [$m^3 \text{H}_2\text{O}/m^3 \text{soil}$].

The relative available soil moisture content is then used to scale the stomatal resistance as followed:

$$g'_s = \xi * g_s \quad (\text{A.4})$$

These factors and formulas are important for calculation of the evaporation rates within the vegetation model. Soil drought influences the stomatal behavior, which close when the water content reaches a certain value (Schulze, Turner, Gollan, and Shackel, 1987; Turner, 1991). This stomatal behavior is also proven with experiments with drying soil while keeping the bulk leaf water potential at a constant level (Schurr, Gollan, and Schulze, 1992). Within ENVI-met the scaled stomata resistance is used to calculate the transpiration of vegetation as balance of mass in the soil by the next equation:

$$m = \rho_a g'_s D_s \quad (\text{A.5})$$

Where

m is the transpiration rate of the plant per square metre of leaf per second

[$mg \text{H}_2\text{O} m^{-2} \text{Leaf} s^{-1}$];

ρ_a is the air density [kgm^{-3}]; and

D_s is the saturation specific humidity with respect to the specific humidity of the air just outside the stomatal pore [$gkg^{-1}s^{-1}$].

The combination of these formulas are the driving factors of the vegetation model. Though, as described before, a second influence on the evaporation rate is the root profile. The Root Area Density (RAD) profile, of any plant, can be given as an input in the database. The last influence on the evaporation rate is the Leaf Area Density (LAD), which defines together with its LAD-profile, the surface of the canopy and thus influences the amount of evaporation. For each individual plant the vertical integrals are taken to determine the transpiration flux and the root uptake for each specific soil layer. This is done by using the LAD en RAD to determine the total flux per area and suction per layer with the following equations:

$$m_{trans} = \rho_w \int_0^z LAD(z) J_{f,trans}(z) dz \quad (\text{A.6})$$

$$S_\eta(-z) = \frac{m_{trans}}{\rho_w} (RAD(-z) D_\eta(-z)) \left(\int_{-z}^0 RAD(-z) D_\eta(-z) dz \right)^{-1} \quad (\text{A.7})$$

To summarize, the vegetation's evaporation rate is depending on the soil moisture content, photosynthetic rate, carbon dioxide concentration and the characteristics of the vegetation. Due these relationships, the vegetation model is impactful on simulating the urban environment. The vegetation model influences, direct or indirectly, both soil and atmosphere conditions of the model.

To assure reliable results for both cases several aspects are assumed. The CO_2 fixation of vegetation within the model is C_3 -fixation for the various types of vegetation, while the RAD and LAD profiles are taken from ENVI-met's database for trees, hedges and grasses.

A.4 Soil model of ENVI-met

The foundation of an urban environment is the soil on which it is build. The soil model, based on the soil parameters of ENVI-met's database, depends on two main aspects. The first aspect is the type of material. The type of material defines how the physical processes behave within the soil structure. One physical process is heat transfer between the surface and under-laying layers. The heat transfer is calculated through the thermal conductivity of the soil profile and its current soil water content.

The soil water content, the second aspect of the soil model, is calculated based on a water balance, taking into account evaporation, water flow, which is defined by Darcy's law (see equation , and root suction, depending on the evaporation and available soil moisture. Darcy's Law is given in three dimensions by:

$$\begin{aligned} q_x &= -K_x \frac{\partial h}{\partial x} \\ q_y &= -K_y \frac{\partial h}{\partial y} \\ q_z &= -K_z \frac{\partial h}{\partial z} \end{aligned} \quad (\text{A.8})$$

The soil model is influenced by the evaporation, vegetation and top of the soil layer, which all are boundary conditions of the air and soil model. The radiative fluxes, described as part of the Atmospheric model of ENVI-met, come down onto the top soil layer. The top of the soil layer is then heated and will influence both the soil model as the atmospheric model. Besides, vegetation has a need for water from their root zone within the soil.

The root zone suction is influenced the water content in the soils. Therefore, it is important to define the soil profiles, its parameters and rootzone correctly within the model. The rootzone is dependent on the vegetation model which is addressed in the previous section(A.3). Within the water balance a volumetric water content in $m^3 H_2O$ per $m^3 soil$ per cell is derived. To calculate the volumetric water content, three values of water contents of each soil are the boundary condition for the water content, which are:

1. The water content at saturation;
2. The water content at field capacity;
3. The water content at wilting point.

ENVI-met approaches the water content in the unsaturated zone, after a rainfall event, by a wetting front based on the Green–Ampt Infiltration equation(Heber Green and Ampt, 1911), and is used with the Clapp and Hornberger Constant(Roger B. Clapp and Hornberger, 1978) for each specific soil to determine the conductivity in the unsaturated zone to determine thermal conductivity. The suction potential within the soil layers is approached by equation A.9:

$$\psi = \psi_s \left(\frac{\theta}{\theta_s} \right)^{-b} \quad (\text{A.9})$$

And the relative hydraulic conductivity in the layer is calculated through equation A.10:

$$\frac{K}{K_s} = \left(\frac{\theta}{\theta_s} \right)^{2b+3} \quad (\text{A.10})$$

Where:

- ψ is the suction potential [L];
- ψ_s is the saturated suction potential [L];
- θ is the soil moisture content in the soil [L^3/L^3];
- θ_s is the saturated soil moisture content of the soil [L^3/L^3];
- b is the Clapp and Hornberger constant;
- K is the specific hydraulic conductivity [L/T];
- K_s is the saturated specific hydraulic conductivity.

When derived with respect to the Darcy's Law, equation A.8, and the depth, the wetting front is calculated and a new specific hydraulic conductivity is determined. These are used to determine the thermal conductivity through the layers in combination with the diffusivity. Based on these factors the thermal conductivity is calculated. The thermal conductivity is important for the storage of thermal energy within the sub-surface of the urban area and therefore contributes to urban temperatures. The thermal conductivity is calculated through:

$$D_s = \frac{1}{b} * K_s \frac{\psi_s}{\theta_s} \quad (\text{A.11})$$

$$D = D_s \left(\frac{\theta}{\theta_s} \right)^{2+1/b} \quad (\text{A.12})$$

Where:

D is the thermal conductivity [L^2/T];

D_s is the saturated diffusivity [L^2/T];

Since the thermal conductivity is influenced by the water content within the sub-surface, can be concluded that the soil water content influences the thermal conditions of the urban environment. Besides the soil water content influences evaporation rates, which influence humidity and ambient temperature. To conclude, the soil model influences the urban temperature, evaporation rate and humidity of the atmospheric model.

A.5 Input data of ENVI-met

To enable a ENVI-met simulation specific information has to be given to the software to enable a simulation. This section discusses the multiple model input variables of ENVI-met. These model input variables are defined by three main aspects, which are the database system, Spaces or Area Input File, and the ENVI guide or the Simulation File. Since Spaces was shortly elaborated during an earlier section, only the two other aspects are discussed. The Database system is discussed regarding its structure and adaptability of the parameters. After which in the following paragraphs the ENVI guide is discussed.

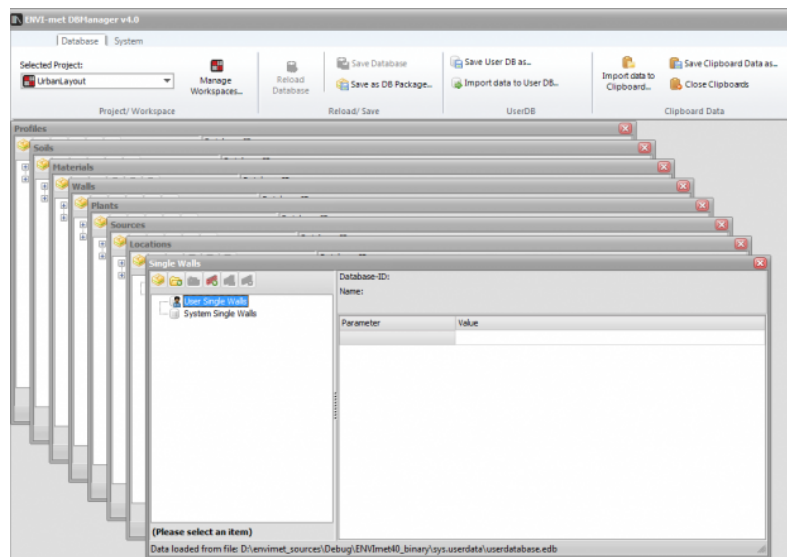


Figure A.1: An overview of the database manager of ENVI-Met. All eight panels can be adapted, to approach reality of that given material, soil or construction element (ENVI-Met GmbH, 2019b).

A.5.1 ENVI-met's database system

The database system is used to define parameters of materials, soils and vegetation, which combined give soil profiles, wall systems and green infrastructure systems, such as green facades and roofs. These parameters can be defined through the database manager, an image of the database manager can be seen in figure A.1,

which exists of the project group and eight panels for all the elements. The database manager is used to define the items of the simulation, which are defined with Spaces. Therefore, to approach the urban environment, the parameters within the database manager should represent reality.

While more accurately defining several parameters is out of the scope, the focus will be on modelling the surfaces, soils and soil-profiles as accurate as possible. These factors influence the subsoil processes on extraction within the unsaturated zone by vegetation. Therefore these factors influence the infiltration and evaporation rate, and therefore also the urban air temperature. The parameters of the subsoil and soil profiles that influence the evaporation, the subsoil flow and infiltration are given by:

Influencing the evaporation:

1. Water content at:
 - (a) field capacity;
 - (b) wilting point and
 - (c) saturation.
2. Plant height;
3. Root zone depth;
4. Leaf Area Density (LAD);
5. Root Area Density (RAD);

Influencing the subsoil flow and infiltration:

1. Matrix potential;
2. Hydraulic conductivity and
3. Clapp and Hornberger constant.

Since the evaporation rate influences the temperature due a change within the energy balance (2.1), and on itself also has an influence on the evaporation rate of the vegetation, the parameters influencing the energy balance within an urban environment have to be representative as well. The energy balance within the urban environment is influenced by physical properties of materials. These are represented within the database system by:

1. Absorption;
2. Transmission;
3. Reflectively or albedo;
4. Emissivity of long-wave radiation;
5. Thermal conductivity and
6. Specific heat.

The ENVI guide

The ENVI guide is used to set-up and initiate a simulation. After constructing the spaces input file and database for the simulation, the starting time, duration and meteorological input can be given. The meteorological input is given at half an hour intervals for several meteorological data which are:

- the absolute temperature in degrees Kelvin;
- the relative humidity in percentage;
- the wind velocity in metres per second;
- the wind direction and
- the precipitation in millimetres.

This data is prompt through a CSV file and converted by ENVI-met for the simulation. Additionally radiation or cloud cover can be given. Since ENVI-met is also capable of calculating the incoming radiation, based on geographical data, this application is used. To correctly process the input, ENVI-met depends on the input of the measurement height of the meteorological data which can be variable per aspect given. This data is then stored and later used for the simulation.

A.5.2 Parent-child relationships within the database

Some of the relevant parameters are defined by their parent-child-relationship, for example the parent of the profiles are the soils. Therefore to define the profiles the various soil elements have to be defined first. The parent-child-relationship within ENVI-met is given in table A.1, which gives insight in the most important databases. As can be seen are the soils, materials and plants databases the most relevant databases to adapt.

A \ B	Soils	Profiles	Materials	Plants	Greening	Walls	Single Walls
Soils	<i>x</i>	P	–	–	P	–	–
Profiles	C	<i>x</i>	–	–	–	–	–
Materials	–	–	<i>x</i>	–	–	P	P
Plants	–	–	–	<i>x</i>	P	–	–
Greening	C	–	–	C	<i>x</i>	–	–
Walls	–	–	C	–	–	<i>x</i>	–
Single Walls	–	–	C	–	–	–	<i>x</i>

Table A.1: The parent-child-relationships within the database of ENVI-met. When A is a parent of B this is shown with a "P". When A is a child of B this is given by a "C". When A is B this is given with a cross-mark(*x*) and if there is no relationship this is given with a dash(–).

A.5.3 The adjustable parameters within each database.

Each database's parameter can be adapted within ENVI-met. This section will primarily describe the three parent groups and their parameters, besides it gives insight in the additional parameters of the child databases.

Firstly the soil database is addressed regarding its adjustable parameters.

Soils	Input	Unit
Type of material	Artificial/Natural	–
Water content at saturation		$m^3 \text{ water} / m^3 \text{ soil}$
Water content at field capacity		$m^3 \text{ water} / m^3 \text{ soil}$
Water content at wilting point		$m^3 \text{ water} / m^3 \text{ soil}$
Matrix potential		m
Hydraulic conductivity		$m/s * 10^{-6}$
Volumetric heat capacity		$J/m^3 K * 10^6$
Clapp & Hornberger constant		–
Heat Conductivity		W/(m*K)

Table A.2: The adjustable parameters within the soil database.

Parameter	Value
Alternative Name	(None) <input type="button" value="..."/>
CO2 Fixation Type	C3 <input type="button" value="v"/>
Leaf Type	Gras <input type="button" value="v"/>
Albedo	0.40000 <input type="button" value="0"/>
Transmittance	0.30000 <input type="button" value="0"/>
Plant height	2.00000 <input type="button" value="0"/>
Root Zone Depth	2.00000 <input type="button" value="0"/>
Leaf Area (LAD) Profile	0.00000,0.00000,0.00000,0.00000,0.00000 <input type="button" value="0"/>
Root Area (RAD) Profile	0.00000,0.00000,0.00000,0.00000,0.00000 <input type="button" value="0"/>
Season Profile	1.00000,1.00000,1.00000,1.00000,1.00000 <input type="button" value="0"/>

Figure A.2: The plants' database can be adjusted on eight parameters.

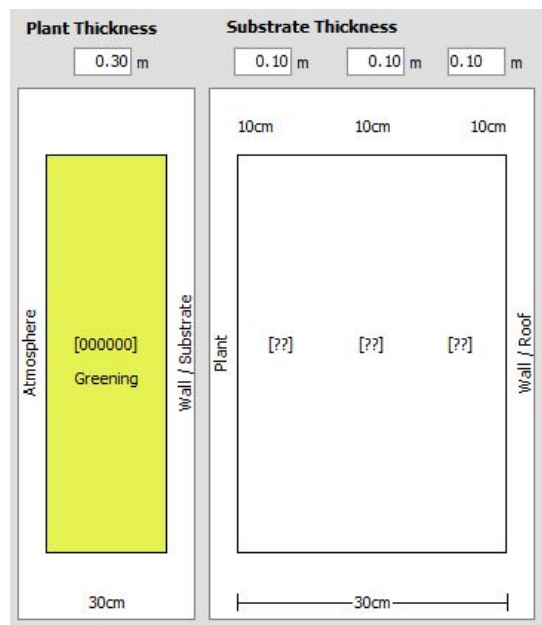


Figure A.3: The adjustable parameters of the roof and wall greening. The plant thickness and typology can be adjusted directly, likewise the LAD and LAI of the greening. Furthermore, an optional layer with variable thickness of substrate can be added, whose parameters are adapted through the soils database.

Chapter - B

Appendix - Multi criteria analysis of second location

Based on the Oranjeboomstraat, Rotterdam, a second location within Eindhoven is chosen. The second location is chosen primarily based on the subsoil. A different subsoil creates the opportunity to determine the effectiveness of measures under different circumstances. The city of Eindhoven is chosen due the sandy subsoil of the city, opposed to the clayey subsoil of Rotterdam. Based on five criteria a street is chosen out of eight potential locations. The chosen location is discussed as a case study in Chapter 4. This appendix discusses the characteristic of the Oranjeboomstraat in Rotterdam after which the profile in Eindhoven is chosen, based on a Multi Criteria Analysis (MCA). The characteristics discussed are:

- Street orientation;
- Building height;
- Building age;
- Dimensions of the cross-section of street profile, and
- Urban heat island effect.

The orientation, building height and dimensions of the street profile are based on the Dutch General Height file or AHN (Rijkswaterstaat, 2020). AHN is a detailed height map of the Netherlands with a resolution of 0.5 metre and 95% has an accuracy of 15cm. Furthermore, building ages are estimated through data from Basisregistratie Adressen en Gebouwen (BAG) through the Waag Society (Spaan, 2015). At last the expected urban heat island effect is estimated through

B.1 The characteristics of the Oranjeboomstraat in Rotterdam

The Oranjeboomstraat is shortly discussed according the five aspects given in the introduction. These collectively form the criteria for the MCA for the second case study. Firstly, street orientation, building height and dimensions of the cross-section are given as the physical properties of the case. Secondly, the building age of the case and at last the estimated urban heat island is discussed.

B.1.1 Physical properties of the Oranjeboomstraat, Rotterdam

Figures 4.2 & 4.8 show the location of Oranjeboomstraat and a cross-section of the current situation. From the map and the cross-section can be concluded that the streets orientation is about -35° out of North. Furthermore can be seen that the housing block has height between 11–15m. While the width of the entire cross-section is 125 metres. The buildings stem from 19 Within the Multi criteria analysis of the second profile this width should be matched as closely as possible.

B.2 Multi criteria analysis for Eindhoven

Initially eight streets have been chosen to be evaluated, from these three streets were left for a final evaluation. The initial evaluation was based on size and likeness of the build area of the Oranjeboomstraat in Rotterdam.

This left the study with three streets, the Boschdijk, Bredalaan and Roosjevoststraat. These three are selected due the total width of the available study case, the presence of a green bank in the middle of the street, and likeness of the street-profile with the Oranjeboomstraat.

The actual multi criteria analysis is then based on the North-South orientation of the main street, the average building height, building age range and total profile width. The final factor is then based on the following

formula:

$$Factor = 2 * \left(\frac{Orientation}{Orientation_{OBS}} \right) + 2 * \frac{height}{height_{OBS}} - \frac{age_{youngest} + age_{oldest}}{age_{youngest,OBS} + age_{oldest,OBS}} - \frac{|Width - Width_{OBS}|}{Width_{OBS}}$$

Table B.1 shows the parameters of the Oranjeboomstraat, Roosjevosstraat, Bredalaan and the Boschdijk. As can be seen is the Bredalaan the highest ranked profile, followed by the Boschdijk and Roosjevosstraat. The Bredalaan is therefore chosen as the second case study to use for this study.

	OBS	Roosjevosstraat	Bredalaan	Boschdijk
Orientation[°]	325	319	286	328
Average building height[m]	15	8.5	11	10
Oldest building [year]	1930	1975	1945	1945
Youngest building [year]	1995	1985	1960	1960
Total profile width	120	100	120	125
Factor		1.25	2.2	2.1

Table B.1: Multi criteria analysis to determine the second profile

Chapter - C

Appendix - Wind evaluation of the street profile.

Since the wind is acting as a dominant influence on temperature and evaporation, a wind stability analysis is performed. The wind stability analysis, based on the four dominant wind directions, is focused on the sensitiveness to wind direction. The simulation is performed on the street-profile of the Oranjeboomstraat, Feijenoord. A simulation of June 23rd 2018 is performed for 24-hours period from 6a.m.. The appendix will discuss the chosen profile, meteorological input and evaluate the output of the simulation.

The street-profile of the Oranjeboomstraat in ENVI-met

The Oranjeboomstraat in Feijenoord is simplified and modelled in ENVI-met with a resolution of 2 by 2 metres. The main model input is geo-reference and urban environment data. Several aspects are given as input for the urban environment. While building materials are not taken into account, situation and dimensions of infrastructure and nature are. Likewise, the elevation and surface morphology is represented within the model. Furthermore, the usage of the basic soil profile of loa.m.y sand is chosen as profile. A relative height-map, with respect to street-level, can be seen in figure C.1. These heights have been given as input for the building blocks. An unusual aspect within these housing blocks can be seen in the map, figure C.1. There is an area which is situated about a metre lower than the surrounding, so this is given as input as well.

Besides modelling the urban environment, meteorological circumstances have to be given as input. The input of these characteristics is discussed in the upcoming section.

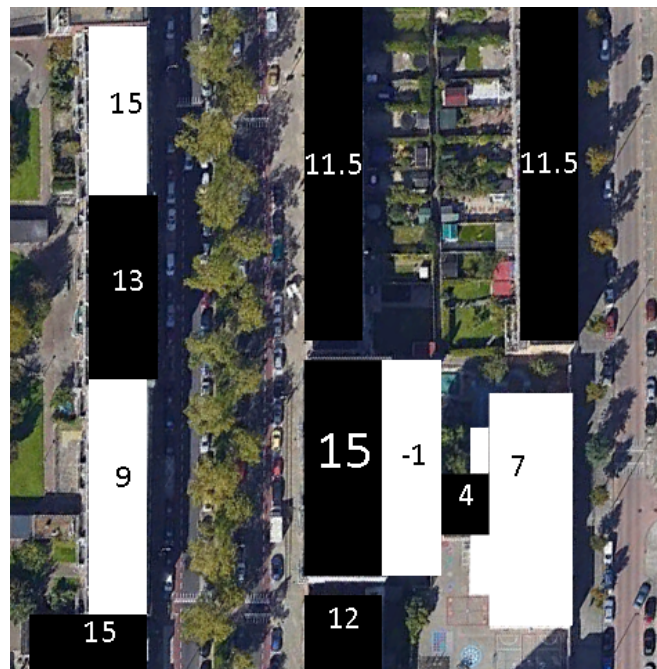


Figure C.1: A relative height map of the Oranjeboomstraat, Rotterda.m.. *The height differences are given with respect to street level. Since ENVI-met cannot handle resolutions for buildings smaller than a metre the values have to be rounded up or down to their respective height.*

Meteorological conditions of the simulation

The goal of the wind evaluation is to get an insight on the sensitivity of temperature to wind. This sensitivity is important since the PET is sensitive to meteorological fluctuations of temperature and wind (Walther and

Goestchel, 2018).

The simulation will not be too complicated to get direct and desired results. To get these results a general approach is chosen to simulate one day within a warm day with minimal wind necessary. The temperatures given for a warm day within ENVI-met are defined as a minimal, or night, temperature of 18°C and a maximum, or day, temperature of 28°C .

Since the intensity of wind has a large effect on temperature and turbulence, is chosen to simulate with a constant low wind velocity. The wind velocity has a value of 1 m/s with a constant direction. Furthermore, no additional meteorological parameters have been defined within the simulation.

The four dominant wind directions

To choose the dominant wind flow is assumed that this comes from either perpendicular or parallel directions, with respect to the street-profile. To define the four dominant wind directions the orientation of the Oranjeboomstraat with respect to the North is determined. The wind directions could be determined after this analysis.

Based on Google Earth, the orientation of the Oranjeboomstraat is at 124° . From this orientation can be concluded that the two parallel and two perpendicular wind flows come from respectively 124° and 304° , and 34° and 214° . These four wind directions are evaluated with respect to each other under equal circumstances. Since each wind direction is evaluated with respect to each other, this gives comparisons A till F, which can be seen in table C.1.

Together with these directions all the simulation's input parameters are defined, an overview can be seen in table C.2. The results of the will be given and discussed now.

Wind direction	34°	124°	214°	304°
East or 34°	x	x	x	x
South or 124°	A	x	x	x
West or 214°	B	C	x	x
North or 304°	D	E	F	x

Table C.1: The evaluated wind directions of the model. *These four wind directions are evaluated with respect to each other, based on their absolute temperature differences. This results in six comparisons, A till F, which will be evaluated.*

Date	Start time	Duration	T_{min}	T_{max}	Wind velocity	Wind direction
2018-06-23	6 a.m.	24 hours	18°C	28°C	1 m/s	34/124/214/304 $^{\circ}$

Table C.2: Overview of the wind sensitivity simulation's input. *A simulation of one day is performed for a warm situation with low wind velocities from multiple directions.*

Results of the wind sensitivity analysis

ENVI-met produces a lot of output, therefore is chosen to evaluate temperatures at three moments of the day. The first moment is right in the morning at 7 a.m., after stabilization of the wind flows. The second moment is chosen around the warmest period of the day around 2 p.m.. The last moment is chosen to be at 2 a.m. when there are no incoming fluxes and temperature differences mainly occur due heat release of materials. For every situation, A till F (see table C.1), a heat map at 2 p.m. and $z=1.80\text{m}$, and a normalized histogram is given of the absolute differences. Every situation is evaluated regarding spatial differences and average temperature distribution, within each map the buildings are included, but for the spatial analysis these are excluded.

Results of situation A with wind from eastern and southern directions.

The first results discussed are the temperature differences between eastern and southern winds with respect to orientation. The results are represented within a spatial map and three combined histograms, which are visible in figure C.2. Within the temperature difference map there is one relatively warmer spot, which are around the buildings on the north-side of the profile. Besides, on the south-side there is a small colder area. Most of the other spaces are in around 0°C difference. This is strengthened by the histogram and table C.3 where for all three times showing the temperature differences have means close to zero with little deviations.

Therefore, the differences between wind from 34° and 124° does not show a significant difference overall on average. Besides, the temperatures show a quite accurate distribution over the entire area, with the only exception near the edges of the area. This peak in temperature can possibly be explained due the lack of nesting grids.

	Mean [$^{\circ}\text{C}$]	Standard deviation [$^{\circ}\text{C}$]	Minimum [$^{\circ}\text{C}$]	Maximum [$^{\circ}\text{C}$]
7 a.m.	-0.007	0.021	-1.25	1.36
2 p.m.	-0.003	0.011	-4.5	4.76
2 a.m.	-0.005	0.013	-3.67	0.39

Table C.3: The mean air temperature, standard deviation, and minimum and maximum values between a 34° and 124° wind with respect to each other.

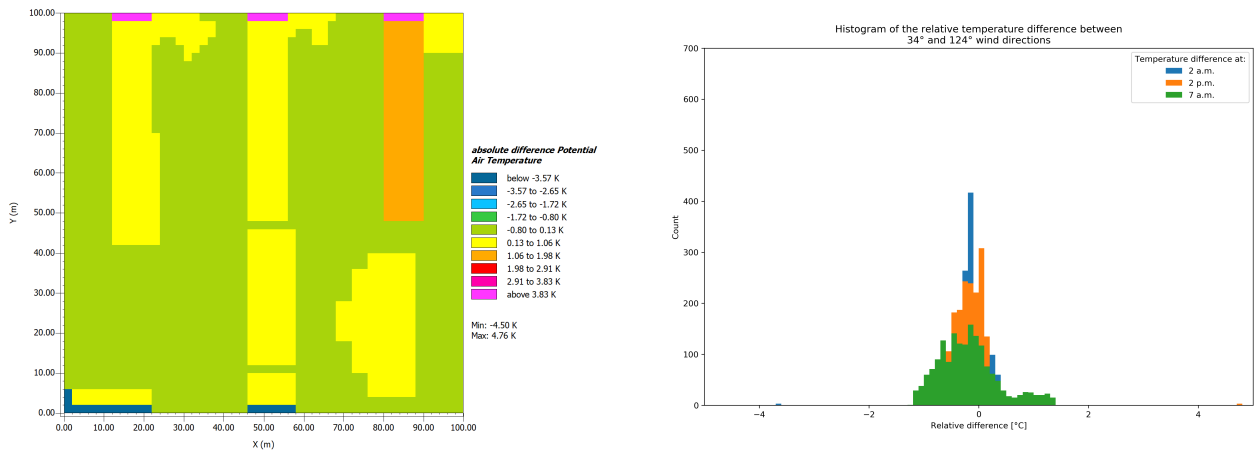


Figure C.2: Comparison A regarding wind from 34° and 124° , which in the map are east and south. Left is a map visible of the temperature difference at 2p.m., and on the right hand side is this data represented in a histogram. The mean fluctuates between -0.007°C , -0.003°C and -0.005°C , with standard deviations of 0.021°C , 0.011°C and 0.013°C respectively.

Results of situation B with wind from eastern and western directions.

The second result shown is the two perpendicular wind directions of 34° and 214° . Figure C.4 and table C.4 show the results of the wind analysis. The mean temperatures are again close to no change with respect to each other and the standard deviations are relatively small. Again at the edges of the simulated areas are some warmer and colder outliers. So also for these two wind directions only small differences can be seen.

	Mean [$^{\circ}\text{C}$]	Standard deviation [$^{\circ}\text{C}$]	Minimum [$^{\circ}\text{C}$]	Maximum [$^{\circ}\text{C}$]
7 a.m.	0.005	0.031	-1.15	1.91
2 p.m.	0.001	0.008	-0.28	4.78
2 a.m.	0.00045	0.018	-3.66	0.75

Table C.4: The mean air temperature, standard deviation, and minimum and maximum values between a 34° and 214° wind with respect to each other.

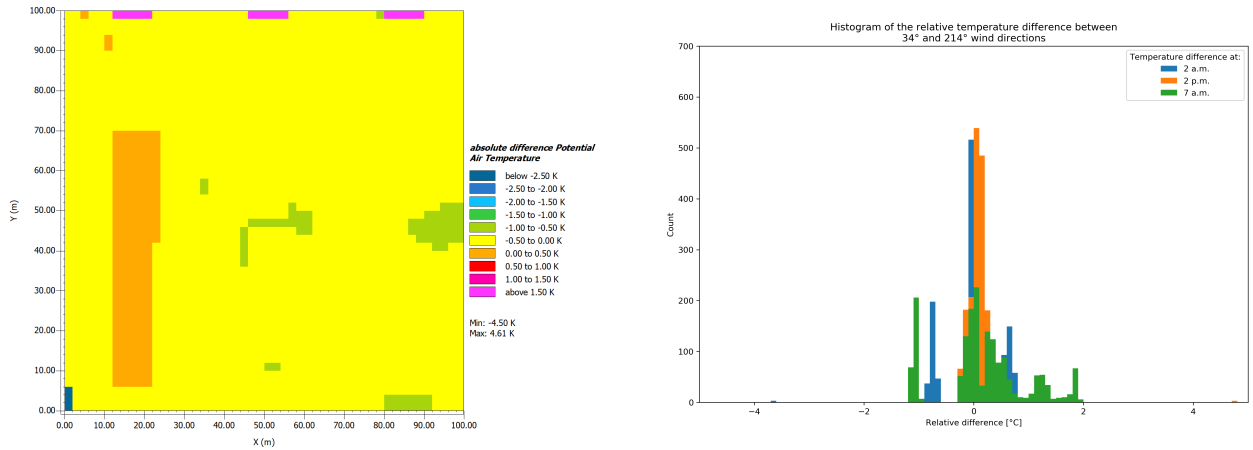


Figure C.3: Comparison B regarding wind from 34° and 214° , which in the map are east and west. *Left is a map visible of the temperature difference at 2p.m., and on the right hand side is this data represented in a histogram. The mean fluctuates between 0.0005°C , 0.001°C and 0.0005°C , with standard deviations of 0.031°C , 0.008°C and 0.018°C respectively.*

Results of situation C with wind from southern and western directions.

The third result shown is the wind directions of 124° and 214° . Figure C.5 and table C.5 show the results of the wind analysis. The mean temperatures are again close to no change with respect to each other and the standard deviations are relatively small. Though this time since there is a clear difference visible at the south-eastern building where a warmer spot develops. But on average for these two wind directions only small differences can be seen.

	Mean [°C]	Standard deviation [°C]	Minimum [°C]	Maximum [°C]
7 a.m.	-0.007	0.021	-0.82	1.54
2 p.m.	-0.003	0.011	-0.50	0.35
2 a.m.	-0.005	0.013	-0.72	0.76

Table C.5: The mean air temperature, standard deviation, and minimum and maximum values between a 124° and 214° wind with respect to each other.

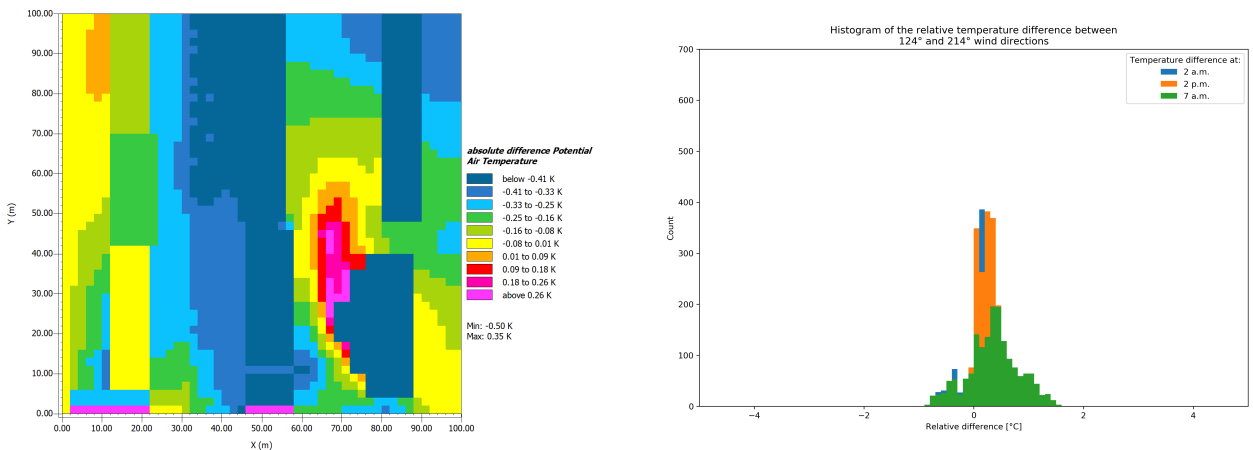


Figure C.4: Comparison C regarding wind from 124° and 214° , which in the map are south and west. *Left is a map visible of the temperature difference at 2p.m., and on the right hand side is this data represented in a histogram. The mean fluctuates between -0.007°C , -0.003°C and -0.005°C , with standard deviations of 0.021°C , 0.011°C and 0.013°C respectively.*

Results of situation D with wind from eastern and northern directions.

The forth result shown is the wind directions of 34° and 304° . Figure C.6 and table C.6 show the results of the wind analysis. The mean temperatures are again close to no change with respect to each other. Besides,

the standard deviations are relatively small. Due these small differences there is also no remarkable locations within the relative heatmap.

	Mean [°C]	Standard deviation [°C]	Minimum [°C]	Maximum [°C]
7 a.m.	-0.0050	0.021	-1.23	1.32
2 p.m.	-0.0050	0.021	-0.56	4.76
2 a.m.	-0.0036	0.015	-3.7	0.67

Table C.6: The mean air temperature, standard deviation, and minimum and maximum values between a 34° and 304° wind with respect to each other.

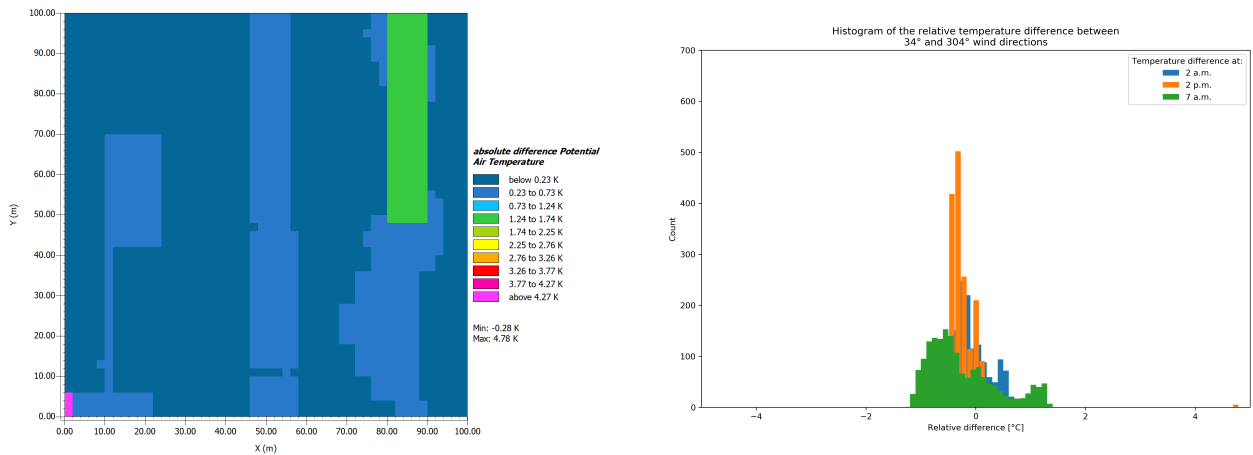


Figure C.5: Comparison D regarding wind from 34° and 304°, which in the map are east and north. Left is a map visible of the temperature difference at 2p.m., and on the right hand side is this data represented in a histogram. The mean fluctuates between -0.005° C, -0.005° C and -0.0036° C, with standard deviations of 0.021° C, 0.021° C and 0.015° C respectively.

Results of situation E with wind from norther and southern directions.

The fifth result shown is the wind directions of 124 and 304°. Figure C.7 and table C.7 show the results of the wind analysis. The mean value and standard deviation of the relative air temperatures are again close to zero. Again only at the edges of the simulated area some larger differences were found.

	Mean [°C]	Standard deviation [°C]	Minimum [°C]	Maximum [°C]
7 a.m.	0.0017	0.016	-1.62	1.68
2 p.m.	0.0012	0.006	-4.76	4.50
2 a.m.	-0.0003	0.0095	-3.97	3.46

Table C.7: The mean air temperature, standard deviation, and minimum and maximum values between a 124° and 304° wind with respect to each other.

Results of situation F with wind from western and northern directions.

The sixth, and last, result shown is the wind directions of 214 and 304°. Figure C.8 and table C.8 show the results of the wind analysis. The mean value and standard deviation of the relative air temperatures are again close to zero. Again only at the edges of the simulated area some larger differences were found.

Discussion and conclusion regarding the influence of wind on the temperature

The changing of the wind direction does not show a significant change on the mean temperature of the Oranjeboomstraat. The standard deviations of the various relative temperatures fluctuates between 0.006-0.31° C, but there are some larger differences of about 4-5° C. The larger differences are mostly found at the edges of

	Mean [°C]	Standard deviation [°C]	Minimum [°C]	Maximum [°C]
7 a.m.	0.0149	0.021	-0.57	2.15
2 p.m.	0.0034	0.019	-4.61	4.5
2 a.m.	0.0025	0.011	-0.59	3.79

Table C.8: The mean air temperature, standard deviation, and minimum and maximum values between a 214° and 304° wind with respect to each other.

the simulated areas.

The wind direction has therefore a minor effect on the average air temperature of the case. The average and standard deviations at several times are not larger than the accuracy (0.25-1°C) of ENVI-met found in other studies (Maggiotto et al., 2014) and thus has changing the wind direction a minimal effect on a day simulation.

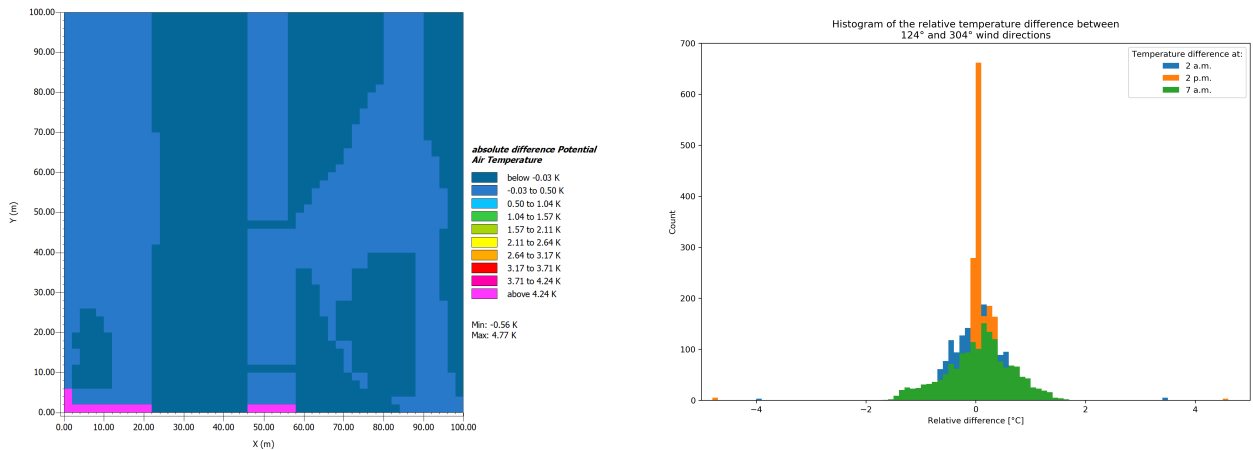


Figure C.6: Comparison E regarding wind from 124° and 304°, which in the map are south and north. Left is a map visible of the temperature difference at 2p.m., and on the right hand side is this data represented in a histogram. The mean fluctuates between 0.0017°C, 0.0012°C and -0.0003°C, with standard deviations of 0.016°C, 0.006°C and 0.0095°C respectively.

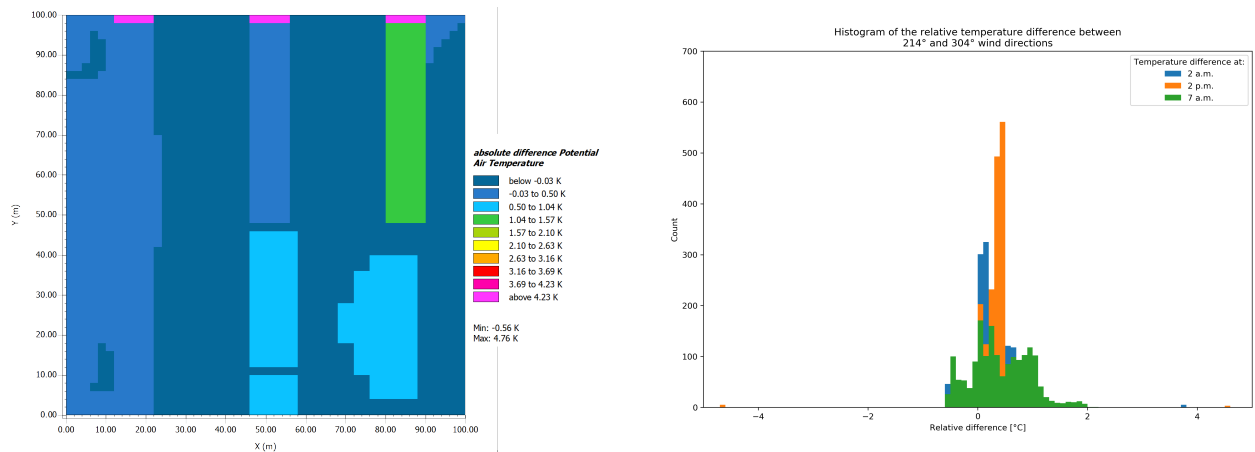


Figure C.7: Comparison F regarding wind from 214° and 304° , which in the map are west and north. Left is a map visible of the temperature difference at 2 p.m., and on the right hand side is this data represented in a histogram. The mean fluctuates between 0.0149°C , 0.0034°C and 0.0025°C , with standard deviations of 0.021°C , 0.019°C and 0.011°C respectively.

Chapter - D

Appendix - additional tables and graphs of the results

Dry Oranjeboomstraat

a.m./p.m.		1	2	3	4	5	6	7	8	9	10	11	12
Median	a.m.	24.66	23.67	22.68	21.69	20.54	21.56	23.22	25.28	27.3	28.48	29.59	30.5
	p.m.	31.27	32.05	32.78	32.85	32.52	31.96	31.18	30.01	28.77	27.7	26.67	25.66
Maximum	a.m.	25.42	24.57	23.72	22.89	21.46	22.18	23.94	26.17	28.46	29.84	31.39	32.68
	p.m.	33.72	34.63	35.41	35.29	34.64	33.44	32.1	30.5	29.14	28.06	27.16	26.28
Minimum	a.m.	24.09	22.99	21.9	20.81	20.17	21.2	22.94	24.51	26.09	27.69	28.75	29.57
	p.m.	30.48	31.31	32.11	32.25	31.95	31.4	30.66	29.57	28.3	27.28	26.31	25.2

Table D.1: Air temperature data of the simulation with the driest soil moisture profile. *The median temperatures fluctuate between 20.54 and 32.85° C, while the absolute minimum and maximum temperatures are 20.17 and 35.41° C.*

Irrigated Oranjeboomstraat

a.m./p.m.		1	2	3	4	5	6	7	8	9	10	11	12
Median	a.m.	24.26	23.3	22.36	21.42	20.5	21.53	23.14	25.11	26.99	28.16	29.17	30.08
	p.m.	30.87	31.66	32.4	32.47	32.15	31.55	30.76	29.58	28.38	27.31	26.25	25.24
Maximum	a.m.	25.13	24.31	23.5	22.7	21.42	22.17	23.87	26.01	28.23	29.57	31.08	32.44
	p.m.	33.55	34.5	35.24	35.03	34.28	33.28	31.96	30.2	28.82	27.68	26.81	25.96
Minimum	a.m.	23.61	22.58	21.53	20.5	20.09	21.15	22.66	24.33	25.9	27.34	28.37	29.26
	p.m.	30.11	30.98	31.78	31.93	31.65	31.08	30.29	29.06	27.86	26.8	25.72	24.65

Table D.2: Air temperature data of the simulation with the wettest soil moisture profile. *The median temperatures fluctuate between 20.5 and 32.47° C, while the absolute minimum and maximum temperatures are 20.09 and 35.24° C.*

Air temperature of the Oranjeboomstraat's green infrastructure with a dry soil

a.m./p.m.		1	2	3	4	5	6	7	8	9	10	11	12
Median	a.m.	24.7	23.72	22.76	21.8	20.57	21.55	23.19	25.06	27.22	28.45	29.46	30.24
	p.m.	31.07	31.85	32.58	32.69	32.37	31.84	31.07	29.97	28.75	27.7	26.68	25.68
Maximum	a.m.	25.31	24.46	23.61	22.77	21.46	22.15	23.76	26.17	28.46	29.84	31.39	32.68
	p.m.	33.72	34.63	35.41	35.29	34.64	33.42	31.78	30.16	28.92	27.95	27.05	26.18
Minimum	a.m.	25.18	24.3	23.44	22.58	21.35	22.09	23.35	25.62	28.06	29.45	30.68	31.84
	p.m.	32.46	33.22	33.79	33.66	33.14	32.49	31.47	30.05	28.85	27.87	26.96	26.06

Table D.3: Green infrastructure's Air temperature data of the simulation with the driest soil moisture profile. *The median temperatures fluctuate between 20.57 and 32.7° C, while the minimum and maximum temperatures of the green infrastructure are 21.35 and 35.41° C respectively.*

Air temperature of the Oranjeboomstraat's green infrastructure with an irrigated soil

a.m./p.m.		1	2	3	4	5	6	7	8	9	10	11	12
Median	a.m.	24.18	23.25	22.32	21.41	20.51	21.43	23.02	24.76	26.63	27.84	28.75	29.67
	p.m.	30.45	31.28	32.09	32.21	31.9	31.33	30.55	29.33	28.14	27.1	26.1	25.13
Maximum	a.m.	25.04	24.2	23.37	22.55	21.42	22.14	23.6	25.77	27.97	29.31	30.76	32.1
	p.m.	33.19	34.14	34.93	34.77	34.14	33.08	31.5	29.86	28.55	27.62	26.75	25.89
Minimum	a.m.	24.85	24.0	23.17	22.34	21.28	22.03	23.26	25.26	27.18	28.41	29.55	30.7
	p.m.	31.57	32.41	33.1	33.05	32.62	31.87	30.84	29.62	28.47	27.51	26.59	25.71

Table D.4: Green infrastructure's Air temperature data of the simulation with the wettest soil moisture profile. *The median temperatures fluctuate between 20.51 and 32.21° C, while the minimum and maximum temperatures of the green infrastructure are 21.28 and 34.93° C respectively.*

Air temperature of the Bredalaan's green infrastructure with a dry soil

a.m./p.m.		1	2	3	4	5	6	7	8	9	10	11	12
Median	a.m.	25.31	24.43	23.56	22.7	20.57	21.15	22.77	24.55	26.4	27.77	28.83	29.5
	p.m.	30.39	31.24	32.05	32.19	31.9	31.36	30.67	29.86	28.97	28.03	27.11	26.2
Maximum	a.m.	25.74	24.92	24.1	23.29	21.01	21.46	23.52	25.84	28.08	29.55	31.01	32.21
	p.m.	33.28	33.82	34.45	34.42	34.0	33.43	32.16	30.46	29.15	28.21	27.38	26.56
Minimum	a.m.	25.39	24.52	23.67	22.82	20.75	21.3	22.92	25.02	27.14	28.52	29.8	30.33
	p.m.	31.24	32.05	32.86	32.91	32.59	32.07	31.39	30.2	29.0	28.06	27.15	26.26

Table D.5: Green infrastructure's Air temperature data of the simulation with the wettest soil moisture profile. *The median temperatures fluctuate between 20.57 and 32.19° C, while the minimum and maximum temperatures of the green infrastructure are 20.75 and 34.45° C respectively.*

Air temperature of the Bredalaan's green infrastructure with an irrigated soil

a.m./p.m.		1	2	3	4	5	6	7	8	9	10	11	12
Median	a.m.	25.19	24.33	23.47	22.63	20.57	21.13	22.65	24.39	26.15	27.43	28.23	29.06
	p.m.	29.96	30.85	31.69	31.88	31.61	31.12	30.45	29.72	28.81	27.87	26.96	26.07
Maximum	a.m.	25.67	24.85	24.04	23.24	21.01	21.44	23.0	25.25	27.32	28.72	29.99	31.37
	p.m.	32.54	33.46	34.18	34.09	33.61	32.97	31.77	30.19	28.93	28.11	27.29	26.48
Minimum	a.m.	25.28	24.43	23.58	22.74	20.75	21.28	22.72	24.67	26.61	27.93	28.97	29.94
	p.m.	30.84	31.75	32.64	32.68	32.27	31.68	30.95	29.94	28.85	27.92	27.02	26.14

Table D.6: Green infrastructure's Air temperature data of the simulation with the wettest soil moisture profile. *The median temperatures fluctuate between 20.57 and 31.88° C, while the minimum and maximum temperatures of the green infrastructure are 20.75 and 34.18° C respectively.*

Chapter - E

Appendix - Comparison of ENVI-met and KNMI data

Below is a table given with KNMI's meteorological data and the adapted data to be modelled within ENVI-met. First the data of Eindhoven is given after which Rotterdam its meteorological input is given.

For both locations the same approach is used the hourly data is interpolated to semi-hourly data. In some cases the wind direction and/or wind velocity have been further adapted to increase stability.

E.1 Input Eindhoven

YYYYMMDD	HH	DD[°]	KNMI's data			
			FH[0.1 m/s]	T[0.1 °C]	RH[0.1 mm]	U[%]
20180727	1	100	10	257	-1	57
20180727	2	120	20	260	0	55
20180727	3	110	20	252	0	55
20180727	4	110	30	243	0	55
20180727	5	120	20	248	0	49
20180727	6	120	20	261	0	42
20180727	7	120	30	281	0	36
20180727	8	130	40	307	0	30
20180727	9	130	40	324	0	26
20180727	10	80	50	339	0	22
20180727	11	110	50	344	0	18
20180727	12	90	50	351	0	18
20180727	13	70	40	351	0	18
20180727	14	90	40	359	0	18
20180727	15	80	40	356	0	19
20180727	16	130	40	357	0	17
20180727	17	80	30	357	0	17
20180727	18	90	40	348	0	18
20180727	19	90	30	330	0	21
20180727	20	70	30	310	0	26
20180727	21	80	20	299	0	28
20180727	22	90	20	285	0	31
20180727	23	240	30	274	0	37
20180727	24	300	40	239	0	61
20180728	1	340	40	232	0	64
20180728	2	270	60	214	13	78
20180728	3	320	30	202	-1	86
20180728	4	40	20	200	0	87
20180728	5	220	20	199	0	90
20180728	6	230	30	200	-1	90
20180728	7	110	10	213	-1	83
20180728	8	200	30	219	-1	83
20180728	9	180	30	212	7	88
20180728	10	180	20	226	-1	84
20180728	11	210	50	260	0	66
20180728	12	230	60	269	0	55
20180728	13	250	80	268	0	50
20180728	14	270	70	257	0	51
20180728	15	250	80	263	0	45
20180728	16	250	80	247	0	41
20180728	17	250	70	245	0	36
20180728	18	250	70	237	0	31
20180728	19	280	40	214	0	38
20180728	20	310	20	194	0	45
20180728	21	310	20	177	0	50
20180728	22	0	10	146	0	64
20180728	23	200	10	134	0	68
20180728	24	100	10	136	0	71
...

YYYYMMDD	HH	DD	FH	T	RH	U
...
20180729	1	100	10	136	0	75
20180729	2	120	20	165	0	59
20180729	3	120	30	168	0	61
20180729	4	150	30	172	0	62
20180729	5	130	20	169	0	63
20180729	6	140	30	190	0	59
20180729	7	160	30	215	0	55
20180729	8	170	50	234	0	45
20180729	9	200	60	257	0	36
20180729	10	200	70	253	0	36
20180729	11	200	70	254	0	34
20180729	12	200	70	263	0	32
20180729	13	190	70	269	0	31
20180729	14	200	60	280	0	24
20180729	15	210	70	280	0	25
20180729	16	230	60	287	0	29
20180729	17	250	70	276	0	33
20180729	18	230	50	266	0	37
20180729	19	230	50	252	0	41
20180729	20	230	20	232	-1	51
20180729	21	230	10	218	0	58
20180729	22	240	10	214	0	63
20180729	23	160	20	219	0	60
20180729	24	170	30	221	0	60
20180730	1	160	30	216	0	63
20180730	2	160	30	215	0	63
20180730	3	170	30	210	0	65
20180730	4	160	30	200	0	69
20180730	5	170	30	206	-1	69
20180730	6	190	30	228	0	62
20180730	7	200	40	252	0	54
20180730	8	190	50	257	0	52
20180730	9	190	60	273	0	46
20180730	10	190	60	282	0	43
20180730	11	200	60	291	0	42
20180730	12	210	60	310	0	35
20180730	13	220	60	308	0	35
20180730	14	230	60	320	0	31
20180730	15	210	60	319	0	29
20180730	16	230	60	308	0	31
20180730	17	260	50	296	0	35
20180730	18	250	30	288	0	42
20180730	19	260	30	274	0	50
20180730	20	310	50	219	0	74
20180730	21	360	30	205	0	78
20180730	22	30	20	195	0	83
20180730	23	30	20	195	0	84
20180730	24	110	10	183	0	88
...

YYYYMMDD	HH	DD	FH	T	RH	U
...
20180731	1	110	10	188	0	86
20180731	2	990	10	186	0	86
20180731	3	170	10	179	0	91
20180731	4	190	10	181	0	89
20180731	5	240	10	193	0	86
20180731	6	140	10	204	0	82
20180731	7	150	30	240	0	68
20180731	8	190	40	247	0	66
20180731	9	210	60	251	0	59
20180731	10	220	70	280	0	45
20180731	11	230	80	271	0	39
20180731	12	250	80	286	0	37
20180731	13	290	50	264	0	45
20180731	14	320	50	274	0	45
20180731	15	290	40	272	0	43
20180731	16	290	40	271	0	41
20180731	17	310	40	264	0	44
20180731	18	320	50	248	0	47
20180731	19	330	40	232	0	53
20180731	20	330	40	212	0	59
20180731	21	10	20	192	0	64
20180731	22	360	20	194	0	64
20180731	23	310	10	180	0	70
20180731	24	40	10	167	0	75
20180801	1	100	10	165	0	74
20180801	2	0	10	146	0	83
20180801	3	230	0	140	0	87
20180801	4	990	10	132	0	89
20180801	5	0	0	139	0	88
20180801	6	0	0	181	0	75
20180801	7	350	10	221	0	59
20180801	8	10	20	237	0	47
20180801	9	340	20	246	0	41
20180801	10	20	30	259	0	38
20180801	11	80	20	270	0	35
20180801	12	360	30	273	0	35
20180801	13	50	30	275	0	36
20180801	14	90	20	286	0	34
20180801	15	100	30	285	0	35
20180801	16	80	20	284	0	35
20180801	17	30	30	287	0	34
20180801	18	20	30	280	0	36
20180801	19	340	30	257	0	47
20180801	20	330	40	228	0	54
20180801	21	340	30	210	0	59
20180801	22	320	20	194	0	65
20180801	23	330	10	187	0	69
20180801	24	340	10	184	0	72

DD.MM.YYYY	HH:MM:SS	ENVI-met's data				
		T[°K]	U[%]	FH [m/s]	DD[°]	P[mm]
27.07.2018	00:00:00	296.85	67	1	110	0
27.07.2018	00:30:00	297.85	62	1	105	0
27.07.2018	01:00:00	298.85	57	1	100	0
27.07.2018	01:30:00	299	56	1.5	110	0
27.07.2018	02:00:00	299.15	55	2	120	0
27.07.2018	02:30:00	298.75	55	2	115	0
27.07.2018	03:00:00	298.35	55	2	110	0
27.07.2018	03:30:00	297.9	55	2.5	110	0
27.07.2018	04:00:00	297.45	55	3	110	0
27.07.2018	04:30:00	297.7	52	2.5	115	0
27.07.2018	05:00:00	297.95	49	2	120	0
27.07.2018	05:30:00	298.6	45.5	2	120	0
27.07.2018	06:00:00	299.25	42	2	120	0
27.07.2018	06:30:00	300.25	39	2.5	120	0
27.07.2018	07:00:00	301.25	36	3	120	0
27.07.2018	07:30:00	302.55	33	3.5	125	0
27.07.2018	08:00:00	303.85	30	4	130	0
27.07.2018	08:30:00	304.7	28	4	130	0
27.07.2018	09:00:00	305.55	26	4	130	0
27.07.2018	09:30:00	306.3	24	4.5	105	0
27.07.2018	10:00:00	307.05	22	5	80	0
27.07.2018	10:30:00	307.3	20	5	95	0
27.07.2018	11:00:00	307.55	18	5	110	0
27.07.2018	11:30:00	307.9	18	5	100	0
27.07.2018	12:00:00	308.25	18	5	90	0
27.07.2018	12:30:00	308.25	18	4.5	80	0
27.07.2018	13:00:00	308.25	18	4	70	0
27.07.2018	13:30:00	308.65	18	4	80	0
27.07.2018	14:00:00	309.05	18	4	90	0
27.07.2018	14:30:00	308.9	18.5	4	85	0
27.07.2018	15:00:00	308.75	19	4	80	0
27.07.2018	15:30:00	308.8	18	4	105	0
27.07.2018	16:00:00	308.85	17	4	130	0
27.07.2018	16:30:00	308.85	17	3.5	105	0
27.07.2018	17:00:00	308.85	17	3	80	0
27.07.2018	17:30:00	308.4	17.5	3.5	85	0
27.07.2018	18:00:00	307.95	18	4	90	0
27.07.2018	18:30:00	307.05	19.5	3.5	90	0
27.07.2018	19:00:00	306.15	21	3	90	0
27.07.2018	19:30:00	305.15	23.5	3	80	0
27.07.2018	20:00:00	304.15	26	3	70	0
27.07.2018	20:30:00	303.6	27	2.5	75	0
27.07.2018	21:00:00	303.05	28	2	80	0
27.07.2018	21:30:00	302.35	29.5	2	85	0
27.07.2018	22:00:00	301.65	31	2	90	0
27.07.2018	22:30:00	301.1	34	2.5	165	0
27.07.2018	23:00:00	300.55	37	3	240	0
27.07.2018	23:30:00	298.8	49	3.5	270	0
...

DD.MM.YYYY	HH:MM:SS	T[°K]	U[%]	FH [m/s]	DD[°]	P[mm]
...
28.07.2018	00:00:00	297.05	61	4	300	0
28.07.2018	00:30:00	296.7	62.5	4	320	0
28.07.2018	01:00:00	296.35	64	4	340	0
28.07.2018	01:30:00	295.45	71	5	305	0.65
28.07.2018	02:00:00	294.55	78	6	270	1.3
28.07.2018	02:30:00	293.95	82	4.5	295	0.65
28.07.2018	03:00:00	293.35	86	3	320	0
28.07.2018	03:30:00	293.25	86.5	2.5	360	0
28.07.2018	04:00:00	293.15	87	2	40	0
28.07.2018	04:30:00	293.1	88.5	2	130	0
28.07.2018	05:00:00	293.05	90	2	220	0
28.07.2018	05:30:00	293.1	90	2.5	225	0
28.07.2018	06:00:00	293.15	90	3	230	0
28.07.2018	06:30:00	293.8	86.5	2	170	0
28.07.2018	07:00:00	294.45	83	1	110	0
28.07.2018	07:30:00	294.75	83	2	155	0
28.07.2018	08:00:00	295.05	83	3	200	0
28.07.2018	08:30:00	294.7	85.5	3	190	0.35
28.07.2018	09:00:00	294.35	88	3	180	0.7
28.07.2018	09:30:00	295.05	86	2.5	180	0.35
28.07.2018	10:00:00	295.75	84	2	180	0
28.07.2018	10:30:00	297.45	75	3.5	195	0
28.07.2018	11:00:00	299.15	66	5	210	0
28.07.2018	11:30:00	299.6	60.5	5.5	220	0
28.07.2018	12:00:00	300.05	55	6	230	0
28.07.2018	12:30:00	300	52.5	7	240	0
28.07.2018	13:00:00	299.95	50	8	250	0
28.07.2018	13:30:00	299.4	50.5	7.5	260	0
28.07.2018	14:00:00	298.85	51	7	270	0
28.07.2018	14:30:00	299.15	48	7.5	260	0
28.07.2018	15:00:00	299.45	45	8	250	0
28.07.2018	15:30:00	298.65	43	8	250	0
28.07.2018	16:00:00	297.85	41	8	250	0
28.07.2018	16:30:00	297.75	38.5	7.5	250	0
28.07.2018	17:00:00	297.65	36	7	250	0
28.07.2018	17:30:00	297.25	33.5	7	250	0
28.07.2018	18:00:00	296.85	31	7	250	0
28.07.2018	18:30:00	295.7	34.5	5.5	265	0
28.07.2018	19:00:00	294.55	38	4	280	0
28.07.2018	19:30:00	293.55	41.5	3	295	0
28.07.2018	20:00:00	292.55	45	2	310	0
28.07.2018	20:30:00	291.7	47.5	2	310	0
28.07.2018	21:00:00	290.85	50	2	310	0
28.07.2018	21:30:00	289.3	57	1.5	282.5	0
28.07.2018	22:00:00	287.75	64	1	255	0
28.07.2018	22:30:00	287.15	66	1	227.5	0
28.07.2018	23:00:00	286.55	68	1	200	0
28.07.2018	23:30:00	286.65	69.5	1	150	0
...

DD.MM.YYYY	HH:MM:SS	T[°K]	U[%]	FH [m/s]	DD[°]	P[mm]
...
29.07.2018	00:00:00	286.75	71	1	100	0
29.07.2018	00:30:00	286.75	73	1	100	0
29.07.2018	01:00:00	286.75	75	1	100	0
29.07.2018	01:30:00	288.2	67	1.5	110	0
29.07.2018	02:00:00	289.65	59	2	120	0
29.07.2018	02:30:00	289.8	60	2.5	120	0
29.07.2018	03:00:00	289.95	61	3	120	0
29.07.2018	03:30:00	290.15	61.5	3	135	0
29.07.2018	04:00:00	290.35	62	3	150	0
29.07.2018	04:30:00	290.2	62.5	2.5	140	0
29.07.2018	05:00:00	290.05	63	2	130	0
29.07.2018	05:30:00	291.1	61	2.5	135	0
29.07.2018	06:00:00	292.15	59	3	140	0
29.07.2018	06:30:00	293.4	57	3	150	0
29.07.2018	07:00:00	294.65	55	3	160	0
29.07.2018	07:30:00	295.6	50	4	165	0
29.07.2018	08:00:00	296.55	45	5	170	0
29.07.2018	08:30:00	297.7	40.5	5.5	185	0
29.07.2018	09:00:00	298.85	36	6	200	0
29.07.2018	09:30:00	298.65	36	6.5	200	0
29.07.2018	10:00:00	298.45	36	7	200	0
29.07.2018	10:30:00	298.5	35	7	200	0
29.07.2018	11:00:00	298.55	34	7	200	0
29.07.2018	11:30:00	299	33	7	200	0
29.07.2018	12:00:00	299.45	32	7	200	0
29.07.2018	12:30:00	299.75	31.5	7	195	0
29.07.2018	13:00:00	300.05	31	7	190	0
29.07.2018	13:30:00	300.6	27.5	6.5	195	0
29.07.2018	14:00:00	301.15	24	6	200	0
29.07.2018	14:30:00	301.15	24.5	6.5	205	0
29.07.2018	15:00:00	301.15	25	7	210	0
29.07.2018	15:30:00	301.5	27	6.5	220	0
29.07.2018	16:00:00	301.85	29	6	230	0
29.07.2018	16:30:00	301.3	31	6.5	240	0
29.07.2018	17:00:00	300.75	33	7	250	0
29.07.2018	17:30:00	300.25	35	6	240	0
29.07.2018	18:00:00	299.75	37	5	230	0
29.07.2018	18:30:00	299.05	39	5	230	0
29.07.2018	19:00:00	298.35	41	5	230	0
29.07.2018	19:30:00	297.35	46	3.5	230	0
29.07.2018	20:00:00	296.35	51	2	230	0
29.07.2018	20:30:00	295.65	54.5	1.5	230	0
29.07.2018	21:00:00	294.95	58	1	230	0
29.07.2018	21:30:00	294.75	60.5	1	235	0
29.07.2018	22:00:00	294.55	63	1	240	0
29.07.2018	22:30:00	294.8	61.5	1.5	200	0
29.07.2018	23:00:00	295.05	60	2	160	0
29.07.2018	23:30:00	295.15	60	2.5	165	0
...

DD.MM.YYYY	HH:MM:SS	T[°K]	U[%]	FH [m/s]	DD[°]	P[mm]
...
30.07.2018	00:00:00	295.25	60	3	170	0
30.07.2018	00:30:00	295	61.5	3	165	0
30.07.2018	01:00:00	294.75	63	3	160	0
30.07.2018	01:30:00	294.7	63	3	160	0
30.07.2018	02:00:00	294.65	63	3	160	0
30.07.2018	02:30:00	294.4	64	3	165	0
30.07.2018	03:00:00	294.15	65	3	170	0
30.07.2018	03:30:00	293.65	67	3	165	0
30.07.2018	04:00:00	293.15	69	3	160	0
30.07.2018	04:30:00	293.45	69	3	165	0
30.07.2018	05:00:00	293.75	69	3	170	0
30.07.2018	05:30:00	294.85	65.5	3	180	0
30.07.2018	06:00:00	295.95	62	3	190	0
30.07.2018	06:30:00	297.15	58	3.5	195	0
30.07.2018	07:00:00	298.35	54	4	200	0
30.07.2018	07:30:00	298.6	53	4.5	195	0
30.07.2018	08:00:00	298.85	52	5	190	0
30.07.2018	08:30:00	299.65	49	5.5	190	0
30.07.2018	09:00:00	300.45	46	6	190	0
30.07.2018	09:30:00	300.9	44.5	6	190	0
30.07.2018	10:00:00	301.35	43	6	190	0
30.07.2018	10:30:00	301.8	42.5	6	195	0
30.07.2018	11:00:00	302.25	42	6	200	0
30.07.2018	11:30:00	303.2	38.5	6	205	0
30.07.2018	12:00:00	304.15	35	6	210	0
30.07.2018	12:30:00	304.05	35	6	215	0
30.07.2018	13:00:00	303.95	35	6	220	0
30.07.2018	13:30:00	304.55	33	6	225	0
30.07.2018	14:00:00	305.15	31	6	230	0
30.07.2018	14:30:00	305.1	30	6	220	0
30.07.2018	15:00:00	305.05	29	6	210	0
30.07.2018	15:30:00	304.5	30	6	220	0
30.07.2018	16:00:00	303.95	31	6	230	0
30.07.2018	16:30:00	303.35	33	5.5	245	0
30.07.2018	17:00:00	302.75	35	5	260	0
30.07.2018	17:30:00	302.35	38.5	4	255	0
30.07.2018	18:00:00	301.95	42	3	250	0
30.07.2018	18:30:00	301.25	46	3	255	0
30.07.2018	19:00:00	300.55	50	3	260	0
30.07.2018	19:30:00	297.8	62	4	285	0
30.07.2018	20:00:00	295.05	74	5	310	0
30.07.2018	20:30:00	294.35	76	4	335	0
30.07.2018	21:00:00	293.65	78	3	0	0
30.07.2018	21:30:00	293.15	80.5	2.5	15	0
30.07.2018	22:00:00	292.65	83	2	30	0
30.07.2018	22:30:00	292.65	83.5	2	30	0
30.07.2018	23:00:00	292.65	84	2	30	0
30.07.2018	23:30:00	292.05	86	1.5	70	0
...

DD.MM.YYYY	HH:MM:SS	T[°K]	U[%]	FH [m/s]	DD[°]	P[mm]
...
31.07.2018	00:00:00	291.45	88	1	110	0
31.07.2018	00:30:00	291.7	87	1	110	0
31.07.2018	01:00:00	291.95	86	1	110	0
31.07.2018	01:30:00	291.85	86	1	125	0
31.07.2018	02:00:00	291.75	86	1	140	0
31.07.2018	02:30:00	291.4	88.5	1	155	0
31.07.2018	03:00:00	291.05	91	1	170	0
31.07.2018	03:30:00	291.15	90	1	180	0
31.07.2018	04:00:00	291.25	89	1	190	0
31.07.2018	04:30:00	291.85	87.5	1	215	0
31.07.2018	05:00:00	292.45	86	1	240	0
31.07.2018	05:30:00	293	84	1	190	0
31.07.2018	06:00:00	293.55	82	1	140	0
31.07.2018	06:30:00	295.35	75	2	145	0
31.07.2018	07:00:00	297.15	68	3	150	0
31.07.2018	07:30:00	297.5	67	3.5	170	0
31.07.2018	08:00:00	297.85	66	4	190	0
31.07.2018	08:30:00	298.05	62.5	5	200	0
31.07.2018	09:00:00	298.25	59	6	210	0
31.07.2018	09:30:00	299.7	52	6.5	215	0
31.07.2018	10:00:00	301.15	45	7	220	0
31.07.2018	10:30:00	300.7	42	7.5	225	0
31.07.2018	11:00:00	300.25	39	8	230	0
31.07.2018	11:30:00	301	38	8	240	0
31.07.2018	12:00:00	301.75	37	8	250	0
31.07.2018	12:30:00	300.65	41	6.5	270	0
31.07.2018	13:00:00	299.55	45	5	290	0
31.07.2018	13:30:00	300.05	45	5	305	0
31.07.2018	14:00:00	300.55	45	5	320	0
31.07.2018	14:30:00	300.45	44	4.5	305	0
31.07.2018	15:00:00	300.35	43	4	290	0
31.07.2018	15:30:00	300.3	42	4	290	0
31.07.2018	16:00:00	300.25	41	4	290	0
31.07.2018	16:30:00	299.9	42.5	4	300	0
31.07.2018	17:00:00	299.55	44	4	310	0
31.07.2018	17:30:00	298.75	45.5	4.5	315	0
31.07.2018	18:00:00	297.95	47	5	320	0
31.07.2018	18:30:00	297.15	50	4.5	325	0
31.07.2018	19:00:00	296.35	53	4	330	0
31.07.2018	19:30:00	295.35	56	4	330	0
31.07.2018	20:00:00	294.35	59	4	330	0
31.07.2018	20:30:00	293.35	61.5	3	350	0
31.07.2018	21:00:00	292.35	64	2	10	0
31.07.2018	21:30:00	292.45	64	2	5	0
31.07.2018	22:00:00	292.55	64	2	0	0
31.07.2018	22:30:00	291.85	67	1.5	335	0
31.07.2018	23:00:00	291.15	70	1	310	0
31.07.2018	23:30:00	290.5	72.5	1	355	0
01.08.2018	00:00:00	289.85	75	1	40	0
01.08.2018	00:30:00	289.75	74.5	1	70	0
01.08.2018	01:00:00	289.65	74	1	100	0
01.08.2018	01:30:00	288.7	78.5	1	132.5	0
01.08.2018	02:00:00	287.75	83	1	165	0
01.08.2018	02:30:00	287.45	85	0.5	197.5	0
01.08.2018	03:00:00	287.15	87	0	230	0
01.08.2018	03:30:00	286.75	88	0.5	262.5	0

E.2 **Input Rotterdam**

YYYYMMDD	HH	DD[°]	KNMI's data			
			FH[0.1 m/s]	T[0.1 °C]	RH[0.1 mm]	U[%]
20180727	4	100	20	230	0	71
20180727	5	100	30	233	0	72
20180727	6	120	30	244	0	62
20180727	7	120	30	259	0	57
20180727	8	120	30	278	0	48
20180727	9	120	40	306	0	39
20180727	10	110	40	321	0	35
20180727	11	120	40	338	0	28
20180727	12	100	50	350	0	26
20180727	13	100	50	359	0	23
20180727	14	90	60	355	0	21
20180727	15	100	50	358	0	19
20180727	16	100	50	337	0	22
20180727	17	100	40	335	0	24
20180727	18	80	40	314	0	35
20180727	19	90	30	308	0	33
20180727	20	100	30	295	0	35
20180727	21	110	30	288	0	36
20180727	22	290	50	240	0	64
20180727	23	300	60	211	0	78
20180727	24	360	30	207	0	80
20180728	1	300	30	203	0	83
20180728	2	240	30	202	0	84
20180728	3	60	20	195	0	85
20180728	4	230	20	202	0	83
20180728	5	230	30	206	-1	82
20180728	6	110	20	202	5	90
20180728	7	220	20	209	2	87
20180728	8	170	20	225	0	83
20180728	9	200	60	237	0	72
20180728	10	220	70	235	0	69
20180728	11	240	70	227	23	87
20180728	12	260	90	215	0	65
20180728	13	250	90	214	0	57
20180728	14	240	100	228	0	50
20180728	15	250	90	221	0	46
20180728	16	250	90	218	0	50
20180728	17	250	90	214	0	51
20180728	18	240	80	203	0	58
20180728	19	250	70	192	0	61
20180728	20	240	50	188	0	59
20180728	21	240	50	184	0	58
20180728	22	240	50	178	0	62
20180728	23	220	40	176	0	66
20180728	24	170	30	172	0	70
...

YYYYMMDD	HH	DD	FH	T	RH	U
...
20180729	1	160	30	177	0	67
20180729	2	160	30	178	0	62
20180729	3	150	30	179	0	59
20180729	4	170	20	177	0	60
20180729	5	140	30	184	0	54
20180729	6	130	40	200	0	51
20180729	7	160	60	210	0	51
20180729	8	180	60	226	0	45
20180729	9	180	60	238	0	41
20180729	10	190	80	246	0	40
20180729	11	210	90	241	0	42
20180729	12	200	80	243	0	40
20180729	13	210	70	220	-1	54
20180729	14	200	60	231	-1	47
20180729	15	200	60	232	-1	51
20180729	16	210	60	240	-1	42
20180729	17	200	60	226	-1	55
20180729	18	190	50	234	-1	51
20180729	19	210	50	234	0	54
20180729	20	200	40	232	0	57
20180729	21	210	60	232	0	60
20180729	22	220	60	227	0	64
20180729	23	170	40	224	0	65
20180729	24	200	40	226	0	63
20180730	1	190	50	226	0	64
20180730	2	200	40	222	0	68
20180730	3	190	40	219	0	71
20180730	4	190	30	218	0	72
20180730	5	190	30	221	0	72
20180730	6	180	40	227	0	70
20180730	7	180	40	230	0	68
20180730	8	200	40	248	0	61
20180730	9	190	50	249	0	61
20180730	10	190	60	265	0	56
20180730	11	200	60	265	0	55
20180730	12	210	60	276	0	53
20180730	13	200	70	279	0	50
20180730	14	190	60	284	0	50
20180730	15	220	60	273	0	53
20180730	16	190	40	272	0	52
20180730	17	210	50	279	0	51
20180730	18	280	60	214	0	77
20180730	19	270	60	194	-1	82
20180730	20	330	20	187	-1	90
20180730	21	0	10	185	0	90
20180730	22	990	10	182	0	90
20180730	23	0	10	185	0	89
20180730	24	80	10	177	0	88
...

YYYYMMDD	HH	DD	FH	T	RH	U
...
20180731	1	110	20	185	0	87
20180731	2	120	10	191	0	84
20180731	3	160	20	190	0	84
20180731	4	150	10	184	0	89
20180731	5	350	10	186	0	88
20180731	6	130	10	211	0	74
20180731	7	140	30	223	0	72
20180731	8	190	50	239	0	70
20180731	9	210	60	257	0	56
20180731	10	260	80	221	-1	72
20180731	11	260	90	229	-1	61
20180731	12	270	60	233	0	58
20180731	13	260	60	234	0	55
20180731	14	270	60	234	0	50
20180731	15	270	60	231	0	49
20180731	16	270	50	230	0	49
20180731	17	290	40	222	0	53
20180731	18	300	30	211	0	58
20180731	19	300	20	192	0	69
20180731	20	0	0	174	0	77
20180731	21	0	10	164	0	81
20180731	22	0	10	161	0	84
20180731	23	0	10	143	0	95
20180731	24	70	10	133	0	96
...

YYYYMMDD	HH	DD	FH	T	RH	U
...
20180801	1	0	10	133	0	97
20180801	2	80	0	137	0	97
20180801	3	990	10	133	0	97
20180801	4	340	10	125	0	98
20180801	5	300	0	137	0	97
20180801	6	990	10	169	0	91
20180801	7	0	10	202	0	74
20180801	8	990	10	215	0	62
20180801	9	300	20	230	0	56
20180801	10	280	30	241	0	56
20180801	11	280	30	245	0	52
20180801	12	290	30	250	0	48
20180801	13	280	30	248	0	50
20180801	14	300	30	251	0	46
20180801	15	290	30	253	0	43
20180801	16	320	40	247	0	43
20180801	17	320	30	243	0	43
20180801	18	340	30	232	0	51
20180801	19	360	20	209	0	58
20180801	20	20	20	189	0	71
20180801	21	330	10	172	0	84
20180801	22	350	10	166	0	88
20180801	23	0	0	167	0	90
20180801	24	990	10	163	0	92

DD.MM.YYYY	HH:MM:SS	ENVI-met's data				
		T[°K]	U[%]	FH [m/s]	DD[°]	P[mm]
27.07.2018	04:00:00	296.15	71	2	100	0
27.07.2018	04:30:00	296.3	71.5	2.5	100	0
27.07.2018	05:00:00	296.45	72	3	100	0
27.07.2018	05:30:00	297	67	3	110	0
27.07.2018	06:00:00	297.55	62	3	120	0
27.07.2018	06:30:00	298.3	59.5	3	120	0
27.07.2018	07:00:00	299.05	57	3	120	0
27.07.2018	07:30:00	300	52.5	3	120	0
27.07.2018	08:00:00	300.95	48	3	120	0
27.07.2018	08:30:00	302.35	43.5	3.5	120	0
27.07.2018	09:00:00	303.75	39	4	120	0
27.07.2018	09:30:00	304.5	37	4	115	0
27.07.2018	10:00:00	305.25	35	4	110	0
27.07.2018	10:30:00	306.1	31.5	4	115	0
27.07.2018	11:00:00	306.95	28	4	120	0
27.07.2018	11:30:00	307.55	27	4.5	110	0
27.07.2018	12:00:00	308.15	26	5	100	0
27.07.2018	12:30:00	308.6	24.5	5	100	0
27.07.2018	13:00:00	309.05	23	5	100	0
27.07.2018	13:30:00	308.85	22	5.5	95	0
27.07.2018	14:00:00	308.65	21	6	90	0
27.07.2018	14:30:00	308.8	20	5.5	95	0
27.07.2018	15:00:00	308.95	19	5	100	0
27.07.2018	15:30:00	307.9	20.5	5	100	0
27.07.2018	16:00:00	306.85	22	5	100	0
27.07.2018	16:30:00	306.75	23	4.5	100	0
27.07.2018	17:00:00	306.65	24	4	100	0
27.07.2018	17:30:00	305.6	29.5	4	90	0
27.07.2018	18:00:00	304.55	35	4	80	0
27.07.2018	18:30:00	304.25	34	3.5	85	0
27.07.2018	19:00:00	303.95	33	3	90	0
27.07.2018	19:30:00	303.3	34	3	95	0
27.07.2018	20:00:00	302.65	35	3	100	0
27.07.2018	20:30:00	302.3	35.5	3	105	0
27.07.2018	21:00:00	301.95	36	3	110	0
27.07.2018	21:30:00	299.55	50	4	200	0
27.07.2018	22:00:00	297.15	64	5	290	0
27.07.2018	22:30:00	295.7	71	5.5	295	0
27.07.2018	23:00:00	294.25	78	6	300	0
27.07.2018	23:30:00	294.05	79	4.5	330	0
...

DD.MM.YYYY	HH:MM:SS	T[°K]	U[%]	FH [m/s]	DD[°]	P[mm]
...
28.07.2018	00:00:00	293.85	80	3	0	0
28.07.2018	00:30:00	293.65	81.5	3	330	0
28.07.2018	01:00:00	293.45	83	3	300	0
28.07.2018	01:30:00	293.4	83.5	3	270	0
28.07.2018	02:00:00	293.35	84	3	240	0
28.07.2018	02:30:00	293	84.5	2.5	330	0
28.07.2018	03:00:00	292.65	85	2	60	0
28.07.2018	03:30:00	293	84	2	145	0
28.07.2018	04:00:00	293.35	83	2	230	0
28.07.2018	04:30:00	293.55	82.5	2.5	230	0
28.07.2018	05:00:00	293.75	82	3	230	0
28.07.2018	05:30:00	293.55	86	2.5	170	0.25
28.07.2018	06:00:00	293.35	90	2	110	0.5
28.07.2018	06:30:00	293.7	88.5	2	165	0.35
28.07.2018	07:00:00	294.05	87	2	220	0.2
28.07.2018	07:30:00	294.85	85	2	195	0.1
28.07.2018	08:00:00	295.65	83	2	170	0
28.07.2018	08:30:00	296.25	77.5	4	185	0
28.07.2018	09:00:00	296.85	72	6	200	0
28.07.2018	09:30:00	296.75	70.5	6.5	210	0
28.07.2018	10:00:00	296.65	69	7	220	0
28.07.2018	10:30:00	296.25	78	7	230	1.15
28.07.2018	11:00:00	295.85	87	7	240	2.3
28.07.2018	11:30:00	295.25	76	8	250	1.15
28.07.2018	12:00:00	294.65	65	9	260	0
28.07.2018	12:30:00	294.6	61	9	255	0
28.07.2018	13:00:00	294.55	57	9	250	0
28.07.2018	13:30:00	295.25	53.5	9.5	245	0
28.07.2018	14:00:00	295.95	50	10	240	0
28.07.2018	14:30:00	295.6	48	9.5	245	0
28.07.2018	15:00:00	295.25	46	9	250	0
28.07.2018	15:30:00	295.1	48	9	250	0
28.07.2018	16:00:00	294.95	50	9	250	0
28.07.2018	16:30:00	294.75	50.5	9	250	0
28.07.2018	17:00:00	294.55	51	9	250	0
28.07.2018	17:30:00	294	54.5	8.5	245	0
28.07.2018	18:00:00	293.45	58	8	240	0
28.07.2018	18:30:00	292.9	59.5	7.5	245	0
28.07.2018	19:00:00	292.35	61	7	250	0
28.07.2018	19:30:00	292.15	60	6	245	0
28.07.2018	20:00:00	291.95	59	5	240	0
28.07.2018	20:30:00	291.75	58.5	5	240	0
28.07.2018	21:00:00	291.55	58	5	240	0
28.07.2018	21:30:00	291.25	60	5	240	0
28.07.2018	22:00:00	290.95	62	5	240	0
28.07.2018	22:30:00	290.85	64	4.5	230	0
28.07.2018	23:00:00	290.75	66	4	220	0
28.07.2018	23:30:00	290.55	68	3.5	195	0
...

DD.MM.YYYY	HH:MM:SS	T[°K]	U[%]	FH [m/s]	DD[°]	P[mm]
...
29.07.2018	00:00:00	290.35	70	3	170	0
29.07.2018	00:30:00	290.6	68.5	3	165	0
29.07.2018	01:00:00	290.85	67	3	160	0
29.07.2018	01:30:00	290.9	64.5	3	160	0
29.07.2018	02:00:00	290.95	62	3	160	0
29.07.2018	02:30:00	291	60.5	3	155	0
29.07.2018	03:00:00	291.05	59	3	150	0
29.07.2018	03:30:00	290.95	59.5	2.5	160	0
29.07.2018	04:00:00	290.85	60	2	170	0
29.07.2018	04:30:00	291.2	57	2.5	155	0
29.07.2018	05:00:00	291.55	54	3	140	0
29.07.2018	05:30:00	292.35	52.5	3.5	135	0
29.07.2018	06:00:00	293.15	51	4	130	0
29.07.2018	06:30:00	293.65	51	5	145	0
29.07.2018	07:00:00	294.15	51	6	160	0
29.07.2018	07:30:00	294.95	48	6	170	0
29.07.2018	08:00:00	295.75	45	6	180	0
29.07.2018	08:30:00	296.35	43	6	180	0
29.07.2018	09:00:00	296.95	41	6	180	0
29.07.2018	09:30:00	297.35	40.5	7	185	0
29.07.2018	10:00:00	297.75	40	8	190	0
29.07.2018	10:30:00	297.5	41	8.5	200	0
29.07.2018	11:00:00	297.25	42	9	210	0
29.07.2018	11:30:00	297.35	41	8.5	205	0
29.07.2018	12:00:00	297.45	40	8	200	0
29.07.2018	12:30:00	296.3	47	7.5	205	0
29.07.2018	13:00:00	295.15	54	7	210	0
29.07.2018	13:30:00	295.7	50.5	6.5	205	0
29.07.2018	14:00:00	296.25	47	6	200	0
29.07.2018	14:30:00	296.3	49	6	200	0
29.07.2018	15:00:00	296.35	51	6	200	0
29.07.2018	15:30:00	296.75	46.5	6	205	0
29.07.2018	16:00:00	297.15	42	6	210	0
29.07.2018	16:30:00	296.45	48.5	6	205	0
29.07.2018	17:00:00	295.75	55	6	200	0
29.07.2018	17:30:00	296.15	53	5.5	195	0
29.07.2018	18:00:00	296.55	51	5	190	0
29.07.2018	18:30:00	296.55	52.5	5	200	0
29.07.2018	19:00:00	296.55	54	5	210	0
29.07.2018	19:30:00	296.45	55.5	4.5	205	0
29.07.2018	20:00:00	296.35	57	4	200	0
29.07.2018	20:30:00	296.35	58.5	5	205	0
29.07.2018	21:00:00	296.35	60	6	210	0
29.07.2018	21:30:00	296.1	62	6	215	0
29.07.2018	22:00:00	295.85	64	6	220	0
29.07.2018	22:30:00	295.7	64.5	5	195	0
29.07.2018	23:00:00	295.55	65	4	170	0
29.07.2018	23:30:00	295.65	64	4	185	0
...

DD.MM.YYYY	HH:MM:SS	T[°K]	U[%]	FH [m/s]	DD[°]	P[mm]
...
30.07.2018	00:00:00	295.75	63	4	200	0
30.07.2018	00:30:00	295.75	63.5	4.5	195	0
30.07.2018	01:00:00	295.75	64	5	190	0
30.07.2018	01:30:00	295.55	66	4.5	195	0
30.07.2018	02:00:00	295.35	68	4	200	0
30.07.2018	02:30:00	295.2	69.5	4	195	0
30.07.2018	03:00:00	295.05	71	4	190	0
30.07.2018	03:30:00	295	71.5	3.5	190	0
30.07.2018	04:00:00	294.95	72	3	190	0
30.07.2018	04:30:00	295.1	72	3	190	0
30.07.2018	05:00:00	295.25	72	3	190	0
30.07.2018	05:30:00	295.55	71	3.5	185	0
30.07.2018	06:00:00	295.85	70	4	180	0
30.07.2018	06:30:00	296	69	4	180	0
30.07.2018	07:00:00	296.15	68	4	180	0
30.07.2018	07:30:00	297.05	64.5	4	190	0
30.07.2018	08:00:00	297.95	61	4	200	0
30.07.2018	08:30:00	298	61	4.5	195	0
30.07.2018	09:00:00	298.05	61	5	190	0
30.07.2018	09:30:00	298.85	58.5	5.5	190	0
30.07.2018	10:00:00	299.65	56	6	190	0
30.07.2018	10:30:00	299.65	55.5	6	195	0
30.07.2018	11:00:00	299.65	55	6	200	0
30.07.2018	11:30:00	300.2	54	6	205	0
30.07.2018	12:00:00	300.75	53	6	210	0
30.07.2018	12:30:00	300.9	51.5	6.5	205	0
30.07.2018	13:00:00	301.05	50	7	200	0
30.07.2018	13:30:00	301.3	50	6.5	195	0
30.07.2018	14:00:00	301.55	50	6	190	0
30.07.2018	14:30:00	301	51.5	6	205	0
30.07.2018	15:00:00	300.45	53	6	220	0
30.07.2018	15:30:00	300.4	52.5	5	205	0
30.07.2018	16:00:00	300.35	52	4	190	0
30.07.2018	16:30:00	300.7	51.5	4.5	200	0
30.07.2018	17:00:00	301.05	51	5	210	0
30.07.2018	17:30:00	297.8	64	5.5	245	0
30.07.2018	18:00:00	294.55	77	6	280	0
30.07.2018	18:30:00	293.55	79.5	6	275	0
30.07.2018	19:00:00	292.55	82	6	270	0
30.07.2018	19:30:00	292.2	86	4	300	0
30.07.2018	20:00:00	291.85	90	2	330	0
30.07.2018	20:30:00	291.75	90	1.5	45	0
30.07.2018	21:00:00	291.65	90	1	120	0
30.07.2018	21:30:00	291.5	90	1	90	0
30.07.2018	22:00:00	291.35	90	1	60	0
30.07.2018	22:30:00	291.5	89.5	1	65	0
30.07.2018	23:00:00	291.65	89	1	70	0
30.07.2018	23:30:00	291.25	88.5	1	75	0
...

DD.MM.YYYY	HH:MM:SS	T[°K]	U[%]	FH [m/s]	DD[°]	P[mm]
...
31.07.2018	00:00:00	290.85	88	1	80	0
31.07.2018	00:30:00	291.25	87.5	1.5	95	0
31.07.2018	01:00:00	291.65	87	2	110	0
31.07.2018	01:30:00	291.95	85.5	1.5	115	0
31.07.2018	02:00:00	292.25	84	1	120	0
31.07.2018	02:30:00	292.2	84	1.5	140	0
31.07.2018	03:00:00	292.15	84	2	160	0
31.07.2018	03:30:00	291.85	86.5	1.5	155	0
31.07.2018	04:00:00	291.55	89	1	150	0
31.07.2018	04:30:00	291.65	88.5	1	70	0
31.07.2018	05:00:00	291.75	88	1	350	0
31.07.2018	05:30:00	293	81	1	60	0
31.07.2018	06:00:00	294.25	74	1	130	0
31.07.2018	06:30:00	294.85	73	2	135	0
31.07.2018	07:00:00	295.45	72	3	140	0
31.07.2018	07:30:00	296.25	71	4	165	0
31.07.2018	08:00:00	297.05	70	5	190	0
31.07.2018	08:30:00	297.95	63	5.5	200	0
31.07.2018	09:00:00	298.85	56	6	210	0
31.07.2018	09:30:00	297.05	64	7	235	0
31.07.2018	10:00:00	295.25	72	8	260	0
31.07.2018	10:30:00	295.65	66.5	8.5	260	0
31.07.2018	11:00:00	296.05	61	9	260	0
31.07.2018	11:30:00	296.25	59.5	7.5	265	0
31.07.2018	12:00:00	296.45	58	6	270	0
31.07.2018	12:30:00	296.5	56.5	6	265	0
31.07.2018	13:00:00	296.55	55	6	260	0
31.07.2018	13:30:00	296.55	52.5	6	265	0
31.07.2018	14:00:00	296.55	50	6	270	0
31.07.2018	14:30:00	296.4	49.5	6	270	0
31.07.2018	15:00:00	296.25	49	6	270	0
31.07.2018	15:30:00	296.2	49	5.5	270	0
31.07.2018	16:00:00	296.15	49	5	270	0
31.07.2018	16:30:00	295.75	51	4.5	280	0
31.07.2018	17:00:00	295.35	53	4	290	0
31.07.2018	17:30:00	294.8	55.5	3.5	295	0
31.07.2018	18:00:00	294.25	58	3	300	0
31.07.2018	18:30:00	293.3	63.5	2.5	300	0
31.07.2018	19:00:00	292.35	69	2	300	0
31.07.2018	19:30:00	291.45	73	1	315	0
31.07.2018	20:00:00	290.55	77	0	330	0
31.07.2018	20:30:00	290.05	79	0.5	337.5	0
31.07.2018	21:00:00	289.55	81	1	345	0
31.07.2018	21:30:00	289.4	82.5	1	348.75	0
31.07.2018	22:00:00	289.25	84	1	352.5	0
31.07.2018	22:30:00	288.35	89.5	1	11.875	0
31.07.2018	23:00:00	287.45	95	1	31.25	0
31.07.2018	23:30:00	286.95	95.5	1	50.625	0
...

DD.MM.YYYY	HH:MM:SS	T[°K]	U[%]	FH [m/s]	DD[°]	P[mm]
...
01.08.2018	00:00:00	286.45	96	1	70	0
01.08.2018	00:30:00	286.45	96.5	1	72.5	0
01.08.2018	01:00:00	286.45	97	1	75	0
01.08.2018	01:30:00	286.65	97	0.5	77.5	0
01.08.2018	02:00:00	286.85	97	0	80	0
01.08.2018	02:30:00	286.65	97	0.5	55	0
01.08.2018	03:00:00	286.45	97	1	30	0
01.08.2018	03:30:00	286.05	97.5	1	5	0
01.08.2018	04:00:00	285.65	98	1	340	0
01.08.2018	04:30:00	286.25	97.5	0.5	320	0
01.08.2018	05:00:00	286.85	97	0	300	0
01.08.2018	05:30:00	288.45	94	0.5	315	0
01.08.2018	06:00:00	290.05	91	1	330	0
01.08.2018	06:30:00	291.7	82.5	1	45	0
01.08.2018	07:00:00	293.35	74	1	120	0
01.08.2018	07:30:00	294	68	1	165	0
01.08.2018	08:00:00	294.65	62	1	210	0
01.08.2018	08:30:00	295.4	59	1.5	255	0
01.08.2018	09:00:00	296.15	56	2	300	0
01.08.2018	09:30:00	296.7	56	2.5	290	0
01.08.2018	10:00:00	297.25	56	3	280	0
01.08.2018	10:30:00	297.45	54	3	280	0
01.08.2018	11:00:00	297.65	52	3	280	0
01.08.2018	11:30:00	297.9	50	3	285	0
01.08.2018	12:00:00	298.15	48	3	290	0
01.08.2018	12:30:00	298.05	49	3	285	0
01.08.2018	13:00:00	297.95	50	3	280	0
01.08.2018	13:30:00	298.1	48	3	290	0
01.08.2018	14:00:00	298.25	46	3	300	0
01.08.2018	14:30:00	298.35	44.5	3	295	0
01.08.2018	15:00:00	298.45	43	3	290	0
01.08.2018	15:30:00	298.15	43	3.5	305	0
01.08.2018	16:00:00	297.85	43	4	320	0
01.08.2018	16:30:00	297.65	43	3.5	320	0
01.08.2018	17:00:00	297.45	43	3	320	0
01.08.2018	17:30:00	296.9	47	3	330	0
01.08.2018	18:00:00	296.35	51	3	340	0
01.08.2018	18:30:00	295.2	54.5	2.5	350	0
01.08.2018	19:00:00	294.05	58	2	0	0
01.08.2018	19:30:00	293.05	64.5	2	10	0
01.08.2018	20:00:00	292.05	71	2	20	0
01.08.2018	20:30:00	291.2	77.5	1.5	355	0
01.08.2018	21:00:00	290.35	84	1	330	0
01.08.2018	21:30:00	290.05	86	1	340	0
01.08.2018	22:00:00	289.75	88	1	350	0
01.08.2018	22:30:00	289.8	89	0.5	60	0
01.08.2018	23:00:00	289.85	90	0	130	0
01.08.2018	23:30:00	289.65	91	0.5	97.5	0